Molecular composition and pharmacology of store-operated calcium entry in sensory neurons

Alexandra-Silvia Hogea

Submitted in accordance with the requirements for the degree of

Doctor of Philosophy

The University of Leeds

School of Biomedical Sciences

September 2018

The candidate confirms that the work submitted is her own and that appropriate credit has been given where reference has been made to the work of others.

Acknowledgements

Firstly, I would like to express my appreciation and thanks to my supervisor, mentor and friend, Professor Nikita Gamper. It has been an amazing time and even if it was filled with challenges, I overcame them thanks to your continued support, guidance and optimism.

I am extremely grateful to Professor David Beech and Dr. Lin Hua Jiang for their guidance at different stages during my early PhD years.

I am very lucky to have met past and present Gamper lab members who contributed greatly to my development as a scientist, who welcomed me in their lives and made Leeds feel more like home. A massive thank you to Shihab Shah for the support and friendship, for being patient during hard times and for celebrating the achievements together. It has been quite a ride! I would also like to express my gratitude to Ewa Jaworska who first introduced me to immunohistochemistry at times when I thought nail polish is just for nails.

Thank you Rosmaliza Ramli, Haixia Gao, Eleni Kyriakopoulou for all your guidance and for being such good friends! Special thank you to my previous students Fred, Dan, Adam and Georgie for choosing to work together for your dissertations.

Finally, deepest gratitude to my parents and to my sister for their unparalleled support and love even if we were miles apart. Thank you to my husband, Iulian, for your love, your patience and your optimism during all these years. It has been an amazing journey thanks to you.

Abstract

In a forever busy pharmaceutical market, the need for analgesic and anti-inflammatory drugs is still in high demand. Various conditions such as rheumatoid arthritis, diabetes or viral infections are frequently associated with persistent and unalleviated pain, therefore uncovering novel pharmacological targets is deemed necessary.

Store-operated calcium entry (SOCE), a complex mechanism orchestrated by calcium release activated calcium (CRAC) channels, has been recently associated with neuropathic and inflammatory pain. Moreover, several attempts to describe the presence of CRAC channel molecular components in pain-sensing DRG and dorsal horn neurons have been made. Yet, the exact identity of CRAC channel complex components, the function of junctional proteins in CRAC channel assembly and the exact role of SOCE within primary afferent neurons remains poorly understood. Here I hypothesized that SOCE functions as a facilitator of Ca^{2+} signalling in inflammatory pain conditions and that junctional proteins offer a supportive role of the CRAC channels assembly in DRG neurons.

To test this, I characterized the localization pattern of CRAC components within DRG neurons by immunohistrochemistry. STIM (1 and 2) and Orai (1 and 3) isoforms were all expressed within primary afferent neurons of different sensory modalities. STIM1 and Orai1 were expressed to a higher degree as compared to their family members and co-localized into puncta upon SOCE activation as demonstrated by proximity ligation assay (PLA). Interestingly, STIM2 revealed a higher preference in large-diameter (presumed mechanosensory) neurons, as compared to STIM1.

To confirm the presence of SOCE, the effect of CRAC inhibitors YM58483 and Synta66 in DRG neurons was also investigated. Both compounds significantly reduced SOCE in DRG neurons; the efficacy of inhibition was dramatically increased by pre-incubation suggesting that these CRAC inhibitors may not act as direct ion channel pore blockers but rather interfere with the CRAC complex functional assembly.

CRAC channel complex assembly relies on the close proximity of the cellular plasma membrane and endoplasmic reticulum, yet, nothing is known thus far about how these membrane junctions are maintained in DRG. This thesis brings evidence of the expression of Junctophilin (JPH) proteins within primary sensory neurons. Amongst the family members, JPH4 was expressed the highest, followed by JPH1 and JPH3, while no expression of JPH2 was observed.

Moreover, experiments using immunocytochemistry revealed that JPH4 is co-expressed with Orai1 and STIM1 in pain-sensing neurons, while PLA demonstrated that both Orai1 and STIM1 co-localize with JPH4 at endoplasmic reticulum (ER)-plasma membrane (PM) junctions upon bradykinin (BK) -induced SOCE.

To test whether JPH4 is a SOCE facilitator, several experiments were performed. Thus, it was demonstrated that STIM1 directly interacts with JPH4 upon ER Ca^{2+} store depletion using immunoprecipitation. Furthermore, knocking-down JPH4 disrupted the Orai1-STIM1 clustering and coupling at the ER-PM junctions as observed by PLA. Interestingly, silencing JPH4 in DRG neurons inhibited SOCE without altering the basal Ca^{2+} pool levels and impaired the subsequent ER Ca^{2+} store refill, as demonstrated by calcium imaging experiments. These observations taken together strengthen the role of JPH4 in facilitating SOCE in DRG neurons.

CRAC channels have been previously considered attractive targets for treatment of inflammatory conditions and more pharmaceutical companies showed an increased interest in developing CRAC modulators in the past decade. The high expression of JPH4 in peripheral sensory neurons, its importance in promoting the CRAC channel assembly and its role on the oscillatory ER Ca^{2+} refill provide evidence for considering JPH proteins as putative targets for treating inflammatory pain.

Contents

Publications/posters

Hogea, A and Gamper, N, (2016), **Modulating store-operated Ca^{2+} entry in sensory neurons**, European Calcium Society Meeting, Valladolid, Spain

List of Figures

List of Tables

Abbreviations

2-APB	2-aminoethoxydiphenyl borate
5-HT	Serotonin
$[Ca^{2+}]i$	Intracellular Ca^{2+} concentration
AC	Adenylyl Cyclase
AMPA	α-amino-3-hydroxy-5-methyl-4-isoxazolepropionic aci
ANO1	Anoctamin-1
AOI	Area of interest
ATP	Adenosine triphosphate
B_1R	Bradykinin receptor 1
B_2R	Bradykinin receptor 2
BDNF	Brain-derived neurotrophic factor
BK	Bradykinin
BSA	Bovine serum albumin
BTP2	3,5-bis(trifluoromethyl)pyrazole
CAD	CRAC activation domain
CaM	Calmodulin
cAMP	Cyclic adenosine monophosphate
CaM	Calmodulin
CAMKII	Calcium /calmodulin-dependent protein kinase II
Ca_V	Voltage gated Ca^{2+} channel
CC1	Coil-coiled domain 1
CCh	Carbachol
CDK	Cyclin-dependent kinase 1
cDNA	Complementary deoxyribonucleic acid
CEPIA	Calcium-measuring organelle entrapped protein indicator
CFA	Complete Freund's adjuvant

CHO	Chinese hamster ovary cells
CICR	Ca^{2+}-induced Ca^{2+}-release
CIF	Calcium influx factor
CIP	Congenital insensitivity to pain
CGRP	calcitonin-gene related peptide
CMD	CRAC modulatory domain
CMT	Charcot Marie Tooth disease
CNS	Central nervous system
Co-IP	Co-immunoprecipitation
COX	Cyclooxygenase
CPA	Cyclopiazonic acid
CRAC	Calcium release-activated calcium channel
DAG	Diacylglycerol
DAPI	4′,6-diamidino-2-phenylindole
DHPR	Dihydropyridine receptors
DMEM	Dulbecco's modified Eagle's medium
DRG	Dorsal root ganglion
EC	Extracellular solution
EC_{50}	Half-maximal (50%) response concentration
EGTA	ethyleneglycol-bis(β-aminoethyl ether)-N,N,N',N'-tetraacetic acid
EDTA	Ethylenediaminetetraacetic acid
EP_2	Prostaglandin receptor 2
ER	Endoplasmic reticulum
ET	Endothelin
FCS	Fetal calf serum
GDAP1	Ganglioside-induced differentiation-associated protein 1
GECI	Genetically encoded calcium indicators
GFP	Green fluorescent protein

GPCR	G-protein coupled receptor
H1	Histamine receptor 1
hASMC	Human aortic smooth muscle cells
HBSS	Hanks balanced salt saline solution
HDL-2	Huntington's Disease like 2
HEK293	Human embryonic kidney 293 cells
HIV	Human immunodeficiency virus
HL-60	Human leukemia-60 cells
HMC	Hypertrophic cardiomyopathy
HRP	Horse radish peroxidase
IASP	International Association for the Study of Pain
IBD	Inflammatory bowel disease
IC_{50}	Half maximal inhibitory concentration
ICC	Immunocytochemistry
ICD	Intracellular domain
I_{CRAC}	Calcium release-activated calcium current
IL-4	Interleukin-4
IP	Immunoprecipitation
IP_X	Prostacyclin receptor x
IP_3	Inositol 1,4,5-trisphosphate
IP_3R	Inositol 1,4,5-triphosphate receptor
$iPLA_2\beta$	Calcium independent phospholipase A2 beta
I_{SOC}	Store operated calcium current
JMC	Junctional membrane complexes
JPH	Junctophilin
KD	Knock-down
Kd	Dissociation constant
LB	Lysogeny broth

MAP	Mitogen activated protein
MORN	Membrane occupation and recognition nexus motifs
mRNA	Messenger ribonucleic acid
NAADP	Nicotinic acid adenine dinucleotide phosphate
Na_V	Voltage-gated Na+ channel
NF200	Neurofilament 200
NGF	Nerve growth factor
NK1	Neurokinin 1 receptor
NMDA	N-methyl-D-aspartate
NSAID	Nonsteroidal anti-inflammatory drug
OASF	ORAI1-activating small fragment
PAR-2	Protease-activated receptor 2
PASMC	Pulmonary Artery Smooth Muscle Cells
PB	Phosphate buffer
PBS	Phosphate buffer saline
PDGF	Platelet-derived growth factor
PFA	Paraformaldehyde
PGE	Prostaglandin receptor
PI3K	Phosphoinositide 3 kinase
PIP_2	Phosphatidylinositol 4,5-bisphosphate
PKA	Protein kinase A
PKC	Protein kinase C
PLA	Proximity ligation assay
PLC	Phospholipase C
PM	Plasma membrane
POAEE	Palmitoleic acid ethyl ester
PSNL	Partial spinal nerve ligation
RBL-2H3	Rat basophilic leukemia cells

RNA	Ribonucleic acid
ROC	Receptor-activated channels
ROI	Region of interest
ROS	Reactive oxygen species
RVM	Rostral ventral medulla
RYR	Ryanodine Receptor
SAM	Sterile alpha motif
SARAF	SOCE-associated regulatory factor
SCID	Severe combined immunodeficiency disorder
SEM	Standard error mean
SERCA	Sarcoplasmic/Endoplasmic Reticulum Ca^{2+}-ATPase
siRNA	Small interference ribonucleic acid
SHD	STIM1 homomerization domain
SNI	Spinal nerve injury
SNL	Spinal nerve ligation
SOAP	STIM1-Orai1 association pocket
SOAR	STIM1-Orai1 activating region
SOCC	Store operated calcium channel
SOCE	Store-operated calcium entry
SOCIC	Store-operated calcium influx complex
SP	Substance P
SPF	Signal peptide fragment
SR	Sarcoplasmic reticulum
STIM	Stromal interacting molecule
TG	Trigeminal ganglion
TIRF	Total internal reflection fluorescence microscopy
TM	Transmembrane
TMEM66	Transmembrane protein 66

TNFα	Tumour necrosis factor alpha
TPC	Two pore channels
TrkA	Tyrosine kinase A
TRP	Transient receptor potential channel
TRPA1	Transient receptor potential ankyrin 1
TRPC	Transient receptor potential canonical
TRPM	Transient receptor potential melastin
TRPV1	Transient receptor potential vanilloid 1
VGCC	Voltage gated Ca^{2+} channel
VMSCs	Vascular smooth muscle cells
VOC	Voltage operated channels
WB	Western blot
YFP	Yellow fluorescent protein

Chapter 1. Introduction

At some point in life, everyone should experience the sensation called pain; the ability to feel it is critical for survival. Patients with congenital insensitivity to pain (CIP), first described by Swanson in 1963, represent rare clinical cases when undetectable body injuries can become fatal. Pain protects us against harmful external stimuli (noxious heat or cold, physical tissue damage or chemical irritants) and internal threats (such as broken bones or infections) (Stemkowski et al. 2012). Thus, without the ability to sense it, our body will not be able to acknowledge trauma and to further protect itself from harm.

Researchers continuously invest resources to attain an in depth understanding of pain mechanisms as well as supporting the demand for analgesics that we are facing nowadays. While acute pain is attenuated once the injured tissue is healed (such as postoperative pain), chronic pain is persistent and its management is challenging. Chronic pain has a multifactorial etiology and is not an extension of acute pain (Mao et al. 2017). For this reason, patients with various conditions such as diabetes, arthritis, neuropathic or cancer-related pain still suffer from unalleviated pain. The current treatments are not sufficient to attenuate pain in certain clinical cases and this affects greatly the quality of patients' lives. For a correct diagnosis and an efficient treatment, the development of novel diagnostic tools and analgesics is extremely necessary and in very high demand.

The following chapter is a review of the most recent and relevant research publications to support the objectives of this thesis. Firstly, I will offer an overview of the general aspects of pain signaling, followed by discussing the importance of store-operated calcium-entry in inflammatory pain and, finally, outlining the role of junctophilin proteins in modulating calcium dynamics.

1.1 Nociception

Our skin and internal organs contain unspecialized peripheral nerve endings of neurons that are responsible for responding to sensorial stimuli (Stemkowski et al. 2012). An interesting characteristic of these neurons is their morphology: a pseudo-unipolar axon projecting from the soma and bifurcating towards the periphery where the stimuli is detected and towards the spinal horn, where they synapse with secondary neurons which in-turn further project signals to the relevant structures in the brain (Devor et al. 1999; Tandrup et al. 1995).

The process by which noxious stimuli are detected is called nociception and the primary afferent neurons that respond to it are referred to as nociceptors (Dubin and Patapoutian, 2010). The somata of primary nociceptors reside in the trigeminal ganglia (TG; 1 pair, for detecting cephalic stimuli) and the dorsal root ganglia (DRG; 29 pairs at each vertebra in humans) (Basbaum et al. 2009).

The nociceptive terminal expresses different proteins that are selectively activated in response to external stimuli. Types of proteins that are most frequently activated during this detection phase are: receptor-activated channels, ROC (e.g. the heat sensor TRPV1), G-protein coupled receptors, GPCR (e.g. bradykinin or histamine receptor), or voltage-operated channels, VOC (e.g. voltage-gated sodium channels) (Bourinet et al. 2014, Stemkowski et al. 2012).

Nociceptors are typically categorized based on fiber size, the type of the sensory stimuli they detect and how fast they conduct an action potential. The three main classes of sensory fibers are:

i) *Aβ fibers*, large myelinated fibers with fast conductivity; they respond to light touch and pressure
ii) *Aδ fibers*, medium thinly myelinated fibers with lower conductivity; they respond to mechanical and/or thermal stimuli
iii) *C fibers*, small non-myelinated fibers with slow conductivity; they respond to mechanical, thermal and/or chemical stimuli.

The myelination of fibers determines the speed of action potential conduction through the axon. Regarding pain, Aδ fibers are responsible for mediating the first component of pain, whereas C fibers detect and propagate the secondary slow pain. Table 1.1 shows the classification of nerve fibers based on diameter, conduction velocity myelination and function.

Type of sensory fiber	Diameter (μm)	Conduction velocity (m/s)	Myelinated?	Function
Aβ fiber	5-12	30-70	Myelinated	fine touch
Aδ fiber	2-5	12-30	Thinly myelinated	light touch fast pain temperature
C fiber	0.5-1	0.5-2	Not myelinated	slow pain temperature

Table 1.1 The classification on sensory fibers based on conduction velocity and size

Other ways to classify peripheral sensory neurons also exist. For instance, C fibers are further subcategorized in two groups: i) 'peptidergic' fibers that express nerve growth factor (NGF) receptor, tyrosine kinase A (TrkA), calcitonin-gene related peptide (CGRP) and Substance P (SP); and ii) 'non-peptidergic' fibers that express the purinergic receptor P2X3 while lacking CGRP or SP (Basbaum et al. 1999, Vuchanova et al. 1998). Recently, sequencing studies have also been used to further subdivide nociceptors however, this is outside the scope of the current thesis. (Usoskin et al. 2015; Li et al. 2016).

1.2 The ascending pathway of pain

An external stimulus, such as noxious heat, activates a sensory receptor found at the nerve endings of nociceptors. This first event is called a receptor potential which involves depolarization of the membrane due to an inward current flow (Basbaum et al. 2009). The receptor potential leads to the the activation of voltage-gated ion channels (such as voltage-gated calcium, sodium and potassium channels) that play a key role in both neurotransmitter release and generation of action potentials (Fletcher A. 2011).

Upon action potential generation, the signal is propagated through the neuronal fiber (axon), thus enabling communication with postsynaptic neurons found in the dorsal horn (Dubin et al. 2010) (Figure 1.1). The dorsal horn of the spinal cord is organized into distinct laminae where nociceptors of different sensory modalities terminate (Figure 1.1). As such, Aβ fibers terminate deeper in the dorsal horn (laminae III, IV, V) whereas Aδ afferents project to both lamina I and lamina V. Interestingly, C fibers reveal distinct projection patterns depending on their subtype: most peptidergic C nociceptors terminate in lamina I and deeper lamina II, while non-peptidergic fibers project in the ventral part of lamina II (Basbaum et al. 2009) (Figure 1.1). Therefore, neurons within laminae I and II are responsive to noxious stimuli (through Aδ and C afferents), neurons in laminae III and IV respond to innocuous stimulation (via Aβ fibers) and neurons in lamina V respond to both noxious and non-noxious stimuli.

Dorsal horn (second order) neurons ascend via the spinothalamic tract and project to different areas of the brain such as the thalamus and the parabrachial nucleus (Figure 1.1). From these areas, third order neurons project to the somatosensory cortex and amygdala, and further to the insular and cingulate cortices where the emotional component of pain is processed (Basbaum et al. 2009) (Figure 1.1). Other second order neurons terminate at the rostral ventral medulla and parabrachial nucleus where descending modulation takes place. Orofacial noxious stimuli detected by the TG nociceptors follow a similar pathway, but via the TG nerve and the subsequent trigemino-thalamic pathway (Basbaum et al. 2009).

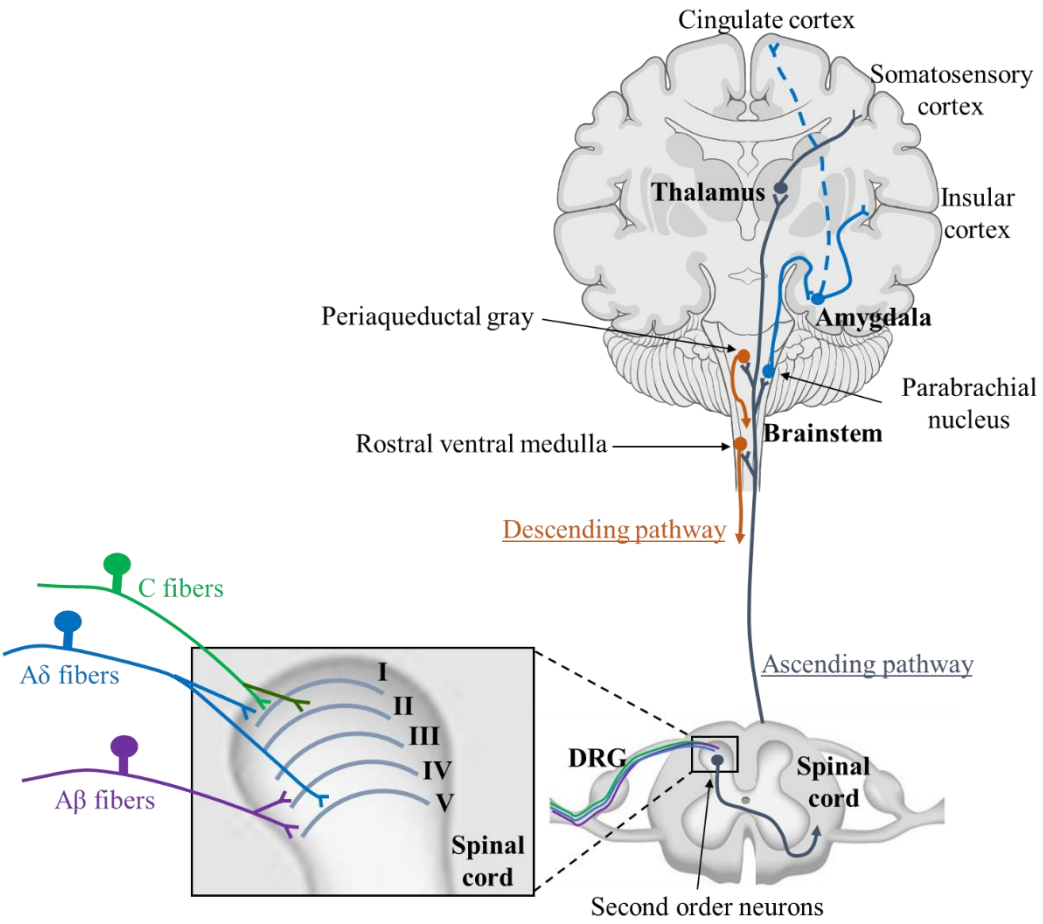

Figure 1.1 Anatomy of the pain pathway. The noxious stimulus is detected at the nociceptive terminal of the primary afferent neurons. These reside in the dorsal root ganglia (DRG) and the trigeminal ganglia (TG, not shown). The dorsal horn reveals a laminar organization where nociceptors terminate. Peptidergic C fibers (green) and Aδ fibers (blue) project superficially in the lamina I of the dorsal horn, while the non-peptidergic C fibers (dark green) terminate in the inner part of lamina II. Laminae III and IV receive input from Aβ fibers, while lamina V neurons are responsive to both noxious and non-noxious stimuli via Aδ and Aβ nociceptors, respectively. Second order neurons project further to different areas of the brain: to the thalamus where information about the location and the intensity of the stimulus is transmitted, to the amygdala via the parabrachial nucleus, where the emotional component of the pain is generated and to the periaqueductal gray and rostral ventral medulla regions where the descending feedback occurs. Figure based on Basbaum et al. 2009.

1.3 Types of pain

Despite the critical role of pain to protect us from harm, not all types of pain are beneficial to the body. Differentiating pain is necessary for diagnostics and treatment, therefore many (sometimes overlapping) classifications have been generated based on various factors such as time course, physiology of pain, intensity and location /type of tissue.

Based on physiology, pain can be classified as *nociceptive* (transient, acute) pain, *neuropathic* (nervous system injury) pain and *inflammatory* (tissue injury) pain. Interestingly, more than one mechanism can be present at once and a patient can suffer more than one type of pain. For example, inflammatory pain signalling is also involved in neuropathic pain (Xu et al. 2011).

Nociceptive pain occurs as a result of noxious stimulation in an otherwise healthy tissue and is based on nociceptor specialization in sensing heat, chemical or mechanical stimuli (Carr et al. 1999). It is characterized as being the physiological, acute type of pain produced by the activation of nociceptors found in internal organs or skin (Carr et al. 1999). This can be referred to as 'healthy pain' which is emplaced to provide protection to the body (see above).

Conversely, *Neuropathic pain* is defined as pain "initiated or caused by a primary lesion or dysfunction in the nervous system" (IASP definition, www.iasp-pain.org) and it appears as hyperalgesia (exaggerated pain sensation subsequent to a noxious stimulus) or allodynia (pain sensation following an innocuous stimulus). (Bridges et al. 2001) Persistent pain secondary to nerve injury is a very complex phenomenon and comprises of pathological remodelling of peripheral afferents and central sensitisation in both the spinal cord and the brain. (Campbell et al.2006). The neuropathic pain signalling pathways have been intensely studied and the ongoing focus on the proteins involved (ion channels, receptors, enzymes) led to some success in the development of targeted pain therapies. Yet, the complexity of neuropathic pain poses substantial challenges to both researchers and clinicians. Viral infections (e.g. with Herpes zoster), cancer therapies (e.g. chemotherapy agents such as paclitaxel) or various diseases (e.g. diabetes) can generate nerve damage and therefore become the main source of unalleviated persistent pain (Campbell et al. 2006). At the moment, the sufferers can only benefit from

drugs that temporary reduce the pain secondary to the nerve injury. As personalised healthcare is moving forward, we are looking towards a future of individual targeted therapies and novel pharmacological targets to be discovered. However, despite the importance of such studies, neuropathic pain is outside the scope of this thesis.

Inflammatory pain is usually generated by a tissue lesion and is one of the five characteristics of inflammation: heat (calor), swelling (tumor), pain (dolor), redness (rubor) and loss-of-function (function laesa). (Kidd et al. 2001). Inflammation generates an immune response which involves the release of numerous signalling factors by immune cells (e.g. leukocytes, neutrophils) and damaged tissue (Figure 1.2). At the injury site, mediators are released from damaged cells into the extracellular space which act on the peripheral terminals of nociceptive afferents by directly activating or sensitizing them to other chemical and physical stimuli (Das V. 2015) (Table 1.2). The receptors they activate fall into three main categories: i) G-protein coupled receptors (GPCR), ii) receptor tyrosine kinases (Trk) and iii) ion channels (Linley et al. 2010).

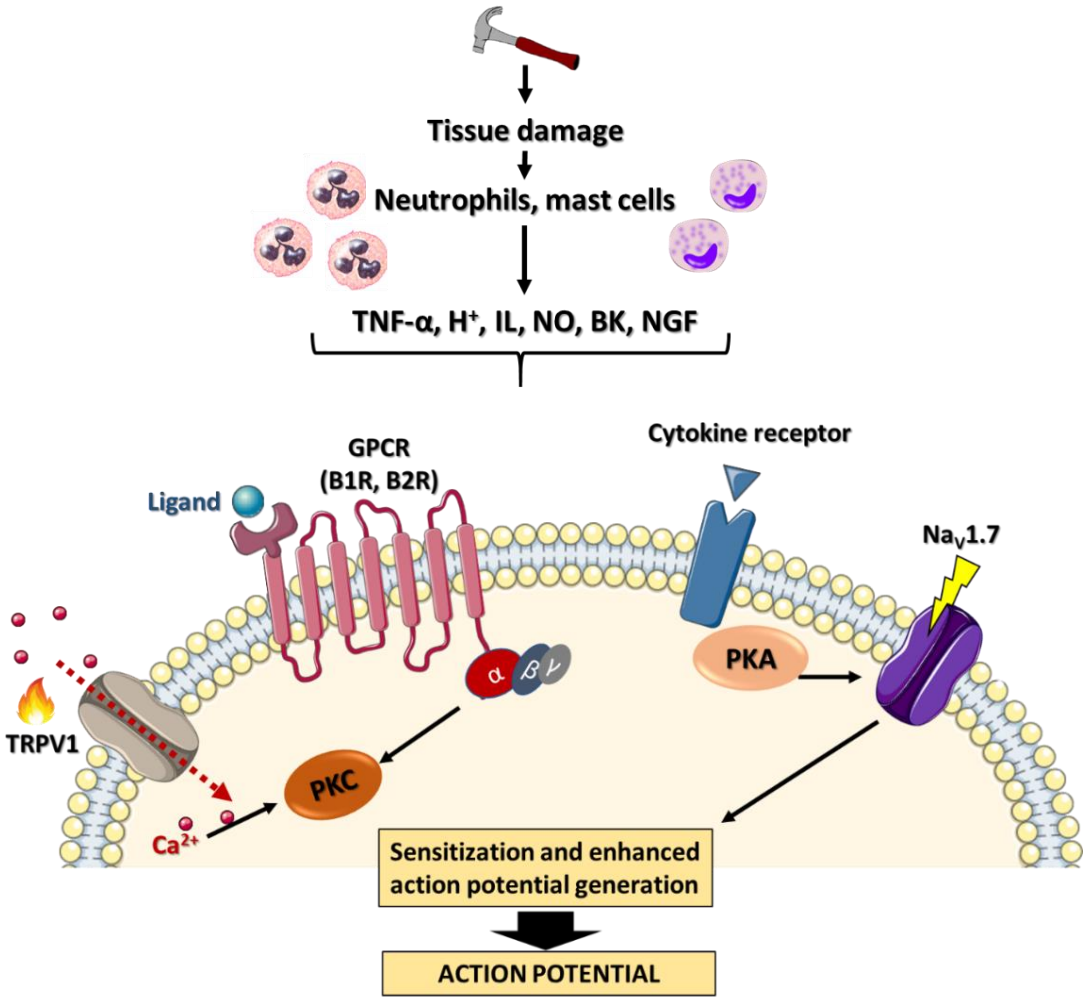

Figure 1.2. Mechanisms of inflammatory pain pathways in peripheral sensory neurons. A tissue lesion generates an immune response and the subsequent release of pro-inflammatory mediators (such as BK). These mediators further act on local peripheral nociceptors (e.g. BK receptors B1, B2) and trigger internal cascades responsible for the generation of an action potential. Figure adapted from Das V. 2015.

Mediator and its source	Tissue target	Receptor	Somatic target
Bradykinin (immune cells, plasma)	Blood vessels Nociceptors	B1R B2R	Thermal Mechanical
Substance P (nociceptors)	Immune cells Blood vessels Nociceptors	NK1R	Thermal Mechanical
Glutamate (microglia, nociceptors)	Nociceptors	mGluR1 mGlu2/3 mGluR5	Thermal Mechanical
Serine proteases (immune cells, nociceptors)	Nociceptors	PAR1 PAR2 PAR4	Thermal Mechanical
Endothelin (endothelial cells)	Blood vessels Nociceptors	ETaR ETbR	Thermal Mechanical Chemical
Serotonin (immune cells)	Nociceptors	5-HT1A 2A, 2B 3, 4, 7	Thermal Mechanical Chemical
Prostaglandin (microglia, nociceptors)	Nociceptors	EP1, 2 EP3B, 3C EP4 DP1, 2	Thermal Mechanical Chemical
CGRP (nociceptors)	Blood vessels Nociceptors Endothelial cells	CRLR RAMP1	Thermal Mechanical
ATP (microglia, nociceptors)	Nociceptors Immune cells Microglia	P2X2, 3, 4, 7 P2Y	Thermal Mechanical
NGF (immune cells, nociceptors)	Nociceptors Immune cells	TrkA GPR30	Thermal Mechanical

Table 1.2 Summary of key inflammatory mediators released during an immune response (This list has been adapted from Jeske NA 2015)

1.4 G-protein coupled receptors

G-protein coupled receptors (GPCRs) form the largest family signalling proteins with approximately 850 members (Geppetti et al. 2015). They are highly involved in mediating pain and itch as they reside in the nerve terminal of sensory neurons. GPCRs sense and respond to stimuli from immune cells, epithelial tissue or the circulation and also have a key role in neurogenic inflammation (Geppetti et al. 2015). G-proteins are generally classified as monomeric G-proteins (or small G-proteins) and heterotrimeric G-proteins (composed of three different subunits α, β and γ) (Geppetti et al. 2015, Purves et al. 2001). G-protein activation alters the function of different downstream effectors, mainly enzymes such as adenylyl cyclase (AC) or phospholipase C (PLC) (Figure 1.3). In turn, these enzymes produce second messengers that activate different intracellular signalling cascades (Purves et al. 2001). Interestingly, specific G-protein subunits trigger different cascades, and therefore the signalling pathway is receptor-dependent (Figure 1.3). As such:

i) Activation of G_s *proteins* triggers the stimulation of adenylyl cyclase (AC) with cyclic adenosine monophosphate (cAMP) being generated. Furthermore, protein kinase A (PKA) is activated and modulates other proteins through phosphorylation, such as voltage gated sodium channels ($Na_V1.7$) (Figure 1.2). These channels are responsible for the depolarization phase of the action potential in various excitable cells (Linley et al. 2010; Bhave et al. 2002). Among the inflammatory GPCR coupled to G_s are prostaglandin receptors EP2, 4 and DP1, prostacyclin (IP) receptor, serotonin (5-HT) receptors and endothelin (ET) receptor A

ii) Opioid receptors, GABAB, dopamine D2 and some other receptors are coupled to $G_{i/o}$ *proteins*; once activated, they promote an analgesic effect by reducing the cAMP levels and further inhibiting presynaptic $Na_V1.7$ channels. Interestingly, it has been shown that bradykinin (BK) has a role in the insertion of delta-opioid receptors in the plasma membrane of peripheral sensory neurons (Linley et al. 2010)

iii) Receptors coupled to $G_{q/11}$ α *subunits* stimulate the plasma membrane phosphatidylinositol-4,5-biphosphate (PIP_2) cleavage by phospholipase C (PLC). This generates two metabolites: inositol triphosphate (IP_3) and diacylglycerol (DAG). DAG activates the protein kinase C (PKC) that targets various ion channels such as the heat sensor, TRPV1, while IP_3 binds to IP_3 receptors (IP_3R) found in the endoplasmic reticulum (ER) membrane, further generating a calcium release from the ER pool into the cytosol (Jung et al. 2004). Among inflammatory GPCR expressed in nociceptors are histamine receptor H_1, BK receptor 2 (B_2R), prostaglandin receptor EP_1, substance P receptor NK_1 and purinergic receptor P2Y.

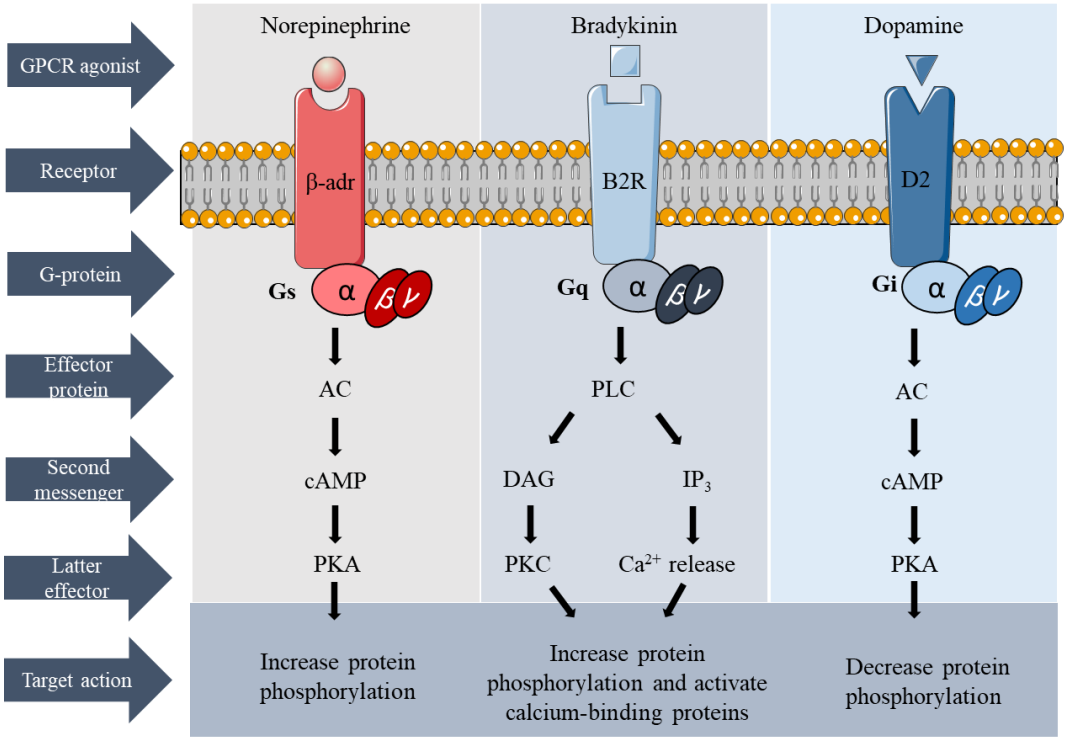

Figure 1.3 Intracellular signalling cascades associated with GPCRs. In all three examples, binding a GPCR agonist to its specific receptor leads to the activation of the G-protein. Further on, downstream effector proteins recruit second messengers and trigger specific pathways (from left to right: Gs, Gq and Gi as examples for heterotrimeric G-proteins). Figure adapted from Purves et al. 2001.

1.5 Ca^{2+} signalling

In the remaining pages of this chapter I will focus on Ca^{2+} signalling as this is the main topic of the current study. Ca^{2+} acts as a ubiquitous secondary messenger regulating a plethora of cellular functions, ranging from gene expression to contractility and from synaptic transition to cell death (Cerella et al. 2010). One recognised role of Ca^{2+} in the nervous system is facilitation of synaptic transmission. Due to the steep Ca^{2+} gradient present between the inside and outside of the cell, voltage-gated Ca^{2+} channel (VGCC) activation allows Ca^{2+} to flood into the cell and increase the cytoplasmic concentration of Ca^{2+}. Further on, Ca^{2+} binds to synaptotagmin-1 (a protein localized to synaptic vesicles) and triggers exocytosis (Clapham et al. 2007). There are multiple calcium-permeable channels involved in pain signalling and VGCCs represent the dominant pathway of calcium entry through depolarization. (Bourinet et al. 2014). These channels can be categorized depending on their mode of action: high voltage activated channels (further classified as L-, N-, P-, Q- and R- types) and low voltage activated channels (T-type) (Bourinet et al. 2014).

Other Ca^{2+}-permeable channels such as N-methyl-D-aspartate (NMDA), transient receptor potential (TRP) or P2X receptors are non-selective calcium-permeable cation channels shown to be expressed in nociceptive neurons and play key roles in pain signalling. (Bourinet et al. 2014). Despite these various channels being important in nociceptive signal transduction, they are outside the scope of this thesis, so they will not be discussed further.

Not all intracellular Ca^{2+} signals are mediated by Ca^{2+} entry from the outside of the cell. A robust Ca^{2+} signalling 'hub' is represented by intracellular Ca^{2+} stores, such as endoplasmic reticulum (ER), mitochondria and Golgi apparatus (Ashby and Tepikin, 2001). In relation to inflammatory pain mechanisms, of particular importance are ER Ca^{2+} stores as these are mobilised downstream of the $G_{q/11}$-coupled GPCR and some other relevant pathways (Geppetti et al. 2015). An important mechanism for the maintenance of ER Ca^{2+} load is through the so-called calcium-release activated-calcium (CRAC) channels. These are activated upon depletion of Ca^{2+} from ER and generate a small inward calcium current called

I_{CRAC} (Parekh 2010, Luik et al. 2006). Activation of ER membrane residents IP_3 and/or ryanodine receptors (RyR) leads to initiation of this process, which was amply named as Store Operated Ca^{2+} Entry (SOCE) (Parekh and Putney 2005)

The following chapter will offer an in depth understanding of this mechanism, its origins and role in excitable and non-excitable cells.

1.5.1 Store operated calcium entry (SOCE)

The concept of SOCE dates to JW Putney's manuscript published in 1986, describing the term "capacitative" calcium entry as the mechanism by which plasma membrane Ca^{2+} channels are activated by intracellular store discharge (Putney JW 1986). Previous studies in the field showed that cytosolic Ca^{2+} can be increased by two main methods: i) cationic influx from the extracellular compartment into the cytoplasm, and ii) depletion of intracellular Ca^{2+} stores. (Bohr et al. 1963; Breemen et al. 1969, Putney et al. 1981). Also, a secondary messenger has been identified to mobilize internal Ca^{2+} release from nonmitochondrial intracellular stores in pancreatic cells; this was found to be the inositol 4,5-trisphosphate (IP_3) (Berridge 1983). Further studies demonstrated that a sesquiterpene lactone, thapsigargin, was able to release Ca^{2+} from the internal stores independently of IP_3 formation (Jackson et al. 1988). After the development of the cytosolic Ca^{2+} indicator fura-2 (Grynkiewics et al. 1986), a report described a transient rise in $[Ca^{2+}]_i$ using thapsigargin as a model of SOCE activation (Takemura et al. 1989). The activity of thapsigargin was attributed to the blockade of the sarco/endoplasmic reticulum Ca^{2+}-ATPase (SERCA) pumps which were subsequently defined as being responsible for refilling the ER stores (Thastrup et al.1990).

JW Putney further investigated the relationship between three key elements of calcium signaling in excitable and non-excitable cells: calcium entry into the cell, calcium release from internal stores and refilling these stores (Putney JW 1986). Similarly, in 1983, Fabiato firstly described the concept of calcium-induced calcium-release (CICR) via ryanodine receptors in

cardiac cells (Fabiato 1983). Altogether, the findings around SOCE were later summarized in 2005 (Parekh AB and Putney JW, 2005) when several mechanisms thought to activate SOCE were reported: i) the presence of diffusible messengers that could link store depletion to replenishment stimulation (Takemura et al. 1989), ii) vesicular fusion suggesting that store-operated calcium channels (SOCC) are diffused in the PM after store depletion (Somasundaram et al. 1995) and iii) conformational coupling: IP_3Rs bind to plasma membrane Ca^{2+} channels in skeletal muscles (Irvine et al. 1990). Later, the molecular identity of the proteins involved in modulating SOCE was revealed.

1.5.2 STIM, Orai and TRPC. Key players in activating SOCE

In 1992, Hoth and Penner reported for the first time recordings of a whole-cell current generated by Ca^{2+} store depletion. They called this Ca^{2+} release-activated Ca^{2+} current, I_{CRAC} (Hoth and Penner 1992). I_{CRAC} was shown to be a small (in the range of few pA/pF) inward rectifying and with a positive reversal potential current. The authors hypothesized that emptying Ca^{2+} stores could generate the activation of a PM current either through a second messenger or by the direct interaction between ER and PM (Hoth and Penner 1992). While most Ca^{2+} channels are permeant to other divalent cations, CRAC channels seemed to be highly Ca^{2+} selective and to be blocked by Ba^{2+} and Mn^{2+} (Hoth and Penner 1992) (Figure 1.4).

At that time, the Drosophila TRP channel was the first non-voltage Ca^{2+} channel known to reside in the PM and to be activated by Ca^{2+} store depletion, but the mechanism underlying this process remained unelucidated (Wes et al. 1995). Later, after the TRPC1-7 family member were identified, TRPC1 was channel thought to contribute to SOCE (Liu et al. 2003). However, the electrophysiological properties of TRPC1-mediated Ca^{2+} currents did not resemble those of I_{CRAC} (e.g. the current is relatively Ca^{2+} selective) and other TRP channels also failed to conduct I_{CRAC} described by Hoth and Penner (Liu et al. 2003). Thus separately,

I_{SOC} was defined as the nonselective current occurring after the activation and opening of PM ion channels in response to ER Ca^{2+} store depletion (Roos et al. 2005, Feske et al. 2006).

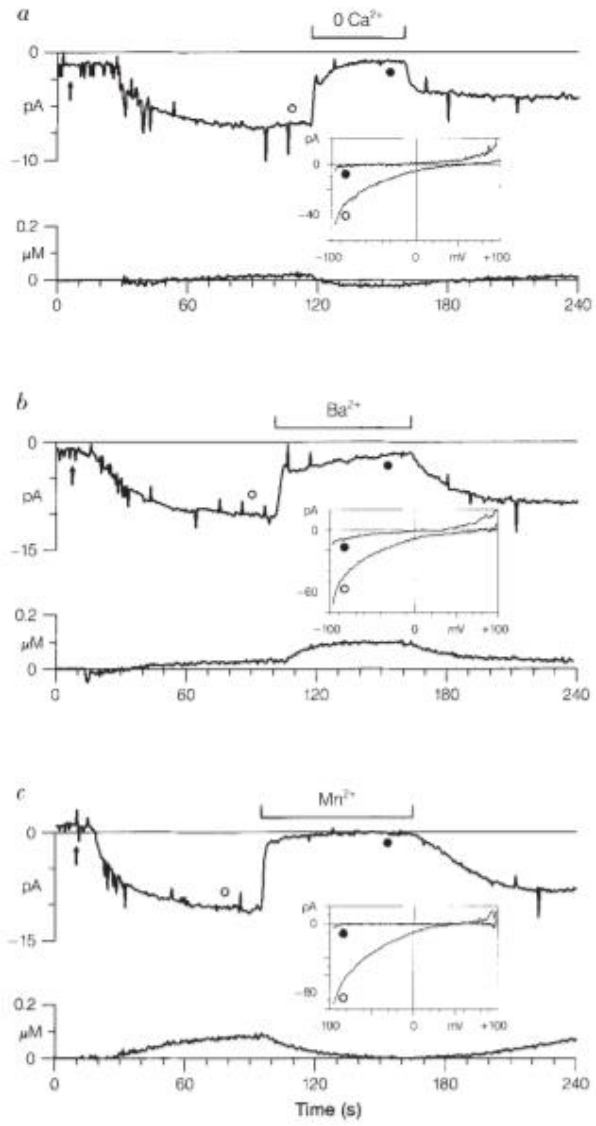

Figure 1.4 Permeability of I_{CRAC} to divalent cations I_{CRAC} was activated by IP_3 and EGTA in a standard buffer containing 10 mM Ca^{2+}. This solution that was then changed to a) Ca^{2+} free solution, b)10 mM Ba^{2+} and c) 10 mM Mn^{2+} in 1mM EGTA. The circles mark the current-voltage relationships during the inward current at 10mM Ca^{2+} (white) and during the application of the test solution (black). Image taken from Hoth and Penner 1992.

A decade later, Roos and colleagues identified the stromal interacting molecule (STIM, initially called SIM) as being key component of SOCE (Roos et al. 2005). Calcium imaging and whole-cell patch clamp single cell recordings showed a decrease in SOCE driven by thapsigargin in RNAi induced knockdown of STIM1 in Drosophila S2 cells (Roos et al 2005). Knocking down the human STIM1 in Jurkat T cells as well as its overexpression in human embryonic kidney (HEK) 293 cells cumulatively confirmed its role in promoting thapsigargin-induced Ca^{2+} entry (Roos et al 2005). The authors highlighted that while STIM1 can trigger SOCE, it cannot form the channel itself. Its main role is to sense changes in the ER Ca^{2+} levels thereby triggering Ca^{2+} entry through plasma membrane channels when these levels drop (Roos et al 2005).

One year later, a genetic screening study revealed that a mutation in human Orai1 caused a severe combined immunodeficiency disorder (SCID) (Feske et al. 2006). It was also the first channelopathy of the immune system ever described at that time. More importantly, in a mechanistic manner, the same study showed that Orai1 mutations in human T cells led to a complete loss of I_{CRAC} (Feske et al. 2006). Orai1 (initially called CRACM1) was thus confirmed as the primary pore-forming component of CRAC channels able to conduct I_{CRAC} upon ER store depletion (Feske et al. 2006, Vig et al. 2006). Vig and colleagues confirmed the role of Orai1 in mediating thapsigargin-induced I_{CRAC} by knockdown experiments in HEK293 and Jurkat T cells (Figure 1.5).

Later, three key properties of Orai1 were described: i) it is sensitive to 2APB (2-aminoethyldiphenyl borate, a non-selective I_{CRAC} inhibitor), ii) it is dependent on calcium concentration, and iii) it is well expressed in human T cells (Lis et al. 2007).

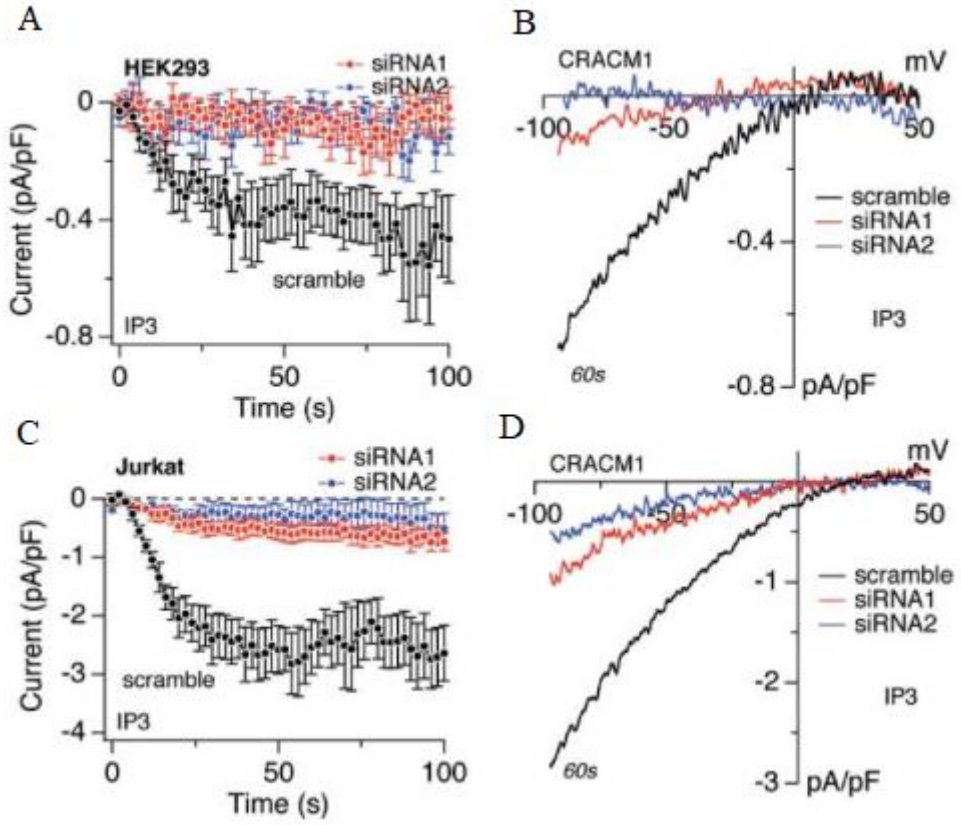

Figure 1.5: Inhibition of I_{CRAC} by CRACM1 (Orai1) siRNAs. Normalized time course of IP_3-induced I_{CRAC} in HEK293 cells (A) and Jurkat cells (C). 10mM BAPTA was used to clamp $[Ca^{2+}]_i$ to near zero. Data shown as average for Scramble and CRACM1-KD with siRNA1 and siRNA2. Representative current-voltage traces of I_{CRAC} at 60 s evoked by 50 ms voltage ramps in HEK293 cells (B) and Jurkat cells (C). Image taken from Vig et al. 2006.

The discovery of STIM, Orai and TRPC proteins led to a further characterization of SOCE: STIM1 is the ER Ca^{2+} sensor, plasma membrane TRPC channels are responsible for the nonselective cation current I_{SOC} and Orai1 channels mediate I_{CRAC}, the highly Ca^{2+} selective current (Roos et al 2005, Feske et al. 2006, Zhang et al. 2006). STIM1 is required to activate calcium entry through both channel types (Roos et al 2005).

1.5.3 STIM isoforms

STIM1 was initially identified in Drosophila S2 cells, but in mammals a second homologue, STIM2, was also described (Roos et al. 2005; Prakriya M 2013). They are both ER-membrane residents highly involved in SOCE.

STIM1 is a 685 amino acid long, 77 kDa in size, protein residing in the ER/SR membrane and has two properties critical for activating SOCE: i) it senses the ER Ca^{2+} store discharge, and ii) after store depletion, it communicates with plasma membrane TRPC or Orai channels to activate I_{SOC} or $I_{CRAC,}$ respectively (Prakriya M 2013). Two splice variants have been determined: STIM1S (S for small, the well-known STIM1 that slowly clusters and form CRAC channels with Orai1) and STIM1L (L for long, 110 kDa variant that interacts with actin and forms permanent clusters with Orai1 independent of SOCE) (Darbellay et al. 2011).

For STIM1 to function as a sensor and Ca^{2+} entry facilitator, several domains important for its role were identified (Figure 1.4). In the ER-luminal N-terminus, STIM1 contains a canonical but hidden EF-hand as well as a sterile-α motif (SAM) (Stathopulos et al. 2006). As previously mentioned, STIM1 is responsible for initializing the first step of SOCE, thus when the ER Ca^{2+} pool is depleted, Ca^{2+} dissociates from the EF hand, followed by the destabilization of the EF-SAM domain, which means it becomes less compact (Fahrner et al. 2013). Extended STIM1 monomers further form oligomers and consequently redistribute into puncta located at ER-PM junctions (Baba et al. 2006).

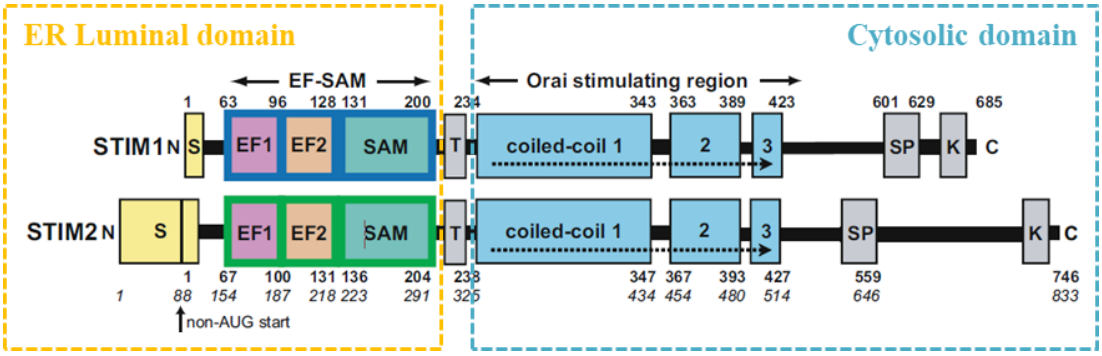

Figure 1.6. The architecture of STIM1 and STIM2 proteins The ER luminal region consists of the N-terminus which includes the signalling peptide, the canonical EF1 hand, the noncanonical EF2 hand and the SAM domain. The transmembrane domain (T) separates the EF-SAM region from the cytosolic domain. The cytosolic region comprises of three coiled-coil domain (CC1, 2 and 3), a serine-proline rich segment (SP) and a lysine rich polybasic domain (K). Figure adapted from Zhu et al. 2017.

In the cytosolic strand, the C-terminus contains three coiled-coil domains (CC1, CC2 and CC3), a serine/proline and a lysine-rich region as well as a CRAC-modulatory-domain (CMD) (Muik et al. 2009; Fahrner et al. 2013). Previous studies identified key regions of the C-terminus sufficient to activate the PM Orai channels: the CRAC activation domain (CAD), STIM1-Orai1 activating region (SOAR), ORAI1-activating small fragment (OASF) and Coiled-coil domain b9 (Ccb9) (Muik et al. 2009; Park et al. 2009). These domains have CC2 and CC3 regions in common, as well as 19 other residues and a STIM1 homomerization domain (SHD) (Fahrner et al. 2013). Interestingly, the deletion of the SHD fragment in the OASF region abolishes the activation of CRAC channels as showed in patch clamp recordings (Muik et al. 2009).

STIM2 (84 kDa molecular weight) differs from STIM1 in the variable domain downstream of the second C-terminal coiled-coil region and does not have a short N-terminal signal peptide sequence as STIM1 does (Johnstone et al. 2010, Soboloff et al. 2012).

Interestingly, the STIM2 EF-hand has a low affinity for Ca^{2+} (Kd~500 µM) and its monomer has a more stable EF-hand than that of STIM1. This observation led to the conclusion that STIM1 is able convert from mono- to oligomeric state in a faster manner (Stathopulos et al. 2006; Zheng et al. 2009).

The C terminus of STIM2 has an additional polybasic domain and a shorter acidic region of an unknown function which was shown to interact with both PIP_2 and PIP_3, while STIM1 has a preference for PIP_2 (Ercang et al. 2009, 2012; Mullins and Park 2009). Moreover, the SOCE-associated regulatory factor (SARAF protein, encoded by the SARAF gene, formerly named transmembrane protein 66 or TMEM66) responds to cytosolic Ca^{2+} elevation after ER Ca^{2+} refill, generating a slow inactivation of STIM2-dependent basal SOCE (Palty et al. 2012). SARAF is an ER resident protein that inhibits SOCE through an unknown mechanism (Palty et al. 2012). Another group reported that the depletion of the acidic Ca^{2+} stores in platelets expressing both STIM1 and STIM2 enhanced both their interactions and the association of STIM2 with the SERCA3 isoform (Zbidi et al. 2011).

There are three different prost-translationally modified STIM2 proteins, as follows:

a) ER-localized hSTIM2: it is a fully cleaved signal peptide and contains the previously identified N-terminus peptide sequence.
b) Cytosolic non-glycosylated pre-STIM2: a full-length version that escapes ER targeting; is responsible for store-independent activation of Orai1 (Graham et al.2011).
c) ER-localized fragment of STIM2: its cleavage results in releasing the N-terminus signal peptide fragment (SPF) into the cytoplasm and it contains a calmodulin binding site (Shen et al. 2005; Graham et al. 2011). Other studies showed that STIM2 has a second, low affinity (1 µm) calmodulin binding site at the lysine-rich C-terminus that is involved in the reduced plasma membrane phospholipase interaction (Bauer et al. 2008; Bhardwaj et al. 2013).

Soboloff and colleagues investigated the role of STIM2 and found that it has an inhibitory effect on SOCE (Soboloff et al. 2006). Brandman and colleagues also showed that knocking-down STIM2 in HEK293, HeLa and HUVEC cells reduced the basal level of cytosolic Ca^{2+} and overexpressing STIM2 led to an increased level of basal Ca^{2+} (Brandman et al. 2007)

1.5.4 Role of STIM isoforms in disease

While the role of STIM and Orai proteins has been intensely studied in relation to various diseases, SOCE has been shown to contribute to normal skeletal muscle function, fatigue or even aging (Thornton et al., Brotto M. 2011). Evidences also show that SOCE is important in muscle contraction during exercise or tetanic stimulations (Pan et al. 2014).

A decade before its role in SOCE was established, the STIM1 gene was initially reported as being highly expressed in skeletal muscle tumors as well as in child malignancies (Sabbioni et al 1997).

Moreover, recent studies have shown that STIM1 is required for platelet activation and mutations might be responsible for the Stormorken (rare disease characterized by mild bleeding) and York (CRAC channelopathy characterized by thrombocytopenia) syndromes in humans (Misceo et al 2014, Markello et al 2015). A missense mutation leading to the replacement of Arginine 304 with tryptophan affects the CC1 fragment of STIM1, which is responsible for maintaining in its STIM1 inactive form. This mutation has been correlated with excessive Ca^{2+} entry, leading to premature platelet activation and subsequent bleeding disorders (Misceo et al 2014). Similarly, mutations in the canonical EF-hand of STIM1 have also been associated with tubular aggregate myopathy in humans (Bohm et al 2013). Other studies have reported that high-calorie diet in pigs increases STIM1 expression in coronary smooth cells, leading to coronary atherosclerosis (Edwards et al 2010).

Studies done in mice lacking STIM1 in smooth muscle cells showed tissue growth deficiency, thus providing evidence for the role of STIM1 in smooth muscle development (Mancarella et al 2013). Recent advances in clinical research confirmed that serum STIM1 levels can be used as a biomarker for restenosis (Li et al 2015).

STIM1/Orai1 mediated SOCE has been associated with breast cancer cell migration in triple negative MDA-MB231 cells, regulating their migration but not proliferation (Yang et al. 2009). Several studies confirmed that STIM1/Orai1 SOCE is involved in breast cancer

metastasis (Yang et al. 2009, Davis et al. 2012). Recent findings reported that STIM1 expression is increased in colorectal cancer tissue samples and further associated with tumour invasion and metastasis (Wang et al. 2015). The same group showed that STIM1 regulates COX-2 but not COX-1 expression in colorectal cancer cells and NSAIDS indomethacin and ibuprofen almost completely reduced STIM1-regulated cell migration.

STIM2 was shown to be highly expressed in different melanoma cells, again having a potential role in metastasis and tumour migration (Stanisz et al. 2014). Other studies reported an increased expression of STIM2 in colorectal as well as in oesophageal squamous cancer cells (Zhu et al. 2014, Sobradillo et al. 2014).

Altered Ca^{2+} signalling has been associated with neurodegeneration and subsequent loss of neuronal function leading to diseases such as Alzheimer's, Huntington's, HIV-induced dementia or Parkinson's. Several studies showed that during oxidative stress, ROS production increases SOCE, leading to cell injury due to excessive Ca^{2+} entry (Nunes and Demaurex 2014). Oxidative stress reduces the affinity of STIM1 for Ca^{2+}, thus facilitating a store-independent activation of STIM1 and an increase in I_{SOC} (Nunes and Demaurex 2014).

The second isoform, STIM2, may also have an important role in mediating neuronal SOCE. Contradictory data suggest that depending on the type of cells, STIM2 might have a conflicting role: STIM2 KD mice were protected from neuronal damage secondary to a cerebral ischemic stroke (Berna-Erro et al. 2009) while another study showed that loss of STIM2 determines hippocampal neuronal loss in mice (Sun et al 2014).

1.5.5 Orai proteins. Structure and function

Plasma membrane resident Orai1 is a 33 kDa molecule with four transmembrane domains; and intracellular N- and C-terminal regions (Feske et al. 2006) As described previously, Orai proteins (particularly Orai1 isoform) are responsible for forming the CRAC channel pore (Mercer et al. 2006, Yamashita et al.2007). The concurrent discovery of both Orai and STIM

proteins led to a wave of interest in these proteins and their role in different excitable and non-excitable cells.

In 2012, Hou X and colleagues answered a widely asked question regarding the structure of Orai1, its multimerization and ability to form contacts with the cytosolic region of STIM1. The group elucidated the crystal structure of the Drosophila CRAC channel pore. Figure 4 shows the channel's hexameric assembly of Orai proteins. Each subunit of Orai1 contains four transmembrane (TM) domains and a helix following TM4 that expands into the cytoplasm (Hou X et al. 2012). The TM helices are arranged in three concentric circles: TM4 helices form the outer ring, the TM2 and TM3 helices form the middle ring, while TM1 helices constitute the inner circle and outline the ion pore (Hou X et al. 2012). Recently, contacts between the TM1 helix and the TM2/3 helices have been reported as critical for STIM1/Orai1 channel gating (Yeung P. S-W et al. 2018). E106 residues found in the TM1 region constitute the Ca^{2+} pore binding site and reflects the main difference between CRAC channels and VGCCs. The E106 ring binds Ca^{2+} specifically and blocks Na^{+} currents through the channels at lower micromolar Ca^{2+} concentrations (Prakriya and Lewis 2006; Gudlur and Hogan 2017; Yang et al. 1993).

Multiple binding models have been described; some models show that Orai1 C-terminal helices are able to interact with STIM1, while other models reflect the binding between a pair of Orai1 TM4 helices and a STIM1 dimer (Hou et al. 2012, Palty et al.2015, Stathopulos et al.2013). Moreover, studies showed that STIM1 also binds to the N-terminal segment of Orai1, thus indicating that this contact might be necessary to modulate the open conformation of the pore (Zhou et al. 2015, 2016).

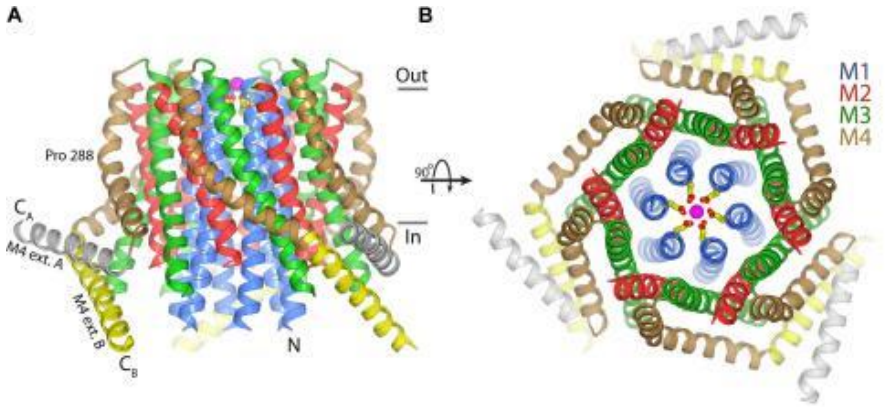

Figure 1.7. The architecture of Orai1. A representation of the structure of the channel showing in a color coded format the four trasmembrane domains of the Orai1 pore: TM1 in blue, TM2 in red, TM3 in green and TM4 in brown. The yellow and grey subunits are extensions of TM4. Figure adapted from Hou et al. 2012.

There are other two isoforms of within this protein family: Orai2 and Orai3, found in mammalian cells. Studies showed that all three proteins are capable to form CRAC-like channels, but Orai1 remains the best-studied protein until now (Lis et al. 2007, Prakriya 2013).

Structurally, these homologues differ in their C-terminal site and the TM3-TM4 loop sequence (Lis et al. 2007). Orai1 contains two glutamates in the C-terminal region, while Orai2 and Orai3 contain three (Lis et al.2007; Frischauf et al. 2009). This structural difference might be responsible for the reduced fast inactivation observed in Orai1 but not in Orai2 or Orai3 (Frischauf et al. 2009; Hoth and Niemeyer 2013). Orai3 also contains the longest extracellular TM3-TM4 loop between the three isoforms (Frischauf et al. 2011). Orai2 displays a moderate level of fast Ca^{2+} dependent inactivation as compared with Orai1 (low) and Orai3 (high) (Zweifach and Lewis 1995). Even-though the crystal structure of Orai1 established in 2012 highlights its hexameric constitution, contradicting studies state that Orai1 may function as a tetramer (Hou and Pedi 2012). Moreover, a ratio of 8 STIM1 to one Orai1 tetramer seems to result in a maximal current density through the CRAC channel, and it is not known whether such dependence exists for other STIM and Orai homologs (Hoover and Lewis 2011, Lis et al. 2011). Other studies reported that Orai2 gives rise to smaller currents than Orai1 and that it may also be able to reduce Orai1 functionality when co-expressed in Jurkat T cells (Alansary

et al. 2014, DeHaven et al. 2007, Inayama et al. 2015). Additionally, Ca^{2+} signals were unchanged in siRNA induced Orai2 or Orai3 knock-out human aortic smooth muscle (hASMC) cells, suggesting that Orai1 plays a key role in SOCE activation while its isoforms may not contribute directly to SOCE (Baryshnikov et al. 2009). Interestingly, high Orai2 expression might correlate with high STIM2 expression in some cells (Hoth and Niemeyer, 2013).

Experiments on HEK293 cells showed that over-expressing Orai3 with STIM1 failed to generate an increase in I_{SOC}, but it moderately increased when Orai2 was over-expressed. The highest I_{SOC} was achieved in the presence of Orai1 (Mercer, 2006). As previously discussed, the N-terminus of Orai1 is key for activating SOCE. This was confirmed by replacing the Orai3 N-terminus region with that of Orai1, resulting in a higher magnitude of I_{SOC}. Vice versa, when the Orai3 N-terminus was inserted into the Orai1 channel, the current was completely abolished (Shuttleworth, 2012).

At this moment in time, there is no definite evidence of the functional role of Orai2 or 3, but it has been proposed that they might mediate SOCE, to a minimal extent, in cells lacking functional Orai1 (Mercer et al. 2006).

1.5.6 Role of Orai isoforms in disease

As mentioned previously, in 2006 a study reported that R91W mutation of human Orai1 was associated with defective SOCE, CRAC channel function and the development of SCID (Feske et al 2006). Several groups then reported that Orai-1 deficient patients presented with a severe immunodeficiencies characterized by the weak T cell activation and impaired cytokine production (McCarl CA et al. 2009; Feske et al. 2009). Moreover, upon vaccination or infection, patients with Orai1 mutations could not mount antigen-specific antibodies (Feske et al. 2009). The question regarding whether other Orai isoforms are able to rescue SOCE in R91W mutant T cells and fibroblasts was also raised. Interestingly, neither Orai2 nor Orai3

was able to activate or maintain I_{SOC} in Orai1 mutant cells of SCID patients (Gwack et al. 2007).

The group tested the effect of endogenously expressed Orai2 and Orai3 as well as that of efficiently delivered proteins to the plasma membrane and both scenarios failed to rescue $I_{SOC.}$ This suggests that, at least in these cell types, the Orai1 isoform plays a vital role in SOCE (Gwack et al. 2007). Interestingly, in some breast cancer cell lines, endogenous SOCE seems to be mediated by Orai3: while estrogen-receptor negative breast cancer cells showed an Orai1-dependent SOCE, the estrogen-receptor positive cells showed that I_{SOC} is mediated through Orai3 (Motiani et al. 2010).

The absence of Orai1 in humans has also been associated with different myopathies: one study reported global muscular hypotonia, reduced head control, decreased endurance and muscle strength as well as respiratory muscle insufficiency in Orai1-null patients (McCarl et al 2009). Orai1 deficient patients also presented a dental enamel defects and difficulties in sweating leading to dry skin and recurrent fever with heat intolerance (McCarl et al 2009; Feske er al. 2009, Feske et al. 2010). As Ca^{2+} influx is required for normal secretion from sweat glands, the absence of Orai1 (resulting in impaired SOCE) has consequences on the function of sweat glands generating hypo- or anhidrosis (Feske et al. 2010).

Similar to the role of STIM1 in thrombosis and haemostasis, Orai1-mediated SOCE is essential for platelet activation and thrombin-dependent coagulation (Bergmeier et al. 2009). Other studies have also shown that mice failed to form thrombus and promote artery occlusion in chemical injured arterial walls, this being associated with Orai1 and STIM1 deficiency (Braun et al. 2009; Varga-Szabo et al. 2008).

1.6 STIM-Orai coupling. CRAC channels

CRAC current was initially observed in T and mast cells and was characterized as a highly selective Ca^{2+} current that is activated as a consequence of a reduction in ER Ca^{2+} levels (Lewis and Cahalan 1989, Zweifach and Lewis 1993). As described in previous sections, the CRAC current is a cationic influx from the extracellular compartment into the cytosol, through the PM resident CRAC channels that comprises of the ER Ca^{2+} sensor STIM and PM pore-forming subunit, Orai. Thus, channel gating is dependent on the direct interaction between STIM and Orai proteins (Gudlur et al 2013). When the ER Ca^{2+} pool is depleted, a conformational rearrangement of STIM1 is induced when its EF hand releases the bound Ca^{2+} ions; the protein becomes more extended and is able to span the ER-PM distance (Muik et al. 2011). Orai channels reside evenly distributed in the PM. STIM1 functions to recruit and cluster with them into forming the CRAC channel at ER-PM junctions (Luik et al. 2006). Studies showed that STIM proteins translocate within the ER membrane which can be optically monitored through so-called 'puncta' formation. This translocation occurs within ~1 minute, is independent of Orai and precedes Orai gating and CRAC channel opening (Liou et al. 2005; Wu et al. 2006). Interestingly, the recruitment of Orai proteins at ER-PM junctions, into puncta, is dependent on STIM1 (Park et al. 2009). In the absence of ER store depletion, all three Orai channels are inactive until STIM1 binding occurs (Lis et al. 2007; Schindl et al. 2009).

However, few studies revealed that a long splice variant of STIM1 (STIM1L) may form clusters with Orai1, independent of store depletion, predominantly in excitable cells (Darbellay et al. 2011). STIM1L has been shown to be present in all skeletal muscles, brain, spleen, liver, lungs and heart, while STIM1S is ubiquitously expressed in all tissues (Darbellay et al. 2011). Simillarly, Sauc and colleagues showed that STIM1L is able to trap and gate Orai1 without the involvement of the ER in murine embryonic fibroblasts (Sauc et al. 2015).

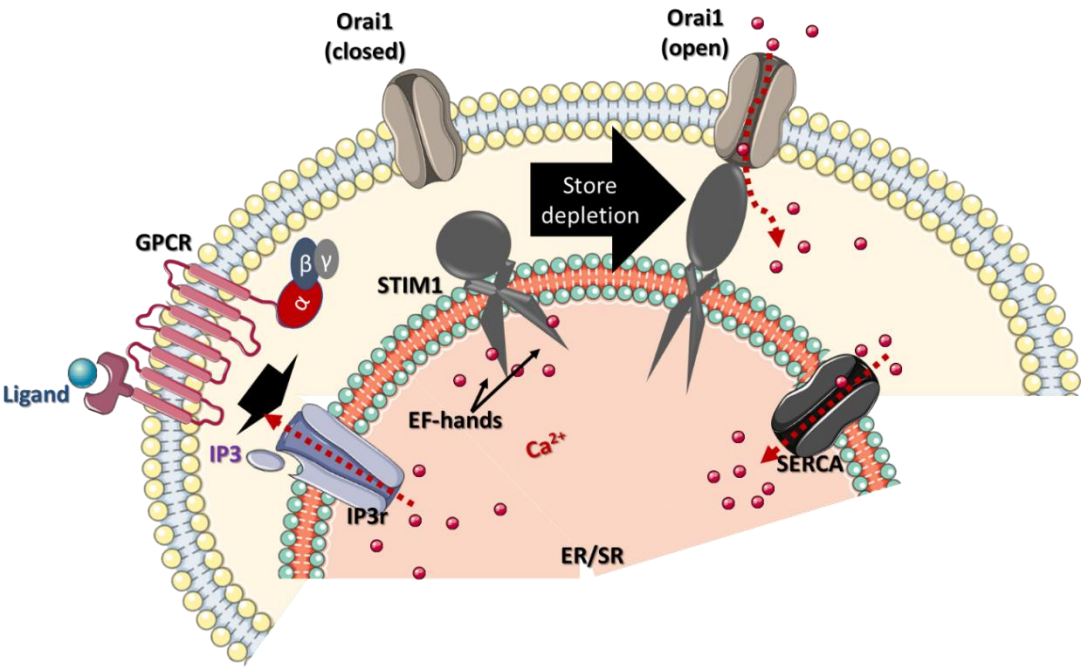

Figure 1.8. Schematic representation of CRAC channel activation.Once triggered by factors such as GPCR agonists (Ligand, blue), ER Ca^{2+} pool starts to deplete and the EF hands of STIM1 release Ca^{2+} as a consequence to the store discharge. This triggers a conformational change in STIM1 structure, followed by its movement into clusters at ER-PM junctions. There it binds to Orai1, followed by the channel formation, pore opening and Ca^{2+} influx into the cytosol. ER residents SERCA pumps facilitate the Ca^{2+} store replenishment and once refilled, CRAC channels deactivate and STIM and Orai proteins return to their resting state.

STIM1 directly binds to the N- and C-termini of Orai1 and recent studies have described the STIM1-Orai1 Association Pocket (SOAP) where leucines L273 and L276 of Orai1 are involved in hydrophobic interactions with STIM1 and negatively charged aspartate of Orai1 further form electrostatic interactions with STIM1 regions (Hou et al. 2012, Stathopulos et al. 2013). While STIM1 binding is primarily achieved by coupling to the Orai1 C-terminus region, studies have also shown that truncating N-terminus elicits an impairment in Orai1 function (Derler et al. 2013, Zhou et al. 2016). Interestingly a STIM1-Orai1 interaction at the N-terminus was also detected, but with a weaker affinity (Derler et al. 2013). Since the crystal structure of Orai1 has been described, the hexameric structure of the channel has been widely accepted, but the stoichiometry of the STIM-Orai complex remains controversial (Hou et al. 2012). A recent study showed that the number of STIM1 molecules is important for the degree

of inactivation of I_{CRAC}, therefore the higher number of STIM1 molecules, the more pronounced I_{CRAC} inactivation (Scrimgeour et el. 2014).

While the structural complexity of the STIM-Orai machinery remains to be determined, it is widely accepted that STIM1 initially couples to the C-terminus of Orai1, involving a conformational rearrangement of its subdomains, including bridging the Orai1 N-terminus in order to fully activate the channel (Fahrner et al. 2017). Orai1, 2 and 3 can form hetero- or homomeric channels and once coupled with STIM1, the TM domains of Orai rearrange, form and open the pore, allowing Ca^{2+} influx. As previously explained, the TM4 of Orai1 forms the outer ring of the pore, TM2 and TM3 helices form the middle ring, while TM1 helix forms the inner pore that is permeable to Ca^{2+} (Hou et al. 2012, Zhou et al. 2010). Close to the external side of the CRAC channel, the so-called Ca^{2+} accumulation region (CAR) includes negatively charged amino acids found between TM1 and TM2 (Frischauf et al. 2015). CAR, found at 1 to 2 nanometres away from the selectivity filter, initially binds up to three Ca^{2+} ions, thus functioning as a Ca^{2+} driver into the pore by locally increasing Ca^{2+} levels (Frischauf et al. 2015; Jha and Muallem 2016). CAR is found in a flexible loop between TM1 and TM2, while the selectivity filter is located in the TM1 helix, comprising of six glutamates (Hou et al. 2012). In the centre of the pore, a hydrophobic segment forms the gate that blocks Ca^{2+} entry in the resting state (Hou et al. 2012).

The activation process of CRAC channels is reversible and the hallmark of the channel is its fast calcium-dependent inactivation (CDI) mechanism. Patch-clamp recordings showed that when cells are hyperpolarized, CDI occurs within tens of milliseconds after the peak of I_{CRAC} (Zweifach and Lewis 1995; Shaw 2013). Fast CDI was linked to a region of acidic residues close to the CAD domain of STIM1 (Lee et al. 2009). Interestingly, other studies showed that Orai1 is also involved in the fast CRAC channel inactivation, through a calmodulin-binding domain found in the N-terminus of Orai1 (Mullins et al. 2016).

Despite the fast mechanism of CDI, the CRAC channel disassembly occurs within tens of seconds following their activation. This is called the slow CRAC inactivation and is triggered

by ER Ca^{2+} store refilling (Liou et al. 2007; Shaw 2013). Once Ca^{2+} ions are taken up by the ER-resident SERCA pumps, it then binds to the EF hand in the N-terminus of STIM1, causing STIM1 de-oligomerization, followed by Orai1-STIM1 disassembly, dissolution of puncta and STIM1's diffusion away from the PM returning to the resting state (Liou et al. 2007).

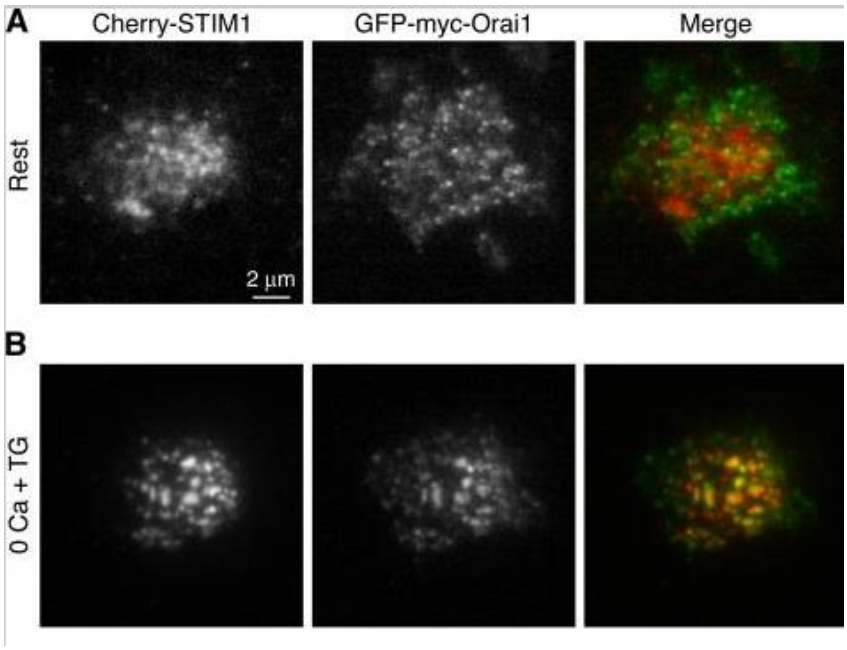

Figure 1.9. Total Internal Reflection Fluorescence (TIRF) imaging of one Jurkat T cell showing STIM1-Orai1 clustering during SOCE. A. At rest, ER located mCherry-STIM1 is widely distributed and out of focus, while GFP-myc-Orai1 is distributed throughout the cell, at the PM and in focus. B. Once SOCE is triggered with thapsigargin (TG) in Ca^{2+} free conditions, STIM1 clusters and expands to reach the PM. Orai1 also changed its initial position. The merged images show that at rest STIM1 and Orai1 do not colocalize, but during SOCE, both proteins translocate and meet at the formed puncta. Figure adapted from Luik et al. 2006.

Several studies found that the activity of CRAC channels could also be regulated through processes such as protein kinase C (PKC) dependent phosphorylation of the N-terminus of Orai1, or cyclin-dependent kinase 1 (CDK1) phosphorylation of STIM1 (Kawasaki et al. 2010; Smyth et al. 2009). The importance of these mechanisms remains to be elucidated.

1.7 Pharmacology of CRAC channels

Calcium influx through CRAC channels regulates different cellular functions such as cell proliferation, gene expression and exocytosis. Since the identification of Orai1-3 and STIM1-2 proteins and their role in SOCE, researchers investigated ways to modulate these channels. As described in previous sections, defects in CRAC channel function were shown to be associated with different human diseases: immunodeficiency, myopathy, anhydrosis, cardiac or pulmonary deficiency. Taken together, the accumulating knowledge regarding the role of CRAC channels in these diseases led to an increased interest in the development of CRAC channel modulators. Due to the complex STIM-Orai machinery, alongside other endogenous proteins thought to be involved in modulating SOCE, multiple proteins have been targeted and several pharmacological agents have been developed. While most of them are still in preclinical studies, some may have the scientific profile to be taken further in to clinical development.

1.7.1 Inducers

The main mechanisms that induce I_{CRAC} are:

a) blockade of sarcoplasmic/endoplasmic reticulum Ca^{2+}-ATPase pumps (with SERCA inhibitors, e.g. **thapsigargin**, **cyclopiazonic acid**);

b) activating IP_3 receptors with GPCR agonists;

c) activating RyR with RyR agonists (e.g. **caffeine**), and

d) using calcium ionophores (e.g. **ionomycin**).

While plenty of endogenous compounds are putative SOCE inducers (such as GPCR agonists: ATP, histamine, epinephrine, BK etc.), **2-aminoethyl diphenyl borate (2-APB)** is one of the few small-molecule CRAC activators used in research. This agent was initially obtained by the esterification of diphenylboronic acid with aminoethanol in ethanol. The procedure was published by Povlock TP and colleagues in 1958. Remarkably, 2-APB seems to be a direct activator of Orai3 channels at 50 μM, both in the presence or absence of STIM1, displaying

large outward low Ca^{2+} selective currents (Peinelt et al. 2008). Interestingly, it has been reported that 2-APB has a dual effect in such a way that it activates SOCE at lower concentrations (3-10 µM) but inhibits calcium influx at higher concentrations (30-50 µM) (DeHaven et al. 2008). This drug is considered a non-selective CRAC channel inhibitor as it acts on multiple other receptors and ion channels such as blocking IP_3R, SERCA pumps, TRPC3, activating TRPV1,2 and 3 and potentiating TRPV6 (also known as CaT1) and TRPM6 (Maruyama et al. 2007, Hu et al. 2004, Missiaern et al. 2001).

Calcium influx factor (CIF), whose molecular identity is still unknown, has been identified by in a variety of cells (Bolotina et al. 2005; Csutora et al. 1999; Kim et al. 1999). CIF is known to be produced in the ER, following Ca^{2+} depletion and its thought to induce the displacement of calmodulin from a PM Ca^{2+}-independent phospholipase $A_2\beta$ ($iPLA_2\beta$), thus leading to SOCE activation (Randriamampita et al. 1993; Smani T et al. 2004). Interestingly, a study showed that following ER Ca^{2+} depletion, STIM1 might initially function as a trigger for CIF production as well as facilitating CIF delivery to its PM target, $iPLA_2\beta$ (Csutora et al. 2008). The identity of CIF and its exact role in mediating I_{CRAC} still remains subject of future research.

Loperamide, a drug widely used for acute diarrhea, is a SOCE enhancer. While it has no direct effect on I_{CRAC}, at 10 to 30 µM concentrations, it has been proposed to function as a CRAC potentiator in cultured HL-60 leukemic cells. (Harper et al. 1997).

Nocodazole (an antineoplastic agent) and **colchicine** (an anti-inflammatory agent, commonly used to treat gout), both causing microtubule depolymerization**,** were also found to enhance I_{CRAC} in STIM1 overexpressing cells (Smyth et al. 2007). Without any direct effect on I_{CRAC}, colchicine substantially potentiated calcium influx in response to submaximal store depletion (Smyth et al. 2007).

While CRAC inducers are widely used as research tools to stimulate SOCE in experimental conditions, a global interest has been given to CRAC inhibitors as putative pharmacological targets especially in inflammatory disorders or autoimmune diseases.

1.7.2 Inhibitors

Similar to other calcium permeable channels, CRAC channels are inhibited by divalent and trivalent cations, possibly due to decreasing Ca^{2+} permeability. Even at low concentrations, **Ni^{2+}, La^{3+}** and **Gd^{3+}** can fully block CRAC channels in cerebral arteriolar smooth muscle cells (Flemming et al. 2003).

Widely known as the TRPV1 activator**, capsaicin** demonstrated an inhibitory effect on CRAC channels (Fischer et al. 2001; Wang et al. 2005). Capsaicin is able to block SOCE in Jurkat T cells in a dose-dependent manner with an IC_{50}=32 µM (Fischer et al.2001). Indo-1 loaded cells showed that capsaicin inhibits SOCE in carbachol (CCh, an acetylcholine receptor activator) treated Jurkat T cells, and fura-2 measurements revealed a reduced capacitative calcium entry in thapsigargin treated P12 cells (Fischer et al. 2001).

BTP2 (YM 58483), a pyrazole derivative, was developed as a tool to inhibit thapsigargin-induced SOCE. It was initially tested in T-lymphocytes and showed a 30-fold selectivity for CRAC channels as compared to VOC channels, with an IC_{50} of 100 nM (Ishikawa et al. 2003). BTP2 might depend on the external calcium concentrations in such a way that the effect of SOCE inhibition was shown to be higher when extracellular Ca^{2+} levels were raised (Zitt et al. 2004). Interestingly, BTP2 seems to have an indirect mechanism on CRAC function as well, by stimulating the opening of TRPM4 channels, leading to membrane depolarization and indirectly reducing calcium influx through CRAC channels (Takezawa et al. 2006).

Diethylstilbestrol, an estrogen receptor agonist, has been found to inhibit I_{CRAC} in mast cells, platelets and aortic myocytes (Zakharov et al. 2004). It has a dose-dependent effect with IC_{50} = 0.1µM. Its inhibitory effect was showed after triggering I_{CRAC} using thapsigargin in whole-cell patch-clamp recordings.

A recent study showed that **oleic acid** inhibits I_{CRAC} in human colorectal adenocarcinoma cells. The inhibitory effect was protein kinase C-independent and it was restored by albumin. By contrast, stearic acid could not reduce I_{CRAC} in colon carcinoma cells (Carrillo et al. 2012).

Another putative CRAC channel blocker is **nocodazole**, an anti-neoplastic agent. Smyth and Putney studied its effects on HEK293 cell lines. Confocal images showed a dispersion of microtubules throughout the ER after nocodazole treatment, presumably preventing formation of the STIM1-Orai1 puncta. Interestingly, in STIM1 overexpressing cells, nocodazole enhanced the capacitative calcium entry through CRAC channels (Smyth et al.2007). **Econazole**, an imidazole derivative used as a fungal agent, demonstrated non-selective CRAC channel blocking effects in mast cells (Franzius et al. 1994). Similar to econazole, **SKF96365,** an imidazole antimycotic, was one of the first developed CRAC channel inhibitors (Franzius et al. 1994). Its effect has been tested in a range of cells with an IC_{50} values of 12 µM in Jurkat T cells (Chung et al. 1994). Both econazole and SKF96365 exhibit a non-specific CRAC channel profile as they also suppress the activity of non-selective cation channels, VGCC, as well as cyclic AMP-gated chloride channels (Chung et al. 1994, Singh et al. 2010).

Several studies mentioned **carboxyamidotriazole** as being a potent SOCE inhibitor. It was proposed to generate mitochondrial depolarization which leads to greater calcium-dependent inactivation of the CRAC channels (Mignen et al. 2005). The use of carboxyamidotriazole has been associated with impaired cancer cell proliferation and invasion and this molecule reached several oncology clinical trials in diseases such as ovarian and cervical cancer, melanoma or renal cell carcinoma (Kohn et al. 1996).

The pharmaceutical company GlaxoSmithKline (GSK) developed a list of novel pyrazole compounds identified as selective CRAC inhibitors, without affecting STIM1 aggregation or STIM1-Orai1 coupling. Among these, **GSK-5498A** inhibits I_{CRAC} with an IC_{50} of 1 µM in HEK cells (Tian et al. 2016; Rice et al 2013), while **GSK-7975A** decreases the POAEE (palmitoleic acid ethyl ester, a mediator of alcohol-related pancreatitis)-evoked cytosolic Ca^{2+} rise in pancreatic acinar cells (Gerasimenko et al. 2013). This finding potentially indicates a

pharmacological role against acute pancreatitis which lacks effective treatment and is life-threatening (Pandol et al. 2007).

Synta Pharmaceuticals also developed a series of CRAC channel inhibitors, amongst which **Synta66** has drawn attention in recent years (Tian et al. 2016). Despite its SOCE inhibitory effect demonstrated on red blood cells (IC_{50}= 3μM), Synta 66 has been shown to reduce the expression of interleukins (IL)-2 and 17 in cells taken from inflamed areas of patients suffering from inflammatory bowel disease (IBD), suggesting its putative role in T-cell signaling (Sabatino et al. 2009).

RO2959, a CRAC channel inhibitor developed by Roche, demonstrated an IC_{50} value of 400nM in RBL-2H3 cells (Jairaman and Prakriya 2013). This molecule can inhibit Orai1 to a greater extent than the other Orai isoforms and can potentially inhibit cytokine production, gene expression and T-cell proliferation as shown in primary CD4+ T cells (Chen et al. 2013).

CalciMedica is a biotech company focused on developing CRAC channel inhibitors for the treatment of inflammatory and autoimmune disorders. Their **CM2489** compound seems to be the first CRAC channel blocker taken forward to human testing. CalciMedica completed a Phase I clinical trial for treating plaque psoriasis with this CRAC inhibitor, leading the exciting pathway of clinical development. In May 2017, the company also received fast-track designation from US FDA for another CRAC channel blocker, **CM4620** which showed promising activity in animal models of pancreatic necrosis and systemic inflammation (CalciMedica, Inc, May24, 2017).

ML-9, a drug known to inhibit myosin light chain kinase, inhibits I_{CRAC} in thapsigargin treated HEK293 cells in a dose-dependent manner with an IC_{50} value of 10 μM (Smyth et al. 2008) Interestingly, confocal and TIRFM recordings showed that the inhibition of I_{CRAC} by ML-9 is due to blocking STIM1 rearrangement, which leads to interrupting STIM1-Orai1 coupling and puncta formation. (Smyth et al. 2008).

1.8 Ca^{2+} microdomains

Components of the Ca^{2+} signalling cascade are frequently organized into the so-called Ca^{2+} microdomains. These are regions within cells that occupy hundreds of nanometres where Ca^{2+} dynamics is locally modulated and Ca^{2+} permeable channels, such as VGCC or CRAC, reside (Berridge, 2006, Parekh, 2008) Microdomains at the ER-PM junctions can modulate Ca^{2+}-dependent processes related to SOCE in both excitable and non-excitable cells (Vaca et al. 2010; Berridge et al. 2006).

Store-Operated Calcium Influx Complex (SOCIC) is considered to be the functional unit of SOCE and is defined as a macromolecular complex that is assembled in response to ER Ca^{2+} depletion, with the purpose to promote Ca^{2+} influx from the extracellular space into the cytoplasm (Vaca et al. 2010). SOCIC comprises of different proteins that assemble and disassemble this complex to modulate Ca^{2+} dynamics. (Vaca et al. 2010). While the main proteins that form SOCIC are STIM1 (the ER Ca^{2+} sensor) and PM Ca^{2+} channels (Orai1 and/or TRPC1), other molecules have been proposed to play a role in capacitive Ca^{2+} entry such as SERCA pumps, calmodulin, IP_3 receptors or junctional proteins. (Putney et al. 2007; Mullins et al. 2009; Varnai et al. 2007).

1.8.1 Sarco/endoplasmic reticulum Ca^{2+} ATP-ase (SERCA)

SERCA pumps have been described as the third element of SOCE (Manjarrés et al. 2010). With high affinity for Ca^{2+}, they have a key role in allowing cytosolic Ca^{2+} to enter the ER and refill the stores. Increased SERCA pumps density at Ca^{2+} microdomains is key to facilitate reloading of the ER Ca^{2+} pool. (Rizutto and Pozzan 2006). Interestingly, it has been shown that SERCA pumps form an outer ring around CRAC channels, but whether they are localized near or exactly at the ER-PM junctions remains unknown. (Manjarres et al. 2010). Inhibitors of SERCA pumps, such as thapsigargin, are widely used by researchers as tools to induce capacitive Ca^{2+} entry. Recent studies highlighted that disrupting Ca^{2+} homeostasis by blocking SERCA can cause apoptosis possibly by extensive ER Ca^{2+} drainage (Sehgal et al. 2017).

1.8.2 Calmodulin

Ca^{2+}-induced Ca^{2+}-release (CICR) takes place in narrow regions between the SR and the t-tubule membrane of cardiac myocytes. These tight associated regions are known as dyads. (Winslow et al. 2011). Dyads have an estimated volume of 3×10^5 nm^3, a diameter of 100 - 200 nm and a height of 10-15 nm and are often referred to as nanodomains (Franzini et al. 1999; Hayashi et al. 2009). At this level, L-type Ca^{2+} channels (LTCCs) are located in the t-tubules of PM, juxtaposed to the RyRs residing in the SR membrane. LTCCs can sense both local and global Ca^{2+} signals through a secondary messenger called calmodulin (CaM) (Winslow et al. 2012). CaM contains 4 EF-hands and binds Ca^{2+} to its C- or N-terminus (up to four ions in total), tethering to LTCCs and mediating Ca^{2+} dependent inactivation. (Winslow et al. 2011).

Interestingly, Ca^{2+} dependent fast inactivation of SOCCs has been previously linked to the interaction of CaM to the N-terminus of Orai1 (Mullins et al. 2009). CaM also has a key role in preventing Ca^{2+} overload by competing with STIM proteins for PM lipids. (Bhardwaj et al. 2013; Malli et al. 2008). A recent study showed that Ca^{2+}-CaM is able to disassemble STIM1 oligomers and therefore deactivate STIM1-Orai1 complexes in HEK293T cells. (Li et al. 2017). SOCE activation causes a cytosolic Ca^{2+} rise through Orai1, therefore leading to charging CaM with Ca^{2+} and its movement closer to the ER-PM junctions where the STIM1-Orai1 complexes are formed. Moreover, Ca^{2+}-CaM has a high affinity for the SOAR of STIM1 (site Orai1 binds to) (Li et al. 2017). Interestingly, the SOAR domain has been shown to have an affinity of approximately 200μM for the Orai1 channel and of 0.2 μM for the Ca^{2+}-CaM which is 1000-fold higher (Li et al 2017, Yuan et al. 2009; Stathopulos et al. 2013). Therefore, in competing with Orai1 for the SOAR domain, Ca^{2+}-CaM is able to pull STIM1 from Orai1 and thus disrupting the CRAC channel assembly (Li et al 2017)

1.8.3 Ca^{2+} permeable channels of the intracellular stores

Inositol 1,4,5-triphosphate (IP_3) activates the ER-resident receptors IP_3R by promoting Ca^{2+} binding to a what was an unidentified stimulatory Ca^{2+} binding site, until recently. (Taylor et al. 2010). Hamada and colleagues recently unveiled the structure of the IP_3R by mutagenesis and X-ray crystallography (Hamada et al. 2017). Over 2000 amino acids have been identified between the IP_3 binding site and the channel itself and several residues have been proposed as candidates for mediating the gating (Hamada et al. 2017).

Functional IP_3R are homo- or hetero- tetrameric channels that allow Ca^{2+} release from the ER into the cytosol (Alzayady et al. 2013). Each monomer is formed by three major domains: 1) the C-terminus comprising of six transmembrane regions; the final transmembrane pair (5-6) and the luminal loop forming the pore (Ramos-Franco et al 1999); 2) the N-terminus containing the IP_3 binding site; and 3) an intervening sequence (Galvan et al 1999). Interestingly, they have modest Ca^{2+} permeability (P_{Ca}/P_K=6) as compared to VGCCs or SOCCs (P_{Ca}/P_K=1000) (Taylor and Tovey 2010). Several studies suggest that SOCE activation requires IP_3R to be in close proximity to the CRAC channels at the PM-ER junctions and that their blockade deactivates already formed CRAC channels suggesting a conformational coupling model for SOCCs (Okeke et al. 2016). Our lab previously reported the importance of IP_3R in the activation of the PM Cl^- channel ANO1. (Jin et al. 2013).

Another important Ca^{2+} release channel found in the SR/ER membrane of cardiac and skeletal muscle cells is RyR (Lanner et al. 2010). There are three isoforms (RyR 1-3) and are the largest known ion channels with a molecular weight higher than 2MDa (Lanner et al. 2010). While they are mainly expressed in skeletal and cardiac muscle cells, RyR2 and RyR3 isoforms has been also identified in areas of the brain such as hippocampus and thalamus (Lai et al. 1992). Similar to IP_3R, RyR are located at Ca^{2+} microdomains, can trigger spontaneous Ca^{2+} sparks and have a role in the excitation-contraction coupling (Lanner et al. 2010).

Recently, a third family of intracellular Ca^{2+} channels has been reported, called two-pore channels (TPC) (Wang et al. 2012). These channels are activated by nicotinic acid adenine

dinucleotide phosphate (NAADP) resulting in Ca^{2+} release from the endo-lysosomal system (Patel et al. 2011; Zhu et al. 2010, Taylor et al. 2010). Interestingly, a number of transient receptor protein (TRP) channels have also been reported to mediate Ca^{2+} release from intracellular stores, in addition to their role in the PM. (Gees et al. 2010).

1.8.4 Junctional proteins

Proteins localised between the ER and PM membranes are known to support the regulation of SOCE and to form junctional membrane complexes (JMCs) (Várnai et al. 2007). Previous studies have identified various components of the JMCs such as junctin (expressed in muscle cells), junctate (a splice isoform of junctin, ubiquitously expressed), mitsugumin (detected in skeletal muscle), sarcalumenin (expressed in cardiac and skeletal muscle) or junctophilins (detected in skeletal and cardiac muscle, neurons and T-cells) (Correll et al. 2017; Srikanth et al. 2012; Hadad et al. 1999; Takeshima et al. 2015).

ER-PM junctions are best understood and described in muscle cells, where JMCs are organized in dyads (in cardiac muscle cells) or triads (in skeletal muscle cells) and one of their key roles is to couple RyRs found in the ER membrane, to VGCCs in the PM membrane. (Berridge et al. 2003). In neurons, JMCs have firstly been described in 1962 as subsurface cisterns and their impairment was associated with different neurodegenerative diseases, including Huntington's disease. (Rosenbluth et al. 1962; Krause et al. 2015).

Junctophilins (JPHs) have been found in all excitable cells as part of JMCs and were intensively studied by Takeshima and colleagues since 2000 (Takeshima et al. 2000). Their first publication described JPHs as JMCs proteins with a hydrophobic segment spanning the ER membrane and a cytosolic domain with affinity for the PM. (Takeshima et al. 2000) The publication mentioned 3 family members and focused on the importance of JPH2 in regulating Ca^{2+} transients in cardiac myocytes, followed by a more thorough characterisation of tissue specific protein expression at mRNA level, later that year. The same research lab reported for the first time, in 2003, the presence of a 4^{th} JPH subtype in both human and mouse genomes

(chromosome 14q11.1 and chromosome 14C1-2, respectively) (Nishi et al 2003). Interestingly, JPH3 and JPH4 were found to be similarly distributed in the brain, predominantly in the hippocampal pyramidal neurons as part of the subsurface cisterns. (Nishi et al. 2003, Moriguchi et al. 2006)

Mammalian JPH family members are composed of eight repeats of the membrane occupation and recognition nexus (MORN) sequence in the cytosolic N-terminus and have high affinity for PM phospholipids. At the same time, their C-termini span the ER/SR membrane. (Kakizawa et al. 2008).

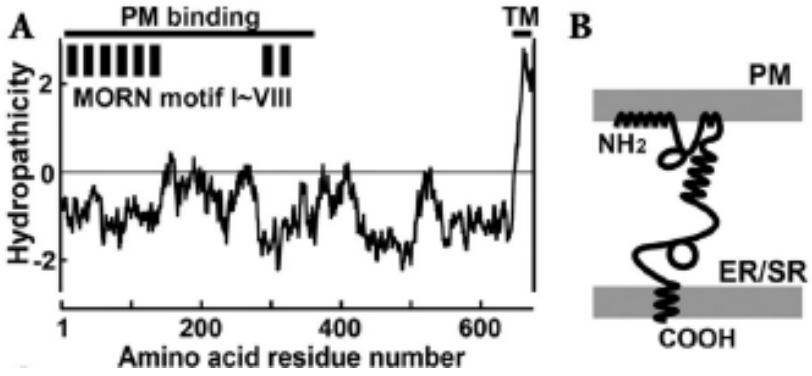

Figure 1.10. The structure of junctophilin proteins. A. Hydropathicity profile of JPH1 (rabbit) showing the PM binding segment (caracterized by repeated MORN motifs) and the transmembrane (TM) segment (or ER/SR membrane spanning section). B. A proposed JPH structure in JMCs showing the C-terminus spanning region in the ER/SR membrane, the cytosolic domain and the N-terminus containing MORN motifs interacting with the PM. Figure adapted from Takeshima et al. 2015.

Junctophilin-1 (JPH1)

JPH1 is a 90 kDa protein, highly expressed in skeletal muscle, identified also at a lower level in the heart, where JPH2 is expressed predominantly. (Takeshima et al. 2000; Phimister et al. 2007). JPH1 was reported in 2000 as a component of PM-SR junctions of rabbit skeletal muscle (Takeshima et al. 2000) and it is now known to have a key role in maintaining the geometry of the muscle JMCs. (Block et al. 1988). It has been shown that silencing JPH1 affects already-formed triads and reduces their overall number in muscle cells. (Hirata et al. 2006). Fewer triads have led to a lower contractile force that concluded with pup death in mice lacking JPH1, presumably due to respiratory failure (Ito et al. 2001). Furthermore, JPH1 proteolysis may contribute to skeletal muscle weakness as seen in a mouse model of muscular dystrophy (Murphy et al. 2013). JPH1 has other roles besides holding the close apposition between the SR membrane and the PM T-tubules: it regulates voltage gated Ca^{2+} entry through direct interactions with dihydropyridine receptors (DHPR) in skeletal muscle cells and also promotes SR stored Ca^{2+} release by interacting with ryanodine receptors (RyR1 isoform) (Golini et al. 2011; Phimister et al. 2007).

Recently, David Pla-Martin and colleagues reported that mutations within JPH1 and ganglioside-induced differentiation-associated protein 1 (GDAP1) gene contribute to severe SOCE impairment (Pla-Martin et al. 2015). GDAP1 plays a role in neuronal development and mutations have been previously associated with neuropatic disorders and more specifically with Charcot-Marie-Tooth disease (CMT) (Pla-Martin et al. 2013). CMT is an inherited condition characterized by progressive muscle weakness and neuropathy. The authors described the case of a 29-year-old Spanish woman with diagnosed with CMT type 2K caused by a GDAP1 R120W mutation (inherited from her father) that also had a R213P mutation in the JPH1 gene (inherited from her mother). She presented a more severe disease phenotype in comparison with her relatives who had only GDAP1 gene mutation (Pla-Martin et al. 2015). Previous studies have shown that CMT neuropathies may also be associated with the impaired distribution of the mitochondria towards the junctional membrane complexes, resulting in a

decrease in SOCE and leading to impaired Ca^{2+} uptake by mitochondria (Pla-Martin et al. 2013).

Junctophilin 2 (JPH2)

Cardiac excitation-contraction (EC) coupling governs the heart muscle contraction and at cellular level it requires a close relationship and precise communication between VGCC located on the T-Tubule and RyR residing on the SR membrane (Brette et al. 2003). Studies have shown that disruptions in this communication, such as changes in T-tubule morphology, are associated with heart failure (Balijepalli et al. 2003).

JPH2, a 74 kDa protein of 696 amino acids, bridges the gap between PM and SR, maintaining the JMC in healthy cardiomyocytes (Takeshima et al. 2000). JPH2 deficiency have been associated with impairment of T-tubule maturation, suggesting that it plays an important role in maintaining the dyadic structure in cardiac muscle cells (Chen et al. 2013). Transgenic JPH2-null mice demonstrated a 90% increase of the distance between SR and sarcolemmal T-tubules (Takeshima et al. 2000). This was associated with spontaneous cardiomyocyte contraction, a reduced amplitude of Ca^{2+} transients as well as irregular Ca^{2+} currents (Takeshima et al. 2000). Calcium-induced calcium-release (CICR) was also impaired in JPH2 KO cardiac cells in vitro, with no effect on the expression or functionality of LTCC (Landstrom et al. 2011).

JPH2 was linked to different types of cardiac disorders such as dilated and hypertrophic cardiomyopathy (HMC) seen in rodent genetic models, or HMC with left ventricular tract obstruction observed in humans (Minamisawa et al. 2004; Landstorm et al. 2011). Several studies have reported that JPH2-altered expression is more frequently associated with HMC incidence as compared to its mutations (<1% HMC) (Landstorm et al. 2012). Interestingly, JPH2-E169K mutation has been recently associated with supraventricular arrhythmia observed in a multi-generation family; a rodent model of this mutation revealed a decreased

RyR2-JPH2 interaction and consecutively an increase in spark frequency (Beavers et al. 2013).

Several studies described skeletal muscle function impairment associated with JPH2 mutations as well (Landstorm et al. 2014). Over-expressing JPH2-S165F mutation resulted in reduced Ca^{2+} release via RyR1, thus reduced CICR followed by hypertrophy (Woo et al. 2010). It was proposed that JPH2-S165F mutation might affect the TRPC3 phosphorylation mediated by PKC (Woo et al. 2008). As TRPC3 is known to modulate RyR1, the JPH2-S165F was considered to indirectly diminish RyR1 function and contribute to skeletal muscle hypertrophy (Woo et al. 20008, 2009, 2010).

Interestingly, dysregulation of JPH2 was associated with microtubule densification due to enhanced polymerization (Zhang et al 2014). Cardiac stress leads to an increase in microtubule density which further results in JPH2 altered redistribution, T-tubule remodelling and EC dysfunction, potentially leading to heart failure (Zhang et al 2014). Furthermore, JPH2 overexpression has been shown to prevent heart failure without affecting the baseline contractile function (Guo et al. 2014).

Junctophilin 3 and 4

Junctophilin 3 (748 amino acids, 81 kDa) and Junctophilin 4 (628 amino acids, 66 kDa) were primarily observed within the brain and studies suggested that their role might be in facilitating the Ca^{2+} crosstalk between PM P/Q-type VGCC and ER RyR (Moriguchi et al. 2006).

Surprisingly, silencing either of the proteins in mice hippocampal neurons resulted in no abnormalities, but the loss of both proteins resulted in impaired Ca^{2+}-dependent K^{+} channel (SK)-dependent afterhyperpolarization, further leading to reduced memory, impaired exploratory activity and death of 5 weeks old mice (Moriguchi et al. 2006). JPH3 seems to serve as a JMC stabiliser, regulating neuronal Ca^{2+} influx and its mutation was linked to Huntington's Disease-like 2 (HDL2), a neurological disorder characterized by motor impairments and cognitive decline leading to dementia (Seixas et al. 2012). JPH3 was also

considered to function as a neuroprotector in elderly populations, hypothesis being confirmed by comparing young versus old JPH3-null mice; ROS dependent tissue oxidation in old mice led to a late-onset neurodegeneration similar to that observed in HDL2 patients (Seixas et al. 2012). Abolished afterhyperpolarization was also observed in cerebellar Purkinje cells of JPH3/4 null mice (Kakizawa et al. 2007). The neuronal JPH3/4 KO resulted in hyperphosphorylation of PKCγ, an impairment in the synaptic maturation contributing to severe motor defects and impaired cerebellar plasticity (Ikeda et al. 2007).

Since their discovery, JPH3 and 4 were mainly investigated in excitable cells, but a recent study reported the presence and the role of JPH4 in T cells (Woo et al. 2016). The authors proposed that in resting cells, JPH4 and junctate form a protein complex that allows STIM1 recruitment after ER Ca^{2+} discharge. The proposed mechanism is that cytosolic CC1-CC2 domains and the ER-luminal domain of STIM1 are interacting with the JPH4-junctate complex as observed in GST pulldown analysis of STIM1 fragments (Woo et al. 2016). The role of JPH4 in T cells may have a high benefit on the development of new pharmacological agents for inflammatory disorders and the presence of both JPH3 and 4 in different brain cells opens the door for further neurobiology research.

1.9 SOCE in neurons

Neurons have been thought to deliver Ca^{2+} influxes mostly through VGCC and receptor activated Ca^{2+} channels (e.g. glutamate or AMPA receptors), but since early 2000's studies have shown the presence of SOCE in excitable cells, including neurons (Akbari et al. 2004; Emptage et al. 2001). The concept of capacitative calcium entry in neuronal cells was originally demonstrated three decades ago (Putney JW 2011), but only later its importance in the development of the nervous system was evidenced (Nishiyama et al. 2000). Altered Ca^{2+} signaling can have serious consequences leading to Ca^{2+} overload, oxidative stress and ROS production, unfolded protein response, autophagy inhibition as well as mitochondrial dysfunction (Bollimuntha et al. 2017). All these issues may further lead to neurological

disorders such as Alzheimer's or Parkinson's disease, HIV-induced dementia, Huntington's, bipolar disorders, as well as ataxia and muscular dystrophy (Bollimuntha et al. 2017).

Different ion channels have been proposed to mediate SOCE in neurons, but TRPC family members attracted interest due to their high expression in the central and peripheral nervous system. Studies have identified TRPC channels to be preferentially expressed in different neuronal populations and thus having distinct functional roles: TRPC1 regulates cell proliferation in neuronal stem cells, TRPC3 and 6 mediate brain-derived neurotrophic factor (BDNF) – dependent neuronal growth and TRPC5 triggers a platelet-derived growth factor (PDGF) medicated neuroprotection (Fiorio et al. 2005; Jia et al. 2007; Yao et al. 2009). Later, Orai and STIM proteins have been shown to be expressed in distinct patterns in the brain and therefore the role of SOCE in neuropathophysiology gained more interest (Kraft et al. 2015).

Orai and STIM isoforms have been identified in both human and murine brain (Kraft et al. 2015). While STIM1 and 2 have similar expression in murine and human brain at mRNA level, Orai1 seems to be less present than Orai3, while Orai2 mRNA has been identified in murine but not in human brain tissue (Lalonde et al.2014). Interestingly, Orai2 and Orai3 seem to co-localize in murine Purkinje cells, STIM1 is highly present in cerebellum and low in the hippocampus, while STIM2 has the opposite expression pattern (Lalonde et al. 2014). In murine hippocampus, STIM1 is highly expressed in neuronal soma, while STIM2 both in soma and dendrites (Hooper et al. 2014).

STIM1's role in Purkinje neurons and cerebellar granule neurons might be to trigger slow glutamate receptor signal and gene transcription, while STIM2 might have a role in preventing memory loss in Alzheimer's disease as it regulates the activity of calmodulin kinase 2 (CAMKII) and stabilizes hippocampal mushroom spines (Hartman et al. 2014; Lalonde et al. 2014; Sun et al. 2014).

Increased expression of STIM1 and Orai1 may lead to neuronal death after an ischemic event, due to cytosolic Ca^{2+} accumulation (Zhang et al. 2014). This is consistent with the fact that

CRAC channels also play a crucial role in thrombus formation. Thus, inhibiting platelet activation with pharmacological agents that target SOCE may prevent or treat ischemic events (Varga-Szabo et al. 2008). A SOCE dysfunction was also associated with Charcot-Marie-Tooth (CMT) disease, characterized by axonal neuropathy or demyelinating of motor and sensory peripheral nerves (Pareyson et al. 2013). This genetic disorder is caused by mutations in GDAP1, whose silencing triggers a partial depletion of the ER Ca^{2+} pool, further reducing the Ca^{2+} influx through SOCE (Barneo-Munoz et al. 2015).

Outside CNS, molecular components of CRAC have been recently found in peripheral neurons, specifically in dorsal root-ganglia (DRG) and dorsal horn neurons (Gemes et al 2011, Munoz and Hu 2016). Previous studies showed that CRAC channels are fully functional in DRGs and that I_{CRAC} is enhanced after nerve injury (Gemes et al. 2011). STIM1, 2 and Orai1, 3 but not Orai2 were identified in DRG neurons and, interestingly, Orai1 and 3 are thought to play a key role in membrane depolarization and neuronal excitability, vital for inter-neuronal signaling and pain transmission (Wei et al. 2017). In a spinal nerve ligation (SNL) rat model, injured DRG L5 neurons revealed an increased I_{CRAC} as compared to control neurons (Gemes et al. 2011). Moreover, while Orai1 and STIM1 expression is not affected after nerve damage, thapsigargin failed to trigger SOCE on injured neurons, suggesting that the nerve injury itself depletes the ER Ca^{2+} stores, activates and maintain I_{CRAC} (Gemes et al. 2011).

The ER Ca^{2+} concentration critically regulates calcium signaling in peripheral nervous system, but Ca^{2+} store replenishment in stimulated DRG neurons is still an undocumented area which requires further research. As previously highlighted, calcium signaling is strongly implicated in inflammatory and neuropathic pain mechanisms and the referenced studies suggest a potential role of CRAC channels in inflammatory GPCR signaling and pain.

1.10 Aims of this study

The above review covered the progress that has been made in the past decade to elucidate the importance of SOCE in excitable and non-excitable cells, but also highlighted the limited knowledge of its role in pain signalling. The overall objective of this study was to characterize SOCE in primary afferent neurons and probe its role in inflammatory signalling cascades. Specific aims of this study are as follows

a) Characterizing the expression of the CRAC components within DRGs.

b) Determining the effect of CRAC inhibitors on ATP and/or BK-induced SOCE.

c) Investigating expression and functional role of junctional proteins, Junctophilins in DRG

d) Exploring the role of SOCE and its components in the maintenance of inflammatory signalling cascades in DRG.

Most of this work was carried out on DRG neurons, but a separate aim was also to investigate whether the effect of CRAC inhibitors YM58483 and Synta66 is dependent on the type of cells, SOCE stage and/or duration of treatment. The overarching aim of this study was to develop mechanistic understanding of SOCE in nociceptive sensory neurons in order to provide new insights for the treatment of inflammatory pain.

Chapter 2. Materials and Methods

2.1 Established cell lines

Human embryonic kidney 293 (HEK 293) cells and Chinese hamster ovary (CHO) cells were used for fluorescent calcium imaging experiments. Cells were cultured on 100 mm culture dishes in Dulbecco's Modified Eagle's medium (DMEM-GlutaMAX, Life Technologies) supplemented with 10% Foetal Calf Serum (FCS, Sigma-Aldrich), 50 U/ml penicillin (Sigma-Aldrich) and 50 µg/ml streptomycin (Sigma-Aldrich) and kept in a humidified incubator (set at 37°C and 5% CO_2). Cells were passaged every 3 days by washing with 10 mL phosphate buffer saline (PBS, Sigma-Aldrich), followed by pipetting for mechanical detachment (for HEK 293 cells) or trypsinization (for CHO cells) with 1 ml Trypsin-EDTA (Invitrogen). Once isolated in a tube, cells were washed twice with fresh DMEM and centrifuged for 5 minutes at 800 rpm (25°C). The cell cone was re-suspended in fresh pre-warmed (37°C) DMEM and cells were seeded at a density of 10^6/ml.

2.1.1 Cell line transfection

For transfection, 24 well plates were prepared consisting of different dilutions of HEK293 or CHO cells. Once cells were adjudged to be ~50-90% confluent 24 hours post-seeding, they were transfected with 100-400 ng DNA using Fugene HD (Promega) according to the manufacturer's instructions. The transfection protocol was optimized by treating the cells with different amounts of plasmid concentration and considering a variable cell confluency. As expected, an efficient transfection has been observed when 400 ng of cDNA plasmid was used and cells were 60-70% confluent. The following day, cells were detached (see above for method depending on cell type), collected and seeded on pre-coated coverslips. Imaging experiments were performed 48 hours post-seeding.

2.2 Primary culture of DRG neurons

All animal work was performed under UK Home Office License and in accordance with the regulations of the UK Animals (Scientific Procedures) Act 1986.

Wistar rats (7 to 14 days old) were sacrificed by exposure to isoflurane overdose, followed by cervical dislocation to confirm the death according to the Home Office Schedule I protocol. Rats were decapitated followed by removal of the spine, which was then sliced longitudinally to expose the spinal cord. Upon removal of the spinal cord, sphere-like DRGs were revealed between vertebras, which were extracted using fine forceps. Ganglia were stored in ice-cold Hanks Balanced Salt Saline (HBSS, Sigma-Aldrich) solution and then transferred into a dissociation solution containing 10 mg/ml dispase (Thermo Fisher Scientific) and 1 mg/ml type 1A collagenase (Sigma-Aldrich) in pre-warmed HBSS. During the dissociation, ganglia were kept in a humidified incubator at 37°C and 5% CO_2 for 13 minutes, followed by gentle trituration to facilitate the dissociation and re-incubated for a further 2 minutes. This protocol has been optimized by previous members of Prof. Nikita Gamper's lab to provide the efficient neuronal survival with regards to the fragility of DRG. A final mechanical dissociation by trituration was performed, followed by addition of ice-cold media (DMEM with GlutaMAX, 10% FCS, penicillin 50 U/ml and streptomycin 50 µg/ml) to halt the dissociation process. Cells were then centrifuged and washed twice for 5 minutes at 800 rpm in ice-cold DMEM media. The cell cone was resuspended in pre-warmed media and 100 µl droplets of the high density cell suspension were placed on 10 mm glass coverslips which were pre-coated with poly-D-lysine (Millipore Ltd) and laminin (Insight Biotechnology) to provide adherence for DRG neurons. Dissociated cells were then incubated for 4 hours to facilitate adhesion and to reduce the risk of apoptosis. Following this, each coverslip was supplemented with 1 ml media for culturing and re-incubated for a minimum of 48 hours prior to experiments.

2.2.1 DRG transfection

Attempts to transfect DRG neurons with either R- or G-CEPIA1*er* were made by choosing a non-viral gene transfer technique. Nucleofection has been shown to be more efficient in transfecting non-dividing cells with respect to other transfection methods (Kirton et al. 2013). This technique combines chemical transduction and electroporation to facilitate the plasmid entry into the nucleus of primary cultured or hard-to-transfect cells (Martinet W et at. 2003). For neurons that required transfection with calcium-measuring organelle-entrapped protein indicators (CEPIA; see below), a Nucleofector® I console (Lonza) was used to transfect DRG neurons. Prior to seeding, cells were resuspended in a rat neuron transfection buffer and mixed with 10 µg of DNA. The solution was then quickly transferred into a Lonza certified cuvette and placed into the nucleofector. Program O-03 was utilized for transfection after which the cells were resuspended in pre-warmed media and seeded onto coverslips. As for standard cultured DRGs, cells were incubated for minimum 48 hours prior to experiments.

2.2.2 DRG knock-down with deliverable small interfering RNA

For gene silencing experiments, small interfering RNA (siRNA) against JPH4 was delivered with Lipofectamine RNAiMAX Transfection Reagent (Thermo Fisher Scientific). To do so, DRG neurons were dissociated as previously described and 48 hours post-seeding the cells were approximately 70% confluent and ready for transfection. Briefly, the cultured neurons were washed with fresh pre-warmed DMEM (without FCS and antibiotics). The transfection reagent and siRNA were mixed in OptiMEM I reduced serum medium (Life Technologies) as per manufacturer's instructions. A scrambled oligomer was also used as a negative control (Table 2.1). Two different siRNA products against JPH4 were used at various concentrations (from 5 to 10 pmol per well)

ell) in both single use and in combination. The diluted siRNA-lipid complex was then added to cells followed by incubation at 37°C for 1 to 3 days. To determine the knock-down (KD) effect, the cells were lysed and analyzed by Western blot as described in Chapter 6.

Product name	Referred to as	Supplier
Silencer Select siRNA against JPH4 (s175513)	siRNA #1	Life Technologies
Silencer Select siRNA against JPH4 (s175511)	siRNA #2	Life Technologies
Silencer Select Negative Control No.1 siRNA	Scrambled oligomer	Life Technologies

Table 2.1: The list of siRNA products used for DRG knock-down experiments.

2.3 Cytosolic calcium imaging using fura-2 AM

Fura-2 is a high affinity calcium indicator, widely used to measure intracellular calcium levels by fluorescence imaging (Paredes et al. 2008). For the experiments detailed in this thesis, fura-2 acetoxymethyl ester (fura-2 AM) was utilized, which is a membrane permeant form of the dye and delivers fura-2 inside the cell once cytosolic esterases remove the acetoxymethyl groups (Paredes et al. 2008). It is a ratiometric calcium indicator that is excited at both 340 and 380 nm and emits at 510 nm. The fluorescence intensity ratio ($R = F_{340}/F_{380}$) is measured at wavelengths where the difference of fluorescence between bound (at 340 nm) and free indicator (at 380 nm) is maximum. This way, the risk of photobleaching or uneven dye loading is reduced as compared to other intensity-based calcium indicators such as Fluo-4.

Prior to recording, plated cells were loaded with fura-2 by incubating them with a mixture of 2 µM fura-2 AM (Thermo Fisher Scientific) and 0.01% pluronic acid (Sigma-Aldrich) in extracellular bath solution (EC, Table 2.3) for 1 hour. The mixture was then removed and cells were washed with EC solution. Fragments of coverslips were placed on the microscope perfusion chamber and EC solution was perfused over the cells through a gravity driven perfusion system at an approximate rate of 2 ml/min. The drug compounds were diluted in EC solution to the required concentration and applied via the perfusion system.

To visualize the cells, an inverted Nikon TE-2000 microscope was connected to a Till Photonics fluorescent imaging system comprising of a Polychrome V monochromator and an IMAGO CCD camera. TILL Vision 4.5.56 software (later upgraded to Live Acquisition 2.2.0) was used for image acquisition and processing. Cells were excited at 340 nm and 380 nm (50 ms exposure) to confirm fura-2 loading and the emission was collected using a UV-2A filter (Nikon). Regions of interest (ROIs) were used to select neurons from snapshots taken to record from and for further post-hoc analysis. Prior to recording, further protocol details were also set (such as duration of excitation, total experiment duration, signal-to-noise parameters). Recordings made were exported and analysed in Microsoft Excel and Origin software.

2.4 Intraorganellar calcium imaging with CEPIA

Calcium-measuring organelle-entrapped protein indicators (CEPIA) are genetically encoded calmodulin-based Ca^{2+} indicators (Suzuki et al. 2014). CEPIAs have been recently described as a new sensitive tool to investigate organellar functions as they are engineered to emit red, green or blue/green fluorescence when binding Ca^{2+} at intraorganellar Ca^{2+} concentrations (Suzuki et al. 2014).

SOCE has been previously investigated by measuring the increase in cytosolic Ca^{2+} levels after store depletion with either SERCA inhibitors or GPCR agonists (Suzuki et al. 2014). Calcium imaging in the ER is therefore another direct mean to analyze SOCE and indicators such as CEPIA allow to do so. I have used R-CEPIA1*er* (Kd = 565 ± 58 μm, Fmax/Fmin = 8.8 ± 0.7) and G-CEPIA1*er* (Kd = 672 ± 23 μm, Fmax/Fmin = 4.7 ± 0.3) (Suzuki et al. 2014). Their high dynamic range proved to be efficient in cultured neurons where Ca^{2+} changes within the ER were mainly studied indirectly by cytosolic Ca^{2+} imaging (Suzuki et al. 2014).

Imaging of ER calcium levels using G-CEPIA1*er* and R-CEPIA1*er* was done in the same manner as fura-2 calcium imaging however excitation was done using 488nm (GFP-B filter cube) and 560nm (G-2A filter cube), respectively.

2.5 CEPIA-cDNA preparation

R- and G- CEPIA1*er* were purchased from Addgene as plasmids in bacteria agar stabs. An agar solution containing 100 µg/ml Ampicillin was prepared and poured in 100 mm diameter Petri dishes. A sterile pipette tip was used to extract the bacteria growing within the agar stab and spread over the solidified agar in the plates. Three different streaks were created to spread and dilute the bacteria. The plates were then incubated at 37°C for 16 to 24 hours and the following day, bacterial colonies were visible. One single colony was used to further prepare a culture of bacteria overnight in a Lysogeny broth (LB) solution containing 100 µg/ml Ampicillin. Plasmid DNA was isolated from the culture using a QIAGEN Plasmid Midi Kit, according to the manufacturer's recommendations. Briefly, the bacterial culture was harvested by centrifugation at 7000 rpm for 15 minutes at 4°C. The bacterial pellet was resuspended in a lysis buffer provided and the supernatant containing plasmid DNA was collected, followed by DNA elution and further on precipitation with room-temperature isopropanol. The pellet DNA was then washed with 70% ethanol, air-dried and dissolved in a suitable volume of alkaline buffer. The plasmid DNA concentration was determined by measuring an absorbance at 260 nm using a NanoDrop spectrophotometer.

Drug	Concentration	Supplier
Thapsigargin	1 µM	LKT Laboratories
ATP	30 µM	Sigma-Aldrich
BK	250 nM	Calbiochem
YM58483	1 µM	Sigma-Aldrich
Synta66	3 µM	provided by Richard Foster, School of Chemistry, University of Leeds

Table 2.2: List of chemicals and drugs used for calcium imaging

Extracellular bath solution (mM)		Ca^{2+} free solution (mM)	
NaCl	160	NaCl	165
KCl	2.5	KCl	2.5
$MgCl_2$	1	$MgCl_2$	1
$CaCl_2$	2	EGTA	1
HEPES	10	HEPES	10
Glucose	10	Glucose	10
	pH 7.4		

Table 2.3: Solutions used for calcium imaging experiments and inducing SOCE

2.6 Immunocytochemistry (ICC)

Cultured DRG neurons were fixed with 4 % ice-cold paraformaldehyde (PFA, Sigma-Aldrich) for 20 minutes. After washing three times with 1x PBS, cells were incubated with a blocking buffer (containing 0.05% Tween 20, 0.25% Triton X-100 and 5% donkey and/ or goat serum in 1X PBS, all products from Sigma-Aldrich) for 1 hour at room temperature. The purpose of this step is to reduce nonspecific background noise and to improve the sensitivity of the assay. Following this, cells were incubated overnight at 4°C with a solution containing one or two primary antibodies, depending on the experimental design. The antibodies were diluted to the required concentration in 5% bovine serum albumin (BSA, Sigma-Aldrich) in 1x PBS. Next day, the cells were washed again with 1x PBS and further incubated with fluorochrome-conjugated secondary antibodies (Table 2.4) diluted in 1 % BSA buffer for 2 hours at room temperature. Coverslips were then washed and mounted on microscope glass slides with 10 µl Vectashield mounting medium supplemented with 4,6 diamidino-2-phenylindole (DAPI, Vector Laboratories). Samples were kept in the dark, at 4°C and imaged with a Carl Zeiss LSM880 inverted confocal microscope and processed with Zeiss ZEN imaging software. For

each staining procedure, a buffer without primary antibody was used as a negative control and cells were detected by nuclei-specific DAPI staining.

2.7 Immunohistochemistry (IHC)

Once fresh ganglia were collected, they were washed with 1x PBS and fixed with 4% ice-cold PFA for 1 hour. The ganglia were then embedded in 10% gelatin (Sigma), solution prepared with distilled water. Once solidified, the gelatin was cut into 1cm³ cubes, each cube containing a ganglion, and further incubated in 4% PFA for 6 to 10 hours at 4°C. The cubes were then washed with 1x PBS and stored in 0.1M phosphate buffer solution (PB, Sigma-Aldrich) at 4°C. Using a microtome blade, DRG sections of approximately 40 µm were cut and wished with 1x PBS. The following steps including blocking and primary/secondary antibody staining were done in the same manner as above. The DRG slices were then mounted with Vectashield plus DAPI, covered with coverslips and sealed with polish prior to imaging. See Table 2.4 for information about the primary and secondary antibodies used for immunocyto- and immunohistochemistry experiments.

To support the validity of the antibodies, control samples without primary antibody treatment were also prepared. Thus, cultured DRG neurons or whole DRG sections were incubated with the buffer alone. The following steps remained unchanged: incubation with secondary antibodies and mounting with Vectashield plus DAPI. Images of the no primary antibody samples were processed in the same way and presented alongside the positive staining in the following chapters. This ensures that the observed staining is due to detecting the antigen by the primary antibody.

Antibodies against STIM, Orai, NF200 and TRPV1 explicitly characterized in previous studies were chosen (see Table 2.4 for details).

At the time of the experiments, the antibodies against JPH proteins were not referenced in any published manuscripts. Therefore, the specificity of these antibodies was also determined by Western blot in tissue homogenates known to express each of the protein (e.g. skeletal muscle

lysate for JPH1, cardiac muscle lysate for JPH2 and cerebellum lysate for JPH3 and JPH4). Specificity of JPH4 antibody has been further confirmed by the JPH4 knockdown. More information can be found in Chapter 5 of this thesis.

The expression of all STIM, Orai and JPH isoforms was investigated in fixed DRG sections. Using Zeiss ZEN software, the number of positively and negatively stained neurons was determined. The mean fluorescence intensity of the whole DRG section was considered the threshold above which a neuron was positive. The cell diameter and mean intensity was calculated for each selected neuron. Further on, the cells were classed depending on the somatic diameter and presented as a frequency distribution. Data is shown as the number of positive neurons of different somatic sizes (± SEM) from the total number of neurons analysed. The somatic diameter intervals were: <10 µm, 10-15 µm, 15-20 µm, 20-25 µm, 25-30 µm, 30-35 µm, 35-40 µm, 40-45 µm and >45 µm.

Antibody	Dilution	Supplier / Reference
Rabbit anti-JPH1	1:200	Biorbyt
Rabbit anti-JPH2	1:200	Biorbyt
Rabbit anti-JPH3	1:200	Biorbyt
Rabbit anti-JPH4	1:200	Biorbyt
Rabbit anti-JPH4	1:200	Sigma-Aldrich
Mouse anti-STIM1	1:200	Abcam / Hájková Z *et al.* 2011
Rabbit anti-STIM2	1:500	Abcam / Bréchard S *et al. 2009*
Mouse anti-Orai1	1:500	Abcam / Guzman R *et al.* 2014
Rabbit anti-Orai1	1:500	Alomone / Qi Z et al. 2016
Rabbit anti-Orai2	1:500	Alomone / Zheng B et al. 2017
Rabbit anti-Orai3	1:500	Alomone / Sabourin J et al. 2016
Mouse anti-NF200	1:2000	Sigma-Aldrich / Rose et al. 2011
Guinea pig anti-TRPV1	1:500	Neuromics / Rose et al. 2011
Donkey anti-mouse Alexa Fluor 488	1:1000	Invitrogen / Rose et al. 2011
Donkey anti-mouse Alexa Fluor 555	1:1000	Invitrogen / Du X et al. 2017
Donkey anti-rabbit Alexa Fluor 488	1:1000	Invitrogen / Li JX et al. 2016
Donkey anti-rabbit Alexa Fluor 555	1:1000	Invitrogen / Du X et al. 2017
Goat anti-guinea pig Alexa Fluor 488	1:1000	Invitrogen / Rose et al. 2011

Table 2.4: Primary and secondary antibodies used for ICC / IHC

2.8 Proximity Ligation Assay (PLA)

PLA is a highly specific proteomic tool that was first developed in 2002 by Fredriksson and colleagues. It aims at detecting and visualizing protein-protein interactions (Fredriksson et al. 2002). PLA uses the principle of two oligonucleotide-labelled antibodies capable of binding when in close proximity (less than 40 nm apart). Two primary antibodies are used to bind the targeted proteins and two oligonucleotide-conjugated secondary antibodies are then used to bind the primary antibodies. When the proteins are found in close proximity, connector oligonucleotides facilitate the formation of a single-stranded DNA circle between the two secondary probes. The use of DNA polymerase promotes the formation of repeated DNA sequences (the 'rolling-cycle amplification') that are further targeted for fluorescent detection.

Thus, acute dissociated DRG neurons were cultured on pre-coated glass microscope slides. Prior to seeding, a hydrophobic barrier pen (Vector Laboratories) was used to delimit a seeding area to approximately 1 cm^2. Two days post-seeding, a Duolink PLA kit (Sigma-Aldrich) was used to perform the experiment as per manufacturer's instructions. Depending on the experimental design, some cells have been treated with the CRAC inhibitor YM58483 for 1 hour and/or store-depleted with BK in Ca^{2+} free solution prior to fixation.

Cells were then fixed with 4% ice-cold PFA for 20 minutes and treated with a permeabilization buffer (composed of 0.05% Tween 20 and 0.25% Triton X in PBS) for 1 hour at room temperature. Further on, the cells were treated with the provided blocking solution for 30 minutes at 37°C, followed by incubation with a diluted primary antibody solution for 12 to 16 hours at 4°C. Next step was to wash the samples and add in oligonucleotide-conjugated secondary antibodies (anti-mouse MINUS and anti-rabbit PLUS PLA probes, Sigma-Aldrich) for 1 hour at 37°C. Further on, the ligation was done by treating the neurons with a solution containing ligase and 5X ligation stock in purified water for 30 minutes at 37°C. Cells were then washed and the amplification step was performed by adding in a solution comprising of polymerase and 5X Amplification stock in purified water for 100 minutes at 37 °C. Finally, the samples were washed and mounted with Duolink mounting medium with DAPI (Sigma-

Aldrich) prior to being sealed. Imaging was performed using a Carl Zeiss LSM880 inverted confocal microscope and images processed by Zeiss ZEN software. Table 2.5 lists the pair of antibodies used to perform different PLA experiments within this thesis.

To validate the PLA approach, I performed negative and positive controls using Orai1 as a target protein. As such, the positive control experiment meant using two primary antibodies against Orai1 (one raised in mouse, one in rabbit) as shown in Table 2.5. Both PLA probes, anti-rabbit PLUS and anti-mouse MINUS, attached to the primary antibodies that previously bound the same Orai1 protein. A PLA-specific fluorescent signal was detected as shown in Chapter 3. Furthermore, a negative control experiment revealed that using only one primary antibody (mouse anti-Orai1) would not suffice for the anti-mouse MINUS and anti-rabbit PLUS probes to bind and reveal any fluorescent puncta (Figure 3.12.A).

Antibody 1	Antibody 2	PLA probe 1	PLA probe 2
Rabbit anti-JPH4	Mouse anti-Orai1	Anti-rabbit PLUS	Anti-mouse MINUS
Rabbit anti-JPH4	Mouse anti-STIM1	Anti-rabbit PLUS	Anti-mouse MINUS
Rabbit anti-Orai1	Mouse anti-STIM1	Anti-rabbit PLUS	Anti-mouse MINUS
Rabbit anti-Orai1	Mouse anti-Orai1	Anti-rabbit PLUS	Anti-mouse MINUS
-	Mouse anti-Orai1	Anti-rabbit PLUS	Anti-mouse MINUS

Table 2.5: Antibodies and probes used for PLA experiments

2.9 Western blot (WB)

WB is a widely used analytical assay to detect protein expression within a sample of tissue homogenate and was introduced in 1979 (Towbin et al. 1979). It is also called immunoblotting and it uses SDS-polyacrylamide gel electrophoresis (SDS-PAGE) to trigger the protein separation within a sample. Once separated, the proteins are transferred on a nitrocellulose or polyvinylidene difluoride (PVDF) membrane and stained with primary and secondary antibodies. The proteins of interest are therefore revealed and the location and intensity of the specific antigen-antibody reaction is analysed.

For the scope of this thesis, WB experiments were performed to determine the expression of JPHs within DRG lysates and to analyse the JPH4-KD efficacy as previously mentioned.

Therefore, DRG neurons from two 7 days old Wistar rats were seeded on 6-well plates. Cells were lysed 48 hours post-seeding with lysis buffer (made of HEPES 50 mM, NaCl 150 mM, Na_3VO_4 183.9 mM, NaF 10 mM, Glycerol 10%, NP-40 1% and EDTA 1mM) supplemented with protease inhibitor. Lysis was boosted by mechanically damaging the cells' membrane with a sterile pipetting tip. The mixture was centrifuged for 10 minutes at 13 000 rpm, at 4°C. To determine the protein concentration, 2µl of the lysate was mixed with 700 µl of diluted spectrophotometer dye (Bio-Rad). The absorbance was read at 595 nm using Jenway 6300 Spectrophotometer and the protein concentration (µg / µl) was calculated using the formula C= Absorbance / 0.0562*2. Further on, an SDS lysate was prepared by mixing 1-part SDS sample buffer with 3-parts of lysate and boiled at 95°C for 5 minutes. The SDS sample buffer is a mixture of 50 µl β-mercaptoethanol (Sigma-Aldrich) and 950 µl 4X Laemmli sample buffer (Bio-Rad). Approximately 30 µg of each denatured protein samples and 8 µl protein marker (Precision Protein Plus, Bio-Rad) were loaded on Mini Protean gels TG (Bio-Rad). Using a Mini-Protean Tetra System connected to a power control (Power Pac HC, Bio-Rad), the samples were electrophoresed at 120 V for 1 hour and 15 minutes or until the marker dye migrated to the bottom of the gel. This step occurred in a running buffer composed of 25 mM Tris-base, 192 mM glycine, 0.1% SDS in purified water).

The proteins were then transferred on a methanol-activated PVDF membrane using a wet-transfer method in transfer buffer (25 mM Tris-base, 192 mM glycine and 20% v/v methanol in purified water). Further on, the membrane was blocked in a 5% milk blocking buffer for 1 hour at room temperature. The membrane was then probed with a diluted primary antibody solution (the required amount of antibody in 5% milk buffer) and incubated overnight on a shaker at 4°C. The following day, the membrane was washed with washing buffer and incubated with a diluted secondary antibody (Table 2.6) in 5% milk buffer for 45 minutes at room temperature. The horse radish peroxidase (HRP)-linked anti-rabbit or anti/mouse secondary antibody was further visualized on the membrane using an enhanced chemiluminescence substrate (Pierce ECL WB Substrate and Super Signal West Femto, Thermo-Scientific). The membrane was then exposed to a Kodak film for 10 seconds up to 10 minutes depending on the assay sensitivity to the targeted proteins. All samples were re-probed for β-actin as a loading control. To do so, the membranes were stripped with stripping buffer (Thermo Scientific) for 20 minutes at room temperature and washed, blocked and re-probed with rabbit anti-β-actin antibody (Cell Signalling) and further performed the same steps as above.

The exposed films were processed using an Xograph machine, scanned and analysed using Image J software. The mean intensity of each band was corrected to background and the band intensity of each targeted protein was made relative to the corresponding loading control, β-actin. Antibody quality control was done using lysates from tissues known to express the protein of interest. In circumstances when it was difficult to interpret the WB results, the protocol was optimized to facilitate a better protein separation, increased the duration of blocking and or washed thoroughly. When needed, other antibodies against the same proteins were used as well as a blocking peptide to confirm the antibody specificity and determine the correct band.

Antibody	Dilution	Supplier
For Western blot experiments:		
Rabbit anti-JPH1	1:500	Biorbyt
Rabbit anti-JPH2	1:500	Biorbyt
Rabbit anti-JPH3	1:500	Biorbyt
Rabbit anti-JPH4	1:500	Biorbyt
Rabbit anti-JPH4*	1:1000	Sigma-Aldrich
* *Blocking peptide*	*1:1000*	*Sigma-Aldrich*
Rabbit anti-β-actin	1:1000	Cell Signaling
HRP-linked anti-rabbit secondary antibody	1:1000	Cell Signaling
HRP-linked anti-mouse secondary antibody	1:1000	Cell Signaling
For Immunoprecipitation experiments:		
Mouse anti-STIM1	1:100	Abcam
Rabbit anti-JPH4	1:500	Biorbyt

Table 2.6: Primary and secondary antibodies used for WB and IP

2.10 Co-immunoprecipitation

Immunoprecipitation (IP) is a widely used technique to detect and purify a specific antigen, while the isolation of protein complexes is known as co-immunoprecipitation (Co-IP) (Phizicky and Fields, 1995). For Co-IP experiments, DRG lysates were prepared as previously described. A pre-cleaning step was done by adding 8 µl of beads (Protein A.G PLUS-Agarose, Santa Cruz Biotechnology) to 500 µg lysate and mixing for 30 minutes at 4°C to reduce the non-specific binding. The mixture was then centrifuged at 9000 rpm for 5 minutes at 4°C. The supernatant was collected and incubated with the appropriate primary antibody for 2 hours at

room temperature. Next day, 20 µl of IP beads were added to the mixture and incubated with rotation overnight at 4°C. The beads were then collected by centrifugation at 9000 rpm for 5 minutes and washed with PBS 3 times. A volume of 60 µl SDS sample buffer was added over the beads followed by boiling them for 5 minutes at 95°C. The next step was to proceed with the gel loading, electrophoresis and transfer as described in the WB method.

This technique was used to determine the interaction between STIM1 and JPH4 in DRG neurons upon SOCE activation (Chapter 6). For this reason, prior to lysis, the cultured neurons were store-depleted with 250 nM BK in Ca^{2+} free solution. Then, the lysate was immunoprecipitated with mouse anti-STIM1 antibody and immunoblotted with rabbit anti-JPH4 antibody (Table 2.6). The membrane was exposed to a Kodak film as previously described, followed by a stripping step and re-probing for STIM1 to confirm the efficacy of the immunoprecipitation.

2.11 Statistical analysis

Student's t-test (unpaired) was used to analyse the mean difference between a control and test group. One-Way ANOVA was used when comparing more than two groups. Statistical significance was established when the p value was ≤ 0.05. All results are provided as mean ± SEM. The n number is equal to the number of samples used for each experiment. Except for the Figure 4.9, three animals per data set were sacrificed to provide the corresponding n number stated in each figure legend (e.g. n= 6 individual samples from 3 different animals). For the imaging experiments, one sample is defined as the mean fluorescence intensity for all neurons analysed per that sample.

Chapter 3. Characterization of CRAC components in DRG neurons

3.1 Introduction

Neurons have the ability to deliver Ca^{2+} signals tailored at modulating specific neuronal functions (Berridge 1998). They use both intra- and extracellular Ca^{2+} sources to regulate Ca^{2+} dependent processes: i) Ca^{2+} influx from the extracellular space is controlled by plasma membrane Ca^{2+} channels, such as VGCCs or ROCs, and ii) Ca^{2+} release from the main intracellular Ca^{2+} source, the ER, is controlled by IP_3R and RyR (Berridge 1998). SOCE, as previously described in Chapter 1, represents another type of Ca^{2+} entry. Initially it was shown to be activated in response to ER Ca^{2+} store depletion in non-excitable cells (Parekh and Putney 2005). Later, CRAC channels were described as carrying the Ca^{2+} current responsible for refilling the ER Ca^{2+} pool (Parekh and Putney 2005, Parekh 2010). For a long time SOCE was not considered to be a source of Ca^{2+} entry in neurons, as these are abundantly populated with VGCCs and ROCs that give access to the extracellular Ca^{2+} reservoir (Putney 2003). In early 2000's a study reported that SOCE is present in hippocampal pyramidal neurons and that it controls neurotransmitter release and contributes to short- and long-term synaptic plasticity (Emptage et al. 2001). Furthermore, impaired SOCE was associated with neurodegenerative disorders such as Alzheimer's or Huntington's disease (Yoo et al. 2000, Wu et al. 2011) and the molecular components of SOCE have been identified to play an important role in synaptic transmission and cognition (Berna-Erro et al. 2009, Hartmann et al. 2014, Klejman et al. 2009).

Besides playing an important role in the central nervous system, the functionality of SOCE was also demonstrated in peripheral neurons. Interestingly, several studies reported that peripheral nerve injury disrupts cytosolic Ca^{2+} homeostasis in sensory neurons and elevated Ca^{2+} levels were linked to diabetic neuropathic pain and chronic inflammatory pain (Fuchs et al. 2005, Fuchs et al. 2007, Gemes et al. 2011, Huang et al. 2002). While the role of CRAC channels has been investigated mainly in dorsal horn neurons and astrocytes (Xia et al. 2014),

several recent studies demonstrated that molecular components of CRAC channels are also present in DRG neurons (Gemes et al. 2011, Gao et al. 2016). Moreover, Wei D and colleagues reported relative mRNA levels and protein expression of Orai and STIM family members in mice DRGs (Wei D et al. 2017). The authors also characterized the functional properties of CRAC channels in DRG neurons by performing Ca^{2+} imaging recordings to test the presence of thapsigargin-induced SOCE within neurons of different sensory modalities (Wei D et al. 2017). Through knock-down experiments, they further highlighted the role of STIM1, STIM2, Orai1 and Orai 3 in modulating SOCE in DRGs and noticed that while Orai2 mRNA level is the highest among all Orai family members, knocking it down had no effect on SOCE (Wei D et al. 2017). Interestingly, both Orai1 and Orai3 are required for thapsigargin-induced neuronal excitability in DRG neurons and knocking-down both proteins prevents membrane depolarization (Wei D et al. 2017). To determine whether depletion of the ER Ca^{2+} pool triggers puncta formation of STIM isoforms, they transfected DRGs with STIM1- or STIM2-YFP. Performing live cell confocal imaging, it was shown that in neurons store depleted with thapsigargin, both STIM isoforms translocated into puncta, but STIM2 to a lesser extent than STIM1 (Wei D et al. 2017). While these recent reports started to address functional role of SOCE and molecular composition of CRAC in sensory neurons, the full picture is still far from being complete.

3.2 Results

Since several attempts were made to characterize the identity and role of CRAC components in peripheral sensory neurons (Wei D et al 2017, Qi et al. 2016, Duncan et al. 2013), this chapter is built to add missing pieces to the puzzle.

Nociceptors are typically categorized based on fiber size and differentiated into groups depending on the type of the sensory stimuli they detect and how fast they conduct an action potential: i) Aβ large myelinated fibers (neuronal somatic diameter usually larger than 45 µm), ii) Aδ medium thinly myelinated fibers (somatic diameter between 25 and 45 µm), and iii) C small non-myelinated fibers (somatic diameter of less than 25 µm) (Basbaum et al. 2009).

Since nociception is associated with Aδ- and C- nerve fibers (conducting fast pain and persistent pain, respectively), it seems reasonable to characterize the presence of SOCE components in DRG neuronal population, based on the somatic size (Suzuki et al. 2010, Rose et al. 2011). For this purpose, I prepared the DRG sections as described in Chapter 2 and used immunohistochemistry assay to characterize the distribution of Orai and STIM subunits in DRG. DAPI staining (blue) was used to identify nuclei. Tissue slices of 40 µm thickness were immunostained with Orai1, Orai2, Orai3, STIM1 and STIM2 antibodies (Table 2.4). To further confirm and characterize the putative role of these proteins, I co-stained the samples with an antibody against the neurofilamental marker NF200 to identify large myelinated neurons. NF200 also reveals positive staining in some, but not all, medium myelinated Aδ fibers. Similarly, to verify whether Orai and/or STIM family members are present in pain signaling C-fibers, I selected TRPV1 as a marker for heat sensitive small-diameter nociceptors.

To ensure consistency and avoid bias, I considered a threshold above which a neuron is stained positively with the required antibody. I measured the mean fluorescence intensity of the whole tissue and used a rounded-up value as a threshold for positive staining (e.g. if the mean intensity is 17, anything above 20 would qualify as positive). I took this conservative approach as this value is already 3 times higher than the background itself (black area including noise).

Using this method will mainly highlight the protein distribution in medium and intense stained cells. It certainly excludes some of the weak (but still positive) stained cells, but importantly, it avoids false positive selection. I have selected the neurons based on their morphological properties: big round-shape cells surrounded by long and thin satellite glial cells.

No primary antibody samples were also prepared as described in Chapter 2. Images were presented alongside positive staining. For co-expression experiments, the samples used as no primary controls were treated with two complimentary secondary antibodies (e.x. Donkey anti-mouse AlexaFluor 555 and Goat anti-guinea pig AlexaFluor 488)

3.2.1 Orai and STIM isoforms are present in DRG neurons.

Immunostaining of DRG sections demonstrated that all STIM and Orai isoforms, except Orai2, are expressed in DRG neurons (Figure 3.1). The nuclear staining of Orai2 was noticed in all samples, independent of antibody dilution (1:200, 1:500 and 1:1000 dilutions were used to test the antibody's affinity to the PFA fixed samples). Further investigations are needed to determine if Orai2 is indeed absent in primary afferent neurons.

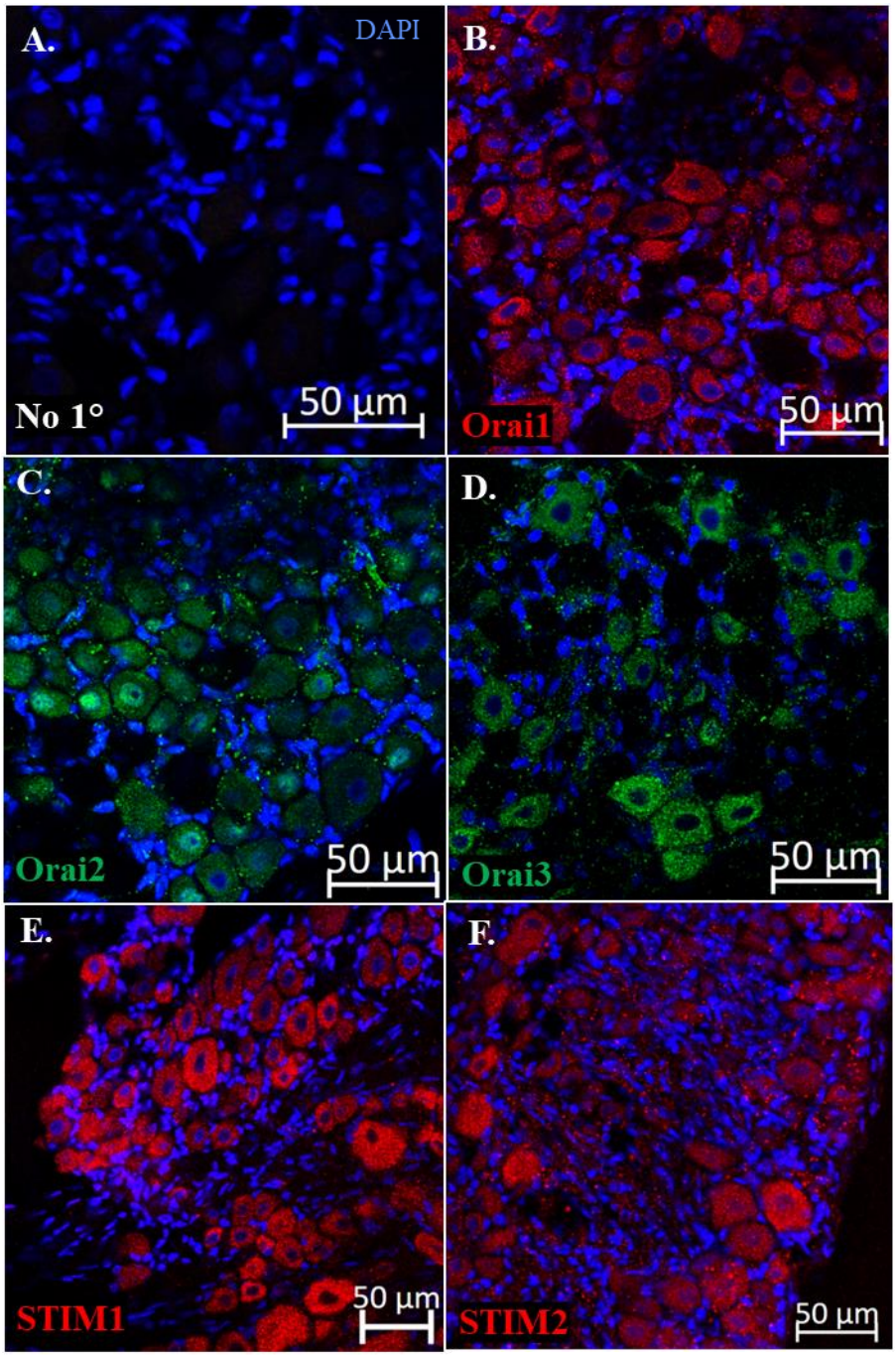

Figure 3.1. The protein expression of Orai and STIM isoforms within DRG neurons. Confocal micrographs for immunostaining with antibodies against Orai1 (B), Orai2 (C), Orai3 (D), STIM1 (E), STIM2 (F) and no-primary control (A). DAPI staining (blue) was used to identify nuclei. Scale bars = 50 µm.

3.2.2 Expression of Orai1 and Orai3 in DRG neurons

Immunohistochemistry experiments revealed that Orai1 was expressed in 74 ± 7% of all neurons. Also, the average somatic diameter of the Orai1-positive cells was 21.5 ± 0.9 µm, very similar to the mean somata size of all DRG neurons analyzed, 21.4 ± 1 µm. There was no evident preference of Orai1 expression in neurons of particular size (Figure 3.2).

As expected, co-staining experiments with neuronal markers NF200 (for medium and large myelinated neurons, Figure 3.3) and TRPV1 (for heat-sensitive nociceptors, Figure 3.4) demonstrated that Orai1 is uniformly distributed within neurons of different sensory modalities.

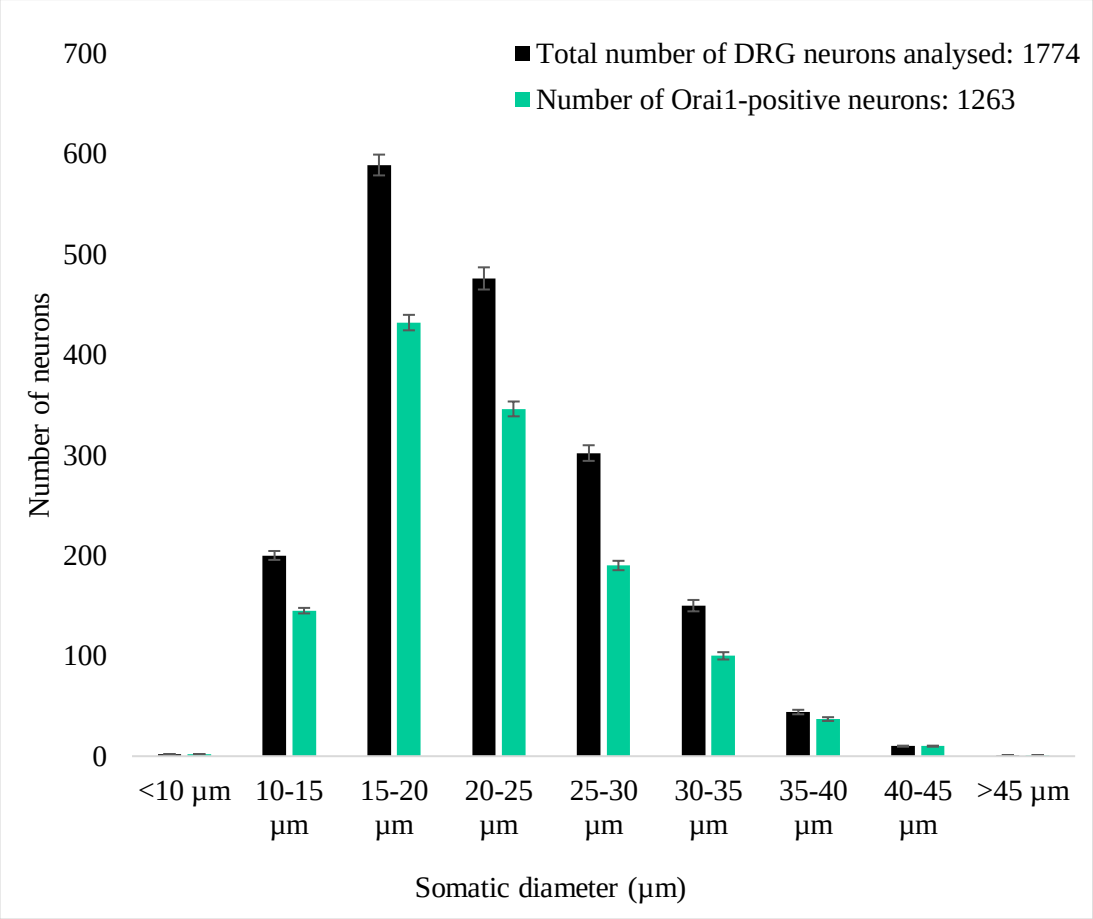

Figure 3.2. The distribution of Orai1 in DRG neurons. A. The somatic diameter of Orai1-positive neurons was measured, presented as a frequency distribution (green) and showed alongside the total number of neurons (black). Data is shown as the number of neurons of different somatic sizes ± SEM, from a total of 1774 neurons analysed (cumulative data from n=10 individual DRG sections).

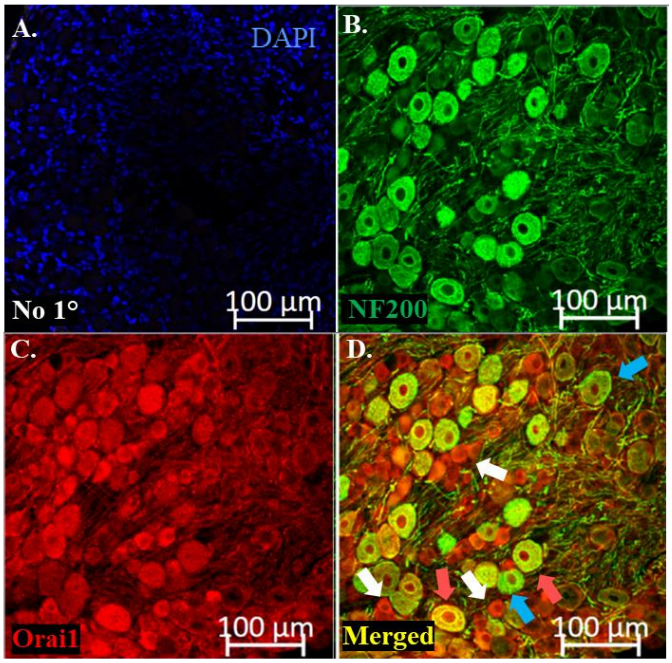

Figure 3.3 The expression of Orai1 in medium and large DRG neurons identified by NF200 marker. A. No-primary antibody control, blue-stained nuclei with DAPI. **B-D** Confocal images of immunostaining with antibodies against NF200 (B, green), Orai1 (C, red) and Co-staining (D, merged). White arrows indicate Orai1 positive neurons, blue arrows indicate NF200 only positive neurons and orange arrows indicate neurons expressing both NF200 and Orai1.

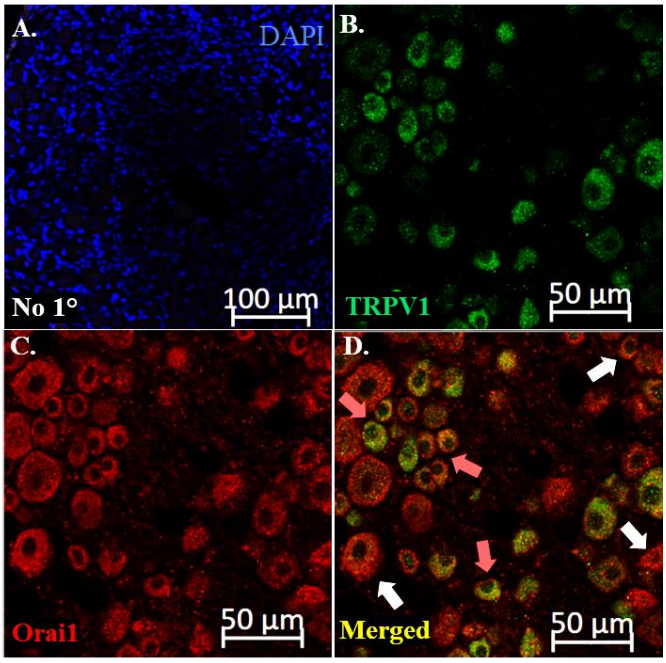

Figure 3.4 The expression of Orai1 in heat-sensing nociceptors identified by TRPV1 marker. A. No-primary antibody control, blue-stained nuclei with DAPI. **B-D** Confocal images of immunostaining with antibodies against TRPV1 (B, green), Orai1 (C, red) and Co-staining (D, merged). White arrows indicate Orai1 positive neurons, Orange arrows indicate neurons expressing both TRPV1 and Orai1.

Orai3 immunostainings demonstrated that this isoform was expressed in 47.6 ± 5.5% of all DRG neurons analyzed (Figure 3.5) and the mean somatic diameter of the Orai3-positive neurons was 22.67 ± 1.69 µm. Similar to Orai1, Orai3 seemed to be expressed uniformly in neurons of all sizes.

Orai1-Orai3 co-staining experiments strengthen the above observations. Figures 3.6 and 3.7 show that neither of the isoforms had a preferred distribution pattern and that Orai3 is less expressed than Orai1 in DRG neurons. Also, out of the total number of Orai1-positive neurons, 56.8 ± 13.4 % of cells were positive for Orai3.

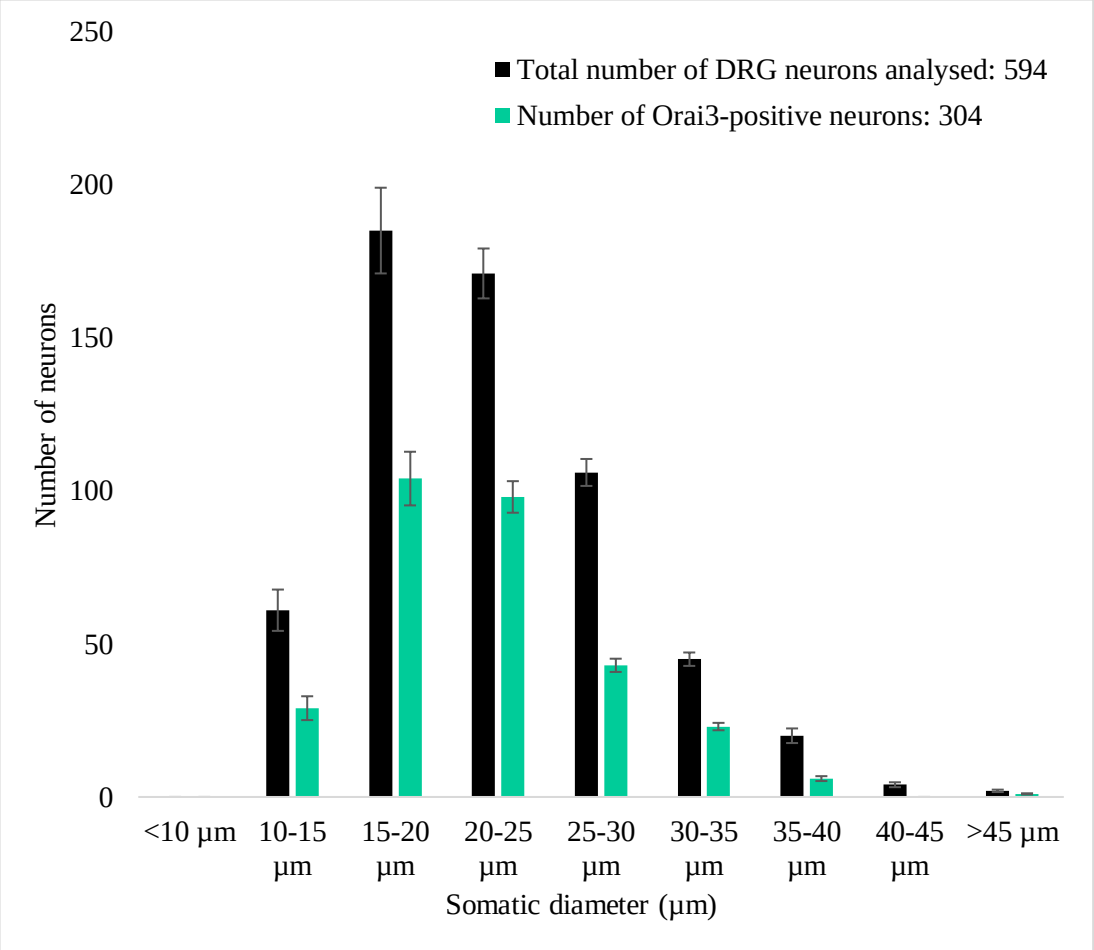

Figure 3.5. The distribution of Orai3 in DRG neurons. A. The somatic diameter of Orai3-positive neurons was measured, presented as a frequency distribution (green) and showed alongside the total number of neurons (black). Data is shown as the number of neurons of different somatic sizes ± SEM, from a total of 594 neurons analysed (cumulative data from n=5 individual DRG sections).

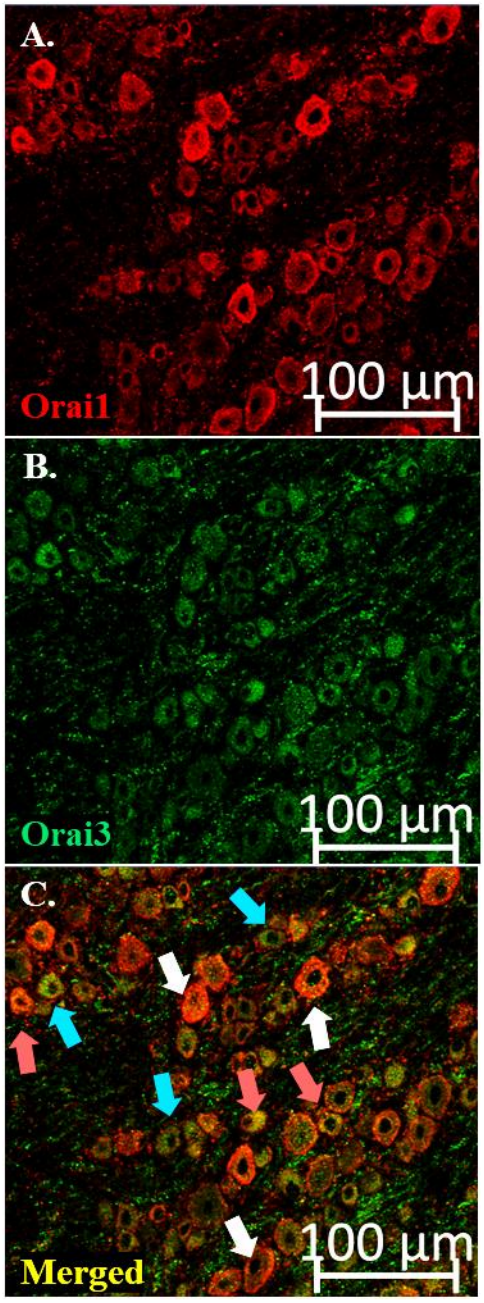

Figure 3.6. Co-localization of Orai1 and Orai3 in DRG neurons. Confocal micrographs of immunostaining with antibodies against Orai1 (A, red) and Orai3 (B, green) and co-staining (C, merged). White arrows indicate Orai1 only positive neurons, blue arrows indicate Orai3 only positive neurons and orange arrows indicate neurons that are positive for both Orai1 and Orai3.

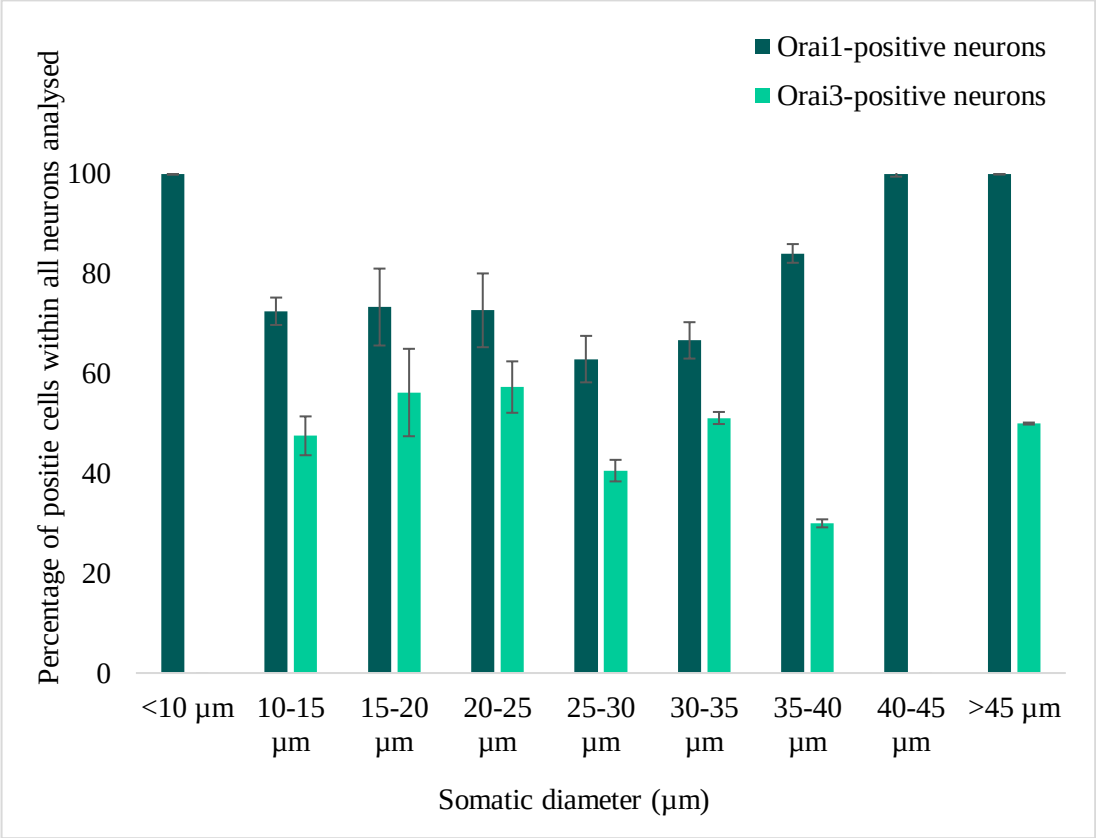

Figure 3.7. The distribution of Orai1 and Orai3 in DRG neurons. A parallel representation of the Orai1 (dark green) and Orai3 (light green) distribution preference within DRG neurons. Data for each isoform represents the percentage of positively-stained neurons as showed in Figure 3.2 and Figure 3.5, respectively.

3.2.3 Expression of STIM1 and STIM2 in DRG neurons

Immunohistochemistry experiments revealed that STIM1 was expressed in 57.4 ± 9.1% of all neurons (505 out of 931 neurons were positive). Furthermore, the mean somatic diameter of the STIM1-positive cells was 23.3 ± 1.2 µm, similar to the average somata size of all DRG neurons analyzed, 23.9 ± 1.5 µm. STIM1 immunostainings did not reveal a localization preference, being expressed uniformly in neurons of all sizes (Figure 3.8).

Co-staining experiments with neuronal markers NF200 (Figure 3.9) and TRPV1 (Figure 3.10) confirmed that STIM1 is expressed in medium and large myelinated neurons, as well as in heat-sensitive nociceptors.

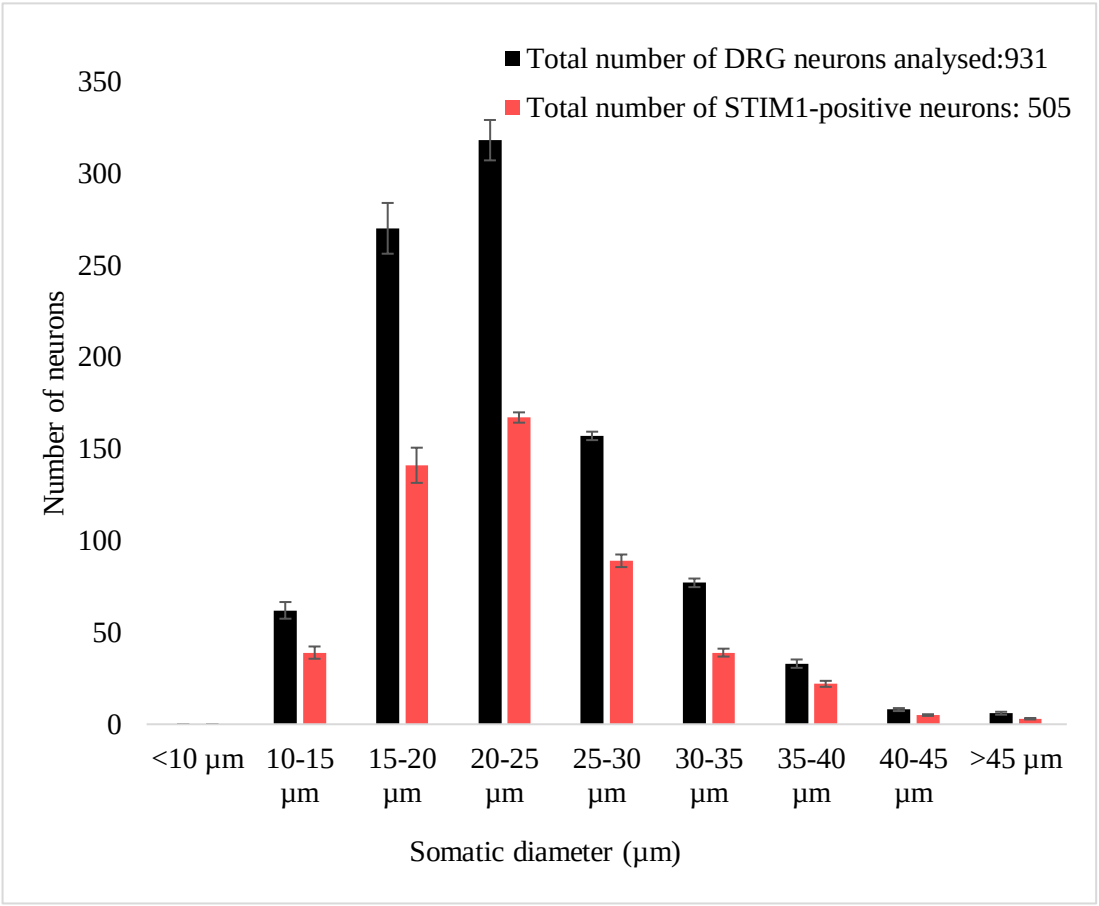

Figure 3.8. The distribution of STIM1 in DRG neurons. A. The somatic diameter of STIM1-positive neurons was measured, presented as a frequency distribution (red) and showed alongside the total number of neurons (black). Data is shown as the number of neurons of different somatic sizes ± SEM, from a total of 931 neurons analysed (cumulative data from n=5 individual DRG sections).

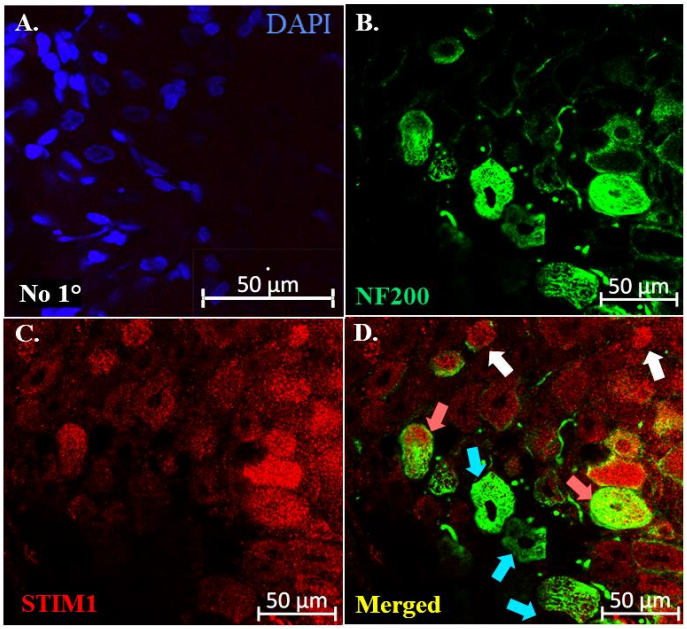

Figure 3.9. Co-localization of STIM1 and NF200 in DRG neurons. A. No-primary antibody control, blue stained nuclei with DAPI. **B-D.** Confocal images of immunostaining with antibodies against NF200 (B, green), STIM1 (C, red) and co-staining (D, merged). White arrows indicate STIM1 positive neurons, blue arrows indicate NF200 only positive neurons and orange arrows indicate neurons expressing both NF200 and STIM1. Scale bars = 50 µm.

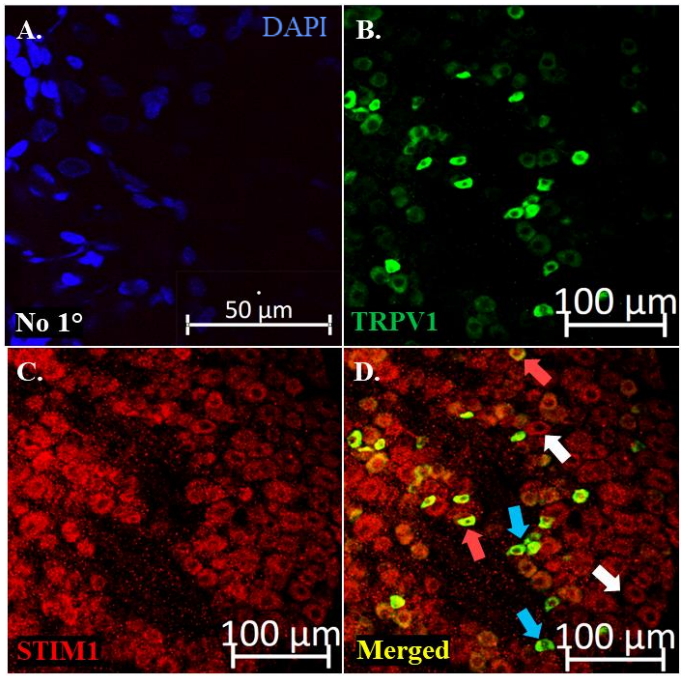

Figure 3.10. Expression of STIM1 in nociceptors expressing TRPV1. A. No-primary antibody control, blue stained nuclei with DAPI. **B-D.** Confocal images of immunostaining with antibodies against TRPV1 (B, green), STIM1 (C, red) and co-staining (D, merged). White arrows indicate STIM1 positive neurons, blue arrows indicate TRPV1 only positive neurons and orange arrows indicate neurons expressing both TRPV1 and STIM1.

STIM2 immunostainings demonstrated that 50.5 ± 9.5% of all DRG neurons analyzed expressed this protein (266 out of 612 neurons were positive) (Figure 3.11). The mean somatic diameter of the STIM2-positive neurons was 25.2 ± 2.6 µm, slightly greater than the overall average of 22.8 ± 2 µm.

STIM1-STIM2 co-staining experiments revealed that 46.7 ± 8.6% of STIM1-positive neurons co-expressed STIM2. Furthermore, Figures 3.12 and 3.13 show that while STIM1 has a uniform distribution throughout neurons of different sizes, STIM2 seemed to be expressed greater in medium and large somata.

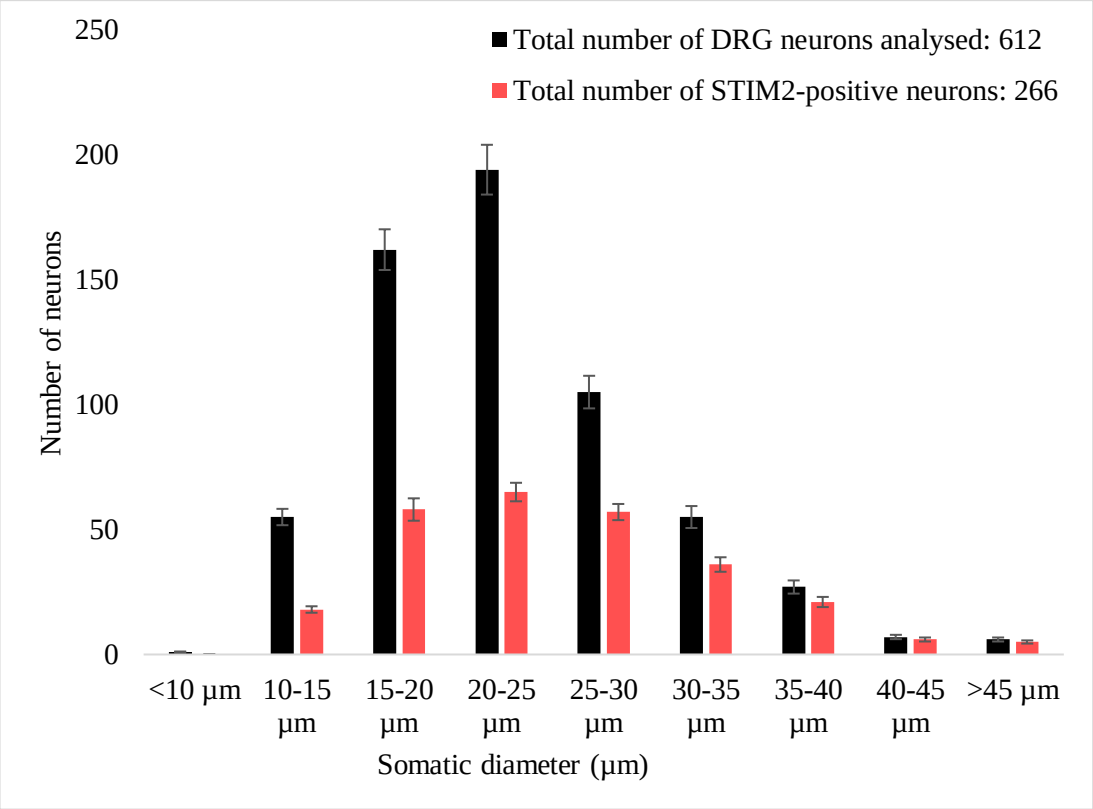

Figure 3.11. The distribution of STIM2 in DRG neurons. A. The somatic diameter of STIM2-positive neurons was measured, presented as a frequency distribution (red) and showed alongside the total number of neurons (black). Data is shown as the number of neurons of different somatic sizes ± SEM, from a total of 612 neurons analysed (cumulative data from n=5 individual DRG sections).

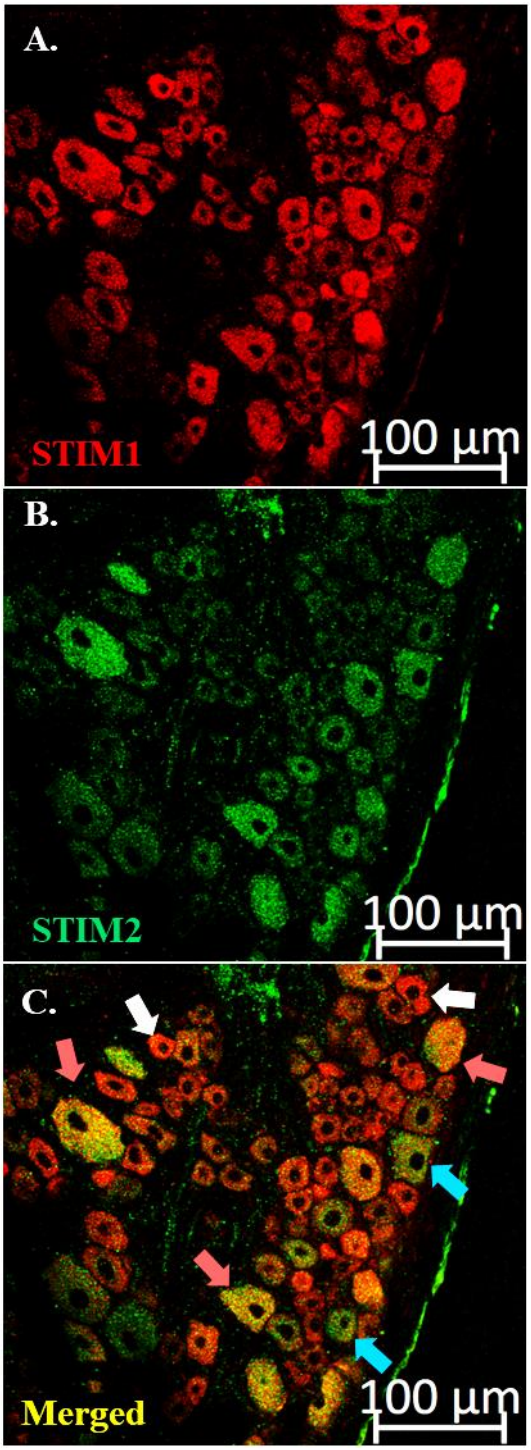

Figure 3.12. Co-localization of STIM1 and STIM2 in DRG neurons. Confocal micrographs of immunostaining with antibodies against STIM1 (A, red) and STIM2 (B, green) and co-staining (C, merged). White arrows indicate STIM1 only positive neurons, blue arrows indicate STIM2 only positive neurons and orange arrows indicate neurons that are positive for both STIM1 and STIM2.

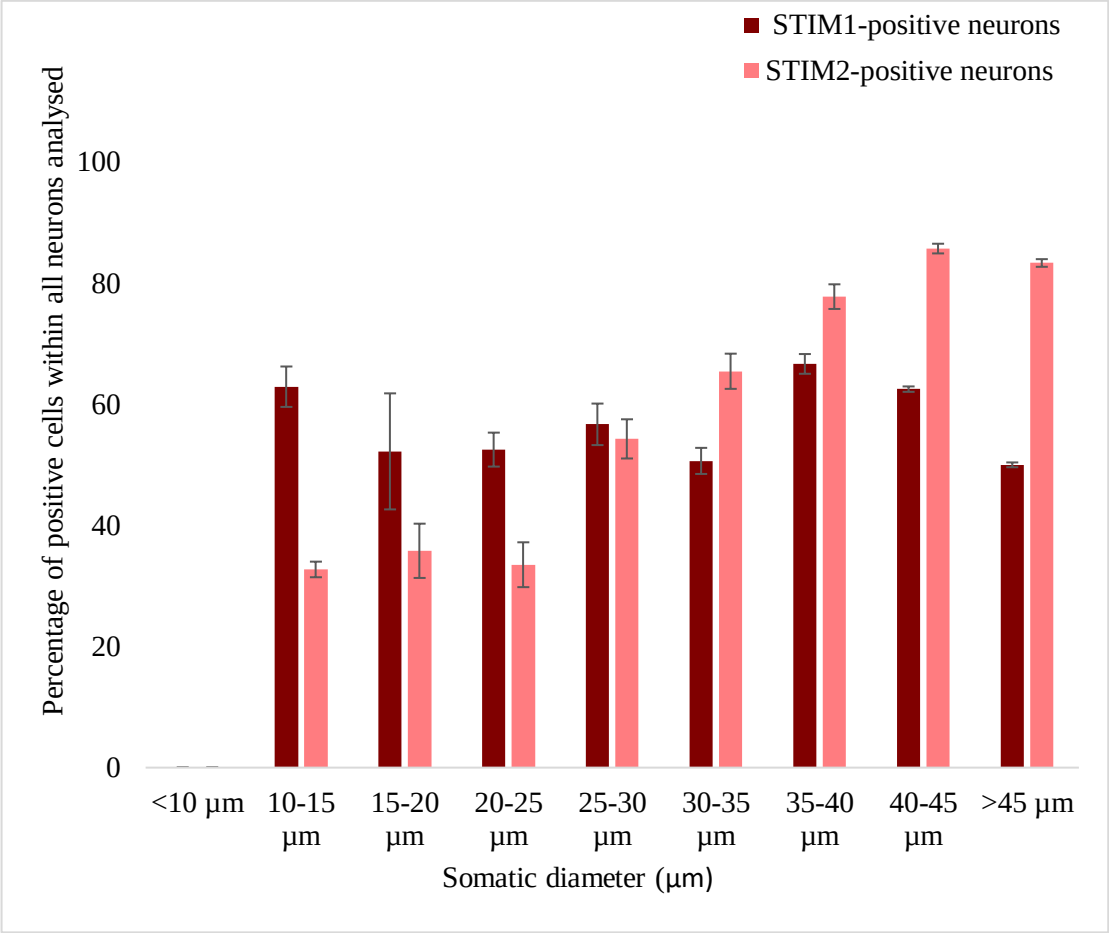

Figure 3.13. The distribution of STIM1 and STIM2 in DRG neurons. A parallel representation of the STIM1 (dark red) and STIM2 (light red) distribution preference within DRG neurons. Data for each isoform represents the percentage of positively-stained neurons as showed in Figure 3.8 and Figure 3.11, respectively.

3.2.4 Orai1 and STIM1 are interacting during SOCE in DRG nociceptors

The presence of SOCE in DRG neurons was demonstrated in several studies (Duncan et al. 2013, Szteyn et al. 2015, Qi et al. 2016). Moreover, attempts were made to clarify which of the CRAC components are present and involved in SOCE. Similar to non-excitable cells, Orai1 and STIM1 were put forward as the main players, while STIM2 and Orai3 were suggested to play supporting roles; yet, these hypotheses require further clarification (Wei D et al. 2017, Gruszczynska-Biegala and Kuznicki 2013). Interestingly, Wei D and colleagues observed that knocking-down either STIM1 or STIM2 in acutely dissociated DRG neurons results in similar SOCE impairment, however, the authors did not mention what types of neurons (e.g. large/small, myelinated/non-myelinated etc.) were tested. Similarly, thapsigargin-induced SOCE was impaired in Orai1 and Orai3 knockdown neurons (Orai1 siRNA proved the highest reduction) and not changed in Orai2 knockdown culture. Importantly, the protein levels of Orai1 and Orai3 in knockdown cultures was reduced only by 30% in this study. The same study also revealed that neurons transfected with STIM1-YFP showed a better puncta formation during SOCE as compared to STIM2-YFP. These findings suggest that between all 5 proteins, STIM1 and Orai1 are the main SOCE drivers in DRG neurons (Wei D et al. 2017).

It is fair to highlight that some of the performed experiments were conducted in transfected cells. For this reason, to test whether the endogenous CRAC components, STIM1 and Orai1, co-localize into puncta to facilitate binding and CRAC pore opening, I performed proximity ligation assay (PLA) targeting endogenously expressed Orai1 and STIM1 proteins in acutely dissociated DRG neurons. This technique aims at detecting protein-protein interactions and is more sensitive than the traditional immunohistochemistry. The proteins of interest are targeted with oligonucleotide-labelled antibodies that are capable of binding when in close proximity (at 40 nm apart). When the proteins are found within 40 nm or less from each other, a fluorescent signal (puncta, dot) is detected by confocal microscopy.

To validate the PLA approach, I performed negative and positive controls using Orai1 as a target protein. The negative control test consisted of a PLA experiment with a single primary antibody against Orai1 (no paired primary antibody was used). Analysis of the PLA-treated probe showed no fluorescent puncta, suggesting that the established protocol does not allow secondary PLA probes to co-localize 'by chance' (Figure 3.14.A).

Moreover, I also ran a positive control experiment where two different primary antibodies against Orai1 (one raised in mouse, one in rabbit) were used (Table 2.5). The reason for this approach is that both PLA probes (anti-mouse plus and anti-rabbit minus) attach to the previously bound antibodies against the same Orai1 protein. The results show fluorescent signals for Orai1-Orai1 PLA, demonstrating that the assay successfully recognizes the proximity of the secondary PLA probes once attached to the same target proteins (Figure 3.14.B).

After this validation, I used PLA as a tool to measure the proximity between Orai1 and STIM1 within DRG nociceptors. DRG neurons were cultured on microscope slides as previously described. Before fixing the cells with 4 % PFA, samples were washed with pre-warmed EC solution containing 2mM Ca^{2+} (Table 2.3). One group of samples were kept in this EC solution, while the other group were bathed in a Ca^{2+} free solution (also containing EGTA) to wash extracellular Ca^{2+}, followed by 5 minutes treatment with 250 nM BK solution (still in Ca^{2+} free conditions). The EC and BK solutions were removed from the control and SOCE induced cells respectively and replaced with 4 % PFA for 20 minutes. The purpose of this experiment was to fix the proteins into their specific cellular location during SOCE and compare the PLA signals to that of the cells with Ca^{2+} levels at rest. Therefore, I tested whether native STIM1 and Orai1 come in close proximity during SOCE as compared to Control (no store-depleted cells).

For measurements, I counted the number of fluorescent puncta with an intensity higher than 10 per each neuron. Then I divided this value by the cross-sectional area and reported the results as the mean number of puncta per μm^2 (Figure 3.15.C).

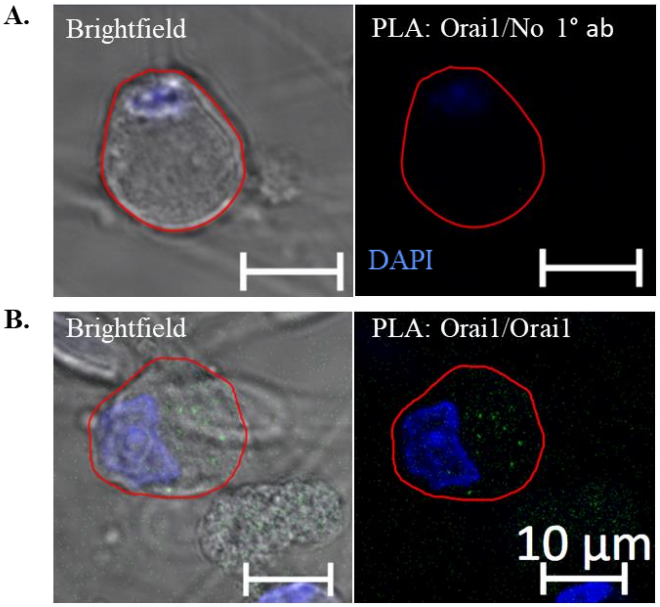

Figure 3.14. PLA protocol validation. A. Negative control based on using only one primary antibody against Orai1. **B.** Positive control based on Orai1-Orai1 PLA. Anti-Orai1 mouse and anti-Orai1 rabbit antibodies were paired to validate the positive PLA signal (green). Scale = 10 µm for all images.

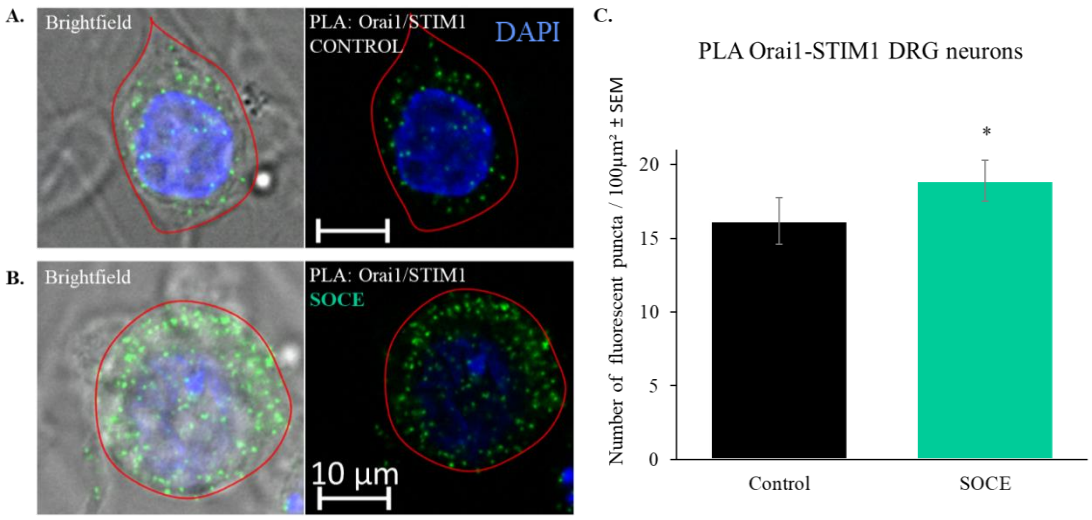

Figure 3.15. Orai1 and STIM1 are in contact during SOCE in DRG cultured neurons. A. Representative image of PLA experiments probing Orai1 and STIM1 proximity in small diameter DRG neurons. The Control group comprises of neurons with Ca^{2+} levels in the resting state. n=27 neurons, N=5 individual experiments. **B.** Representative image of PLA experiments probing Orai1 and STIM1 proximity during SOCE. This group was treated with 250 nM BK in Ca^{2+} free solution prior to fixation. n=33 neurons, N=6 individual experiments. **C**. Plot showing the number of fluorescent puncta per µm² for Orai1-STIM1 proximity in control versus depleted neurons. Scale = 10 µm, unpaired Student's t test, *p<0.05.

3.3 Discussion

This chapter demonstrates the localization pattern of CRAC components within DRG neurons and confirms that endogenously expressed STIM1 and Orai1 isoforms are co-localizing into puncta upon ER Ca^{2+} store depletion. These observations are important in the context of pain research as it has been previously shown that upon nerve injury SOCE is increased and cytosolic Ca^{2+} levels are elevated (Duncan et al. 2013, Gao et al. 2015).

3.3.1 STIM1, STIM2, Orai1 and Orai3 are expressed in DRG neurons

Immunohistochemical characterization of STIM and Orai proteins in DRG sections was carried out and further analyzed based on somatic size and co-localization with nociceptive neuronal markers.

Previous attempts were made to examine the CRAC components and SOCE in control and injured sensory neurons (Xia et al. 2014, Gao et al. 2015, Wei et al. 2017, Qi et al. 2016). While spinal cord dorsal horn neurons and have been the subject for several recent studies (Xia et al. 2014, Gao et al. 2015, Gemes et al. 2011), the presence of Orai and STIM isoforms within first-order neurons located in DRGs needed further clarification. DRG neurons express a variety of receptors and ion channels which modulate the membrane excitability but only recently an attempt was made to determine which STIM/Orai proteins are present and functional in DRGs (Qi et al. 2016, Wei et al. 2017). Relative mRNA levels and protein expression of each isoform has been determined and it was suggested that Orai1 and Orai3 may form homomultimers and contribute to SOCE in DRG neurons (Wei et al. 2017). Moreover, the same study reported that knocking-down both proteins abolishes membrane depolarization and thapsigargin-induced spike frequency, suggesting that these proteins are required for SOCE-induced neuronal excitability (Wei et al. 2017).

However, the exact preferred distribution of Orai and STIM family members within DRGs remained unelucidated. Therefore, this chapter brought evidence for the neuronal distribution of STIM/Orai proteins within DRGs based on different diameter neurons. Interestingly,

amongst SOC family (STIM and Orai isoforms), STIM1 and Orai3 seemed to be uniformly distributed throughout the DRG (Figures 3.5 and 3.8). Orai1 showed the highest overall expression of approximately 74% and it was identified in all large neurons that were analyzed, as opposed to Orai3 that showed a lower expression (Figure 3.7). While Wei and colleagues demonstrated that Orai1 and Orai3 together are responsible for SOCE in DRG neurons, my results revealed that some neurons express Orai3 alone which may lead to differences in SOCE activation and I_{SOC} properties (Figure 3.6). Further investigations are needed to confirm the homo/heterogeneity of Orai isoforms within sensory neurons and to establish their functional role depending on the neuronal subset they populate.

My attempts to investigate the expression of Orai2 failed to determine its distribution pattern in sensory neurons as the confocal images mainly revealed high nuclear staining. Wei and colleagues observed a high mRNA level of Orai2 in DRG, but knocking it down had no effect on SOCE (Wei et al. 2017). Future work might include testing the specificity of other antibodies against Orai2.

3.3.2 STIM2 is highly expressed in large myelinated sensory neurons

STIM2 distribution analysis demonstrated that while it was expressed only in 50% of all neurons analyzed, 34% of the small neurons (diameter <25 μm) revealed positive staining, while 80% of larger neurons (>40 μm) expressed this isoform (Figure 3.13). Hence, STIM2 is preferentially expressed by the myelinated fibers within the DRG. By contrast, STIM1 was uniformly distributed in neurons of all sizes suggesting that it might facilitate SOCE in pain sensing neurons greater than STIM2, while STIM2 might have a role in touch sensation as it was highly expressed in large mechanosensory neurons.

Other groups observed that STIM1 and STIM2 have a different Ca^{2+} sensitivity in such a way that STIM2 might restore Ca^{2+} levels only when there is a subtle decrease in the ER Ca^{2+} concentration (Gruszczynska-Biegala and Kuznicki 2013, Brandman et al. 2007). In contrary, a significant decrease (e.g. triggered by thapsigargin or a GPCR agonist) stimulates STIM1-

Orai1 interaction. A reason for this might be that STIM1 clusters approximately 70-times faster than STIM2 and is able to saturate Orai1 binding sites before STIM2 does (Stathopulos et al. 2009). Similarly, another group reported that STIM2 associates with and promotes STIM1 puncta formation in acinar cells and enhances SOCE at low agonist concentrations (Ling Ong et al. 2015). Low levels of stimulations seem to be enough for STIM2 to produce a physiological response, which complements the fast STIM1 mobilization when ER Ca^{2+} stores are substantially depleted (Ling Ong et al. 2015).

In conclusion, this ability of STIM2 to enable SOCE is relevant when there is less ER Ca^{2+} store depletion and when STIM1 diffuses freely within the ER membrane (Ling Ong et al. 2015). These observations alongside my findings, may suggest that STIM2 alone could have a functional role in touch sensation through mechanoreceptors and associated with STIM1 in pain sensing nociceptors. More investigations are needed to validate this hypothesis in DRG neurons, but STIM2 is clearly not a negligible protein.

3.2.4 Endogenous Orai1 and STIM1 are in contact during SOCE in DRG nociceptors

Orai1 and STIM1 remain the most plausible candidates to form the CRAC amongst their family members as they were shown to be expressed and function in a wide range of cells, including DRG and dorsal horn neurons (Xia et al. 2014, Gao et al. 2015, Qi et al. 2016). While a number of studies reported puncta formation and protein mobilization into clusters in transfected sensory neurons (Wei et al. 2017, Gao et al. 2016), to my knowledge, no attempts to research the interaction between endogenously expressed Orai1 and STIM1 proteins in DRG neurons were made.

Here I aimed at testing whether these proteins come in close apposition upon SOCE activation by running a PLA test that specifically two target proteins when these are within <40 nm of each other. The purpose of this experiment was to determine whether endogenously expressed Orai1 and STIM1 form complexes at the so-called ER-PM junctions of DRG neurons after BK-induced SOCE.

BK is a pro-inflammatory mediator released by immune cells after a tissue injury. In physio/pathological conditions, pro-inflammatory mediators (such as histamine or BK) act on the peripheral terminals of nociceptive afferents and either bind and activate specific receptors or sensitize them to other chemical or physical stimuli (Das V. 2015). BK has been shown to be a pain mediator in different organs and its effect is mediated via its receptors B_1R and B_2R (Steranka et al. 1988, Dray et al.1993). The stimulation of B_2R is known to activate the PLC pathway which results in the release of IP_3 and subsequent SOCE activation (Das V 2015).
Here I demonstrated (Figure 3.15) that upon ER Ca^{2+} store depletion with BK in Ca^{2+} free solution, more STIM1-Orai1 PLA puncta is detected per neuron, suggesting that these proteins move closer to each other and presumably form contacts in order to trigger Ca^{2+} influx. This experiment is particularly important because it shows that endogenously expressed STIM1 and Orai1 proteins are found within less than 40nm of each other after SOCE activation with BK.

Here I characterized the expression of STIM and Orai family members in primary afferent neurons. The next chapter aims at investigating the effect of CRAC inhibitors on inflammatory-mediated SOCE in DRG neurons.

Chapter 4. Pharmacology of CRAC channel inhibitors YM58483 and Synta66

4.1 Introduction

Since their discovery, CRAC channels gained growing interest and became pharmacological targets in several therapeutic areas such as immunology, cancer or allergy (McCarl et al. 2009, Motiani et al. 2010, Calcimedica Inc, 2017). A general interest in developing CRAC channel modulators is confirmed by the high number of patents issued in the past 8 years (Pevarello et al.2014). The strong correlation between genetic defects in Orai and/or STIM proteins and disorders ranging from immunodeficiency syndromes to Huntington's disease, triggered large investment in both academia and industry, into research in this area. Small biotech companies such as Synta Pharmaceuticals and Calcimedica are currently leading the way with several CRAC modulators in the pipeline however recently, large companies such as GSK and Hoffman-La Roche have also initiated major drug discovery initiatives in this field.

Due to the complexity of the machinery behind CRAC channels, several tools to assess their properties have been made available in the last decade. Experimentally, activating SOCE is possible by stimulating ER Ca^{2+} store depletion with agents such as SERCA pump inhibitors (e.g. thapsigargin, cyclopiazonic acid), calcium ionophores (e.g. ionomycin) or by triggering GPCR-mediated processes such as the activation of PLC pathway (Bird et al. 2008, Putney 2010). With growing knowledge regarding the molecular components of CRAC channels, an opportunity to investigate ways to inhibit SOCE led to the development of drugs that act either by blocking the Orai1 pore, or by interfering with the Orai1-STIM1 coupling machinery (Putney 2010, Parekh et al. 2010).

Historically, lanthanides Gd^{3+} and La^{3+} were widely used to block SOCE. Another group of blockers is represented by the fairly non-selective compounds 2-APB (Putney 2010) and ML-9 (a myosin light chain kinase inhibitor). 2-APB was shown to inhibit STIM1 translocation at the ER-PM junctions, but also to strongly inhibit I_{CRAC} through Orai1 channels (Peinelt et al.

2008). Interestingly, whilst widely being used as an inhibitor at higher concentrations, 2-APB also potently activates SOCE at 3-10 μM (DeHaven et al. 2008).

SOCE is a mediator of lymphocyte function with an important role in promoting inflammatory processes (Feske et al. 2012). Several pyrazole derivatives (BTP1, BTP2 and BTP3) have been shown to inhibit SOCE and the subsequent T-cell cytokine production (Trevillyan et al. 2001). Amongst them, BTP2 (also called YM58483, here referred to as YM) demonstrated the highest potency (Trevillyan et al. 2001). This drug has been proven to inhibit I_{CRAC} in T-cells with an IC_{50} of 10nM (Ishikawa et al. 2003, Zitt et al. 2004). YM's greater potency and channel selectivity resulted in a more preferential usage compared to 2-APB amongst research groups. For this reason, the current chapter investigated the SOCE inhibitory effect of this compound in DRG neurons.

Interestingly, multiple studies reported distinct protocols designed to assess the efficacy of YM. Several groups used YM in an acute manner (e.g. during SOCE) (Ishikawa et al. 2003) whereas others have used YM for longer periods of time (Zitt et al. 2004). While it is not clear whether the potency of YM is dependent on the duration of treatment, specific application timepoint (e.g. before or after SOCE initiation) and/or the type of cells, an attempt to evaluate the time-dependence of this drug's action has been made (Zitt et al. 2004). These authors preincubated Jurkat cells with YM for various periods of time and performed patch-clamp experiments to monitor I_{CRAC}. They showed that at 200 nM YM needs at least 2 hours to develop full I_{CRAC} inhibition, which contradicts the acute effect reported by Ishikawa and colleagues (Zitt et al. 2004, Ishikawa et al. 2003).

The effect of YM on immune cells and cytokine production generated a wider interest to investigate whether this compound may have analgesic properties, given that pain is frequently associated with immune responses (Gao R et al. 2013, Gao XH et al. 2015, Xia et al. 2014). A comprehensive study reported that YM effectively relieves spared nerve injury (SNI) pain, formalin-induced nociception as well as pain generated by mechanical, thermal or chemical stimuli (Gao R. et al. 2013). Moreover, in a collagen-induced arthritis (CIA) model,

YM was able to prevent the onset of inflammation and reduce pain hypersensitivity (Gao XH et al. 2015). The I_{CRAC} inhibitory effect of the drug was also tested on acutely dissociated DRG and dorsal horn neurons with results suggesting that YM is not only able to reduce the production and release of pro-inflammatory mediators, but also inhibits SOCE within pain-sensing neurons (Gemes et al. 2011, Gao R et al. 2013, Wei et al. 2017). These cumulative observations on YM's effects on cytokine production and reducing SOCE in nociceptors suggest that this drug might be a plausible candidate for relieving pain in a clinical setting.

Synta Pharmaceutical have also developed a range of SOCE inhibitors. Synta66 (Synta) has drawn a particular attention and has been tested in several studies (Putney 2010, Li et al. 2011). Similar to YM, Synta has been shown to down-regulate the production of cytokines and reduce thapsigargin-induced I_{CRAC} in Jurkat T cells with an IC_{50} of ~1 µM (Sabatino et al. 2009). This molecule also demonstrated high I_{CRAC} inhibition potency in vascular smooth muscle cells (VSMC), with an IC_{50} of 43 nM (Li et al. 2011). It was also proposed that Synta may have high CRAC specificity, proven by the lack of effect on TRPC1/5 channels or ATP receptors, which are known to contribute to SOCE in several cell types (Li et al. 2011). Moreover, experiments on VSMCs expressing YFP-tagged STIM1 showed that Synta does not affect the ER Ca^{2+} store discharge, the ability of STIM1 to sense Ca^{2+} depletion or STIM1 clustering into puncta (Li et al. 2011).

The effect of Synta was also tested on thapsigargin-induced SOCE in DRG neurons and calcium imaging experiments revealed that acute application of 30 µM of this inhibitor reduced Ca^{2+} influx by approximately 35% (Wei et al. 2017). Interestingly, the same group reported that 10 µM YM also inhibits SOCE by ~30% when applied immediately once SOCE reached maximal levels (Wei et al. 2017).

It is important to point out that the effects of YM, Synta and other similar SOCE inhibitors were mainly tested using patch-clamp techniques (to measure changes in I_{CRAC}) or calcium imaging (to analyse changes of cytosolic Ca^{2+v}once store-depletion and subsequent SOCE occur). Therefore, these studies generally report the effect of CRAC inhibitors observed in the

cytoplasm, while lacking information about their effect on the ER Ca^{2+} levels. Tools to directly measure intraorganellar Ca^{2+} concentration were previously used in research, but to a lesser degree (Palmer et al. 2004). Recently, genetically encoded Ca^{2+} indicators (GECI) and the Ca^{2+}-sensitive photoprotein aquaporin were described as tools to target Ca^{2+} within intracellular compartments (Bonora et al. 2013). The latest improved GECI are termed calcium-measuring organelle-entrapped protein indicators (CEPIA); they have a high dynamic range, better spatiotemporal resolution and are applicable to many cell types including neurons (e.g. Purkinje cells) (Suzuki et al. 2014).

The aims of the experiments reported in this chapter are to investigate the effects of two CRAC inhibitors, YM and Synta on the SOCE process and dynamics of ER Ca^{2+} in sensory neurons. Primarily, the protocols were optimised in an established cell line and subsequently the effects of the drugs were investigated in cultured DRG neurons.

4.2 Results

To test the effect of YM and Synta on the ER Ca^{2+} pool refill, I used R-CEPIA1*er* or G-CEPIA1*er* indicators to run intraorganellar Ca^{2+} imaging. The delivery of cDNA in CHO cells was done according to the manufacturer's recommendations and the protocol is detailed in Chapter 2. Time-dependence of transfection efficiency of R-CEPIA1*er* plasmid was determined by incubating the cells for 24, 48 and 72 hours at 37°C and 5% CO_2. Direct visualization of the transfected cells revealed that the optimal cell density and transfection efficiency (30% fluorescent cells, 60-70% cell confluence) was achieved after 48 hours of incubation.

A pilot experiment was run to determine whether SOCE activation by inhibiting SERCA pumps or by stimulating endogenous GPCRs reveal different store depletion/refill patterns. CHO cells expressing R-CEPIA1*er* were treated with 1 µM thapsigargin in Ca^{2+} free solution

to activate SOCE followed by re-introduction of 2 mM Ca^{2+} into the extracellular solution to promote store-operated Ca^{2+} influx (Figure 4.1).

CHO cells endogenously express purinergic receptors P2Y which are coupled with $G_{q/11}$-proteins and are activated by ATP (Erb et al 2012). Once stimulated, a PLC-dependent cascade generates the formation of IP_3 which further triggers the ER Ca^{2+} release through IP_3R. Thus, I also investigated the effect of ATP on the Ca^{2+} store depletion and refill. For this purpose, I stimulated SOCE by treating the cells with 30 µM ATP in Ca^{2+}free solution, followed by the re-addition of 2 mM Ca^{2+} (Figure 4.2).

The first experimental protocol revealed that thapsigargin depleted the ER stores slowly and incompletely, which is in line with what is known about SERCA inhibitors; they act as ER Ca^{2+} uptake blockers and generate a slow passive Ca^{2+} leakage into the cytosol modulated by RyR (Chelu and Wehrens 2007). Once exposed back to Ca^{2+}, only several cells revealed a partial store refill, while the others did not indicate any Ca^{2+} uptake back into the ER. Interestingly, depleting the stores by activating endogenous P2Y receptors with ATP demonstrated a much stronger and faster (within 30 s) store depletion. Once Ca^{2+} was re-introduced into the extracellular solution, it was up-taken rapidly and reached a plateau after 2 minutes.

The results of this pilot experiment suggest that stimulating $G_{q/11}$-coupled GPCR provides a better way of controlling the ER Ca^{2+} content as compared to thapsigargin.

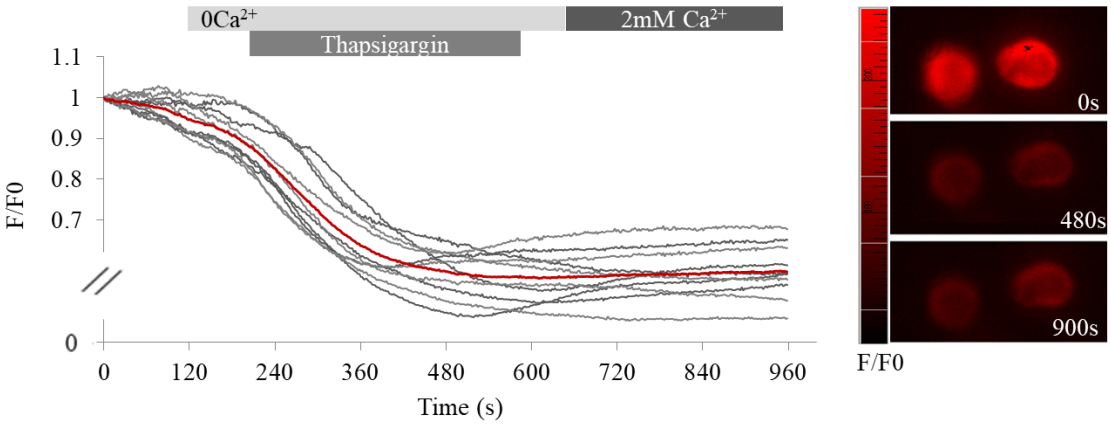

Figure 4.1. Thapsigargin-induced ER Ca^{2+}store depletion in CHO cells expressing R-CEPIA1*er*. Left panel, calcium imaging traces of individual cells (grey) and average (red). Right panel, representative image of the ER Ca^{2+} fluorescence at rest (time = 0s), during store depletion (time = 480 s) and during Ca^{2+} exposure to activate SOCE (time = 900 s).

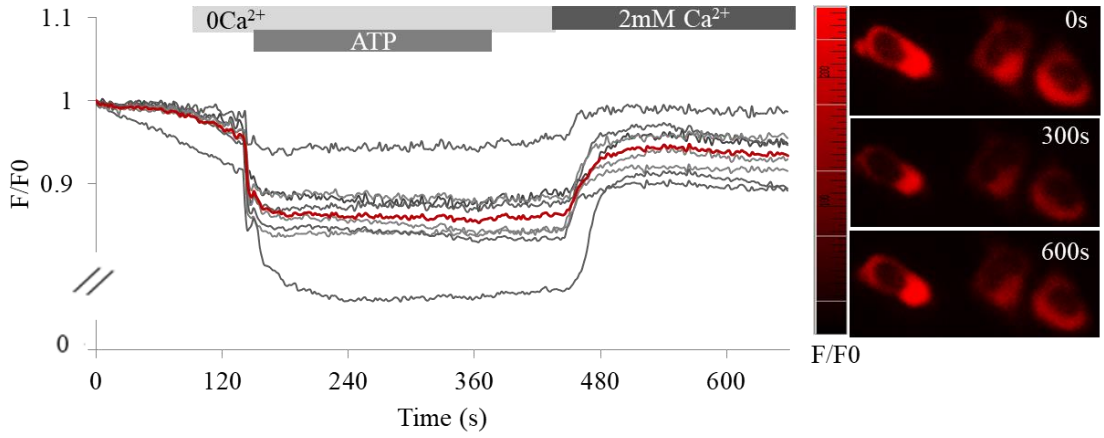

Figure 4.2. ATP-induced ER Ca^{2+}store depletion in CHO cells expressing R-CEPIA1er. Left panel, calcium imaging traces of individual cells (grey) and average (red). Right panel, representative image of the ER Ca^{2+} fluorescence at rest (time = 0s), during store depletion (time = 300 s) and during Ca^{2+} exposure to activate SOCE (time = 600 s).

4.2.1 YM58483 and Synta66 reduce the ER Ca^{2+} store refill in a time-dependent manner

Several studies have highlighted that CRAC inhibitors reveal a more pronounced effect when cells are treated for longer (Zitt et al. 2004). According to Zitt and colleagues, 200 nM YM demonstrated maximal SOCE inhibition when Jurkat T cells were treated for two hours prior to store-depletion. Multiple groups also revealed that CRAC inhibitors have a spontaneous effect when applied immediately after SOCE activation (Ishikawa et al. 2003).

To clarify these scenarios, I further investigated if the inhibitory effect of YM and Synta varies depending on the stage of the experiment: i) during SOCE, ii) during ER Ca^{2+} store depletion, or iii) when Ca^{2+} levels are at rest (pre-treatment for 1 hour prior to store depletion)

To do so, CHO cells were transfected with R-CEPIA1*er* as previously described and 1 µM YM and 3 µM Synta were used as indicated in Figures 4.4 and 4.6. The pre-incubation experiment was performed in EC solution containing either of the drugs. SOCE was induced with 30 µM ATP in Ca^{2+} free solution (treatment for 5 minutes).

The refill/depletion ratio in these three scenarios was compared with that of the control cells (no YM treatment; n=6). The refill/depletion ratio was determined as the maximum normalised fluorescence intensity (F/F_0) corresponding to the refill stage divided by the minimum normalised fluorescence intensity (F/F_0) corresponding to the depletion phase (Figure 4.3).

Figure 4.5. highlights that YM reduced the ER Ca^{2+} levels by 13.5 % in cells treated during SOCE, by 27.8 % in cells treated at store depletion and by 48.6 % in pre-incubated cells (n=6, p=0.009 Student's t test).

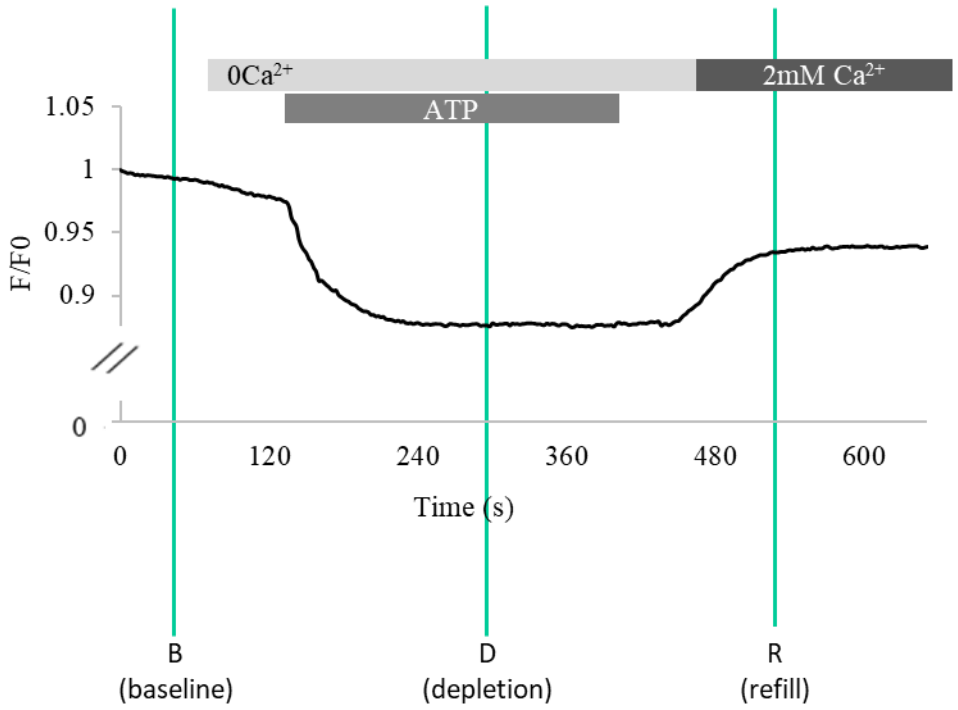

Figure 4.3. Representative image revealing the calculation for the Refill/Depletion ratio. Baseline (B) represents the F/F_0 at t=50s (before Ca^{2+} free solution was applied), Depletion (D) represents the minimal F/F_0 value during ATP treatment (ER Ca^{2+} pool depletion) and Refill (R) is the maximal F/F_0 value recorded during the Ca^{2+} re-addition phase (SOCE). Refill/Depletion ratio= (R-D)/(B-D). This calculation was used to represent data in Figures 4.5 (for YM) and 4.7 (for Synta).

A. Control

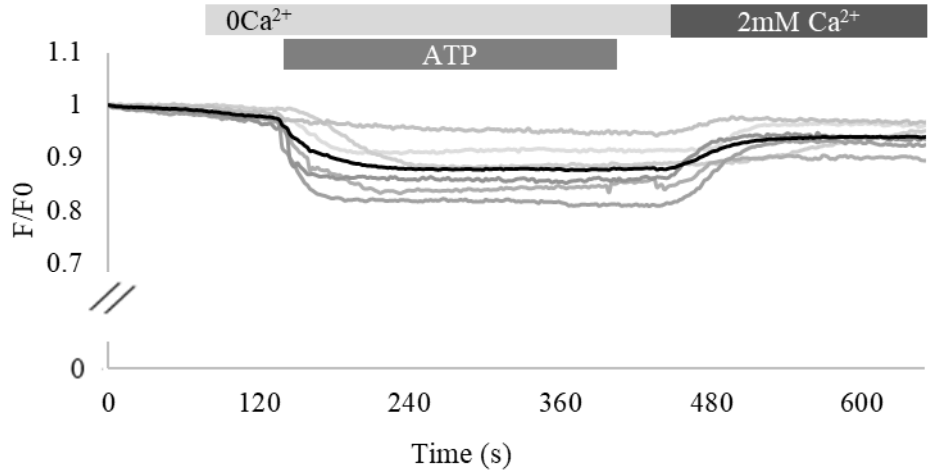

B. YM at refill

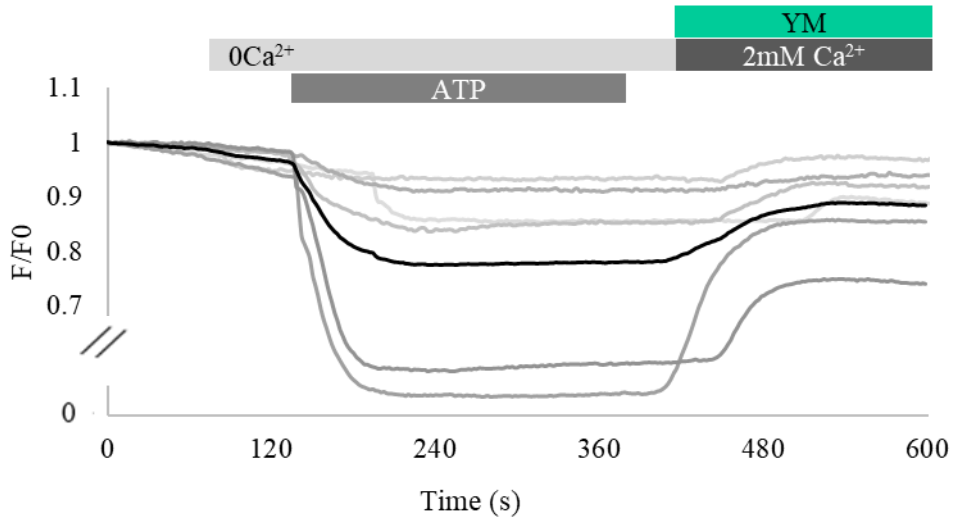

C. YM at depletion

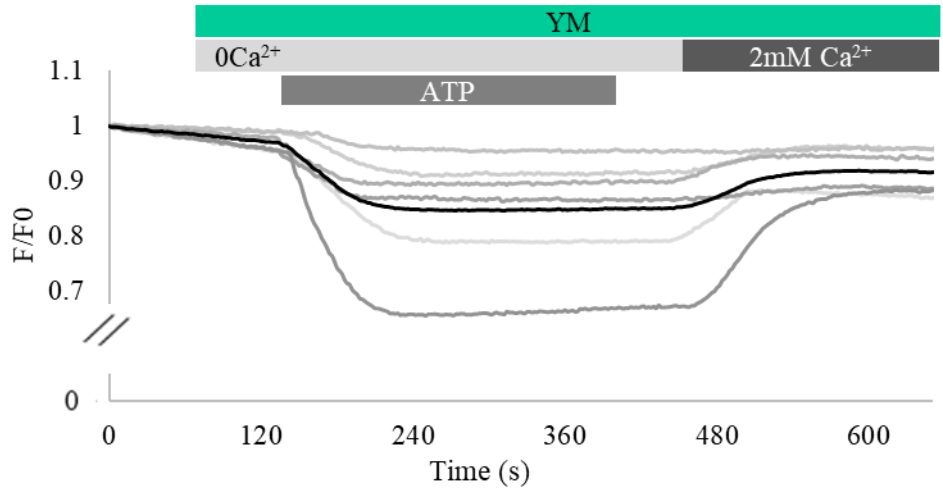

D. YM 1h pre-incubation

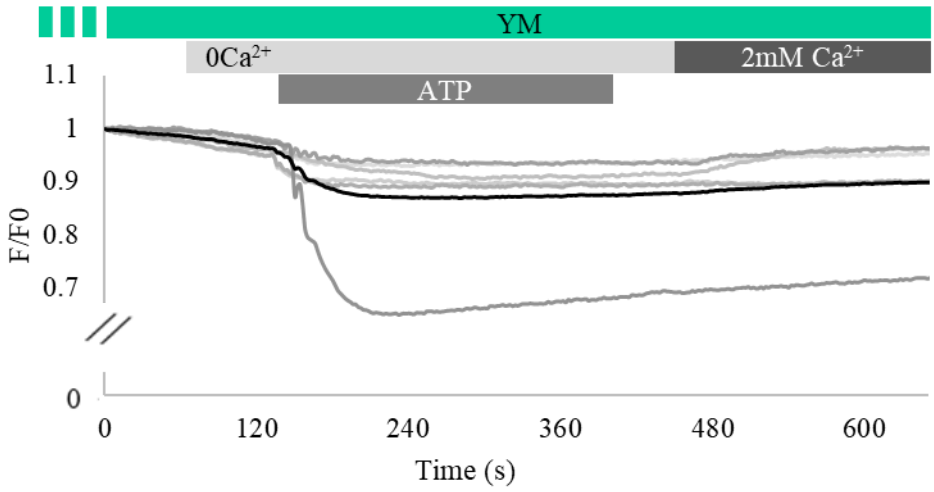

Figure 4.4. The state-dependence effect of YM on the ER Ca^{2+} store refill after ATP-induced SOCE. CHO cells overexpressing R-CEPIA1*er* revealed an unaltered ER Ca^{2+} uptake upon SOCE in non-treated group (A). Cells treated with YM revealed a variable ER replenishment depending on the time of administration: during SOCE only (B), during ER Ca^{2+} depletion phase and further on (C) and when pre-incubated for 1 hour prior to store depletion and for the duration of the experiment (D). Grey lines are individual experiments (n=6 for all data sets), black traces represent the mean for control and YM treated groups, respectively.

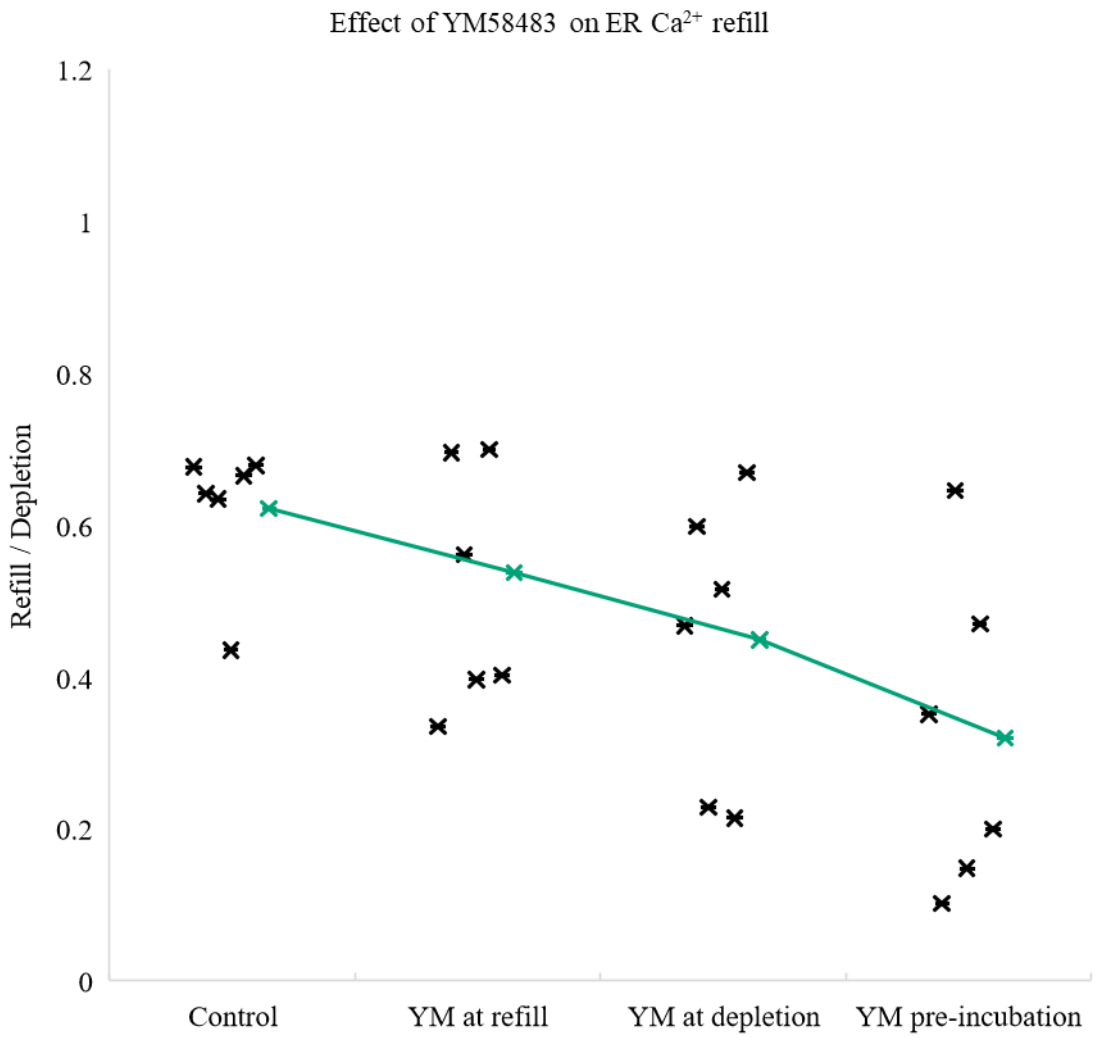

Figure 4.5. YM significantly inhibits the ER Ca^{2+} store recharge in a time-dependent manner. Analysis of experiments shown in Figure 4.4. Data is shown as Refill/Depletion ratio. Black marks are individual experiments (n=6 for each group) and green marks are mean values. *, $p<0.05$, One-Way ANOVA.

Similarly, 3 µM Synta was used to treat CHO cells expressing R-CEPIA1*er* in the same three different scenarios. Thus, cells were exposed to Synta during SOCE (Figure 4.6. B), when store-depletion was stimulated (Figure 4.6. C) and for 1 hour prior to experiment, including the duration of the recording (Figure 4.6. D).

The effect of this drug on the ER Ca^{2+} refill is summarised in Figure 4.7 where the refill/depletion ratio is shown. When cells were treated with Synta during the store refill period, ER Ca^{2+} uptake was reduced by 30.7 % (n=6, p=0.008, Student's t test), when applied during the whole discharge-recharge phase it decreased the store uptake by 45.0 % (n=6, p=0.0017, Student's t test) and when cells were pre-treated with Synta for 1 hour they revealed a reduced ER Ca^{2+}uptake by 53.70 % (n=6, p=0.00019, Student's t test).

A. Control

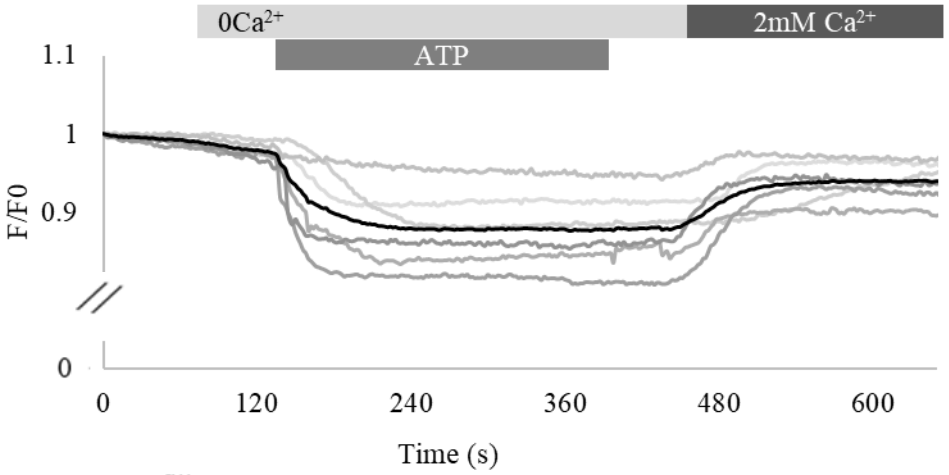

B. Synta66 at refill

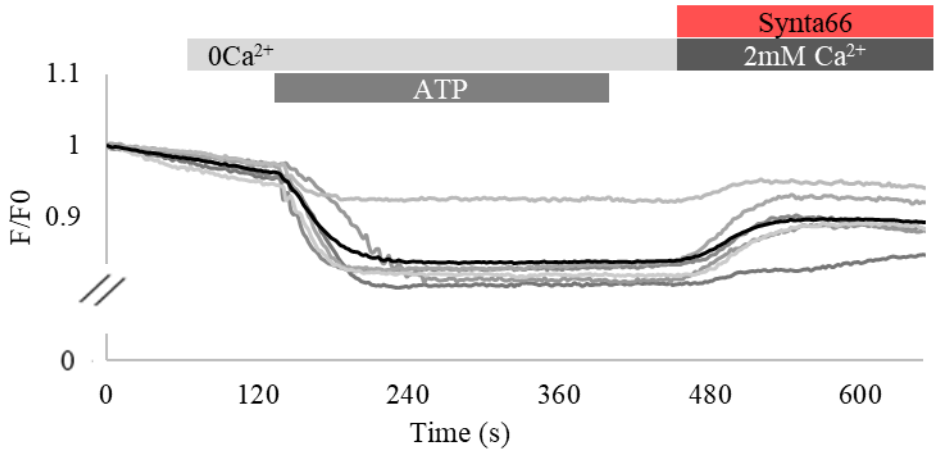

C. Synta66 at depletion

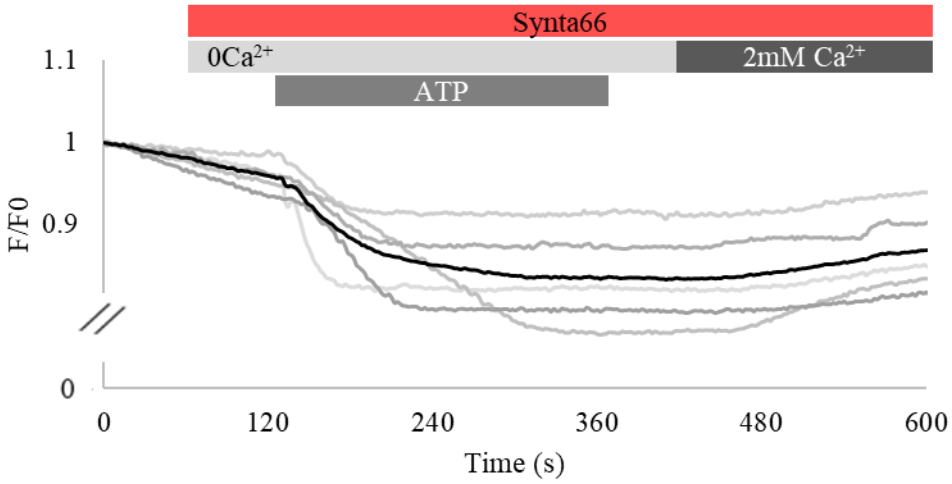

D. Synta66 1h pre-incubation

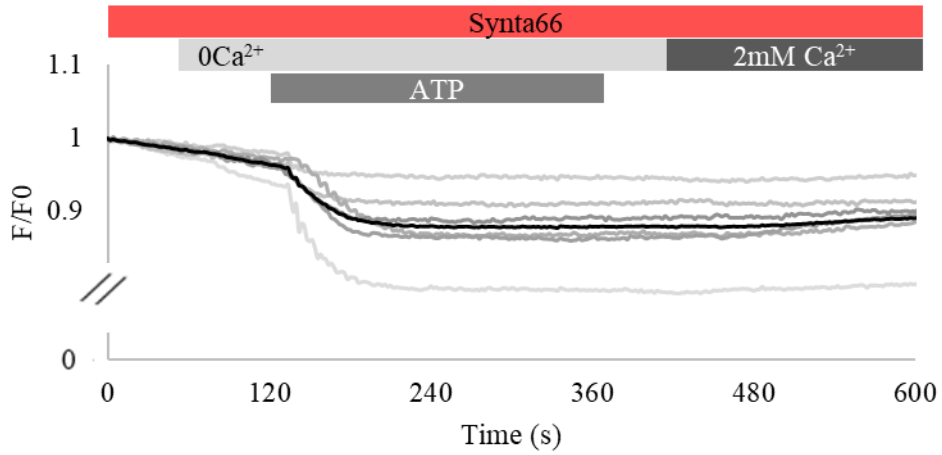

Figure 4.6. The state-dependence effect of Synta on the ER Ca^{2+} store refill after ATP-induced SOCE. CHO cells overexpressing R-CEPIA1*er* revealed an unaltered ER Ca^{2+} uptake upon SOCE in non-treated group (A). Cells treated with Synta revealed a slightly variable ER replenishment depending on the time of administration: during SOCE only (B), during ER Ca^{2+} depletion phase and further on (C) and when pre-incubated for 1 hour prior to store depletion, including during the duration of the experiment (D). Grey lines are individual experiments (n=6 for all data sets), black traces represent the mean for control and YM treated groups, respectively.

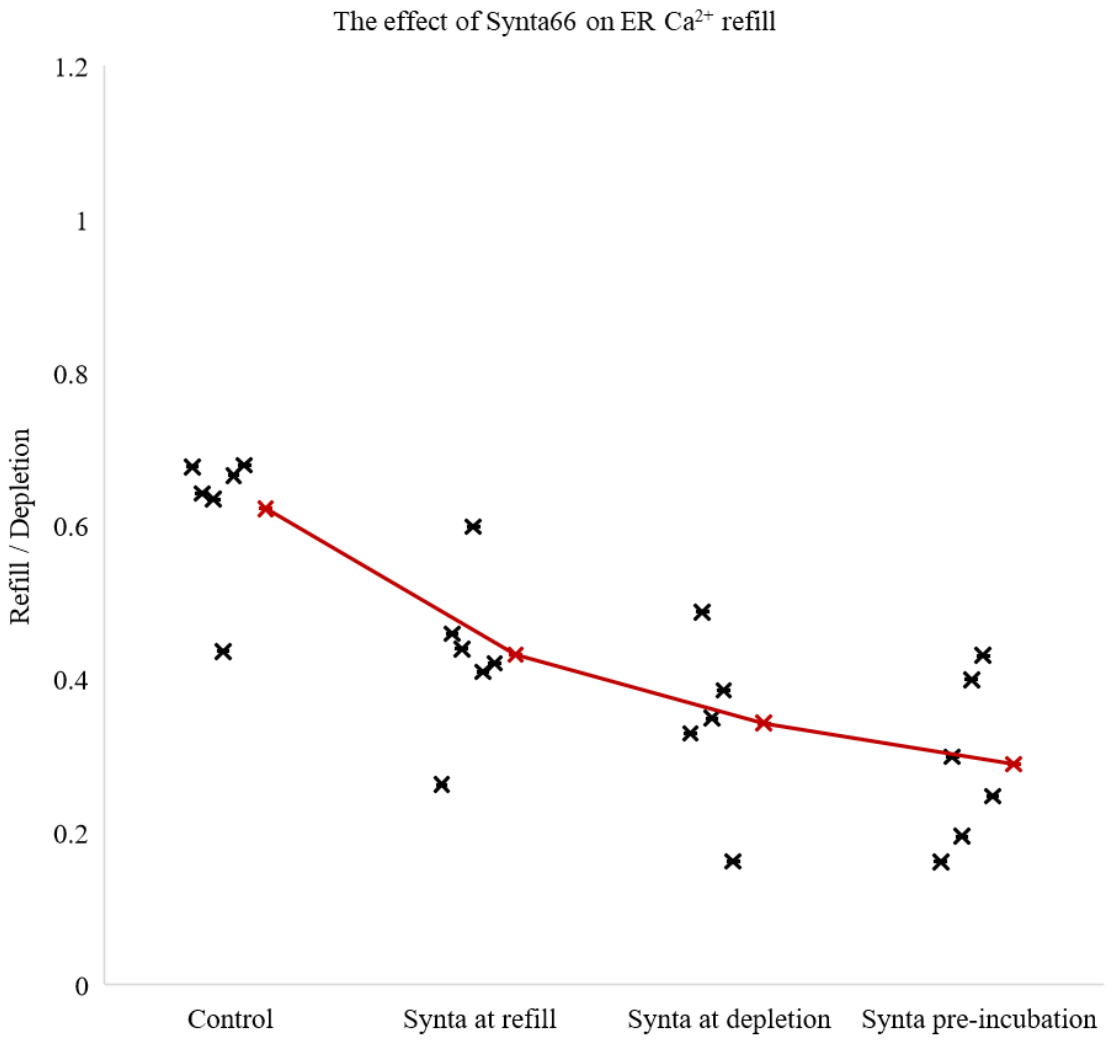

Figure 4.7. Synta significantly inhibits the ER Ca^{2+} store recharge in a time-dependent manner. Analysis of experiments shown in Figure 4.6. Data is shown as Refill/Depletion ratio. Black marks are individual experiments (n-6 for each group) and green marks are mean values. ***, $p<0.001$ One-Way ANOVA.

4.2.2 YM58483 and Synta66 reduce the ER Ca^{2+} store refill in BK treated cells.

One of the pro-inflammatory mediators released after a tissue injury is BK. Not only is BK a potent vasodilator able to reduce the peripheral vascular resistance, but it also contributes to the release of prostaglandin E_2 by binding to B_2 receptors (Shin et al. 2002). Pain sensing neurons highly express B2R and BK contributes to pain signalling by triggering PLC-dependent intracellular cascades, followed by the ER Ca^{2+} store depletion upon IP_3R stimulation. To investigate whether YM and Synta inhibit SOCE and subsequent ER Ca^{2+} refill in BK- treated DRG neurons, I optimized the experimental protocol based on the results presented above. Firstly, I transfected HEK293 cells with G-CEPIA1*er* and B2R and incubated them for 48 hours prior to the experiment day. To maximize the effect of CRAC inhibitors observed in ATP experiments, I pre-treated the cells with either 1 µM YM or 3 µM Synta for 1 hour. Cells were also continuously exposed to each of the drugs during the recording. SOCE was induced with 250 nM BK in Ca^{2+} free solution, followed by the re-addition of 2 mM Ca^{2+} (Figure 4.8. A).

Both YM and Synta significantly reduced the ER Ca^{2+} uptake shown as Refil/Depletion ration ± SEM (Unpaired Student's t-test, $p<0.05$, $n=6$ for all three groups) (Figure 4.8. B).

Interestingly, this experiment reveals a higher inhibitory potency of both drugs in BK-treated G-CEPIA1*er*-HEK cells over-expressing B2R as compared to ATP-treated CHO cells expressing R-CEPIA1*er*. In the BK scenario, YM and Synta reduced the ER Ca^{2+} uptake by 71.5 % and 62.36 %, respectively, which is 22.9 % higher for YM and 8.7 % higher for Synta as compared to the ATP experiments.

In conclusion, differences between the cell type, the Ca^{2+} indicator and the SOCE activator may generate some variability in Ca^{2+} measurements even in identical experimental designs and unchanged drug concentrations.

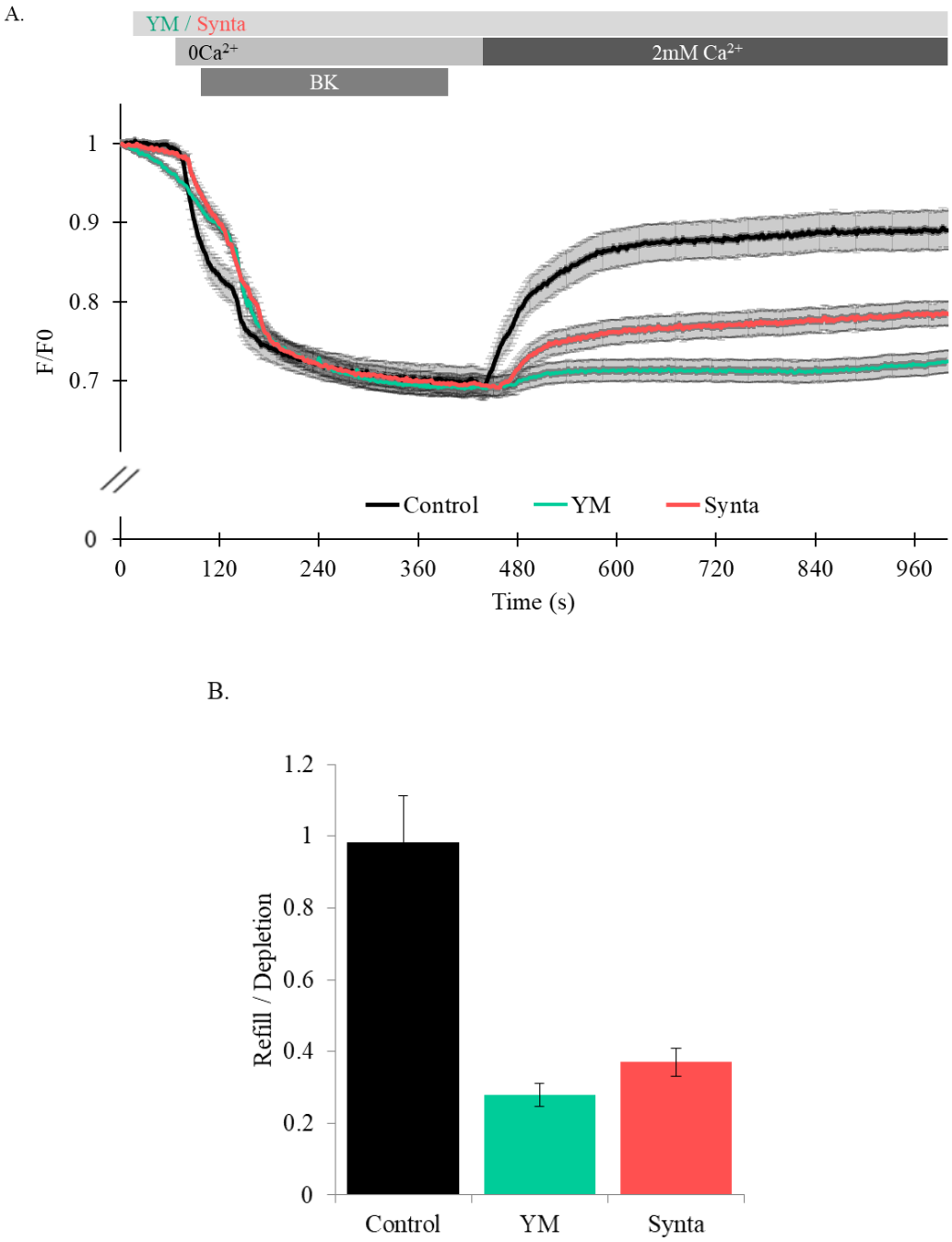

Figure 4.8 YM and Synta significantly inhibit the ER Ca^{2+} store refill after the BK-induced store depletion. A. Calcium imaging traces of HEK293 cells co-transfected with the G-CEPIA1*er* and B_2R in control conditions (black), and after the 1 hr pre-treatment with YM (green) or Synta (red); shown are mean F/F_0± SEM (n=6 for each group). B. ER Ca^{2+} content upon SOCE shown as a Refill/Depletion ratio. Values represent mean ± SEM; *, $p \leq 0.05$, One-Way ANOVA.

4.2.3 YM58483 and Synta66 alter SOCE in small diameter DRG neurons

To test whether YM and Synta demonstrate the same inhibitory effect in cultured sensory neurons, I transfected acutely dissociated DRGs with G-CEPIA1*er* or R-CEPIA1*er* as described in Chapter 2. Both genetically encoded Ca^{2+} indicators were successfully expressed in glial cells, but only G-CEPIA1*er* was present in a very small proportion of neurons. The transfection of primary neurons has been proven challenging and for this reason, only a small number of individual experiments were successfully completed.

The highlights of this attempt are that DRG neurons pre-treated with 1 μM YM revealed a reduced ER Ca^{2+} uptake upon BK-induced SOCE (Figure 4.9). YM potently inhibited SOCE such that the ER Ca^{2+} levels after Ca^{2+} add-back recovered to 37.4 % of the levels seen in the Control group (*, p= 0.04, Unpaired Student's t test, n=3 experiments for each group).

To further confirm the effect of both CRAC inhibitors in DRG neurons, I measured changes in the cytosolic Ca^{2+} load by the ratiometric dye fura-2. Similar with the previous experiments, I induced SOCE with 250 nM BK in Ca^{2+} free solution for 4 minutes, followed by re-addition of 2 mM Ca^{2+} to the extracellular solution to facilitate I_{CRAC}. Both YM and Synta were applied 1 hour prior to calcium imaging and this incubation was done simultaneously with the fura-2 loading. CRAC inhibitors were also applied throughout the recording. Neurons were initially selected based on their morphological properties and after running the experimental protocol, only those responsive to BK were included in the analysis.

Intriguingly, neither YM nor Synta altered the Ca^{2+} release from the ER pool induced by BK (Figure 4.10.B), but as expected, both drugs drastically reduced Ca^{2+} influx in DRG neurons (Figure 4.10.C). More precisely, YM inhibited SOCE by 93.0 % while Synta by 85.1 %.

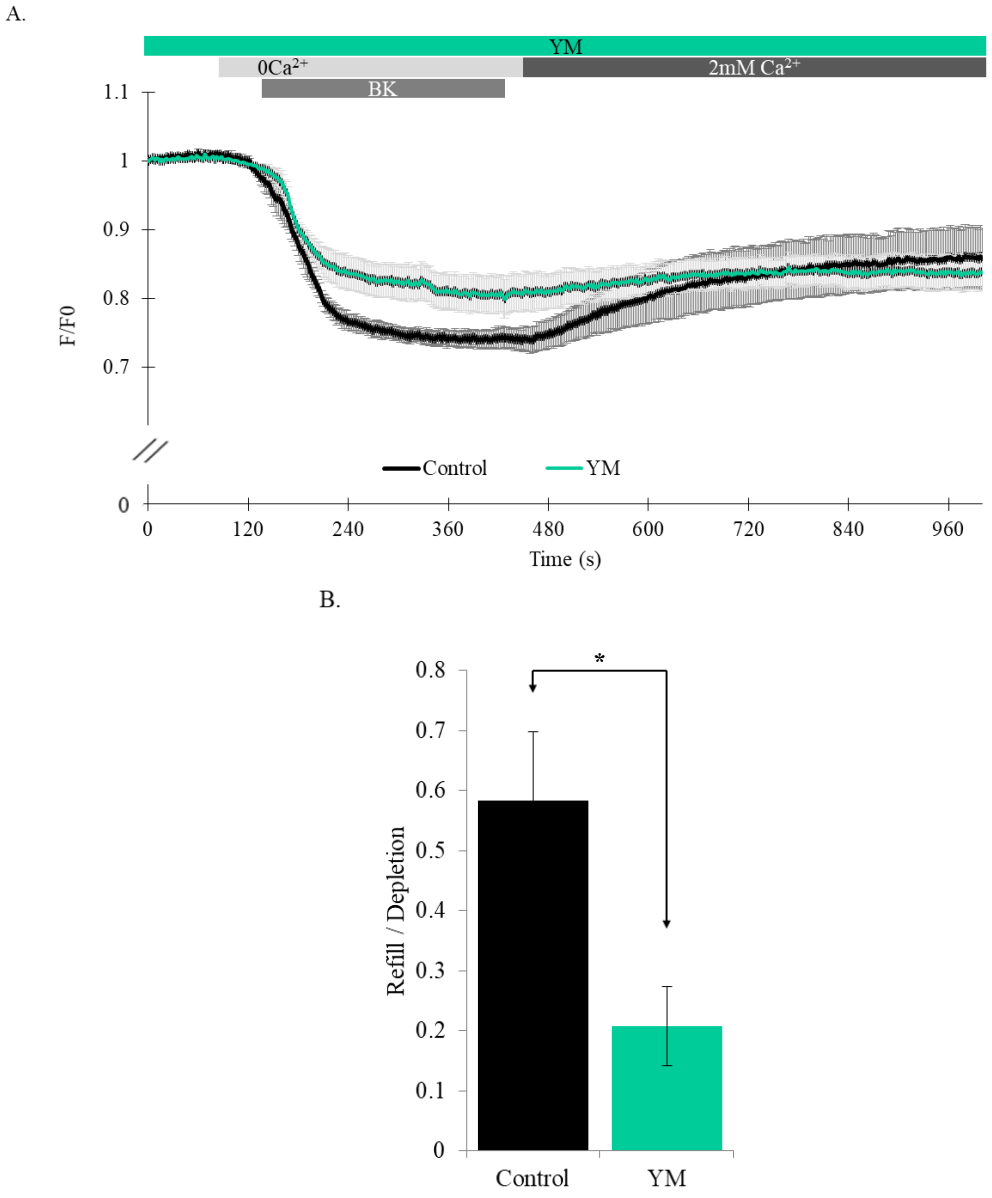

Figure 4.9 YM significantly inhibits the ER Ca^{2+} store refill after the BK-induced store depletion in DRG neurons. A. Calcium imaging traces offura2-AM loaded DRG neurons in control conditions (black), and after the 1 hr pre-treatment with YM (green) shown are mean F/F_0± SEM (n=3 for each group). B. ER Ca^{2+} content upon SOCE shown as a Refill/Depletion ratio. Values represent mean ± SEM; *, $p<0.05$, compared with Control group by unpaired Student's t-test.

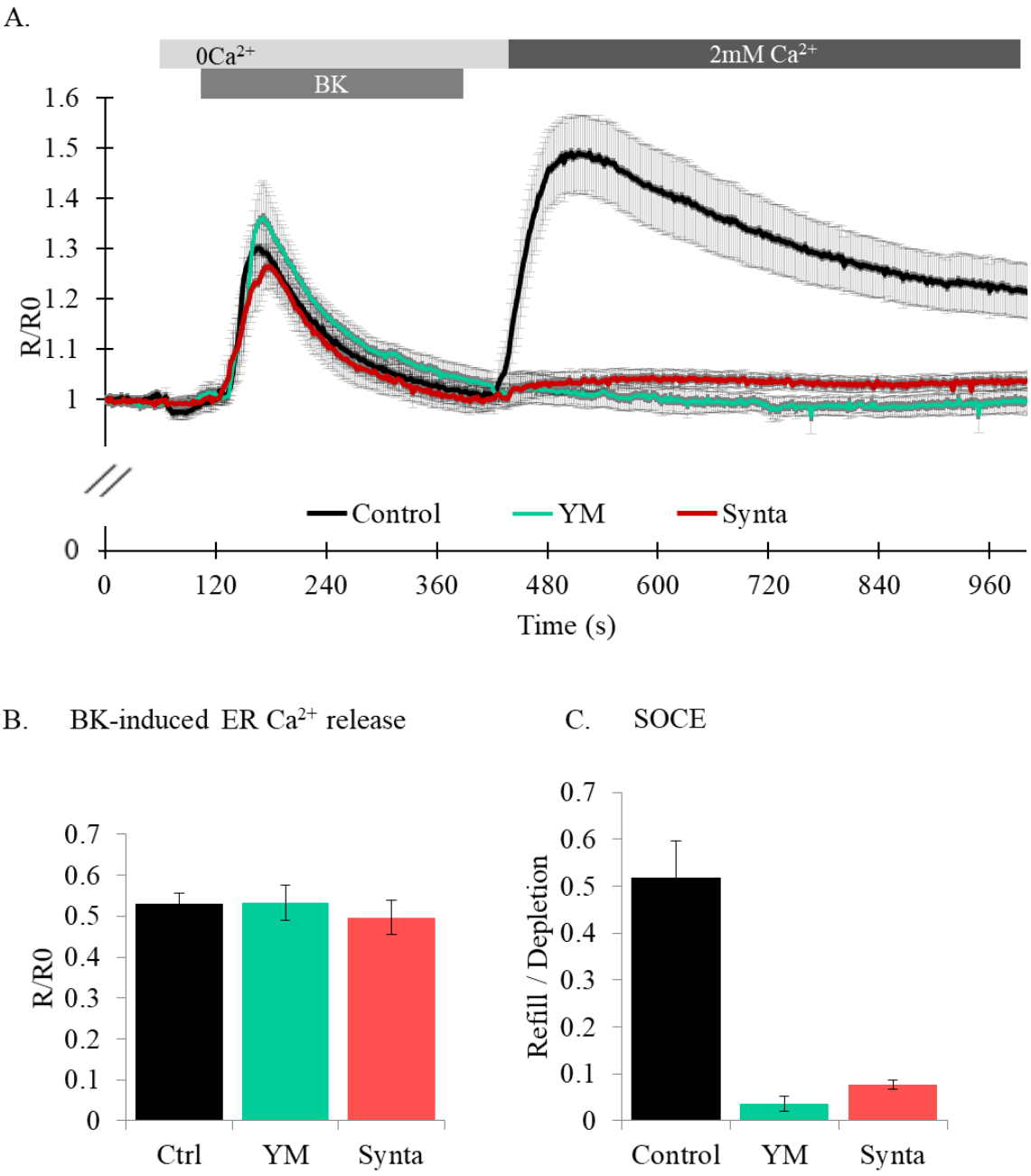

Figure 4.10 YM and Synta significantly inhibit SOCE in DRG neurons. A. Calcium imaging traces of the BK-induced store depletion and Ca^{2+} add-back-induced SOCE in DRG neurons of control neurons (black) and neurons pre-treated with YM (green) or Synta (red); shown are mean $R/R_0 \pm$ SEM (n=6 for each group). B. The effect of YM and Synta on the BK-dependent Ca^{2+} release from the ER pool. C. The effect of YM and Synta on BK-induced SOCE. Values represent mean ± SEM; ***, $p \leq 0.001$ One-Way ANOVA.

4.2.4 Lack of effect of YM on STIM1-Orai1 dynamics at ER-PM junctions

An important mechanism behind the activation of SOCE is the coupling between STIM1 and Orai1 at ER-PM junctions (Parekh and Putney 2005). This happens once ER Ca^{2+} levels drop enough to trigger STIM1 into extending, clustering and binding to the PM resident Orai1 (Parekh and Putney 2005, Putney 2010). The presence of both proteins in DRG neurons has been detailed in Chapter 3 of this thesis. As demonstrated, YM is a potent SOCE inhibitor that prevents ER Ca^{2+} store recharge in various cells, including DRG neurons. As demonstrated above, the maximal SOCE inhibition efficacy of either YM or Synta was achieved only after pre-incubation of the cells prior to store depletion, while acute application of either drug during SOCE had limited effect. This 'state-dependence' of the effect argued against simple ion channel pore block as a main mechanism of the CRAC inhibitors. Therefore, I also tested whether pre-treatment with YM affects STIM1-Orai1 coupling using the proximity ligation assay.

DRG neurons were cultured on microscope slides as previously described. Before PFA fixation, cells were pre-incubated for 1 hour with 1 µM YM, while the control group was kept in fresh extracellular solution. Both control and treated cells were subjected to store-depletion with 250 nM BK in Ca^{2+} free solution to stimulate STIM1-Orai1 coupling and subsequent SOCE activation. PLA signal was determined with LSM880 Zeiss microscope. The number of fluorescent puncta per μm^2 in YM treated cells was compared to the control group (Figure 4.11). The results showed prominent STIM1-Orai1 PLA signal in both groups with no significant difference in the number or fluorescent puncta. This result is in good agreement with the lack of effect of YM (or Synta) on the BK-induced Ca^{2+} release from the ER (Figure 4.10.B) and suggests that YM does not affect the ability of STIM1 to sense the Ca^{2+} discharge, nor its re-arrangement and movement closer to the PM where Orai1 resides. It is therefore unlikely that YM impairs SOCE by interfering with CRAC channel forming mechanism. The mechanism of the YM (or Synta) action remains to be elucidated; perhaps it interferes with

the assembly of the functional CRAC even though STIM1-Orai1 interaction still occurs, alternatively, these compounds may block the CRAC channel at a very slow rate.

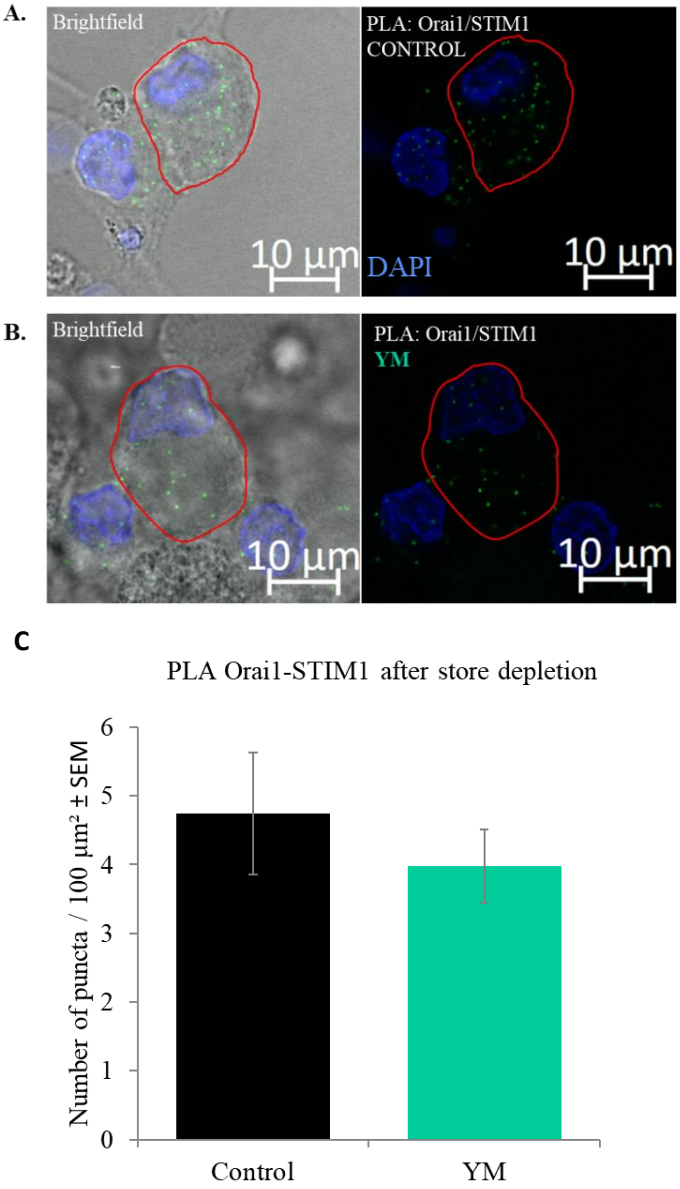

Figure 4.11. YM does not affect the Orai1 - STIM1 coupling in DRG neurons. Representative image of Orai1-STIM1 PLA signal in small diameter DRG neurons in control group, (A, store-depleted and non-treated with CRAC inhibitor, n=5) and YM-treated group (B, store-depleted and pre-treated with YM for 1 hour, n=5).

4.3 Discussion

This chapter aimed at investigating the effect of two widely used CRAC inhibitors in DRG neurons: YM58483 and Synta66. Firstly, I optimized the drug application protocol to determine their effects on ER Ca^{2+} loading in SOCE-induced scenarios, in CHO cells transfected with R-CEPIA1*er*. Secondly, I investigated the effect of these CRAC inhibitors on BK-induced SOCE in DRG neurons and whether YM alters the STIM1-Orai1 interaction in nociceptors.

4.3.1 YM58483 and Synta66 reduces the ER Ca^{2+} store refill in a ”state”-dependent manner

Several groups reported that CRAC inhibitors, including YM, demonstrate a spontaneous inhibitory effect on SOCE which was not evident in my experiments (data not shown). For this reason, I hypothesized that the efficacy of inhibition may depend on the state of the STIM1-Orai1 complex. Hence, I designed an experimental paradigm to test how the effect of YM and Synta varies dependent on the time of drug application (Figure 4.4 and 4.6). Zitt and colleagues attempted to demonstrate the dose and time-dependence of YM in Jurkat T cells and showed that whilst a spontaneous SOCE-inhibitory effect was still observed, the maximal inhibition happened after 2 hours of treatment with 200 nM YM. Their results were achieved by measuring cytosolic Ca^{2+} levels, however this current chapter focuses on the effects of both YM and Synta on the ER Ca^{2+} content specifically, given by ER targeted Ca^{2+} imaging. When cells were only treated during SOCE or during store-depletion, a reduced level of ER Ca^{2+} refill was noticed, but to a lower degree as compared to when the cells were pre-treated for 1 hour prior to store-depletion (Figures 4.5 and 4.7). This finding suggests that CRAC inhibitors might interfere with the STIM/Orai machinery or may simply require a longer duration of treatment for a greater effect. A partial effect on the ER Ca^{2+} refill may still result in subsequent SOCE activation, whereas preventing store replenishment completely would impair further Ca^{2+} influx generated by CRAC channels.

4.3.2 YM58483 and Synta66 reduce the ER Ca^{2+} store refill in BK treated cells.

In order to mimic an inflammatory-pain signalling scenario, I used BK as a model for GPCR-induced SOCE. BK is an endogenously released compound with pro-algesic and pro-inflammatory properties. Amongst other mediators (ATP, Histamine, Substance P), it is synthetized locally, once a tissue is injured. To measure the effect of pro-longed treatment with YM and Synta on BK-induced store-depletion, I over-expressed B_2R and G-CEPIA1*er*-in HEK cells and showed that both drugs significantly prevented the restoration of the ER Ca^{2+} levels. This experiment also confirms the previous results obtained with the ATP-induced SOCE scenario and serves as a pilot prior to investigating the effect of CRAC inhibitors in pain sensing neurons.

4.3.3 YM58483 and Synta66 alter SOCE in pain sensing DRG neurons

Transfecting acutely dissociated DRG neurons with either R-or G-CEPIA1*er* proved to be challenging, therefore a limited number of cells were recorded and only the effect of YM on DRG neurons was tested. Despite of these limitations, a significant reduction in the ER Ca^{2+} uptake induced by YM preincubation was observed (Figure 4.9.B). To continue investigating the effect of CRAC inhibitors in this paradigm, a new transfection method (or even viral gene delivery) should be considered to better deliver the vectors inside the neurons.

To further strengthen the results observed at the ER Ca^{2+}compartment in DRG neurons, I also measured the Ca^{2+} dynamics at the cytosolic level. Wei and colleagues recently reported that 10 µM YM and 30 µM Synta inhibit thapsigargin-induced SOCE in DRG neurons (Wei et al. 2017). Interestingly, both drugs were applied acutely, immediately after maximal SOCE was reached. Using this methodology, YM and Synta demonstrated an inhibitory effect of approximately 30 % (Wei et al. 2017). The findings detailed in this chapter demonstrate that even at 10-times lower concentration (as compared to that used by Wei and colleagues), 1 hour pre-incubation with 1 µM YM and 3 µM Synta revealed SOCE inhibition by 93.04 % and 85.14 %, respectively (Figure 4.10.C). Moreover, neither YM nor Synta affected the Ca^{2+}

release from the stores during BK application (Figure 4.10.B), suggesting that these drugs interfere only with mechanisms underlying SOCE (either by blocking the channel's pore at a slower rate, or by affecting the CRAC channel formation).

4.3.4 Lack of effect of YM on STIM1-Orai1 movement at ER-PM junctions

A widely accepted mechanism for SOCE activation is through STIM1 sensing the ER Ca^{2+} store discharge, its extension and clustering at ER-PM junctions. This is followed by its binding to PM resident Orai1 protein and forming the CRAC channels that open and allow Ca^{2+} influx (Putney 2010, Luik et al. 2006). This is a reversible process, as when the ER Ca^{2+} pool recharges, STIM1 and Orai1 unbind and return to their resting states diffusing freely in the ER and plasma membrane, respectively (Luik et al. 2006, Park et al. 2009). Since SOCE inhibition by either YM or Synta observed in the present study was most efficacious in a scenario when cells were preincubated with the drugs prior to store depletion and SOCE activation, it is logical to hypothesise that the mechanism of the drug action in this case could be the interference with the CRAC channel assembly.

To test whether YM may interfere with STIM1-Orai1 coupling, I investigated if pre-treatment of small-diameter DRG neurons for 1 hour with YM reduces formation of STIM1-Orai1 complexes (as detected with the PLA assay). For this experiment, all cells were store-depleted and SOCE-induced with BK, for consistency with calcium imaging experiments. Interestingly, YM did not demonstrate an inhibitory effect on Orai1-STIM1 puncta formation (Figure 4.11). This suggests that the drug may not affect the ability of STIM1 to sense store depletion (the latter process is actually not affected by either of the drugs), nor its movement closer to PM to recruit Orai1 proteins. These results are consistent with a recent study investigating the effects of Synta on STIM1 clustering in vascular smooth muscle cells (Li et al. 2011). The authors reported that Synta may not act by affecting store depletion, its sensing by STIM1 nor inhibiting the re-arrangement and subsequent movement of STIM1 at the ER-PM junctions (Li et al. 2011) Having said that, the resistance of STIM1-Orai1 machinery to YM and Synta (as assessed with PLA in this study and with fluorescence microscopy by Li

and colleagues) does not rule out a possibility that the drugs may interfere in some way with the physical coupling between the proteins and formation of functional ion channel pore. From a pharmacological perspective, CRAC channels inhibitors such as YM and Synta reveal a high therapeutic potential in chronic and inflammatory pain conditions. They have the ability to impair cytokine release at tissue injury (Gao R. et al. 2013), to inhibit SOCE and subsequent ER Ca^{2+} refill as demonstrated in the current study and further preventing and reducing different types of pain as seen in animal models (Gao XH et al. 2015, Rigaud et al. 2009, Gao R. et al. 2013).

The previous sections revealed the identity of CRAC components and confirmed the presence of BK-mediated SOCE in pain sensing neurons. CRAC channels are formed at the ER-PM junctions, thus the following chapter aims at identifying and characterizing the junctional proteins that might facilitate the channel assembly and subsequent SOCE activation in primary afferent neurons.

Chapter 5. Characterization of Junctophilin proteins in DRG neurons

5.1 Introduction

Junctional membrane complexes (JMCs) between the PM and the ER are common structures of all excitable cells (Landstorm et al 2014). Their main role is to promote the communication between ion channels residing in these membranes (Takeshima et al. 2000, Kakizawa et al. 2008). They are highly important in facilitating SOCE as STIM1 translocation and its interaction with Orai1 happens at the already formed ER-PM junctions (Fahrner et al. 2013). The junctophilin (JPH) family of proteins was discovered almost two decades ago and since then, their critical role in coordinating JMCs was intensely studied (Landstorm et al. 2014). Four JPH family members have been identified to date and their expression profiles were found to be tissue-specific (Landstorm et al. 2014).

JPH1 is highly expressed in skeletal muscle and to a lower degree in cardiomyocytes (Murphy et al. 2013). Despite of being itself a structural support to the JMCs, JPH1 also interacts directly with caveolin-3 (Cav3), which is an important structural component of the muscle cells that forms invaginations of the sarcolemmal membrane (Gazzero et al. 2010). At the ER, JPH1 interacts with RyR1 which modulates the Ca^{2+} release from the sarcoplasmic reticulum (SR), while at the PM it interacts with the L-type calcium channels (LTCC) (Landstorm et al. 2014). Lack of JPH1 has been associated with the development of muscular dystrophy, including respiratory failure leading to early death in mice (Ito et al. 2001).

JPH2 is highly expressed in cardiac muscle cells, also binding Cav3 and co-localizing with LTCC and RyR2 in rat cardiomyocytes (Minamisawa et al. 2004). It plays an important role in maintaining the dyadic ultrastructure of cardiac muscle cells and a reduced expression of JPH2 has been linked to hypertrophic cardiomyopathy and arrhythmia in mice models as well as in humans (Landstorm et al. 2011).

JPH3 and JPH4 are present in neurons of the brain (Landstorm et al. 2014). They are involved in Ca^{2+} homeostasis and facilitate the crosstalk between N-methyl D-aspartate (NMDA) and

RyR in hippocampal neurons and Purkinje cells (Moriguchi et al. 2006). Furthermore, the impaired Ca^{2+} dynamics in JPH3/4 knock-out mice was linked to memory loss, a reduced exploratory activity and irregular limb reflexes (Moriguchi et al. 2006). In humans, a strong correlation between JPH3 and Huntington-disease like syndrome (HDLS) has been described (Landstorm et al. 2014, Holmes et al. 2001). A recent study in Venezuela reported that 25% of the subjects with HDLS had JPH3 mutations (Paradisi et al. 2013). While the cohort of this study was small (16 patients in total), larger studies would be beneficial to clarify the link between JPH3 and HDLS.

Allen Spinal Cord Atlas, a comprehensive map of gene expression through the mouse spinal cord, revealed that JPH3 and JPH4 might be present within young mouse spinal cord and DRGs (http://mousespinal.brain-map.org/). To my knowledge, no other attempt to investigate the JPHs' expression and functional role within sensory neurons has been done, thus this chapter aims at verifying and further on characterizing the presence of JPH family members in DRG neurons.

5.2 Results

Since literature holds no evidence of JPH proteins being expressed in DRG neurons, I attempted to investigate the protein levels of JPHs using Western blot (WB) and immunohistochemistry (IHC) assays.

Acutely dissociated DRG neurons were lysed and further prepared as described in Chapter 2. As a positive control for the WB experiments, I simultaneously prepared other tissue lysates as follows: a skeletal muscle sample as a positive control for JPH1, a cardiac muscle sample for JPH2 and a cerebellum sample for JPH3 and JPH4.

For the IHC experiments, DRGs were collected, fixed and sliced as previously described. Antibodies against JPH1, 2, 3 and 4 (Table 2.4) were used to stain DRG slices at different dilutions (1:200, 1:500 and 1:1000) to optimize the IHC protocol. A dilution of 1:200 for each anti-JPH antibody was found to be optimal and consistent with the manufacturer

recommendations. The overall approach was similar to the previous chapter where I characterized the expression of CRAC components within DRGs. Here, I counted the number of positively stained neurons (for anti-JPH1, 3 and 4 antibodies) and presented my findings as the percentage of neurons expressing each specific JPHs out of the total neuronal population, based on the somatic diameter. I also co-stained with neuronal markers NF200 and TRPV1 to identify medium/large myelinated neurons, as well as heat-sensitive small-diameter nociceptors.

5.2.1 JPH1, JPH3 and JPH4 are expressed in DRG neurons

To determine whether junctophilin proteins might be expressed in DRGs, I first performed a Western blot analysis and found that all JPH proteins were detected in their specific control tissues (Figure 5.1) and bands were of the predicted molecular weight (with the exception of that for JPH4, see below). JPH1, 3 and 4 were detected in DRG while JPH2 was not present (Figure 5.1.B). Interestingly, JPH4 antibody revealed a double band in the DRG, one of which was of the predicted molecular weight (66 kDa), yet, only a lighter band was detected in the brain sample. (Figure 5.1.D). These results suggest the presence of an alternatively spliced gene product or a post-transcriptional modification of the JPH4 in the brain. The experiments were repeated as follows: preparations from 3 animals were used with 6 different lysates per tissue sample; all the repeats returned similar results. Moreover, using a different antibody against JPH4 (Sigma, Table 2.6) revealed the same differences between brain and DRG lysates and all bands were eliminated by using a blocking peptide (Table 2.6). Further confirmation of the JPH4 antibody specificity was obtained using the siRNA knock-down approach (see next chapter).

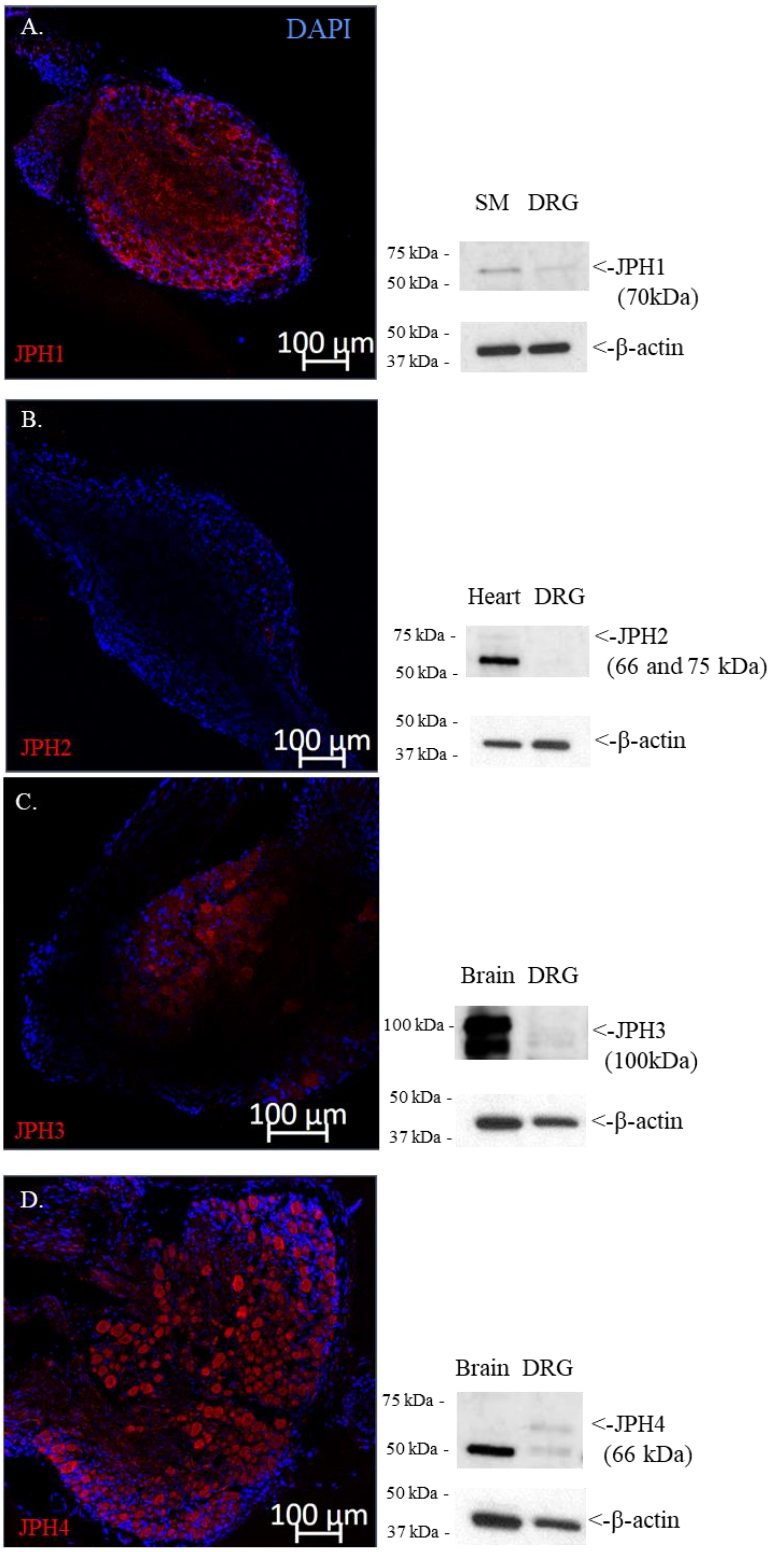

Figure 5.1. The protein expression of JPH isoforms within DRG neurons. Left panel - Representative confocal images of immunostaining with antibodies against JPH1 (A), JPH2 (B), JPH3 (C) and JPH4 (D). **Right panel**- Western blot analyses of the JPH family members in DRG and positive control tissue lysates (Skeletal muscle, SM, for JPH1, Heart for JPH2 and Brain for JPH3 and 4). These are representative results of n=6 individual experiments. Red is JPH labelling and Blue is nuclei labelling with DAPI.

5.2.3 Expression of JPH1 in DRG neurons

Immunostaining of DRG sections demonstrated that JPH1 is expressed in 50.5 ± 3.1 % of all neurons and the average somatic diameter of the positively-stained cells was 22.5 ± 1.2 µm. This was similar to the mean size of all measured DRG neurons, 21.8 ± 0.7 µm; there was no apparent preference in JPH1 expression in neurons of particular size (Figure 5.2.). A representative image of the localization of JPH1 within PFA-fixed DRG sections is also shown in Figure 5.1.A. Furthermore, co-staining experiments demonstrated that JPH1 co-localizes with NF200 in 68.9 ± 9.1 % of the medium and large myelinated neurons (n=3, Figure 5.3 is a representative example) and is expressed within 70.2 ± 10.2 % of the TRPV1-postive nociceptors (n=3, Figure 5.4 is a representative example). Taken together, these observations suggest that JPH1 is expressed in neurons of different sensory modalities, including heat-sensitive nociceptors.

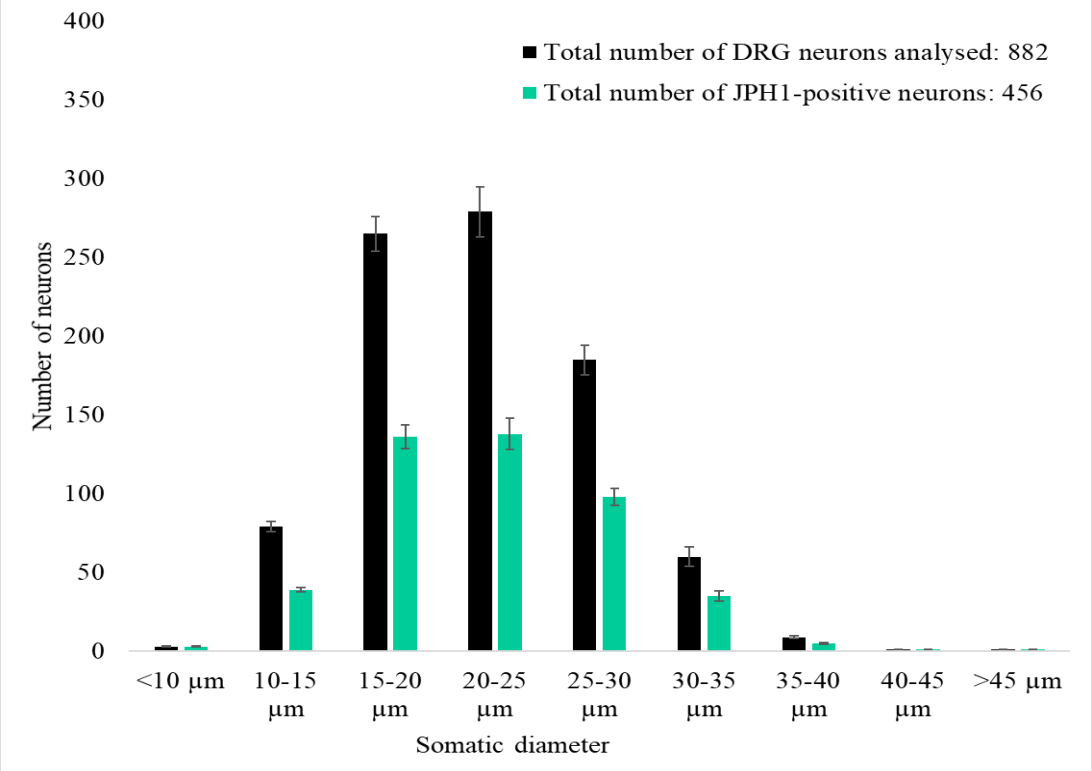

Figure 5.2 The distribution of JPH1 in DRG neurons. The somatic diameter of JPH1-positive neurons was measured, presented as a frequency distribution (green) and showed alongside the total number of neurons (black). Data is shown as the number of neurons of different somatic sizes ± SEM, from a total of 882 neurons analysed (cumulative data from n=6 individual DRG sections).

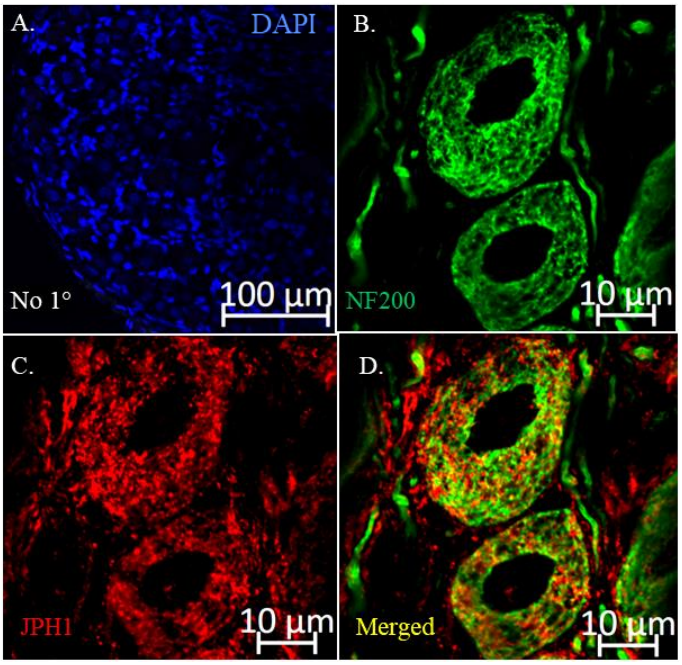

Figure 5.3 The expression of JPH1 in medium and large DRG neurons identified by NF200 marker. A. No-primary antibody control, blue-stained nuclei with DAPI. **B-D** Confocal images of immunostaining with antibodies against NF200 (B, green), JPH1 (C, red) and Co-staining (D, merged).

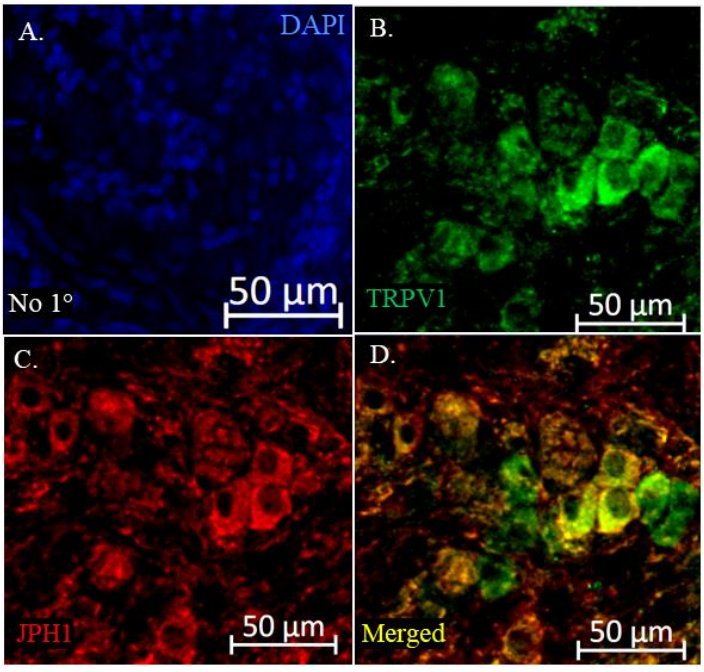

Figure 5.4 The expression of JPH1 in heat-sensing nociceptors identified by TRPV1 marker. A. No-primary antibody control, blue-stained nuclei with DAPI. **B-D** Confocal images of immunostaining with antibodies against TRPV1 (B, green), JPH1 (C, red) and Co-staining (D, merged).

5.2.4 Expression of JPH3 in DRG neurons

Immunohistochemistry experiments revealed that 38.37 ± 4.83 % of DRG neurons express JPH3 protein, thus this isoform seems to be less abundant in this tissue as compared to JPH1. The mean size of JPH3-positive neurons was 20.8 ± 0.6 µm, similar to the overall mean somatic diameter in these samples: 20.5 ± 0.4 µm. The somatic size comparison revealed that JPH3 is similarly expressed in neurons of various sensory modalities (Figure 5.5). Moreover, co-staining experiments with neuronal markers demonstrated that JPH3 is expressed within 55.8 ± 10.1 % of NF200-positive neurons and within 55.1 ± 19 % of heat-sensitive nociceptors

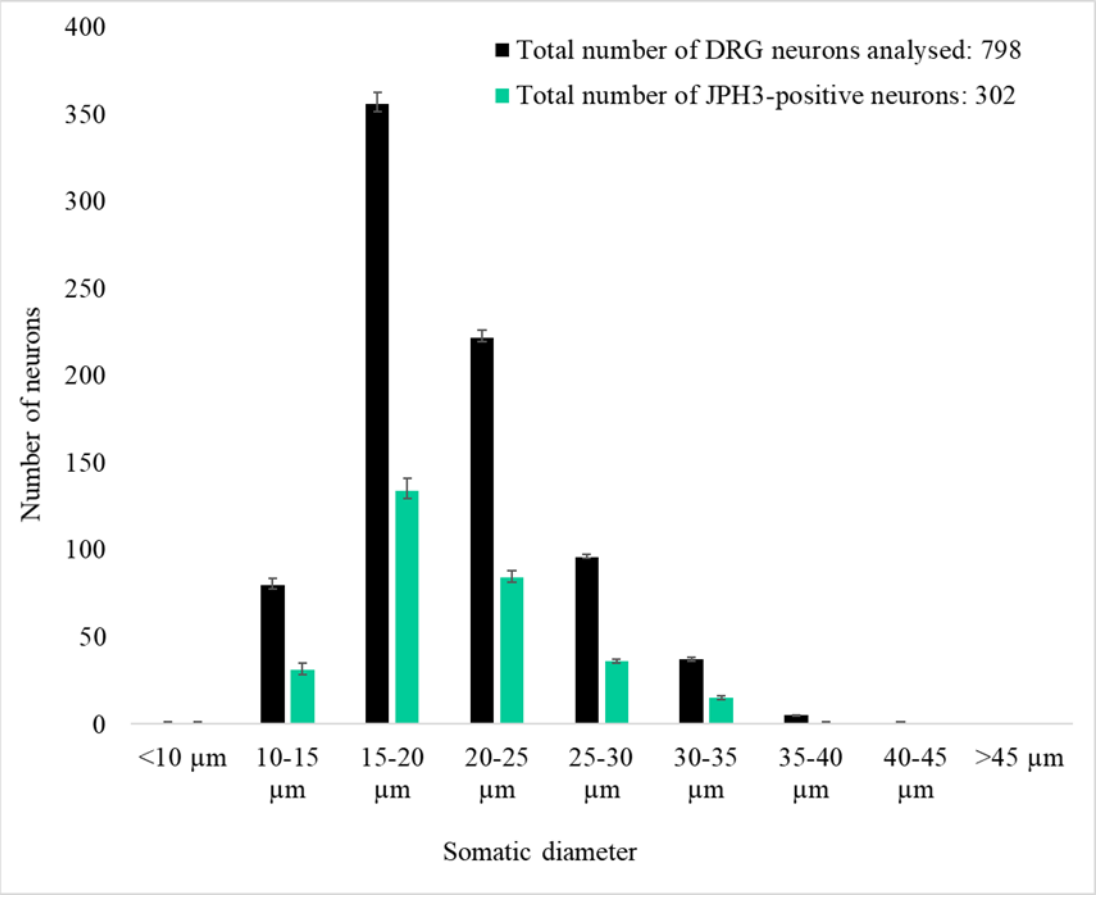

Figure 5.5 The IHC distribution of JPH3 in DRG neurons. The somatic diameter of JPH3-positive neurons was measured, presented as a frequency distribution (green) and showed alongside the total number of neurons analysed (black). Data is shown as the number of neurons of different somatic sizes ± SEM, from a total number of 882 neurons (cumulative data from n=6 individual DRG sections).

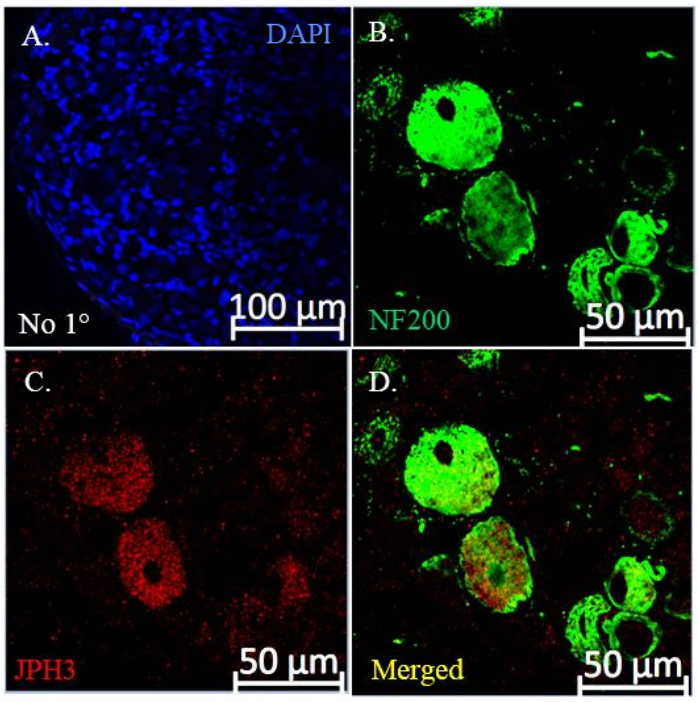

Figure 5.6 The expression of JPH3 in medium/large DRG neurons identified by NF200 marker. A. No-primary antibody control, blue-stained nuclei with DAPI. **B-D** Confocal images of immunostaining with antibodies against NF200 (B, green), JPH3 (C, red) and Co-staining (D, merged).

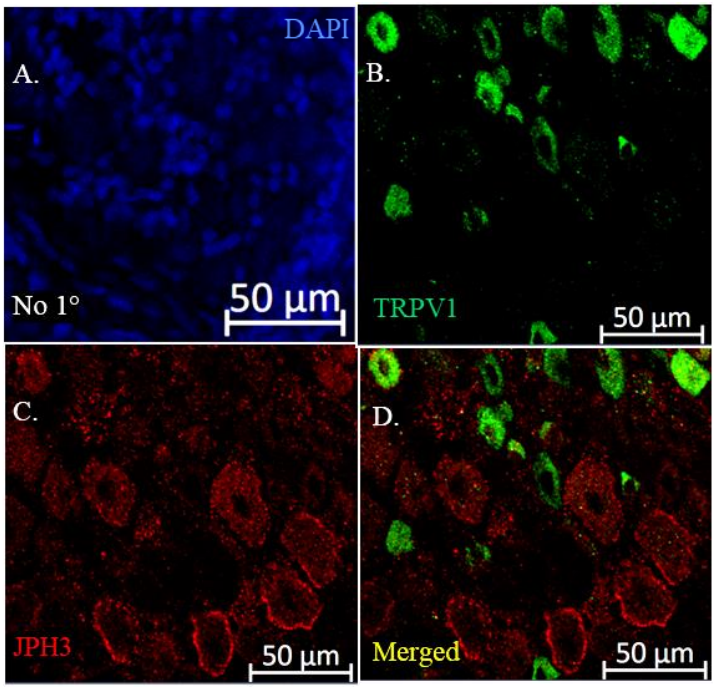

Figure 5.7 The expression of JPH3 in heat-sensing nociceptors identified by TRPV1 marker. A. No-primary antibody control, blue-stained nuclei with DAPI. **B-D** Confocal images of immunostaining with antibodies against TRPV1 (B, green), JPH3 (C, red) and Co-staining (D, merged).

5.2.5 Expression of JPH4 in DRG neurons

Interestingly, JPH4 immunostainings showed that this protein is expressed in 71.5 ± 6% of DRG neurons with a uniform distribution amongst somas of all sizes (Figure 5.8), making JPH4 the most abundantly expressed JPH isoform in DRG. NF200 and TRPV1 co-localization experiments demonstrated that JPH4 is highly co-expressed with these neuronal markers, therefore it is present in 75.1 ± 10 % of the medium and large myelinated Aδ fibers (n=3, Figure 5.9 is a representative example) as well as in 84 ± 6.3 % of the heat-sensitive C-fibers (n=3, Figure 5.10 is a representative example). Similar to the other isoforms, the average somatic diameter of JPH4, 22.2 ± 0.8 µm, did not differ to that of the overall neuronal population (21.88 ± 0.7 µm), further confirming that JPH4 does not reveal a preferred distribution pattern.

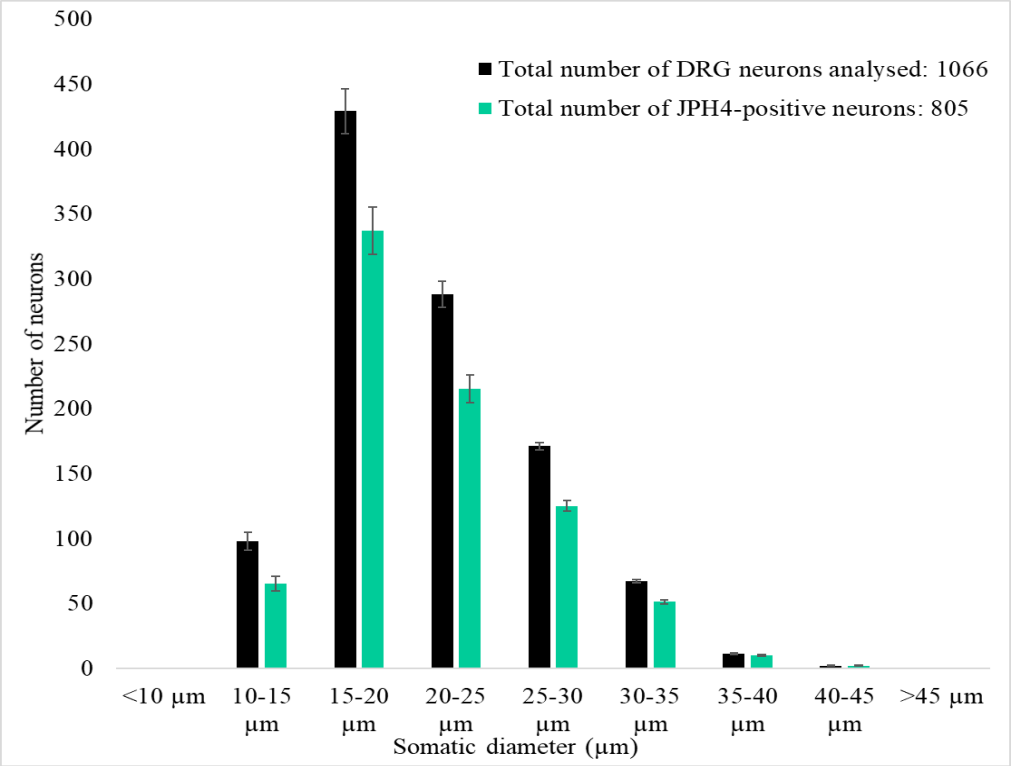

Figure 5.8 The IHC distribution of JPH4 in DRG neurons. The somatic diameter of JPH4-positive neurons was measured, presented as a frequency distribution (green) and showed alongside the total number of neurons (black). Data is shown as the number of neurons of different somatic sizes ± SEM, from a total number of 882 neurons (cumulative data from n=6 individual DRG sections).

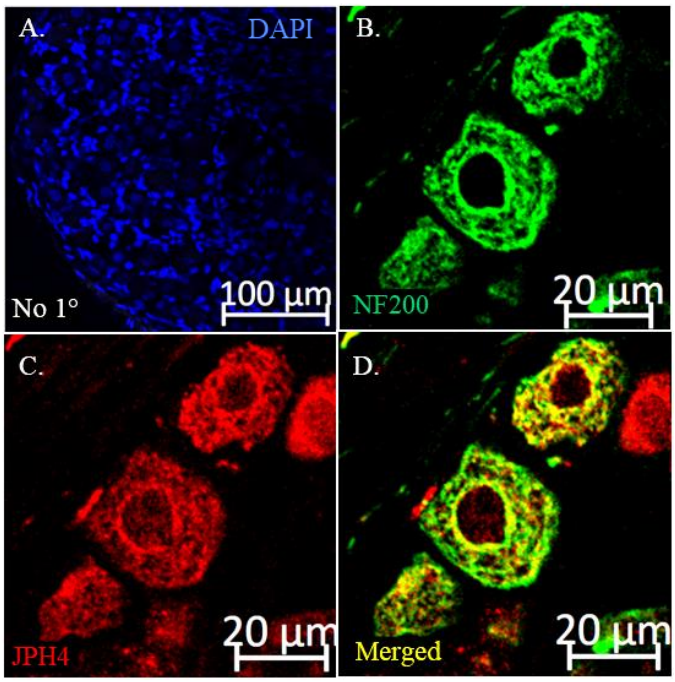

Figure 5.9 Expression of JPH4 in medium/large DRG neurons identified by NF200 marker. A. No-primary antibody control, blue-stained nuclei with DAPI. **B-D** Confocal images of immunostaining with antibodies against NF200 (B, green), JPH4 (C, red) and Co-staining (D, merged).

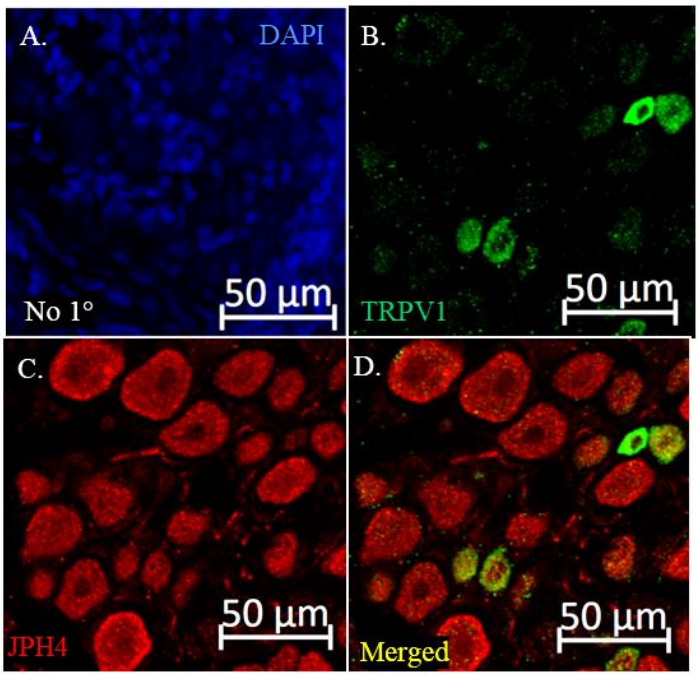

Figure 5.10 Expression of JPH4 in heat-sensing nociceptors identified by TRPV1 marker. A. No-primary antibody control, blue-stained nuclei with DAPI. **B-D** Confocal images of immunostaining with antibodies against TRPV1 (B, green), JPH4 (C, red) and Co-staining (D, merged).

5.3 Discussion

JPH proteins have been previously shown to have an important role in supporting SOCE in excitable cells (Takeshima et al. 2000, Landstorm et al. 2014). Since the presence of JPH3 and 4 within the brain has been confirmed (Nishi et al. 2003) and their mutations were correlated with impaired Ca^{2+} influx leading to neurodegenerative disorders (Seixas et al. 2012), I aimed at investigating whether JPHs are also expressed in primary sensory neurons. The presence of JPHs at ER-PM junctions of nociceptors may offer a supportive role for activating and/or maintaining SOCE in the context of pain signaling. Thus, this chapter also investigated the localization patterns of JPHs within DRG neurons of different sensory modalities.

5.3.1 JPH proteins are present in first order sensory neurons

Western blot analysis was carried out to determine the protein expression of JPH family members within DRG cultured neurons. The relative expression of these isoforms is shown in Figure 5.1 and the results suggest that JPH4 might be expressed at the highest level, followed by JPH1, JPH3 and JPH2 (the last isoform did not reveal any evident band as compared to its positive controls). To further investigate the protein levels and the preferred distribution of JPHs, IHC assay was performed. This experiment revealed that JPH4 isoform is expressed in a higher number of neurons (71%) as compared to JPH1 (50%) and JPH3 (38%) ($p<0.0001$, χ^2 test). No positive staining for JPH2 has been determined, suggesting that this protein might not be present in DRGs. These findings are consistent with the mRNA levels reported in the Allen Spinal Cord Atlas (http://mousespinal.brain-map.org/). However, the expression of JPH1 was thought to be specific for muscle cells (skeletal and to a lesser degree, cardiac) (Landstorm et al. 2014). Surprisingly, the experiments reported in this chapter revealed some expression of JPH1 in DRG by Western blot and Immunohistochemistry approaches. This finding should be further investigated to confirm its presence and most importantly its role within DRG neurons.

5.3.2 JPH1, 3 and 4 are uniformly distributed within neurons of different sensory modalities

A previous attempt to determine the expression of JPH3 and 4 within the brain was made (Nishi et al. 2003) but less is known about the presence of junctional proteins within DRG neurons. Thus, once the expression of JPHs within primary sensory neurons was confirmed, I aimed at determining their localization pattern in this tissue. Interestingly, JPH1, 3 and 4 revealed a uniform distribution within nociceptors of different sizes (Figures 5.2, 5.5, 5.8). This observation suggests that JPHs might facilitate Ca^{2+} dynamics independent of the stimulus type (from light touch to noxious stimuli). In addition, the mean somatic diameter for JPH1 (21.8 μm), JPH3 (20.8 μm) and JPH4 (22.2μm) did not differ from the mean overall neuronal size, further confirming an invariable distribution within DRG neurons.

5.3.3 JPH1, 3 and 4 are expressed in heat-sensitive nociceptors

As mentioned in previous chapters, SOCE is present in DRG neurons and the overexpression of CRAC components might be correlated to different types of pain (Wei et al. 2017). Orai and STIM proteins are localized uniformly within neurons of different sizes, except STIM2 who demonstrated a preference towards the medium-large somata. To determine whether junctophilin proteins might facilitate SOCE in Aδ and C-fibers, I co-stained with neuronal markers NF200 and TRPV1. The results revealed that JPH4 and JPH1 have a strong co-localization pattern with both markers, while JPH3 demonstrated a lower co-expression. However, these observations are based on a dataset comprising of 3 individual experiments per IHC pair and more images are required to clarify the co-expression of JPHs with specific neuronal markers in peripheral sensory neurons This finding suggests that JPH4, JPH1 and, to a lower degree, JPH3 might be involved in facilitating STIM-Orai coupling at ER-PM junctions in DRG neurons. The overall conclusion of the experiments reported above is that in TRPV1-positive nociceptors, which are believed to be the main type of DRG neurons mediating inflammatory pain responses, the major JPH isoform is JPH4. While the expression

of JPH1 and JPH3 should not be neglected, the following chapter will attempt to investigate the functional role of JPH4 in relation to inflammatory pain.

Chapter 6. The role of Junctophilin 4 in primary sensory neurons

6.1 Introduction

SOCE was initially reported as the main source for Ca^{2+} entry in non-excitable cells (Parekh AB and Putney JW, 2005) and since then, the role of Orai/STIM proteins in inflammation and inflammatory pain has been intensely studied (Yamashita et al. 2007, Feske et al 2006, 2009, Xia et al. 2014, Gemes et al 2011). Thus, disrupting SOCE in T-cells was shown to affect the release of pain-generating cytokines (Gao X et al. 2016). However, it was soon discovered that the role of SOCE in inflammatory pain is not only limited to non-excitable cells. For instance, it was shown that silencing CRAC components or inhibiting CRAC channels in DRG and dorsal horn neurons directly affects the excitability of nociceptors (Gao X et al. 2016, Gemes et al 2011). These two somehow synergic mechanisms culminate with an overall reduced painful sensation. The role of junctional proteins that facilitate the communication between STIM and Orai in neurons was less studied. While the presence of JPH3 and JPH4 in brain tissue was described (Nishi et al 2003, Moriguchi et al. 2006), no further evidence of their expression in sensory neurons was reported.

The previous chapter demonstrated that amongst the Junctophilin family members, JPH1, 3 and 4 are expressed in primary-afferent neurons and JPH4 is expressed to a higher degree in nociceptors. Interestingly, the role of JPH4 in facilitating SOCE in T-cells was recently reported (Woo et al. 2016). Firstly, the authors demonstrated that JPH4 is located within the ER-PM junctions of T-cells and, secondly, it interacts with STIM1. To investigate the interaction, JPH4 and STIM1 were overexpressed in T cells and Co-Immunoprecipitation, Total Internal Reflection Fluorescence (TIRF) as well as Ca^{2+} imaging experiments were performed (Woo et al. 2016). The results highlight that JPH4 might modulate SOCE by forming protein complex with junctate. Both JPH4 and junctate have the ability to interact with STIM1 (junctate by its ER-luminal terminus and JPH4 by its cytoplasmic region) (Woo et al. 2016, Treves et al. 2004). Interestingly, high expression of JPH4 promoted STIM1 clustering even when Ca^{2+} levels were at rest, but without affecting these levels. In addition,

STIM2 may also interact with JPH4 for maintaining the basal ER Ca^{2+} levels. Further studies are required to determine the exact role of STIM2 and whether it is also recruited by JPH4/junctate complex at ER-PM junctions. Woo and colleagues provided supporting information about the role of JPH4 in recruiting STIM1 and promoting SOCE in T cells. Previous chapters of this thesis demonstrated that Orai1, STIM1 and JPH4 are highly expressed in DRG neurons, including pain-sensing nociceptors. Therefore, this chapter aims at investigating the role of JPH4 in primary afferent neurons, its interaction with STIM1 and its function as a SOCE facilitator in relation to inflammatory pain.

6.2 Results

Previous chapter have brought evidence of the expression of JPH4 in DRG neurons. As Orai1 and STIM1, the main CRAC components in primary sensory neurons, are expressed in a similar pattern to that of JPH4, I hypothesized that JPH4 co-localizes with either of these proteins in DRG neurons and that it might facilitate SOCE by promoting STIM1 to ER-PM junctions.

6.2.1 JPH4 co-localizes with Orai1 and STIM1 in DRG neurons

To test this, DRG sections were prepared and immunostained with antibodies against JPH4 and Orai1 or STIM1. Figures 6.1.A and 6.2.A show that neurons positive for JPH4 are also positive for Orai1 or STIM1. Interestingly, JPH4 reveals a filament-like intracellular structure with a preferred distribution towards the PM rather than being randomly diffused in the cytoplasm (Figure 6.1.C). JPH4 and Orai1 are co-expressed in cultured DRG neurons and, interestingly, reveal a relatively similar intracellular distribution pattern as shown in Figure 6.1.B. JPH4 and STIM1 are also co-expressed in cultured neurons. Interestingly. while STIM1 prefers a diffused intracellular location (being an ER membrane resident), JPH4 was largely visible at the PM and to a lesser extent in the deeper cellular volume (Figure 6.2.B). These observations suggest that JPH4 might be present at the ER-PM junctions of DRG neurons,

while STIM1 and Orai1 are more likely to be uniformly distributed throughout the ER and PM, respectively.

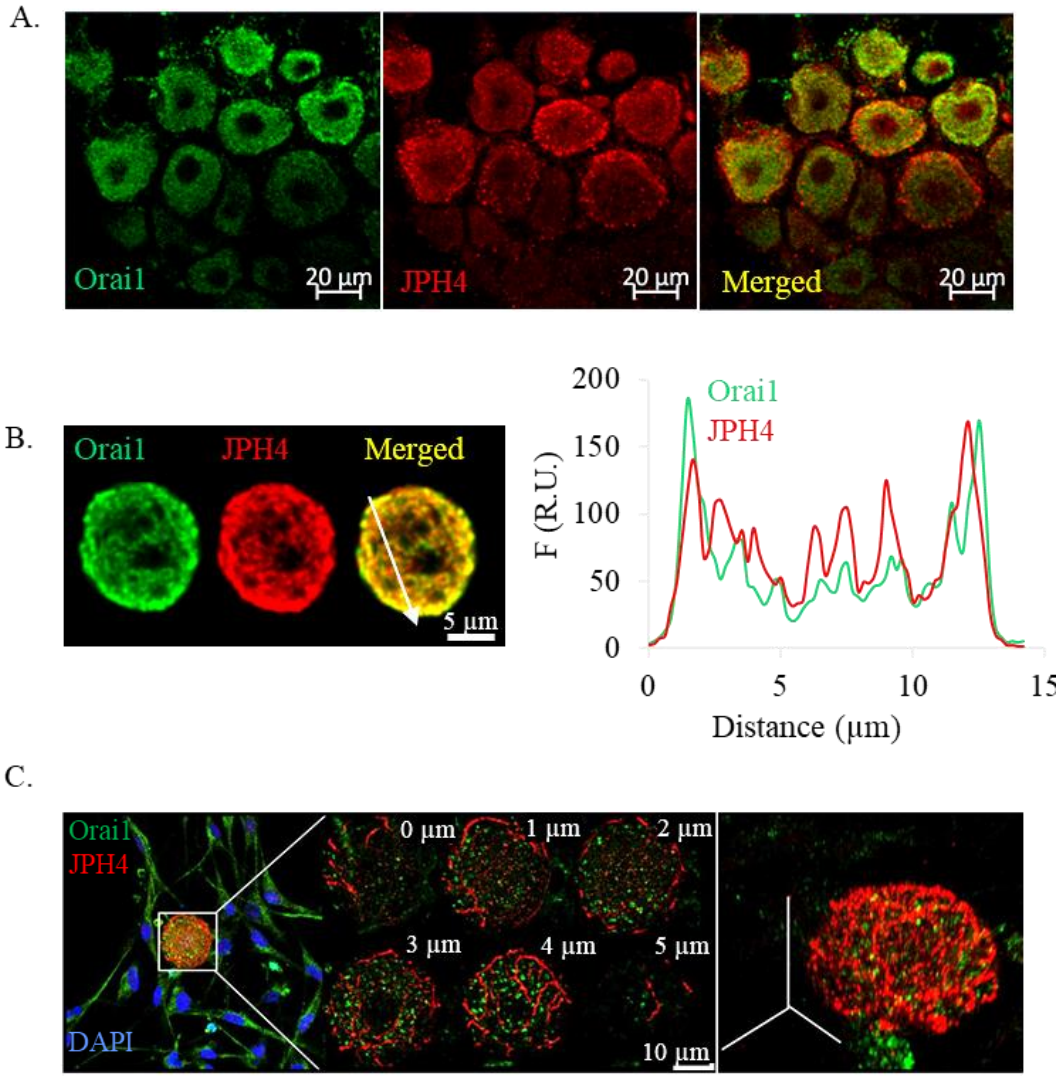

Figure 6.1. JPH4 is co-expressed with Orai1 in DRG neurons. A. Immunohistochemical identification of Orai1 (green) and JPH4 (red) in PFA-fixed DRG sections. **B.** Immunocytochemical identification of Orai1 and JPH4 in small cultured DRG neuron (left panel) and the fluorescence intensity line scan to illustrate the localization for each protein (right panel). **C.** Airyscan image (Z-stack of 1 µm optical sections) of a cultured DRG neuron revealing a specific cisternae-like localization of JPH4 (red) near the plasma membrane. C-right panel is a 3D representation of the same neuron.

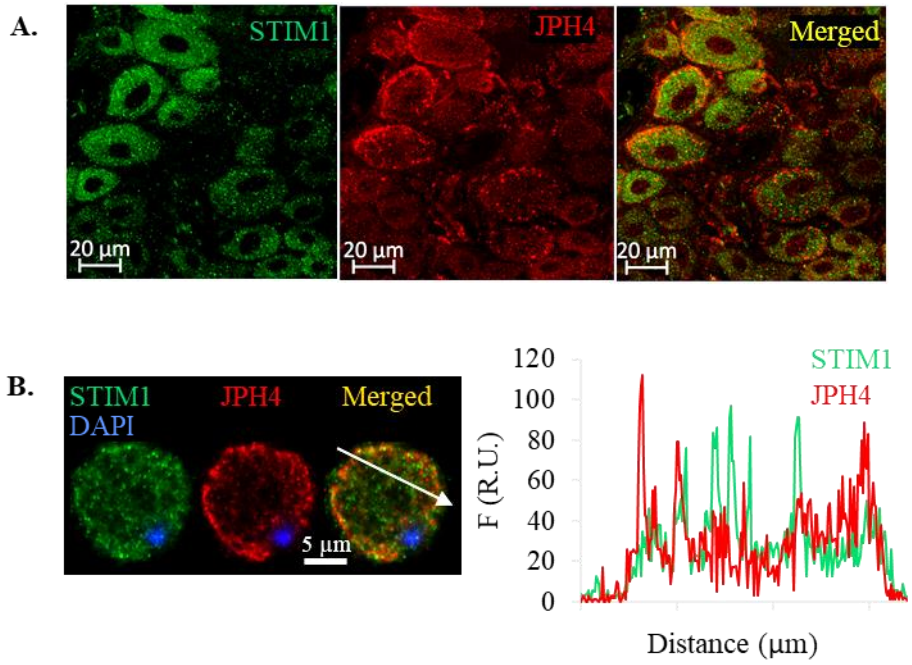

Figure 6.2. JPH4 is co-expressed with STIM1 in DRG neurons. A. Immunohistochemical identification of STIM1 (green) and JPH4 (red) in PFA fixed DRG sections. **B.** Immunocytochemical identification of STIM1 and JPH4 in small cultured DRG neuron (left panel) and the fluorescence intensity line scan to illustrate the localization for each protein (right panel).

6.2.2 JPH4 interacts with STIM1 to promote SOCE

To further investigate the role of JPH4 in sensory neurons, I performed a co-immunoprecipitation (Co-IP) experiment to determine if JPH4 and STIM1 physically interact during SOCE. Acutely dissociated DRG neurons were treated with extracellular buffer (the control group) and with BK in Ca^{2+} free solution (the SOCE stimulated group). Cells were then prepared for Co-IP as described in Chapter 2.

Immunoprecipitates from DRG neurons endogenously expressing JPH4 and STIM1 revealed a weak interaction between the two proteins when Ca^{2+} levels were at rest. This could be caused by protein interactions during cell lysis, but further investigations are needed to confirm. A thicker and darker band for STIM1 was detected once SOCE was activated, suggesting a substantial increase in JPH4-STIM1 interaction upon ER Ca^{2+} store depletion (Figure 6.3.A).

To confirm this interaction, I also investigated if the fluorescent PLA signal between JPH4 and STIM1 is enhanced upon SOCE activation. The experimental protocol was similar to the one described in Chapter 3, where I demonstrated that Orai1 and STIM1 cluster and presumably form contacts after BK-induced SOCE in DRG nociceptors. The results demonstrate that PLA signal between STIM1 and JPH4 is significantly enhanced by the SOCE activation (Figure 6.3 B and C). This suggests that while some JPH4 and STIM1 molecules are already in close proximity at rest, the amount of interacting molecules is greatly increased after BK-induced ER Ca^{2+} store depletion, further suggesting that JPH4 might facilitate SOCE by recruiting STIM1 at the ER-PM junctions.

Interestingly, PLA experiments aiming at the interaction between JPH4 and Orai1 also demonstrated that upon BK-induced SOCE, the two proteins revealed a higher number of fluorescent puncta (Figure 6.4).

Immunoprecipitation experiments for detecting a direct interaction between JPH4 and Orai1 were not performed. An optimized protocol should be used to accommodate the overlapping molecular weight of Orai1 (a 33 kDa protein) to the heavy chain fragment (dark thick bands seen at 50 kDa in Figure 6.3.A) in the IP experiment.

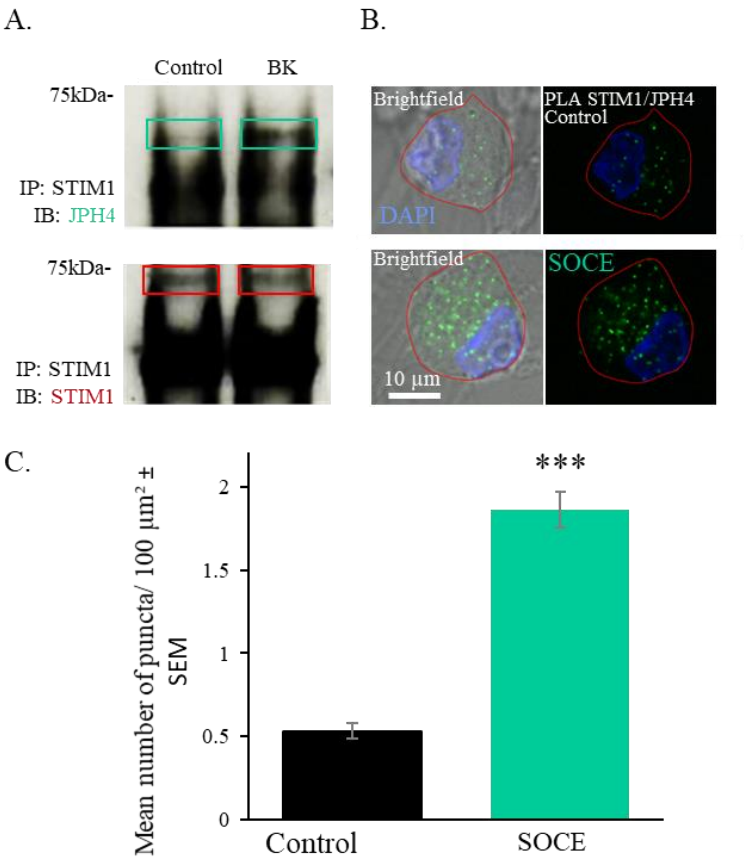

Figure 6.3. JPH4 interacts with STIM1 in DRG neurons. A. JPH4 co-immunoprecipitates with STIM1. Immunoprecipitation was performed with the anti-STIM1 antibody from DRG neurons and immunoblotted for the detection of JPH4 (the band within the green box) and STIM1 (the band within the red box). Cells were left untreated (Control) or treated with BK in Ca^{2+} free solution to induce store-depletion before lysis. **B, C**. Fluorescent PLA signals between STIM1 and JPH4 in cultured DRG neurons: representative example (B), number of fluorescent puncta per 100 µm² (C), Data shown as mean ± SEM, $p<0.001$, Student's t-test.

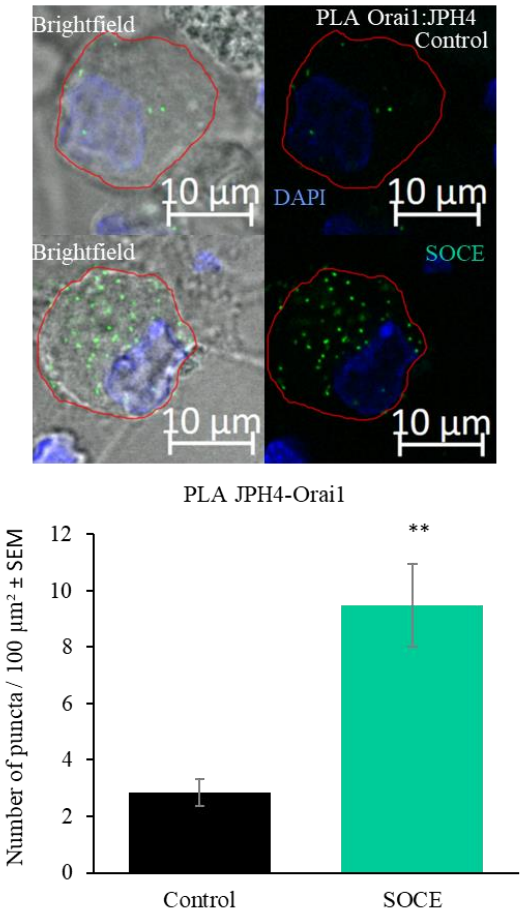

Figure 6.4. Orai1 moves closer to JPH4 upon BK-induced SOCE in DRG neurons. Fluorescent PLA signals between Orai1 and JPH4 in cultured DRG neurons, before and after store depletion with BK. A, representative example; B, number of fluorescent puncta per 100 µm². Data shown as mean ± SEM, $p<0.001$, Student's t-test.

6.2.3 Silencing JPH4 in DRG neurons disrupts Orai1-STIM1 interaction

Previous experiments suggested that STIM1 might interact with JPH4 after Ca^{2+} store depletion, prior to Orai1 binding. Thus, I investigated if silencing JPH4 in DRG neurons disrupts the Orai1-STIM1 machinery. For this purpose, I optimized an experimental protocol to silence JPH4 in cultured DRG neurons. I transfected cultured cells with Lipofectamine RNAiMAX and Silencer Select (Ambion) siRNA oligonucleotides against JPH4 (see Table 2.1) under the manufacturer's recommendations. I also used a scrambled oligomer as a negative control. Two different siRNA products targeting JPH4 were used at various concentrations in both single use and combination to optimize the protocol. I also tested different exposure times to the transfection mixture and determined the silencing effect by both IHC and WB. Silencer Select s175511 (here called siRNA2) demonstrated the highest efficacy of reducing JPH4 protein expression in DRG neurons 48 hours post transfection and at the highest recommended dose. Figure 6.5 shows a reduction in JPH4 expression by approximately 60% in WB analysis and by 40% in IHC assay.

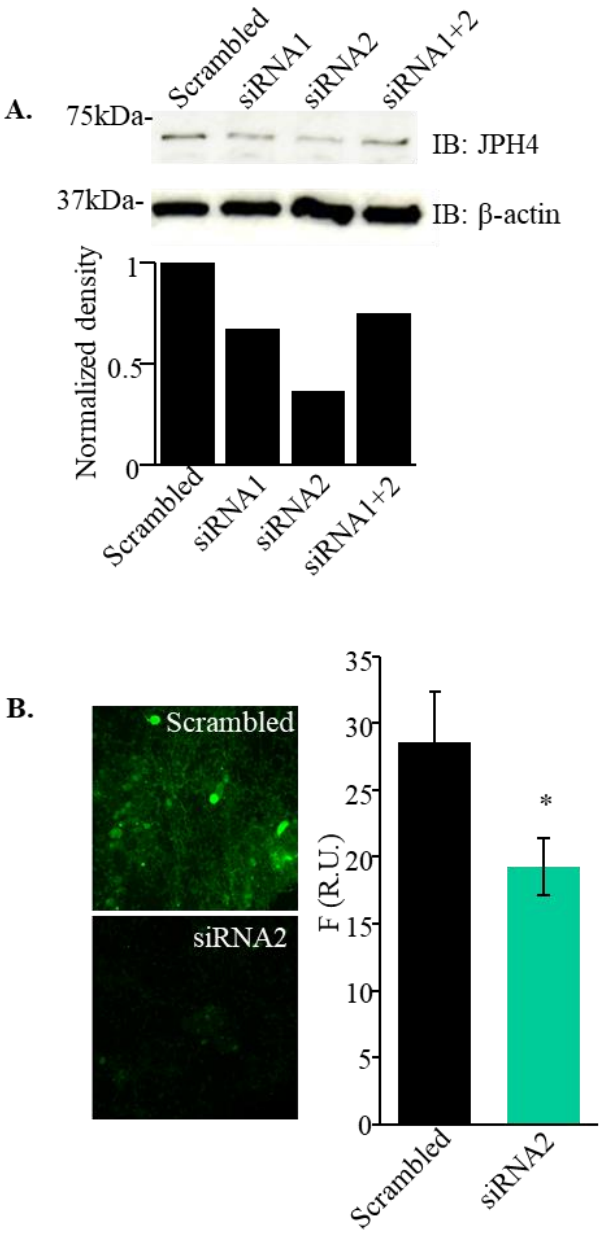

Figure 6.5. Silencing JPH4 in DRG neurons. A. Western blot analysis demonstrating that siRNA2 reduces the expression of JPH4 higher than siRNA1 or combination treatment. **B.** Immunocytochemical assay of Scrambled oligomer (as a negative control) versus JPH4-siRNA2 treated DRG neurons reveals a decreased JPH4 antibody-specific fluorescence by confocal microscopy. Data shown as mean ± SEM, n=6 for both data sets.

Even though this experiment does not provide a complete JPH4 depletion, I decided to test whether silencing JPH4 in DRG neurons using the optimized protocol with siRNA2 would reveal any disruption between Orai1 and STIM1 after BK-induced SOCE.

Thus, PLA experiments aiming at the interaction between Orai1 and STIM1 were performed on JPH4 silenced DRG neurons and compared with the negative control. Upon SOCE activation, Orai1-STIM1 PLA signals revealed a higher number of fluorescent puncta as compared to non-depleted cells in the negative control group (Figure 6.6). This is consistent with my previous finding described in Chapter 3. Interestingly, in the JPH4 silenced group, no significant difference between the number of puncta in store-depleted and non-depleted neurons was detected (Figure 6.7). This experiment was performed with the help of Dr. Shihab Shah.

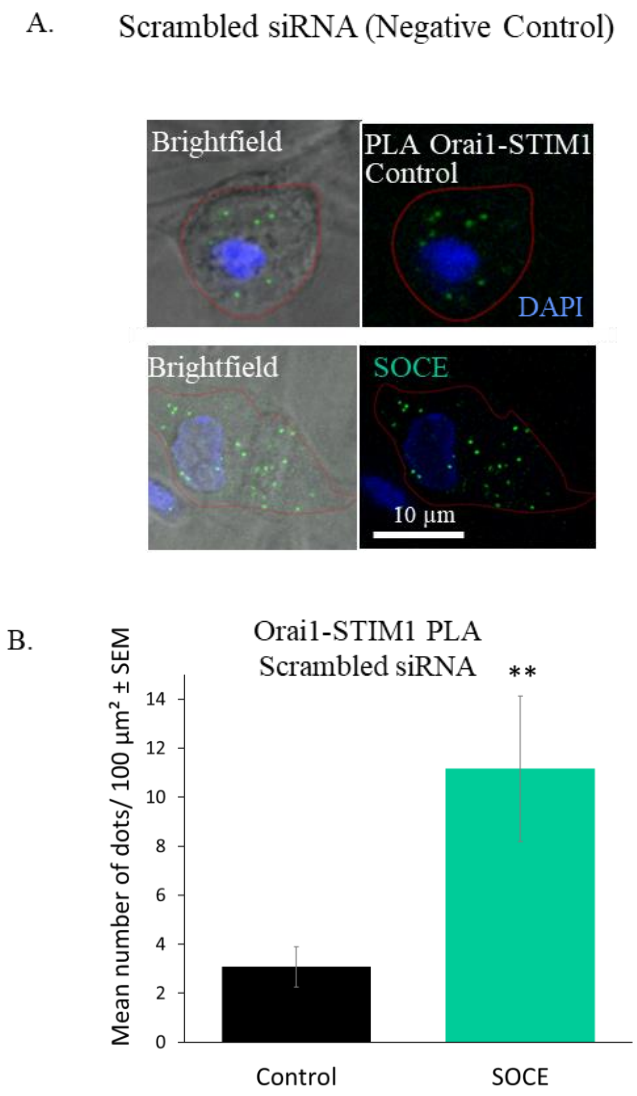

Figure 6.6. Orai1 and STIM1 translocate at ER-PM junctions after BK-induced SOCE in the negative control group. A. Representative example of fluorescent PLA signals between Orai1 and STIM1 in cultured DRG neurons. **B.** The number of fluorescent puncta per 100 µm². Data shown as mean ± SEM, $p<0.001$, Student's t-test, Control n=5, SOCE n-6.

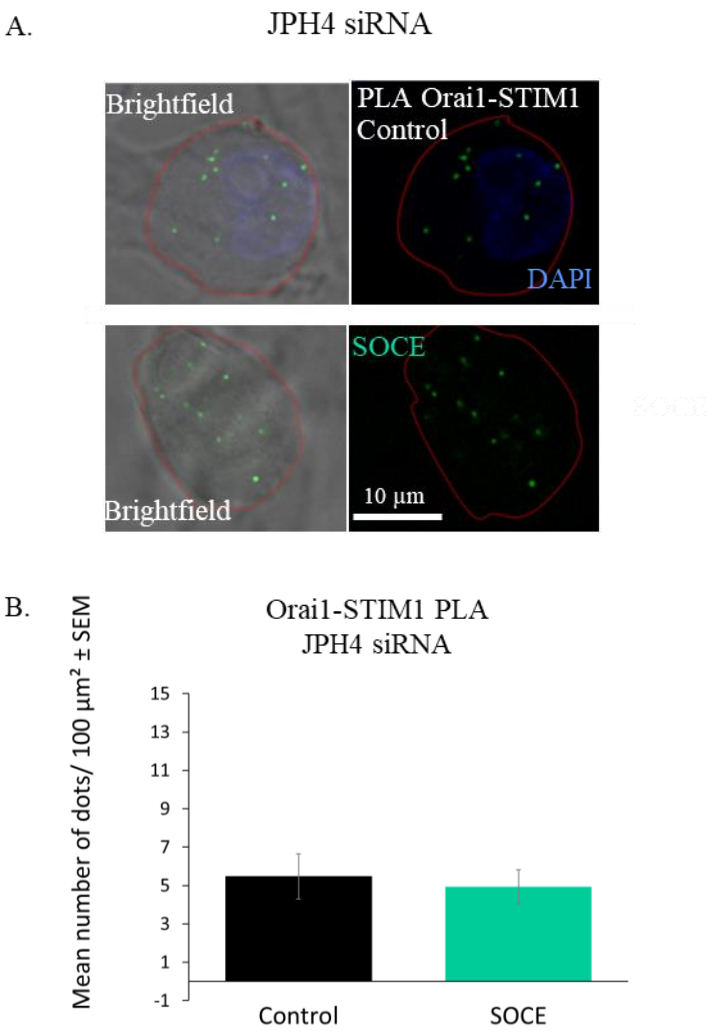

Figure 6.7. Orai1 and STIM1 translocation is disrupted in JPH4-KD sensory neurons. A. Representative example of fluorescent PLA signals between Orai1 and STIM1 in cultured DRG neurons. **B.** The number of fluorescent puncta per 100 µm². Data shown as mean ± SEM, $p<0.001$, Student's t-test, Control n=5, SOCE n=6.

6.2.4 Silencing JPH4 impairs SOCE but does not affect the ER Ca^{2+} levels at rest in DRG neurons

Calcium imaging experiments were then performed to determine whether reducing the expression of JPH4 in DRG neurons has any impact on BK-induced SOCE. To do so, I transfected the neurons with JPH4-siRNA2 (using Lipofectamine RNAiMAX as a vehicle) as described previously. Similarly, Scrambled Oligomer transfections were used as a negative control. Two days post-transfection, cells were loaded with Fura-2AM for 1 hour and washed with extracellular buffer thereafter. For consistency, the experimental design was kept in line with all previous experiments focused on inducing SOCE in DRG neurons. Thus, Ca^{2+} stores were depleted with 250 nM BK in Ca^{2+} free solution and Fura2 fluorescent levels were measured. Figure 6.8 shows that silencing JPH4 in DRG neurons reduces the BK-induced SOCE by approximately 45% ($p<0.05$, Student T test). Interestingly, the amplitudes of the cytosolic Ca^{2+} transients induced by BK during store depletion did not significantly differ between the two groups, although a reduction of 14% in JPH4-siRNA treated cells was noticed ($p<0.05$, Student's t test; Figure 6.8.B).

These results suggest that JPH4 might be involved in facilitating SOCE yet, the basal ER Ca^{2+} levels could be maintained even with such partial SOCE impairment.

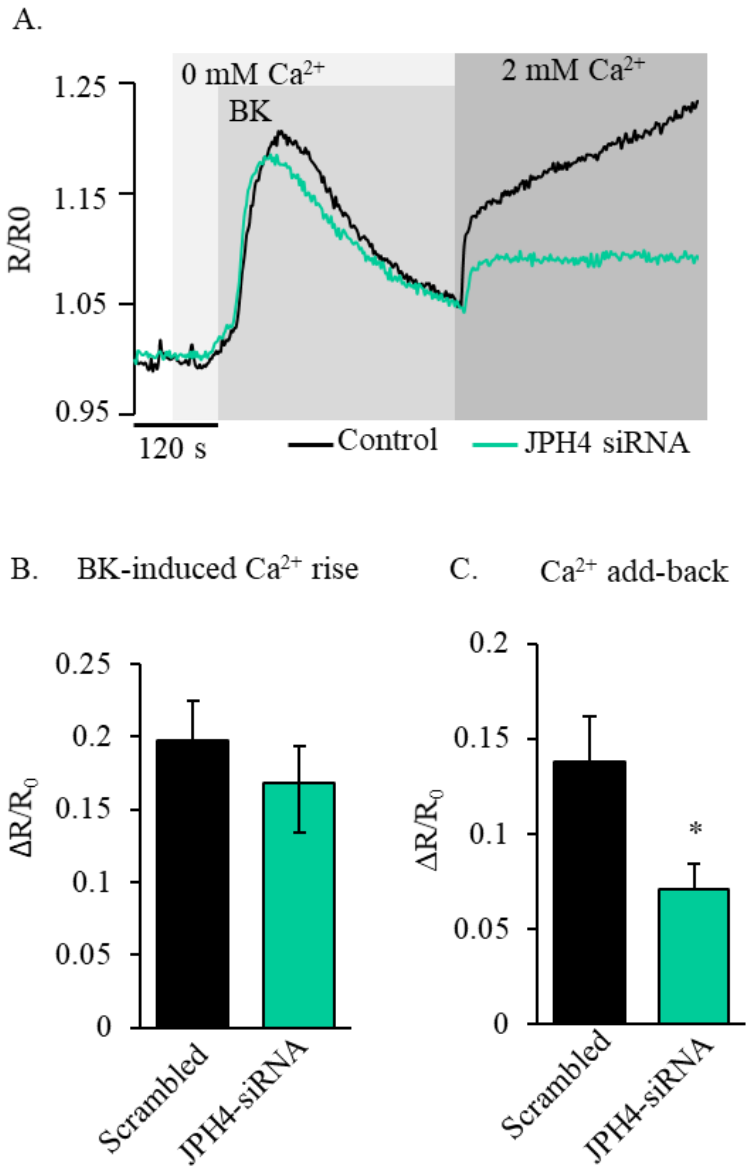

Figure 6.8. JPH4-KD impairs SOCE in DRG neurons. A. Representative example of Fura2 calcium imaging recording of typical store depletion/Ca^{2+} add back experiments in control and JPH4-KD cells, as indicated. **B**, **C** summary data for experiments as these shown in A; the effect of JPH4 KD on the amplitude of the BK-induced Ca^{2+} transients (B) and SOCE during the Ca^{2+} re-addition phase (C). Data is shown as mean ± SEM, $p<0.05$ Student's t test.

The previous experiment demonstrated that silencing JPH4 in DRG neurons generated a reduced SOCE and, presumably, a lower ER Ca^{2+} uptake. To determine the impact of the reduced Ca^{2+} store refill on subsequent SOCE activation, I designed an experimental protocol where two rounds of store depletion were applied in sequence. To avoid desensitization and tachyphylaxis common for the $G_{q/11}$ coupled receptors, the DRG neurons were treated with two different GPCR-agonists. Thus, cultured cells were initially treated with 30 µm ATP to activate endogenous $G_{q/11}$-coupeld P2Y receptors expressed in DRG neurons (Gerevich et al. 2004), Following a Ca^{2+} pool refill phase, BK was applied to stimulate again the IP_3-dependent store depletion, this time by activating B_2R. It has to be pointed out that while DRG neurons also express ionotropin $P2X_2/P2X_3$ receptors (Gerevich et al. 2004), the agonist application was performed in Ca^{2+} free conditions (in line with previous protocols), thus contribution of these receptors to intracellular Ca^{2+} levels was excluded by the experimental design. The aim of this experiment was to investigate the role of JPH4 in an active store refill in intensive DRG stimulation scenarios (as e.g. under the persistent tissue inflammation). Figure 6.9 shows that the secondary (BK-induced) Ca^{2+} release from the stores was indeed reduced by 40% in JPH4-silenced neurons as compared to control.

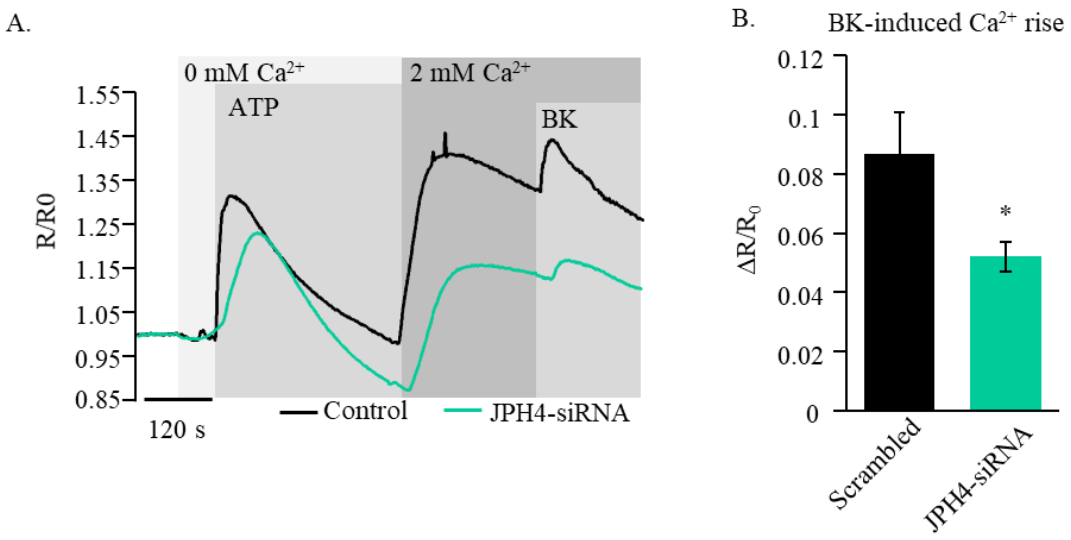

Figure 6.9. JPH4-KD impairs the ER Ca^{2+} pool refill with consequences on the subsequent store depletion. A. Representative example of Fura2 calcium imaging recording in sensory neurons. First store depletion was induced by ATP (30 μM) in the Ca^{2+} free buffer; Ca^{2+} was then added back to the extracellular buffer and secondary IP_3-dependent store depletion with BK (250 nM) was performed. **B.** Fura-2 measurements of BK-induced store depletion in Scrambled Oligomer treated (negative control) and JPH4-KD (siRNA2 treated) DRG neurons. Data is shown as mean ± SEM, $p<0.05$ Student's t-test.

6.3 Discussion

JPH4 has been recently shown to have an important role in facilitating SOCE in T cells and, alongside JPH3, to modulate Ca^{2+} dynamics in hippocampal neurons (Woo et al 2016, Takeshima et al 2003). Chapter 5 of this thesis demonstrated the expression of JPH4 in DRG neurons of different sensory modalities, including small pain-sensing nociceptors. As STIM1 and Orai1 have a similar expression pattern to that of JPH4, the current chapter aimed at investigating whether JPH4 might function as a SOCE promoter in DRG neurons.

6.3.1. JPH4 is co-expressed with Orai1 and STIM1 in primary sensory neurons

The IHC/ICC experiments demonstrated that JPH4 was co-expressed with both Orai1 and STIM1 in primary afferent neurons. Interestingly, ICC experiments highlighted that JPH4 reveals a filament-like staining pattern in the PM, wrapping the neuron as shown in Figure 6.1. It is likely that it might follow the ER cisternae that runs alongside the PM. This image was recorded at different sections through the neuron: starting from the lowest Z level, followed by moving the optical focus up by 1 µm until I reached the other edge of the cell. This pattern has been observed in repeated experiments and further investigations are needed to determine the exact nature of the JPH4-positive cisternae in DRG neurons.

Co-staining with an antibody against STIM1 revealed that JPH4 was expressed mainly at the PM level, while STIM1 populated the intracellular space as expected. It is important to mention that JPH4 is residing in the ER, but its MORN motifs interact with the PM and thus contribute to forming the ER-PM junctions. By contrast, when Ca^{2+} levels are at rest, STIM1 moves freely in the ER membrane reason why a diffused intracellular distribution was observed. Woo and colleagues also demonstrated that after thapsigargin-induced store discharge, STIM1-YFP move into pre-formed junctions detected by mCh-JPH4 in Jurkat T cells.

6.3.2 JPH4 interacts with STIM1 in DRG neurons

The Co-IP experiments (immunoblotting JPH4 in a STIM1 immunoprecipitate sample, Figure 6.3.A) revealed that STIM1 and JPH4 directly interacted upon SOCE stimulation with BK. This finding suggests that discharging the ER Ca^{2+} pool in DRG neurons triggers the translocation of STIM1 at the ER-PM junctions and its binding to JPH4.

This result was consistent with those reported by Woo and colleagues. The authors transfected HEK293 cells with FLAG-STIM1 and GFP-JPH4 and immunoprecipitated with either anti-STIM1 or anti-JPH4 antibody, while blotting for the detection of JPH4 (with anti-GFP antibody) or STIM1 (with anti-FLAG antibody), respectively. Similar with my observations, thapsigargin-induced store depletion generated STIM1-JPH4 interaction, also confirmed by GST pulldown analyses (Woo et al. 2016). Moreover, the same authors reported that JPH4 colocalizes with junctate at the ER-PM junctions of T-cells, form a protein complex and both bind STIM1 in order to facilitate SOCE (Woo et al. 2016). Junctate is an IP_3R- associated protein with a role in modulating ER Ca^{2+} release and facilitating SOCE by recruiting STIM1 into ER-PM junctions (Treves et al. 2004, Srikanth et al. 2012). Previous studies demonstrated that junctate has a structural role into sustaining the ER-PM junctions of T cells where STIM1 and Orai1 cluster, interact and form CRAC channels (Srikanth et al. 2012). To my knowledge, there is no evidence of the expression of this protein in rodent DRG neurons in the literature or in the Allen Mouse Spinal Cord atlas. But mouse cloning studies demonstrated that it is present in brain, heart, spleen, lung, kidney, liver and stomach (Hong et al 2001). Whether JPH4 on its own is sufficient to promote the CRAC channel assembly in DRG neurons remains to be determined. As other junctophilin proteins also seem to be expressed in this tissue (such as JPH1 and JPH3), but to a lesser degree, it is appealing to investigate a putative role of these in SOCE further.

Moreover, PLA analysis further confirmed that both STIM1 and Orai1 come in closer proximity to JPH4 in DRG neurons after BK-induced store depletion. Detecting fluorescent PLA signal between JPH4-STIM1 and JPH4-Orai1 in the non-treated cells demonstrated that

a number of these proteins are already found at the ER-PM junctions (the distance between the inner leaflet of the PM and the ER membrane at junctions is of approximately 20nm), but once the ER Ca^{2+} discharge was induced, further movement and clustering into junctions was revealed by a stronger PLA signal (Figures 6.3 and 6.4). Whether Orai1 directly interacts with JPH4 or further scaffolds are necessary remains to be determined.

6.3.3 Silencing JPH4 in DRG neurons disrupts Orai1-STIM1 interaction

Chapter 3 of this thesis reported that Orai1 and STIM1 come in closer proximity once store depletion is triggered in DRG neurons. Experiments in the current chapter suggested that STIM1 might be recruited by JPH4 at ER-PM junctions, presumably prior to coupling to Orai1. To investigate its role in promoting the formation of CRAC channels, small interfering RNA (siRNA) was used to reduce the expression of JPH4 in DRG neurons. Further on, changes in the fluorescent PLA signal between Orai1-STIM1 were determined. Figures 6.6 and 6.7 demonstrate that downregulation of JPH4 expression reduces Orai1-STIM1 PLA signal in BK-treated neurons as compared to control. These results suggest that lacking JPH4 may impair STIM1 recruitment at ER-PM junctions, further disrupting the CRAC machinery and, presumably, inhibiting SOCE. Taken together, these results strongly suggest that JPH4 is indeed an important component of CRAC channel complex assembly in DRG neurons.

6.3.4 Silencing JPH4 in DRG neurons inhibits SOCE and further impairs the ER Ca^{2+} store refill

To investigate further the role of JPH4 in SOCE, ER store refill and GPCR-induced Ca^{2+} signalling in DRG neurons, JPH4-silenced neurons were store-depleted with BK in the extracellular Ca^{2+} free solution (for consistency, all BK-induced SOCE experiments reported in this thesis were performed by applying the same protocol design). Interestingly, reducing the expression of JPH4 did not alter the basal Ca^{2+} pool levels (Figure 6.8.B), but it

significantly impaired SOCE as shown by a reduced Ca^{2+} influx as compared to control (Figure 6.8.C).

Alongside the BK, other inflammatory mediators released after tissue injury are histamine, 5-hydroxytriptamine (5-HT), adenosine triphosphate (ATP), nitric oxide and ions such as K^+ or H^+ (Kidd and Urban 2001). ATP is also involved in peripheral pain signalling by activating ligand-gated P2X receptors as well as metabotropic P2Y receptors in small nociceptive neurons (Liang et al. 2010, Gerevich and Illes 2004). Previous studies reported that GPCR-activated SOCE demonstrated an oscillatory behaviour as the ER Ca^{2+} pool depletes and refills continuously upon IP_3R or RyR activation (Suzuki et al. 2014). Thus, if a disruption in the Ca^{2+} store uptake occurs, further SOCE-activating processes should be inhibited. Figure 6.9 reveals that a lower expression of JPH4 in DRG neurons impairs ATP-induced SOCE, followed by a decrease in the ER Ca^{2+} uptake and, further on, a reduced BK-induced Ca^{2+} transients. As expected, lower intraorganellar Ca^{2+} levels would subsequently generate lower Ca^{2+} release levels. Moreover, the JPH4-KD was achieved only partially, thus a slow ER Ca^{2+} refill could be expected. Even in this condition, a strong and repetitive stimulation could lead to a deficiency in the recovery of the ER Ca^{2+} levels and, further on, to a reduced neuronal excitability.

An attempt to reduce the expression of JPH4 protein *in vivo* was made by collaborators at Hebei Medical University. The aim of this experiments was to determine changes in the nocifensive behaviour in JPH4 knockout mice as compared to naïve mice. JPH4-KD did not modify the basal thermal or mechanical sensitivity but reduced the BK-induced nociception (data not shown, manuscript in preparation).

All these observations taken together strengthen the hypothesis that JPH4 may have a functional role in recruiting STIM1 at ER-PM junctions, facilitating the CRAC channel assembly and thus mediating inflammatory-related SOCE in pain-sensing neurons. CRAC components have been previously reported as attractive targets for novel analgesic or anti-inflammatory compounds. The results presented in this chapter may lead the road to further

investigations to determine whether junctional proteins, such as JPH4, might be considered as pharmacological targets for inflammatory pain as well.

Chapter 7. General discussion

This study aimed at identifying the CRAC components in DRG neurons, investigating the effects of CRAC inhibitors and determining the role of junctophilin proteins to modulate SOCE in the context of inflammatory pain.

7.1 SOCE is driven mainly by the STIM1/Orai1 machinery in pain-sensing DRG neurons

Neurons use intra- and extracellular Ca^{2+} sources to generate intricate Ca^{2+} signals and the main intracellular Ca^{2+} pool is the ER. Ca^{2+} levels in this organelle are controlled by IP_3R, RyR and SERCA pumps (Berridge 1998). Elevated SOCE was previously associated with neuropathic and inflammatory pain and the presence of molecular components of CRAC channels were reported in primary afferent neurons (Fuchs et al. 2007, Gemes et al. 2011, Wei et al. 2017).

Amongst STIM and Orai family members, it has been suggested that all except Orai2 are expressed and mediate SOCE in DRGs (Wei et al. 2017). Current clamp recordings on Orai1 and Orai3 double knock-down neurons showed a reduced thapsigargin-induced membrane depolarization and spike frequency as compared to control (Wei et al. 2017). This suggests that Orai1 and Orai3 play a key role in SOCE-mediated excitability in peripheral sensory neurons.

Furthermore, fura-2 experiments revealed that thapsigargin-induced SOCE was negatively correlated with the somatic diameter, thus a more robust Ca^{2+} influx occurred in smaller neurons, frequently associated with nociceptors (Wei et al. 2017).

In this thesis I investigated the distribution pattern of STIM and Orai isoforms by immunohistochemistry (Chapter 3) and demonstrated that all proteins except Orai2 are indeed expressed in DRG neurons, which is in line with the observations of Wei and colleagues.

Moreover, the immunostainings revealed that STIM1 and Orai1 remain the most plausible candidates for the CRAC channel as they were expressed to a higher degree in DRG neurons as compared to STIM2 and Orai3. Would this imply they are involved in inflammatory pain signalling? To answer this, I determined whether endogenously expressed STIM1 and Orai1 proteins co-localize into puncta upon BK-induced SOCE, as to my knowledge, attempts to investigate similar scenarios were made only in sensory neurons transiently overexpressing these SOCE components (Gao et al. 2016, Wei et al. 2017). BK, amongst other inflammatory mediators that are released upon tissue injury, acts on the peripheral nerve terminals by activating or sensitizing specific receptors (Das V. 2015). The stimulation of B_2R is known to activate the PLC pathway which results in the release of IP_3 and DAG from PIP_2 (Das V 2015). The main role of IP_3 is to trigger ER Ca^{2+} store depletion through IP_3R, and the lowering in Ca^{2+} levels is further sensed by the ER resident STIM1. Further on, STIM1 clusters and interacts with Orai1 at the ER-PM junctions to mediate SOCE (Liou et al. 2005). Here I reported that BK-induced SOCE triggers the STIM1-Orai1 protein mobilization at the ER-PM junctions in DRG neurons, and therefore this process might have a functional role in inflammatory pain signalling.

7.2 STIM2 is expressed highly in large mechanosensory neurons

Interestingly, immunohistochemistry experiments revealed that STIM1, Orai 1 and Orai 3 are uniformly distributed throughout DRG neurons of all sizes, without any obvious bias towards neurons of a particular size. By contrast, the STIM2 distribution analysis demonstrated that only 34% of the smaller somata (diameter <25 µm) express STIM2, while 80% of larger neurons (>40 µm) revealed positive staining. Hence, STIM2 is preferentially expressed by the myelinated fibers within the DRG.

Previous studies reported that STIM2 could mediate SOCE when a partial ER Ca^{2+} store depletion occurs (and STIM1 is at rest). Moreover, STIM1 was shown to be 70 times faster to saturate Orai1 binding sites as compared to STIM2 and it responds quicker to a significant ER

Ca^{2+} drop (Stathopulos et al. 2009, Gruszczynska-Biegala and Kuznicki 2013). Considering these observations and my findings, it could be hypothesized that: i) in small pain sensing neurons STIM1 is mainly responsible for mediating SOCE, and ii) in large mechanosensory neurons STIM2 could enable SOCE and thus having a role in touch sensation. More investigations are needed to validate the different functions of STIM isoforms in DRG neurons.

Wei and colleagues also reported that thapsigargin induced-SOCE is more robust in small and medium-sized neurons (Wei et al.2017). The reason for this could be the higher expression of STIM1 as compared to STIM2 in small pain sensing nociceptors and the opposite for large myelinated neurons.

7.3 CRAC inhibitors reduce BK-induced SOCE in pain sensing neurons

Since the discovery of the CRAC channel, CRAC inhibitors were developed and widely used as tools for research. Biotech and pharmaceutical companies developed a range of small molecules to inhibit SOCE (McCarl et al. 2009). Several CRAC modulators are now in the pipeline with positive outcomes observed in Phase I clinical trials in immunology and allergy (Calcimedica Inc, 2017). SOCE plays a key role in inflammatory processes and its inhibition is associated with a decrease in cytokine production and subsequent pain alleviation as observed in *in vivo* studies (Gao XH et al. 2015). This thesis revealed that CRAC inhibitors YM and Synta potently reduced BK-induced SOCE in DRG neurons. Wei and colleagues recently reported that 10 µM YM and 30 µM Synta inhibited thapsigargin-induced SOCE by 30% in primary afferent neurons (Wei et al. 2017). In another study cyclopiazonic acid (CPA)-induced SOCE was reduced by approximately 50% when DRG neurons where treated with 3 µM YM and by approximately 15% when treated with 1 µM YM (Gao R et al. 2013). Both research groups applied the drugs acutely, immediately after maximal SOCE was reached. In this study I report that 1 µM YM and 3 µM Synta inhibited BK-induced SOCE by approximately 90%. The concentration I used was 10 times lower as compared to that used by

Wei and colleagues, but neurons were treated for 1 hour prior to store depletion. CHO cells experiments with the ER Ca^{2+} indicator R-CEPIA1*er* demonstrated that YM and Synta inhibit SOCE (and subsequent ER Ca^{2+} refill) greater in the pre-incubation paradigm, as compared to cells being treated during store depletion or during SOCE. Furthermore, PLA experiments revealed that even though YM shows a greater effect when cells were pre-incubated, it may not interfere with processes such as STIM1 Ca^{2+} sensing, its re-arrangement or movement to junctions. Similar results were reported for Synta in vascular smooth muscle cells (Li et al. 2011). This being said, the resistance of STIM1-Orai1 coupling machinery to either of the drugs does not rule out a possibility that YM or Synta may interfere with the formation of the ion channel pore or interfere with the STIM1-Orai1 interaction in such a way that while not affecting clustering, it nevertheless inhibits the formation of functional STIM1-Orai1 complex. The slow kinetics of YM and Synta and the necessity of pre-treatment do suggest that, unlike most ion channel inhibitors, these compounds are unlikely to block SOCE via a simple pore blocking mechanism. This is a novel finding that warrant further investigation, especially in light potential therapeutic applications of the SOCE inhibitors. Indeed, both YM and Synta demonstrated a high therapeutic potential in both neuropathic and inflammatory pain (Gao XH et al. 2015, Wei et al. 2017). They were shown to alter the cytokine release at tissue injury and to alleviate acute and chronic pain in animal models (Sabatino et al. 2009, Wei et al. 2017, Gao XH et al. 2015, Qi et al. 2016, Gemes et al. 2011). In conclusion, this current study provides evidence that YM and Synta complimentary inhibit SOCE in primary afferent neurons this effect is in good agreement with previously reported reduction of cytokine release by these compounds

7.4 Junctophilin proteins are expressed in DRG neurons

Junctional membrane complexes (JMC) between the ER and PM are structures that mediate the communication between proteins residing in these membranes (Takeshima et al. 2000). Junctophilin (JPH) proteins are important components of JMCs and they promote STIM1

translocation at the already formed ER-PM junctions. Thus, the interaction with Orai1 is facilitated and SOCE can be triggered (Fahrner et al. 2013). The expression of JPHs has been observed to be tissue-specific: JPH1 has been identified in skeletal muscle and to a lower degree in cardiomyocytes (Murphy et al. 2013), JPH2 in cardiac muscle cells (Minamisawa et al. 2004), JPH3 and JPH4 in neurons of the brain (Landstorm et al. 2014) and, to date, JPH4 has been the only family member identified in T cells (Landstorm et al. 2014). In both rodents and humans, lack of JPH proteins has been linked to muscular dystrophy (JPH1), arrhythmia (JPH2) and Hungtington-disease like syndrome (JPH3/4) (Ito et al. 2001, Minamisawa et al. 2004, Moriguchi et al. 2006, Paradisi et al. 2013). To my knowledge, literature holds no evidence of JPH proteins being expressed in peripheral sensory neurons, only the Allen Spinal Cord Atlas showing JPH3 and 4 gene expression mapped across the mouse spinal cord and DRGs (http://mousespinal.brain-map.org/).

This thesis for the first time reports the expression of JPH3 and 4 proteins in primary afferent neurons. Surprisingly, JPH1, thought to localize preferentially in skeletal muscle, has been also identified in approximately 50% of DRG neurons. All three proteins showed a uniform distribution within neurons of different sensory modalities, suggesting they might facilitate SOCE induced by a variety of stimuli. Furthermore, I demonstrated that these proteins are expressed in heat-sensitive nociceptors, with JPH4 to express at a higher degree than JPH1 and JPH3. TRPV1-positive nociceptors are believed to be the main type of primary afferent neurons that mediate inflammatory responses, thus I hypothesize that all three proteins might mediate Ca^{2+} dynamics in pain-sensing neurons.

7.5 JPH4 facilitates STIM1-Orai1 coupling in pain sensing neurons

Out of the three JPH proteins identified in DRG neurons, JPH4 was found to be expressed at the highest levels (assuming that the affinities of the JPH antibodies used in this study are comparable). Moreover, it was identified in approximately 80% of heat-sensitive nociceptors further suggesting that it might facilitate SOCE in inflammatory-pain scenarios. Here I

reported that STIM1 and Orai1 are co-expressed with JPH4 in DRG neurons and that both co-localized with JPH4 after store depletion. Interestingly, JPH4 revealed a filament-like localization with a preferred distribution towards the PM. It is likely to follow the ER cisternae that run alongside the PM. When Ca^{2+} levels are at rest, JPH4 co-localized partially with Orai1 towards the PM, but no co-localization of JPH4 and STIM1 was observed. As expected, STIM1 diffuses freely in the ER membrane and only when store depletion occurs it translocates at the ER-PM junctions.

Woo and colleagues recently reported that JPH4 mediates SOCE in T cells by forming a complex with junctate and recruiting STIM1 at the ER-PM junctions. Similarly, I demonstrated that STIM1 directly interacted with JPH4 after stimulation with BK, further suggesting that JPH4 might have a functional role in promoting the formation of CRAC channels in nociceptors.

To strengthen these observations, knock-down experiments revealed that STIM1-Orai1 interaction is disrupted in neurons lacking JPH4, thus this junctional protein is an important component of the CRAC channel complex assembly in pain sensing neurons.

Woo and colleagues demonstrated that both JPH4 and junctate bind STIM1 to facilitate SOCE in T cells. To my knowledge, there is no evidence of the expression of junctate in DRG neurons, but a research group identified it in brain (Hong et al. 2001). Whether JPH4 acts on its own to promote the CRAC channel assembly or if other scaffolding or supporting molecules are recured remains to be determined.

7.6 JPH4 facilitates SOCE in relation to inflammatory pain

My experiments demonstrated that silencing JPH4 disrupts STIM1-Orai1 interaction in pain sensing neurons. As a consequence of this disruption, in conditions of BK stimulation, a decreased SOCE was observed. Importantly, the basal Ca^{2+} levels remained unaffected. A limitation of this experiment was that only partial knock-down of JPH4 was achieved and this

could be the reason why SOCE was not completely abolished. Also, other junctional proteins might facilitate the CRAC channel assembly alongside JPH4. Therefore, in conditions of vigorous stimulation, similar to that occurring in the inflammatory milieu, neurons expressing less JPH4 were still able to refill their stores, albeit at a slower rate. Partial store replenishment affects subsequent SOCE and thus contributes to a decreased neuronal excitability in relation to inflammatory-mediated pain.

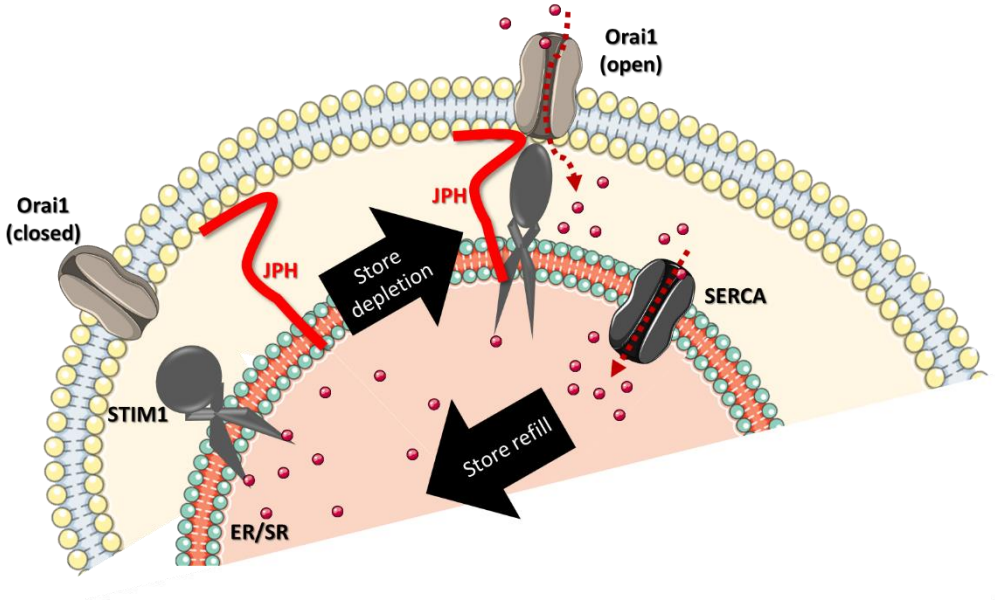

Figure 7.1. Schematic representation of STIM1 recruitment by JPH4. After ER Ca^{2+} pool depletion, STIM1 expands and clusters at the ER-PM junctions where it interacts with junctional proteins such as JPH. JPH4 has been shown to promote STIM1 recruitment in DRG neurons and to offer a supportive role to BK-induced SOCE.

Importantly, these observations were confirmed in the in vivo JPH4 knockdown experiments conducted in collaboration with researchers at Hebei Medical University. In these experiments, unilateral in vivo knock down of JPH4 in rats was performed using an intrathecal injection of cholesterol-conjugated JPH4 siRNA (the same sequence as the siRNA#2 used in this study). Knocking-down JPH4 in mice DRGs did not alter the basal thermal or mechanical sensitivity but significantly reduced the BK-induced pain-related (‘nocicefensive’) behaviour (data not shown, manuscript in preparation).

In conclusion, the work presented in this thesis brings evidence for:

a) the expression pattern of STIM/Orai components in DRG neurons of distinct sensory modalities,
b) the presence of inflammatory mediator (e.g. BK) - induced SOCE in DRG neurons,
c) the CRAC state-dependence effect of SOCE inhibitors YM and Synta
d) the identity and localization pattern of JPH proteins in primary afferent neurons and
e) the functional role of JPH4 in promoting CRAC channel assembly and mediating BK-induced SOCE in primary afferent neurons.

7.7 Future directions

The data presented in this study strengthen the importance of SOCE in inflammatory pain signalling and addressed some of the controversial issues surrounding the efficacy of CRAC inhibitors. The above-mentioned results are also fascinating observations regarding the putative role of JPHs (and JPH4 in particular) in facilitating pain signalling during inflammation.

SOCE is a complex and reversible mechanism that offers the possibility to target a range of proteins to develop novel therapies. Either CRAC channel components or their interacting partners are plausible candidates for future anti-inflammatory and/or analgesic drugs.

STIM 2, Orai 2 and Orai 3 are the isoforms that did not get as much attention from researchers as the other family members did. The impact they may have on facilitating SOCE in a range of scenarios (e.g. STIM2 have been reported to trigger SOCE when a partial ER Ca^{2+} store depletion occurs) should make them attractive for further research. For example, due to the distinct localization pattern of STIM isoforms, I speculate that STIM2 might be involved in mediating SOCE at lower pain thresholds as compared to STIM1.

Here I also reported that JPH4 promotes SOCE in stimulated primary afferent neurons. Whether JPH1 and/or 3 also play a key role in inflammatory pain signalling remains to be determined. One way to investigate this could involve knocking down JPH1 and JPH3 *in vitro* and *in vivo*, running Co-IP and PLA experiments to determine if JPHs form protein complexes upon SOCE stimulation, or if they function individually.

To summarise, the findings reported in this thesis provided evidence for the importance of CRAC components and brought to the surface the role of JPH proteins in the context of inflammatory pain. While researchers are continuously looking to better understand the mechanisms of pain signalling and to find novel pharmacological targets for analgesics, these results will hopefully contribute to building up knowledge in this field.

7.8 Study limitations

The current study has several limitations that could be addressed in future research, as follows:

The DRG neurons were used as a model of SOCE in relation to inflammatory pain signalling. While primary afferent neurons are widely used *in vitro* in all types of pain models (Xiao et al. 2007), the main caveat for using them is that DRG dissociation requires axotomy, thus limiting the results interpretation to the isolated cells (Malin et al. 2007). However, for confirming the hypothesis that JPH4 is important in inflammatory pain signalling, *in vivo* experiments using different pain models were performed by collaborators at Hebei University as described in Chapter 6.

Widely used in molecular biology research, CHO and HEK cell lines were used as analogues of SOCE and intracellular signalling of DRGs. The main reason to experiment on these established cell lines was to reduce the number of sacrificed animals. However, as compared to DRG neurons, these are non-excitable cells and the results may differ due to the lack of specific neuronal proteins such as voltage activate channels.

Bradykinin (250 nM) was used as a mechanism of depleting the ER luminal Ca^{2+} and stimulating SOCE. The concentration I used was tested and confirmed by previous lab members in DRG neurons, however I have not performed any other dosing regimens. It is indeed possible that higher doses of bradykinin could deplete the ER stores better or faster.

Proximity ligation assay (PLA) is a proteomic technique that uses the principle of two oligonucleotide-labelled antibodies that are capable to bind when are found within 40 nm of each other. While the technique is believed to be sensitive due to the detection of the amplified DNA, its sensitivity can be modulated by adjusting the incubation time during the rolling circle amplification. However, for the purpose of this study, I have followed the manufacturer's instructions, but different results may be obtained if amplification conditions would be tuned. Furthermore, there is a risk of not detecting several protein pairs due to the spatial uncertainty introduced by the IgG (primary and secondary) complex, which can be 10-20 nm in size itself, adding further distance to that between the target proteins. Also, already formed CRAC channels may not be detected.

For PLA analysis, I counted the number of puncta with an intensity higher than 10 per each neuron and presented the results as the number of puncta per 100 μm^2. I chose an intensity threshold of 10 as less than that was showing as diffused fluorescence. However, a weak intensity may still be a positive signal, but I took a conservative approach to avoid false negative results.

Similarly, the Immunohistochemistry (IHC) experiments were analysed by selecting the mean fluorescence intensity per DRG section. Indeed, this approach limits the number of neurons counted as positive as those with weak intensity were not considered. Furthermore, there is a limited blinding (assessing the Orai and STIM protein expression) that might have biased the analysis for the IHC, even though the same approach was used throughout all experiments and my findings are similar to what other groups reported (see Chapter 3).

The main limitation of the Co-immunoprecipitation (Co-IP) experiment is that the result mainly suggests that STIM1 and JPH4 are precipitating together as part of a protein complex. Whether they bind directly or indirectly through other proteins cannot be elucidated solely by this method. However, the Co-IP result alongside the PLA in JPH4 KD DRG neurons strongly suggest that JPH4 is involved in the mechanism of SOCE either as a direct or indirect partner with the CRAC components.

The experimental design for optimising the YM and Synta66 application (time) protocol has its limitations as well. Mainly, the design was based on previous literature (see Chpater 4), however a time-exposure variability would have been more appropriate to determine if i) YM and/or Synta are dependent on the state of SOCE, and if ii) YM and/or Synta are dependent on the treatment duration. The current experiment revealed that both drugs are more efficient if incubated 1h prior to store depletion, but whether an incubation time longer than 1h provides a better depletion (or even Ca^{2+} store abolition), remains to be determined.

YM and Synta are pyrazole-derivative drugs that were developed as SOCE inhibitors. However, their mechanism of action remains unknown. Recent literature determined that YM can interact with other Ca^{2+} handling proteins such as TRPM4 channels (Takezawa et al. 2006). The potency of YM as an agonist of TRPM4 is thought to be 100 times higher than that of CRAC channels, as shown in T-cells (Putney et al. 2010). To my knowledge, the selectivity of Synta against a panel of proteins was not yet tested. If YM or Synta activate plasma membrane Ca^{2+} channels, this may contribute to a depolarization and a reduced Ca^{2+} entry through CRAC channels. Thus, it cannot be ruled out that other proteins may contribute to the results presented in this thesis. Knock-down experiments and using specific inhibitors may provide further evidence about the drugs' selectivity. Furthermore, the basal Ca^{2+} levels could also be measured to determine if the drugs influence the overall ER loading during the incubation phase as compared to the acute treatment.

For testing the ER Ca^{2+} fluctuations I used CEPIA sensors as described in Chapter 2.5 However, I have not tested other ER Ca^{2+} indicators and therefore I relied on the specificity

and transfection efficacy as described by Suzuki and colleagues. Another limitation would be not measuring the dye saturation and not calculating the Ca^{2+} concentration which may affect the overall depletion/refill ratio. Moreover, to determine whether the fluorescence intensity decreases with time, running an experiment to determine the bleaching time of the Ca^{2+} indicator would be necessary.

Two STIM1 splice variants have been observed: STIM1S (S for small, 90 kDa) and STIM1L (L for long, 115 kDa) (Darbellay et al. 2011). While STIM1S slowly clusters to form CRAC channels in response to ER Ca^{2+} depletion, STIM1L was shown to colocalize with Orai1, interact with actin and form permanent clusters independent of SOCE (Darbellay et al. 2011). To my knowledge, the different expression of STIM1L and STIM1S in DRG neurons was not determined yet, however the PLA experiments presented in this thesis revealed fluorescent puncta between Orai1 and STIM1 when Ca^{2+} levels are at rest. This may be due to the permanent clusters formed between STIM1L and Orai1 as described by Darbellay and colleagues. To test this hypothesis, specific antibodies can be used to determine the expression (and role) of the two STIM1 splice variants in DRG neurons.

References

Akbari, Y., et al. (2004). "Presenilin regulates capacitative calcium entry dependently and independently of gamma-secretase activity." Biochem Biophys Res Commun 322(4): 1145-1152.

Alansary, D., et al. (2014). "Patch-clamp measurement of ICRAC and ORAI channel activity." Cold Spring Harb Protoc 2014(6): 602-607.

Alzayady, K. J., et al. (2013). "Functional inositol 1,4,5-trisphosphate receptors assembled from concatenated homo- and heteromeric subunits." J Biol Chem 288(41): 29772-29784.

Ashby, M. C. and A. V. Tepikin (2001). "ER calcium and the functions of intracellular organelles." Semin Cell Dev Biol 12(1): 11-17.

Baba, Y., et al. (2006). "Coupling of STIM1 to store-operated Ca^{2+} entry through its constitutive and inducible movement in the endoplasmic reticulum." Proc Natl Acad Sci U S A 103(45): 16704-16709.

Balijepalli, R. C., et al. (2003). "Depletion of T-tubules and specific subcellular changes in sarcolemmal proteins in tachycardia-induced heart failure." Cardiovasc Res 59(1): 67-77.

Barneo-Munoz, M., et al. (2015). "Lack of GDAP1 induces neuronal calcium and mitochondrial defects in a knockout mouse model of charcot-marie-tooth neuropathy." PLoS Genet 11(4): e1005115.

Baryshnikov, S. G., et al. (2009). "Orai1, a critical component of store-operated Ca^{2+} entry, is functionally associated with Na+/Ca^{2+} exchanger and plasma membrane Ca^{2+} pump in proliferating human arterial myocytes." Am J Physiol Cell Physiol 297(5): C1103-1112.

Basbaum, A. I. (1999). "Spinal mechanisms of acute and persistent pain." Reg Anesth Pain Med 24(1): 59-67.

Bauer, M. C., et al. (2008). "Calmodulin binding to the polybasic C-termini of STIM proteins involved in store-operated calcium entry." Biochemistry 47(23): 6089-6091.

Beavers, D. L., et al. (2013). "Mutation E169K in junctophilin-2 causes atrial fibrillation due to impaired RyR2 stabilization." J Am Coll Cardiol 62(21): 2010-2019.

Bergmeier, W., et al. (2009). "R93W mutation in Orai1 causes impaired calcium influx in platelets." Blood 113(3): 675-678.

Berna-Erro, A., et al. (2009). "STIM2 regulates capacitive Ca^{2+} entry in neurons and plays a key role in hypoxic neuronal cell death." Sci Signal 2(93): ra67.

Berridge, M. J. (1993). "Inositol trisphosphate and calcium signalling." Nature 361(6410): 315-325.

Berridge, M. J. (1998). "Neuronal calcium signaling." Neuron 21(1): 13-26.

Berridge, M. J. (2006). "Calcium microdomains: organization and function." Cell Calcium 40(5-6): 405-412.

Berridge, M. J., et al. (2003). "Calcium signalling: dynamics, homeostasis and remodelling." Nat Rev Mol Cell Biol 4(7): 517-529.

Bhardwaj, R., et al. (2013). "Oligomerization and Ca^{2+}/calmodulin control binding of the ER Ca^{2+}-sensors STIM1 and STIM2 to plasma membrane lipids." Biosci Rep 33(5).

Bhave, G., et al. (2002). "cAMP-dependent protein kinase regulates desensitization of the capsaicin receptor (VR1) by direct phosphorylation." Neuron 35(4): 721-731.

Bird, G. S., et al. (2008). "Methods for studying store-operated calcium entry." Methods 46(3): 204-212.

Block, B. A., et al. (1988). "Structural evidence for direct interaction between the molecular components of the transverse tubule/sarcoplasmic reticulum junction in skeletal muscle." J Cell Biol 107(6 Pt 2): 2587-2600.

Bohm, J., et al. (2013). "Constitutive activation of the calcium sensor STIM1 causes tubular-aggregate myopathy." Am J Hum Genet 92(2): 271-278.

Bohr, D. F. (1963). "Vascular Smooth Muscle: Dual Effect of Calcium." Science 139(3555): 597-599.

Bollimuntha, S., et al. (2017). "Neurological and Motor Disorders: Neuronal Store-Operated $Ca(^{2+})$ Signaling: An Overview and Its Function." Adv Exp Med Biol 993: 535-556.

Bolotina, V. M. and P. Csutora (2005). "CIF and other mysteries of the store-operated Ca^{2+}-entry pathway." Trends Biochem Sci 30(7): 378-387.

Bonora, M., et al. (2013). "Subcellular calcium measurements in mammalian cells using jellyfish photoprotein aequorin-based probes." Nat Protoc 8(11): 2105-2118.

Bourinet, E., et al. (2014). "Calcium-permeable ion channels in pain signaling." Physiol Rev 94(1): 81-140.

Brette, F. and C. Orchard (2003). "T-tubule function in mammalian cardiac myocytes." Circ Res 92(11): 1182-1192.

Bridges, D., et al. (2001). "Mechanisms of neuropathic pain." Br J Anaesth 87(1): 12-26.

Brotto, M. (2011). “Aging, sarcopenia and store-operated calcium entry: a common link?” Cell Cycle 10(24): 4201-2.

Campbell, J. N. and R. A. Meyer (2006). "Mechanisms of neuropathic pain." Neuron 52(1): 77-92.

Carr, D. B. and L. C. Goudas (1999). "Acute pain." Lancet 353(9169): 2051-2058.

Carrillo, C., et al. (2012). "Oleic acid inhibits store-operated calcium entry in human colorectal adenocarcinoma cells." Eur J Nutr 51(6): 677-684.

Caterina, M. J., et al. (2000). "Impaired nociception and pain sensation in mice lacking the capsaicin receptor." Science 288(5464): 306-313.

Caterina, M. J., et al. (1997). "The capsaicin receptor: a heat-activated ion channel in the pain pathway." Nature 389(6653): 816-824.

Cerella, C., et al. (2010). “The dual role of calcium as messenger and stressor in cell damage, death, and survival.” Int J Cell Biol 2010: 546163.

Chantelau, E. A. (2015). "Nociception at the diabetic foot, an uncharted territory." World J Diabetes 6(3): 391-402.

Chelu, M. G. and X. H. Wehrens (2007). "Sarcoplasmic reticulum calcium leak and cardiac arrhythmias." Biochem Soc Trans 35(Pt 5): 952-956.

Chen, G., et al. (2013). "Characterization of a novel CRAC inhibitor that potently blocks human T cell activation and effector functions." Mol Immunol 54(3-4): 355-367.

Chung, S. C., et al. (1994). "Inhibition by SK&F 96365 of Ca^{2+} current, IL-2 production and activation in T lymphocytes." Br J Pharmacol 113(3): 861-868.

Clapham, D. E. (2007). "Calcium signaling." Cell 131(6): 1047-1058.

Correll, R. N., et al. (2017). "Mitsugumin 29 regulates t-tubule architecture in the failing heart." Sci Rep 7(1): 5328.

Csutora, P., et al. (2008). "Novel role for STIM1 as a trigger for calcium influx factor production." J Biol Chem 283(21): 14524-14531.

Csutora, P., et al. (1999). "Calcium influx factor is synthesized by yeast and mammalian cells depleted of organellar calcium stores." Proc Natl Acad Sci U S A 96(1): 121-126.

Darbellay, B., et al. (2011). "STIM1L is a new actin-binding splice variant involved in fast repetitive Ca^{2+} release." J Cell Biol 194(2): 335-346.

Das, V. (2015). "An introduction to pain pathways and pain "targets"." Prog Mol Biol Transl Sci 131: 1-30.

Davis, F. M., et al. (2012). "Non-stimulated, agonist-stimulated and store-operated Ca^{2+} influx in MDA-MB-468 breast cancer cells and the effect of EGF-induced EMT on calcium entry." PLoS One 7(5): e36923.

DeHaven, W. I., et al. (2008). "Complex actions of 2-aminoethyldiphenyl borate on store-operated calcium entry." J Biol Chem 283(28): 19265-19273.

DeHaven, W. I., et al. (2007). "Calcium inhibition and calcium potentiation of Orai1, Orai2, and Orai3 calcium release-activated calcium channels." J Biol Chem 282(24): 17548-17556.

Derler, I., et al. (2013). "The action of selective CRAC channel blockers is affected by the Orai pore geometry." Cell Calcium 53(2): 139-151.

Devor, M. (1999). "Unexplained peculiarities of the dorsal root ganglion." Pain Suppl 6: S27-35.

Di Sabatino, A., et al. (2009). "Targeting gut T cell Ca^{2+} release-activated Ca^{2+} channels inhibits T cell cytokine production and T-box transcription factor T-bet in inflammatory bowel disease." J Immunol 183(5): 3454-3462.

Dray, A., et al. (1993). "Bradykinin and inflammatory pain." Trends Neurosci 16(3):99-104.

Dubin, A. E. and A. Patapoutian (2010). "Nociceptors: the sensors of the pain pathway." J Clin Invest 120(11): 3760-3772.

Duncan, C., et al. (2013). "Painful nerve injury decreases sarco-endoplasmic reticulum Ca(2)(+)-ATPase activity in axotomized sensory neurons." Neuroscience 231: 247-257.

Edwards, J. M., et al. (2010). "Exercise training decreases store-operated Ca^{2+}entry associated with metabolic syndrome and coronary atherosclerosis." Cardiovasc Res 85(3): 631-640.

Emptage, N. J., et al. (2001). "Calcium stores in hippocampal synaptic boutons mediate short-term plasticity, store-operated Ca^{2+} entry, and spontaneous transmitter release." Neuron 29(1): 197-208.

Erb, L. and G. A. Weisman (2012). "Coupling of P2Y receptors to G proteins and other signaling pathways." Wiley Interdiscip Rev Membr Transp Signal 1(6): 789-803.

Ercan, E., et al. (2012). "Di-arginine signals and the K-rich domain retain the Ca(2)(+) sensor STIM1 in the endoplasmic reticulum." Traffic 13(7): 992-1003.

Ercan, E., et al. (2009). "A conserved, lipid-mediated sorting mechanism of yeast Ist2 and mammalian STIM proteins to the peripheral ER." Traffic 10(12): 1802-1818.

Fahrner, M., et al. (2013). "The STIM1/Orai signaling machinery." Channels (Austin) 7(5): 330-343.

Fahrner, M., et al. (2017). "The STIM-Orai Pathway: The Interactions Between STIM and Orai." Adv Exp Med Biol 993: 59-81.

Feske, S. (2009). "ORAI1 and STIM1 deficiency in human and mice: roles of store-operated Ca^{2+} entry in the immune system and beyond." Immunol Rev 231(1): 189-209.

Feske, S. (2010). "CRAC channelopathies." Pflugers Arch 460(2): 417-435.

Feske, S., et al. (2006). "A mutation in Orai1 causes immune deficiency by abrogating CRAC channel function." Nature 441(7090): 179-185.

Feske, S., et al. (2012). "Ion channels and transporters in lymphocyte function and immunity." Nat Rev Immunol 12(7): 532-547.

Fiorio Pla, A., et al. (2005). "Canonical transient receptor potential 1 plays a role in basic fibroblast growth factor (bFGF)/FGF receptor-1-induced Ca^{2+} entry and embryonic rat neural stem cell proliferation." J Neurosci 25(10): 2687-2701.

Fischer, B. S., et al. (2001). "Capsaicin inhibits Jurkat T-cell activation by blocking calcium entry current I(CRAC)." J Pharmacol Exp Ther 299(1): 238-246.

Flemming, R., et al. (2003). "Pharmacological profile of store-operated channels in cerebral arteriolar smooth muscle cells." Br J Pharmacol 139(5): 955-965.

Foskett, J. K., et al. (2007). "Inositol trisphosphate receptor Ca^{2+} release channels." Physiol Rev 87(2): 593-658.

Franzini-Armstrong, C., et al. (1999). "Shape, size, and distribution of $Ca(^{2+})$ release units and couplons in skeletal and cardiac muscles." Biophys J 77(3): 1528-1539.

Franzius, D., et al. (1994). "Non-specific effects of calcium entry antagonists in mast cells." Pflugers Arch 428(5-6): 433-438.

Fredriksson, S., et al. (2002). "Protein detection using proximity-dependent DNA ligation assays." Nat Biotechnol 20(5): 473-477.

Frischauf, I., et al. (2009). "Molecular determinants of the coupling between STIM1 and Orai channels: differential activation of Orai1-3 channels by a STIM1 coiled-coil mutant." J Biol Chem 284(32): 21696-21706.

Frischauf, I., et al. (2011). "Cooperativeness of Orai cytosolic domains tunes subtype-specific gating." J Biol Chem 286(10): 8577-8584.

Frischauf, I., et al. (2015). "A calcium-accumulating region, CAR, in the channel Orai1 enhances Ca($^{2+}$) permeation and SOCE-induced gene transcription." Sci Signal 8(408): ra131.

Fuchs, A., et al. (2005). "Painful nerve injury decreases resting cytosolic calcium concentrations in sensory neurons of rats." Anesthesiology 102(6): 1217-1225.

Galvan, D. L., et al. (1999). "Subunit oligomerization, and topology of the inositol 1,4, 5-trisphosphate receptor." J Biol Chem 274(41): 29483-29492.

Gao, R., et al. (2013). "Potent analgesic effects of a store-operated calcium channel inhibitor." Pain 154(10): 2034-2044.

Gao, X., et al. (2016). "STIMs and Orai1 regulate cytokine production in spinal astrocytes." J Neuroinflammation 13(1): 126.

Gao, X. H., et al. (2015). "A store-operated calcium channel inhibitor attenuates collagen-induced arthritis." Br J Pharmacol 172(12): 2991-3002.

Gees, M., et al. (2010). "The role of transient receptor potential cation channels in Ca^{2+} signaling." Cold Spring Harb Perspect Biol 2(10): a003962.

Geppetti, P., et al. (2015). "G Protein-Coupled Receptors: Dynamic Machines for Signaling Pain and Itch." Neuron 88(4): 635-649.

Gerasimenko, J. V., et al. (2013). "Ca^{2+} release-activated Ca^{2+} channel blockade as a potential tool in antipancreatitis therapy." Proc Natl Acad Sci U S A 110(32): 13186-13191.

Gerevich, Z. and P. Illes (2004). "P2Y receptors and pain transmission." Purinergic Signal 1(1): 3-10.

Golini, L., et al. (2011). "Junctophilin 1 and 2 proteins interact with the L-type Ca^{2+} channel dihydropyridine receptors (DHPRs) in skeletal muscle." J Biol Chem 286(51): 43717-43725.

Graham, S. J., et al. (2011). "A cytosolic STIM2 preprotein created by signal peptide inefficiency activates ORAI1 in a store-independent manner." J Biol Chem 286(18): 16174-16185.

Gruszczynska-Biegala, J. and J. Kuznicki (2013). "Native STIM2 and ORAI1 proteins form a calcium-sensitive and thapsigargin-insensitive complex in cortical neurons." J Neurochem 126(6): 727-738.

Grynkiewicz, G., et al. (1985). "A new generation of Ca^{2+} indicators with greatly improved fluorescence properties." J Biol Chem 260(6): 3440-3450.

Gudlur, A. and P. G. Hogan (2017). "The STIM-Orai Pathway: Orai, the Pore-Forming Subunit of the CRAC Channel." Adv Exp Med Biol 993: 39-57.

Gudlur, A., et al. (2013). "STIM-ORAI interactions that control the CRAC channel." Curr Top Membr 71: 33-58.

Guo, A., et al. (2014). “Overexpression of junctophilin-2 does not enhance baseline function but attenuates heart failure development after cardiac stress.” PNAS 111(33): 12240-12245.

Gwack, Y., et al. (2007). "Biochemical and functional characterization of Orai proteins." J Biol Chem 282(22): 16232-16243.

Hadad, N., et al. (1999). "Cardiac sarcalumenin: phosphorylation, comparison with the skeletal muscle sarcalumenin and modulation of ryanodine receptor." J Membr Biol 170(1): 39-49.

Hamada, K., et al. (2017). "IP3-mediated gating mechanism of the IP3 receptor revealed by mutagenesis and X-ray crystallography." Proc Natl Acad Sci U S A 114(18): 4661-4666.

Harper, A. A. and S. N. Lawson (1985). "Conduction velocity is related to morphological cell type in rat dorsal root ganglion neurones." J Physiol 359: 31-46.

Harper, J. L., et al. (1997). "Loperamide: a positive modulator for store-operated calcium channels?" Proc Natl Acad Sci U S A 94(26): 14912-14917.

Hartmann, J., et al. (2014). "STIM1 controls neuronal Ca(2)(+) signaling, mGluR1-dependent synaptic transmission, and cerebellar motor behavior." Neuron 82(3): 635-644.

Hayashi, T., et al. (2009). "Three-dimensional electron microscopy reveals new details of membrane systems for Ca^{2+} signaling in the heart." J Cell Sci 122(Pt 7): 1005-1013.

Hirata, Y., et al. (2006). "Uncoupling store-operated Ca^{2+} entry and altered Ca^{2+} release from sarcoplasmic reticulum through silencing of junctophilin genes." Biophys J 90(12): 4418-4427.

Holmes, S. E., et al. (2001). "A repeat expansion in the gene encoding junctophilin-3 is associated with Huntington disease-like 2." Nat Genet 29(4): 377-378.

Hong, C. S., et al. (2001). "Molecular cloning and characterization of mouse cardiac triadin isoforms." Gene 278(1-2): 193-199.

Hooper, R., et al. (2014). "Neuronal STIMulation at rest." Sci Signal 7(335): pe18.

Hoth, M. and B. A. Niemeyer (2013). "The neglected CRAC proteins: Orai2, Orai3, and STIM2." Curr Top Membr 71: 237-271.

Hoth, M. and R. Penner (1992). "Depletion of intracellular calcium stores activates a calcium current in mast cells." Nature 355(6358): 353-356.

Hou, X., et al. (2012). "Crystal structure of the calcium release-activated calcium channel Orai." Science 338(6112): 1308-1313.

Huang, T. J., et al. (2002). "Diabetes-induced alterations in calcium homeostasis in sensory neurones of streptozotocin-diabetic rats are restricted to lumbar ganglia and are prevented by neurotrophin-3." Diabetologia 45(4): 560-570.

Ikeda, A., et al. (2007). "Abnormal features in mutant cerebellar Purkinje cells lacking junctophilins." Biochem Biophys Res Commun 363(3): 835-839.

Inayama, M., et al. (2015). "Orai1-Orai2 complex is involved in store-operated calcium entry in chondrocyte cell lines." Cell Calcium 57(5-6): 337-347.

Ishikawa, J., et al. (2003). "A pyrazole derivative, YM-58483, potently inhibits store-operated sustained Ca^{2+} influx and IL-2 production in T lymphocytes." J Immunol 170(9): 4441-4449.

Ito, K., et al. (2001). "Deficiency of triad junction and contraction in mutant skeletal muscle lacking junctophilin type 1." J Cell Biol 154(5): 1059-1067.

Jackson, T. R., et al. (1988). "A novel tumour promoter, thapsigargin, transiently increases cytoplasmic free Ca^{2+} without generation of inositol phosphates in NG115-401L neuronal cells." Biochem J 253(1): 81-86.

Jairaman, A. and M. Prakriya (2013). "Molecular pharmacology of store-operated CRAC channels." Channels (Austin) 7(5): 402-414.

Jeske, N. A. (2015). "Peripheral scaffolding and signaling pathways in inflammatory pain." Prog Mol Biol Transl Sci 131: 31-52.

Jha, A. and S. Muallem (2016). "The CAR that drives Ca^{2+} to Orai1." Sci Signal 9(418): fs5.

Jia, Y., et al. (2007). "TRPC channels promote cerebellar granule neuron survival." Nat Neurosci 10(5): 559-567.

Jin, X., et al. (2013). "Activation of the Cl- channel ANO1 by localized calcium signals in nociceptive sensory neurons requires coupling with the IP3 receptor." Sci Signal 6(290): ra73.

Johnstone, L. S., et al. (2010). "STIM proteins: integrators of signalling pathways in development, differentiation and disease." J Cell Mol Med 14(7): 1890-1903.

Jung, J., et al. (2004). "Phosphorylation of vanilloid receptor 1 by Ca^{2+}/calmodulin-dependent kinase II regulates its vanilloid binding." J Biol Chem 279(8): 7048-7054.

Kakizawa, S., et al. (2007). "Junctophilin-mediated channel crosstalk essential for cerebellar synaptic plasticity." EMBO J 26(7): 1924-1933.

Kawasaki, T., et al. (2010). "Protein kinase C-induced phosphorylation of Orai1 regulates the intracellular Ca^{2+} level via the store-operated Ca^{2+} channel." J Biol Chem 285(33): 25720-25730.

Kidd, B. L. and L. A. Urban (2001). "Mechanisms of inflammatory pain." Br J Anaesth 87(1): 3-11.

Kim, H. Y. and M. R. Hanley (1999). "Calcium influx factor (CIF) as a diffusible messenger for the activation of capacitative calcium entry in Xenopus oocytes." Mol Cells 9(3): 326-332.

Kirton, H. M., et al. (2013). "Transient overexpression of genes in neurons using nucleofection." Methods Mol Biol 998: 55-64.

Klejman, M. E., et al. (2009). "Expression of STIM1 in brain and puncta-like co-localization of STIM1 and ORAI1 upon depletion of Ca($^{2+}$) store in neurons." Neurochem Int 54(1): 49-55.

Kohn, E. C., et al. (1996). "Clinical investigation of a cytostatic calcium influx inhibitor in patients with refractory cancers." Cancer Res 56(3): 569-573.

Kraft, R. (2015). "STIM and ORAI proteins in the nervous system." Channels (Austin) 9(5): 245-252.

Krause, A., et al. (2015). "Junctophilin 3 (JPH3) expansion mutations causing Huntington disease like 2 (HDL2) are common in South African patients with African ancestry and a Huntington disease phenotype." Am J Med Genet B Neuropsychiatr Genet 168(7): 573-585.

Lai, F. A., et al. (1992). "Expression of a cardiac Ca($^{2+}$)-release channel isoform in mammalian brain." Biochem J 288 (Pt 2): 553-564.

Lalonde, J., et al. (2014). "Store-operated calcium entry promotes the degradation of the transcription factor Sp4 in resting neurons." Sci Signal 7(328): ra51.

Landstrom, A. P. and M. J. Ackerman (2012). "Beyond the cardiac myofilament: hypertrophic cardiomyopathy- associated mutations in genes that encode calcium-handling proteins." Curr Mol Med 12(5): 507-518.

Landstrom, A. P., et al. (2014). "The junctophilin family of proteins: from bench to bedside." Trends Mol Med 20(6): 353-362.

Landstrom, A. P., et al. (2011). "Junctophilin-2 expression silencing causes cardiocyte hypertrophy and abnormal intracellular calcium-handling." Circ Heart Fail 4(2): 214-223.

Lanner, J. T., et al. (2010). "Ryanodine receptors: structure, expression, molecular details, and function in calcium release." Cold Spring Harb Perspect Biol 2(11): a003996.

Lee, K. P., et al. (2010). "An endoplasmic reticulum/plasma membrane junction: STIM1/Orai1/TRPCs." FEBS Lett 584(10): 2022-2027.

Lee, K. P., et al. (2009). "Molecular determinants of fast Ca^{2+}-dependent inactivation and gating of the Orai channels." Proc Natl Acad Sci U S A 106(34): 14687-14692.

Lewis, R. S. and M. D. Cahalan (1989). "Mitogen-induced oscillations of cytosolic Ca^{2+} and transmembrane Ca^{2+} current in human leukemic T cells." Cell Regul 1(1): 99-112.

Li, J., et al. (2011). "Nanomolar potency and selectivity of a Ca(2)(+) release-activated Ca(2)(+) channel inhibitor against store-operated Ca(2)(+) entry and migration of vascular smooth muscle cells." Br J Pharmacol 164(2): 382-393.

Li, X., et al. (2017). "Calmodulin dissociates the STIM1-Orai1 complex and STIM1 oligomers." Nat Commun 8(1): 1042.

Linley, J. E., et al. (2010). "Understanding inflammatory pain: ion channels contributing to acute and chronic nociception." Pflugers Arch 459(5): 657-669.

Liou, J., et al. (2007). "Live-cell imaging reveals sequential oligomerization and local plasma membrane targeting of stromal interaction molecule 1 after Ca^{2+} store depletion." Proc Natl Acad Sci U S A 104(22): 9301-9306.

Liou, J., et al. (2005). "STIM is a Ca^{2+} sensor essential for Ca^{2+}-store-depletion-triggered Ca^{2+} influx." Curr Biol 15(13): 1235-1241.

Lis, A., et al. (2007). "CRACM1, CRACM2, and CRACM3 are store-operated Ca^{2+} channels with distinct functional properties." Curr Biol 17(9): 794-800.

Liu, X., et al. (2003). "TRPC1 is required for functional store-operated Ca^{2+} channels. Role of acidic amino acid residues in the S5-S6 region." J Biol Chem 278(13): 11337-11343.

Luik, R. M., et al. (2006). "The elementary unit of store-operated Ca^{2+} entry: local activation of CRAC channels by STIM1 at ER-plasma membrane junctions." J Cell Biol 174(6): 815-825.

Malin, S.A., et al. (2007). “Production of dissociated sensory neuron cultures and considerations for their use in studying neuronal function and plasticity.” Nat Protoc 2(1): 152-60.

Malli, R., et al. (2008). "Cytosolic Ca^{2+} prevents the subplasmalemmal clustering of STIM1: an intrinsic mechanism to avoid Ca^{2+} overload." J Cell Sci 121(Pt 19): 3133-3139.

Mancarella, S., et al. (2013). "Targeted STIM deletion impairs calcium homeostasis, NFAT activation, and growth of smooth muscle." FASEB J 27(3): 893-906.

Manjarres, I. M., et al. (2010). "The sarco/endoplasmic reticulum Ca($^{2+}$) ATPase (SERCA) is the third element in capacitative calcium entry." Cell Calcium 47(5): 412-418.

Markello, T., et al. (2015). "York platelet syndrome is a CRAC channelopathy due to gain-of-function mutations in STIM1." Mol Genet Metab 114(3): 474-482.

Maschalidi, S., et al. (2017). "UNC93B1 interacts with the calcium sensor STIM1 for efficient antigen cross-presentation in dendritic cells." Nat Commun 8(1): 1640.

McCarl, C. A., et al. (2009). "ORAI1 deficiency and lack of store-operated Ca^{2+} entry cause immunodeficiency, myopathy, and ectodermal dysplasia." J Allergy Clin Immunol 124(6): 1311-1318 e1317.

Meissner, G. (1994). "Ryanodine receptor/Ca^{2+} release channels and their regulation by endogenous effectors." Annu Rev Physiol 56: 485-508.

Mercer, J. C., et al. (2006). "Large store-operated calcium selective currents due to co-expression of Orai1 or Orai2 with the intracellular calcium sensor, Stim1." J Biol Chem 281(34): 24979-24990.

Mignen, O., et al. (2005). "Carboxyamidotriazole-induced inhibition of mitochondrial calcium import blocks capacitative calcium entry and cell proliferation in HEK-293 cells." J Cell Sci 118(Pt 23): 5615-5623.

Misceo, D., et al. (2014). "A dominant STIM1 mutation causes Stormorken syndrome." Hum Mutat 35(5): 556-564.

Molliver, D. C., et al. (1995). "Presence or absence of TrkA protein distinguishes subsets of small sensory neurons with unique cytochemical characteristics and dorsal horn projections." J Comp Neurol 361(3): 404-416.

Motiani, R. K., et al. (2010). "A novel native store-operated calcium channel encoded by Orai3: selective requirement of Orai3 versus Orai1 in estrogen receptor-positive versus estrogen receptor-negative breast cancer cells." J Biol Chem 285(25): 19173-19183.

Muik, M., et al. (2011). "STIM1 couples to ORAI1 via an intramolecular transition into an extended conformation." EMBO J 30(9): 1678-1689.

Mullins, F. M., et al. (2009). "STIM1 and calmodulin interact with Orai1 to induce Ca^{2+}-dependent inactivation of CRAC channels." Proc Natl Acad Sci U S A 106(36): 15495-15500.

Mullins, F. M., et al. (2016). "Orai1 pore residues control CRAC channel inactivation independently of calmodulin." J Gen Physiol 147(2): 137-152.

Murphy, R. M., et al. (2013). "Ca^{2+}-dependent proteolysis of junctophilin-1 and junctophilin-2 in skeletal and cardiac muscle." J Physiol 591(3): 719-729.

Nishi, M., et al. (2003). "Coexpression of junctophilin type 3 and type 4 in brain." Brain Res Mol Brain Res 118(1-2): 102-110.

Nishiyama, M., et al. (2000). "Calcium stores regulate the polarity and input specificity of synaptic modification." Nature 408(6812): 584-588.

Nunes, P. and N. Demaurex (2014). "Redox regulation of store-operated Ca^{2+} entry." Antioxid Redox Signal 21(6): 915-932.

Ong, H. L., et al. (2015). "STIM2 enhances receptor-stimulated Ca(2)(+) signaling by promoting recruitment of STIM1 to the endoplasmic reticulum-plasma membrane junctions." Sci Signal 8(359): ra3.

Palmer, A. E., et al. (2004). "Bcl-2-mediated alterations in endoplasmic reticulum Ca^{2+} analyzed with an improved genetically encoded fluorescent sensor." Proc Natl Acad Sci U S A 101(50): 17404-17409.

Palty, R. and E. Y. Isacoff (2016). "Cooperative Binding of Stromal Interaction Molecule 1 (STIM1) to the N and C Termini of Calcium Release-activated Calcium Modulator 1 (Orai1)." J Biol Chem 291(1): 334-341.

Palty, R., et al. (2012). "SARAF inactivates the store operated calcium entry machinery to prevent excess calcium refilling." Cell 149(2): 425-438.

Pan, Z., et al. (2014). "Store-operated Ca^{2+} entry in muscle physiology and diseases." BMB Rep 47(2): 69-79.

Pandol, S. J., et al. (2007). "Acute pancreatitis: bench to the bedside." Gastroenterology 132(3): 1127-1151.

Paradisi, I., et al. (2013). "Huntington disease-like 2 (HDL2) in Venezuela: frequency and ethnic origin." J Hum Genet 58(1): 3-6.

Paredes, R. M., et al. (2008). "Chemical calcium indicators." Methods 46(3): 143-151.

Parekh, A. B. (2008). "Ca^{2+} microdomains near plasma membrane Ca^{2+} channels: impact on cell function." J Physiol 586(13): 3043-3054.

Parekh, A. B. (2010). "Store-operated CRAC channels: function in health and disease." Nat Rev Drug Discov 9(5): 399-410.

Parekh, A. B. and J. W. Putney, Jr. (2005). "Store-operated calcium channels." Physiol Rev 85(2): 757-810.

Pareyson, D., et al. (2013). "Dominant Charcot-Marie-Tooth syndrome and cognate disorders." Handb Clin Neurol 115: 817-845.

Park, C. Y., et al. (2009). "STIM1 clusters and activates CRAC channels via direct binding of a cytosolic domain to Orai1." Cell 136(5): 876-890.

Patel, S., et al. (2011). "The endo-lysosomal system as an NAADP-sensitive acidic $Ca(^{2+})$ store: role for the two-pore channels." Cell Calcium 50(2): 157-167.

Peinelt, C., et al. (2008). "2-Aminoethoxydiphenyl borate directly facilitates and indirectly inhibits STIM1-dependent gating of CRAC channels." J Physiol 586(13): 3061-3073.

Pevarello, P., et al. (2014). "$Ca(^{2+})$ release-activated $Ca(^{2+})$ channel inhibitors." Pharm Pat Anal 3(2): 171-182.

Phimister, A. J., et al. (2007). "Conformation-dependent stability of junctophilin 1 (JP1) and ryanodine receptor type 1 (RyR1) channel complex is mediated by their hyper-reactive thiols." J Biol Chem 282(12): 8667-8677.

Phizicky, E. M. and S. Fields (1995). "Protein-protein interactions: methods for detection and analysis." Microbiol Rev 59(1): 94-123.

Pla-Martin, D., et al. (2013). "Silencing of the Charcot-Marie-Tooth disease-associated gene GDAP1 induces abnormal mitochondrial distribution and affects Ca^{2+} homeostasis by reducing store-operated Ca^{2+} entry." Neurobiol Dis 55: 140-151.

Prakriya, M. (2013). "Store-operated Orai channels: structure and function." Curr Top Membr 71: 1-32.

Prakriya, M. and R. S. Lewis (2006). "Regulation of CRAC channel activity by recruitment of silent channels to a high open-probability gating mode." J Gen Physiol 128(3): 373-386.

Purves, D., et al. (2001) “G-proteins and their molecular targets.” Neuroscience. 2nd edition

Putney, J. W., Jr. (1986). "A model for receptor-regulated calcium entry." Cell Calcium 7(1): 1-12.

Putney, J. W., Jr. (2003). "Capacitative calcium entry in the nervous system." Cell Calcium 34(4-5): 339-344.

Putney, J. W., Jr. (2007). "Recent breakthroughs in the molecular mechanism of capacitative calcium entry (with thoughts on how we got here)." Cell Calcium 42(2): 103-110.

Putney, J. W. (2010). "Pharmacology of store-operated calcium channels." Mol Interv 10(4): 209-218.

Putney, J. W. (2011). "Origins of the concept of store-operated calcium entry." Front Biosci (Schol Ed) 3: 980-984.

Putney, J. W., Jr., et al. (1981). "Receptor regulation of calcium release and calcium permeability in parotid gland cells." Philos Trans R Soc Lond B Biol Sci 296(1080): 37-45.

Qi, Z., et al. (2016). "The Central Analgesic Mechanism of YM-58483 in Attenuating Neuropathic Pain in Rats." Cell Mol Neurobiol 36(7): 1035-1043.

Ramos-Franco, J., et al. (1999). "Location of the permeation pathway in the recombinant type 1 inositol 1,4,5-trisphosphate receptor." J Gen Physiol 114(2): 243-250.

Randriamampita, C. and R. Y. Tsien (1993). "Emptying of intracellular Ca^{2+} stores releases a novel small messenger that stimulates Ca^{2+} influx." Nature 364(6440): 809-814.

Rayns, D. G., et al. (1968). "Surface features of striated muscle. I. Guinea-pig cardiac muscle." J Cell Sci 3(4): 467-474.

Rigaud, M., et al. (2009). "Axotomy depletes intracellular calcium stores in primary sensory neurons." Anesthesiology 111(2): 381-392.

Rizzuto, R. and T. Pozzan (2006). "Microdomains of intracellular Ca^{2+}: molecular determinants and functional consequences." Physiol Rev 86(1): 369-408.

Roos, J., et al. (2005). "STIM1, an essential and conserved component of store-operated Ca^{2+} channel function." J Cell Biol 169(3): 435-445.

Rose, K., et al. (2011). “Transcriptional repression of the M channel subunit Kv7.2 in chronic nerve injury.” Pain 152(4): 742-54.

Rosenbluth, J. (1962). "Subsurface cisterns and their relationship to the neuronal plasma membrane." J Cell Biol 13: 405-421.

Sabbioni, S., et al. (1997). "GOK: a gene at 11p15 involved in rhabdomyosarcoma and rhabdoid tumor development." Cancer Res 57(20): 4493-4497.

Sauc, S., et al. (2015). “STIM1L traps and gates Orai1 channels without remodelling the cortical ER.” J Cell Sci 128(8).

Schindl, R., et al. (2009). "Plasticity in Ca^{2+} selectivity of Orai1/Orai3 heteromeric channel." Proc Natl Acad Sci U S A 106(46): 19623-19628.

Scrimgeour, N. R., et al. (2014). "Structural and stoichiometric determinants of Ca^{2+} release-activated Ca^{2+} (CRAC) channel Ca^{2+}-dependent inactivation." Biochim Biophys Acta 1838(5): 1281-1287.

Sehgal, P., et al. (2017). "Inhibition of the sarco/endoplasmic reticulum (ER) Ca($^{2+}$)-ATPase by thapsigargin analogs induces cell death via ER Ca($^{2+}$) depletion and the unfolded protein response." J Biol Chem 292(48): 19656-19673.

Seixas, A. I., et al. (2012). "Loss of junctophilin-3 contributes to Huntington disease-like 2 pathogenesis." Ann Neurol 71(2): 245-257.

Shaw, P. J., et al. (2013). "Molecular regulation of CRAC channels and their role in lymphocyte function." Cell Mol Life Sci 70(15): 2637-2656.

Shin, J., et al. (2002). "Bradykinin-12-lipoxygenase-VR1 signaling pathway for inflammatory hyperalgesia." Proc Natl Acad Sci U S A 99(15): 10150-10155.

Shuttleworth, T. J. (2012). "Orai3--the 'exceptional' Orai?" J Physiol 590(2): 241-257.

Singh, A., et al. (2010). "The transient receptor potential channel antagonist SKF96365 is a potent blocker of low-voltage-activated T-type calcium channels." Br J Pharmacol 160(6): 1464-1475.

Smani, T., et al. (2004). "A novel mechanism for the store-operated calcium influx pathway." Nat Cell Biol 6(2): 113-120.

Smyth, J. T., et al. (2007). "Role of the microtubule cytoskeleton in the function of the store-operated Ca^{2+} channel activator STIM1." J Cell Sci 120(Pt 21): 3762-3771.

Smyth, J. T., et al. (2008). "Ca^{2+}-store-dependent and -independent reversal of Stim1 localization and function." J Cell Sci 121(Pt 6): 762-772.

Smyth, J. T., et al. (2009). "Phosphorylation of STIM1 underlies suppression of store-operated calcium entry during mitosis." Nat Cell Biol 11(12): 1465-1472.

Soboloff, J., et al. (2012). "STIM proteins: dynamic calcium signal transducers." Nat Rev Mol Cell Biol 13(9): 549-565.

Sobradillo, D., et al. (2014). "A reciprocal shift in transient receptor potential channel 1 (TRPC1) and stromal interaction molecule 2 (STIM2) contributes to Ca^{2+} remodeling and cancer hallmarks in colorectal carcinoma cells." J Biol Chem 289(42): 28765-28782.

Stanisz, H., et al. (2014). "Inverse regulation of melanoma growth and migration by Orai1/STIM2-dependent calcium entry." Pigment Cell Melanoma Res 27(3): 442-453.

Stathopulos, P. B. and M. Ikura (2013). "Structure and function of endoplasmic reticulum STIM calcium sensors." Curr Top Membr 71: 59-93.

Stathopulos, P. B., et al. (2006). "Stored Ca^{2+} depletion-induced oligomerization of stromal interaction molecule 1 (STIM1) via the EF-SAM region: An initiation mechanism for capacitive Ca^{2+} entry." J Biol Chem 281(47): 35855-35862.

Stathopulos, P. B., et al. (2013). "STIM1/Orai1 coiled-coil interplay in the regulation of store-operated calcium entry." Nat Commun 4: 2963.

Steranka, L.R., et al. (1988). “Bradykinin as a pain mediator: reeptors are localized to sensory neurons, and antagonists have analgesic actions.” Proc Natl Acad Sci U S A 85(9):3245-9.

Sun, S., et al. (2014). "Reduced synaptic STIM2 expression and impaired store-operated calcium entry cause destabilization of mature spines in mutant presenilin mice." Neuron 82(1): 79-93.

Suzuki, H., et al. (2010). “Characterization of sensory neurons in the dorsal root ganglia of *Bax*-deficient mice.” Brain Res 1362: 23-31.

Suzuki, J., et al. (2014). "Imaging intraorganellar Ca^{2+} at subcellular resolution using CEPIA." Nat Commun 5: 4153.

Szteyn, K., et al. (2015). "Divergence in endothelin-1- and bradykinin-activated store-operated calcium entry in afferent sensory neurons." ASN Neuro 7(2).

Takemura, H. and J. W. Putney, Jr. (1989). "Capacitative calcium entry in parotid acinar cells." Biochem J 258(2): 409-412.

Takeshima, H., et al. (2015). "Ca(2)(+) microdomains organized by junctophilins." Cell Calcium 58(4): 349-356.

Takeshima, H., et al. (2000). "Junctophilins: a novel family of junctional membrane complex proteins." Mol Cell 6(1): 11-22.

Takezawa, R., et al. (2006). "A pyrazole derivative potently inhibits lymphocyte Ca^{2+} influx and cytokine production by facilitating transient receptor potential melastatin 4 channel activity." Mol Pharmacol 69(4): 1413-1420.

Tandrup, T. (1995). "Are the neurons in the dorsal root ganglion pseudounipolar? A comparison of the number of neurons and number of myelinated and unmyelinated fibres in the dorsal root." J Comp Neurol 357(3): 341-347.

Taylor, C. W., et al. (1999). "Expression of inositol trisphosphate receptors." Cell Calcium 26(6): 237-251.

Taylor, C. W. and S. C. Tovey (2010). "IP(3) receptors: toward understanding their activation." Cold Spring Harb Perspect Biol 2(12): a004010.

Thastrup, O., et al. (1990). "Thapsigargin, a tumor promoter, discharges intracellular Ca^{2+} stores by specific inhibition of the endoplasmic reticulum Ca2(+)-ATPase." Proc Natl Acad Sci U S A 87(7): 2466-2470.Thornton, A.M., et al. (2011). “Store-operated Ca(2+) entry (SOCE) contributes to normal skeletal muscle contractility in young but not in aged skeletal muscle.” Aging 3(6): 621-34.

Tian, C., et al. (2016). "Store-operated CRAC channel inhibitors: opportunities and challenges." Future Med Chem 8(7): 817-832.

Towbin, H., et al. (1979). "Electrophoretic transfer of proteins from polyacrylamide gels to nitrocellulose sheets: procedure and some applications." Proc Natl Acad Sci U S A 76(9): 4350-4354.

Treves, S., et al. (2004). "Junctate is a key element in calcium entry induced by activation of InsP3 receptors and/or calcium store depletion." J Cell Biol 166(4): 537-548.

Trevillyan, J. M., et al. (2001). "Potent inhibition of NFAT activation and T cell cytokine production by novel low molecular weight pyrazole compounds." J Biol Chem 276(51): 48118-48126.

Vaca, L. (2010). "SOCIC: the store-operated calcium influx complex." Cell Calcium 47(3): 199-209.

Van Breemen, D. and C. Van Breemen (1969). "Calcium exchange diffusion in a porous phospholipid ion-exchange membrane." Nature 223(5209): 898-900.

Varnai, P., et al. (2007). "Visualization and manipulation of plasma membrane-endoplasmic reticulum contact sites indicates the presence of additional molecular components within the STIM1-Orai1 Complex." J Biol Chem 282(40): 29678-29690.

Vig, M., et al. (2006). "CRACM1 is a plasma membrane protein essential for store-operated Ca^{2+} entry." Science 312(5777): 1220-1223.

Wang, J. Y., et al. (2015). "STIM1 overexpression promotes colorectal cancer progression, cell motility and COX-2 expression." Oncogene 34(33): 4358-4367.

Wang, X., et al. (2012). "TPC proteins are phosphoinositide- activated sodium-selective ion channels in endosomes and lysosomes." Cell 151(2): 372-383.

Wei, D., et al. (2017). "Orai1 and Orai3 Mediate Store-Operated Calcium Entry Contributing to Neuronal Excitability in Dorsal Root Ganglion Neurons." Front Cell Neurosci 11: 400.

Wes, P. D., et al. (1995). "TRPC1, a human homolog of a Drosophila store-operated channel." Proc Natl Acad Sci U S A 92(21): 9652-9656.

Winslow, R. L. and J. L. Greenstein (2011). "Cardiac myocytes and local signaling in nano-domains." Prog Biophys Mol Biol 107(1): 48-59.

Woo, J. S., et al. (2010). "S165F mutation of junctophilin 2 affects Ca^{2+} signalling in skeletal muscle." Biochem J 427(1): 125-134.

Woo, J. S., et al. (2008). "TRPC3-interacting triadic proteins in skeletal muscle." Biochem J 411(2): 399-405.

Woo, J. S., et al. (2016). "Junctophilin-4, a component of the endoplasmic reticulum-plasma membrane junctions, regulates Ca^{2+} dynamics in T cells." Proc Natl Acad Sci U S A 113(10): 2762-2767.

Wooten, M., et al. (2014). "Three functionally distinct classes of C-fibre nociceptors in primates." Nat Commun 5: 4122.

Wu, J., et al. (2011). "Neuronal store-operated calcium entry pathway as a novel therapeutic target for Huntington's disease treatment." Chem Biol 18(6): 777-793.

Wu, M. M., et al. (2006). "Ca^{2+} store depletion causes STIM1 to accumulate in ER regions closely associated with the plasma membrane." J Cell Biol 174(6): 803-813.

Xia, J., et al. (2014). "Native store-operated calcium channels are functionally expressed in mouse spinal cord dorsal horn neurons and regulate resting calcium homeostasis." J Physiol 592(16): 3443-3461.

Xiao, W.H, et al. (2007). “Persistent low-frequency spontaneous discharge in A-fiber and C-fiber primary afferent neurons during an inflammatory pain condition.” Anestethesiology 107(5):813-21.

Xu, Q. and T. L. Yaksh (2011). "A brief comparison of the pathophysiology of inflammatory versus neuropathic pain." Curr Opin Anaesthesiol 24(4): 400-407.

Yamashita, M., et al. (2007). "Orai1 mutations alter ion permeation and Ca^{2+}-dependent fast inactivation of CRAC channels: evidence for coupling of permeation and gating." J Gen Physiol 130(5): 525-540.

Yang, J., et al. (1993). "Molecular determinants of Ca^{2+} selectivity and ion permeation in L-type Ca^{2+} channels." Nature 366(6451): 158-161.

Yang, S., et al. (2009). "Orai1 and STIM1 are critical for breast tumor cell migration and metastasis." Cancer Cell 15(2): 124-134.

Yao, H., et al. (2009). "TRPC channel-mediated neuroprotection by PDGF involves Pyk2/ERK/CREB pathway." Cell Death Differ 16(12): 1681-1693.

Yeung, P. S., et al. (2018). "Mapping the functional anatomy of Orai1 transmembrane domains for CRAC channel gating." Proc Natl Acad Sci U S A 115(22): E5193-E5202.

Yoo, A. S., et al. (2000). "Presenilin-mediated modulation of capacitative calcium entry." Neuron 27(3): 561-572.

Yuan, J. P., et al. (2009). "SOAR and the polybasic STIM1 domains gate and regulate Orai channels." Nat Cell Biol 11(3): 337-343.

Zakharov, S. I., et al. (2004). "Diethylstilbestrol is a potent inhibitor of store-operated channels and capacitative Ca($^{2+}$) influx." Mol Pharmacol 66(3): 702-707.

Zbidi, H., et al. (2011). "STIM1 and STIM2 are located in the acidic Ca^{2+} stores and associates with Orai1 upon depletion of the acidic stores in human platelets." J Biol Chem 286(14): 12257-12270.

Zhang, C., et al. (2014). "Microtubule-mediated defects in junctophilin-2 trafficking contribute to myocyte transverse-tubule remodeling and Ca^{2+} handling dysfunction in heart failure." Circulation 129(17): 1742-1750.

Zhang, S. L., et al. (2006). "Genome-wide RNAi screen of Ca($^{2+}$) influx identifies genes that regulate Ca($^{2+}$) release-activated Ca($^{2+}$) channel activity." Proc Natl Acad Sci U S A 103(24): 9357-9362.

Zhou, Y., et al. (2016). "The STIM1-binding site nexus remotely controls Orai1 channel gating." Nat Commun 7: 13725.

Zhou, Y., et al. (2010). "Pore architecture of the ORAI1 store-operated calcium channel." Proc Natl Acad Sci U S A 107(11): 4896-4901.

Zhu, J., et al. (2017). "The STIM-Orai Pathway: STIM-Orai Structures: Isolated and in Complex." Adv Exp Med Biol 993: 15-38.

Zhu, M. X., et al. (2010). "TPCs: Endolysosomal channels for Ca^{2+} mobilization from acidic organelles triggered by NAADP." FEBS Lett 584(10): 1966-1974.

Zhu, X., et al. (1995). "Molecular cloning of a widely expressed human homologue for the Drosophila trp gene." FEBS Lett 373(3): 193-198.

Zhu, X., et al. (1996). "trp, a novel mammalian gene family essential for agonist-activated capacitative Ca^{2+} entry." Cell 85(5): 661-671.

Zitt, C., et al. (2004). "Potent inhibition of Ca^{2+} release-activated Ca^{2+} channels and T-lymphocyte activation by the pyrazole derivative BTP2." J Biol Chem 279(13): 12427-12437.

Zweifach, A. and R. S. Lewis (1993). "Mitogen-regulated Ca^{2+} current of T lymphocytes is activated by depletion of intracellular Ca^{2+} stores." Proc Natl Acad Sci U S A 90(13): 6295-6299.

Zweifach, A. and R. S. Lewis (1995). "Rapid inactivation of depletion-activated calcium current (ICRAC) due to local calcium feedback." J Gen Physiol 105(2): 209-226.